METHODS FOR ELECTRICAL STIMULATION CONTROL OF LOWER LIMBS IN INDIVIDUALS WITH SPINAL CORD INJURY

ANA CAROLINA CARDOSO DE SOUSA

TESE DE DOUTORADO EM ENGENHARIA DE SISTEMAS ELETRÔNICOS E DE AUTOMAÇÃO
DEPARTAMENTO DE ENGENHARIA ELÉTRICA

FACULDADE DE TECNOLOGIA

UNIVERSIDADE DE BRASÍLIA

UNIVERSIDADE DE BRASÍLIA
FACULDADE DE TECNOLOGIA
DEPARTAMENTO DE ENGENHARIA ELÉTRICA

METHODS FOR ELECTRICAL STIMULATION CONTROL OF LOWER LIMBS IN INDIVIDUALS WITH SPINAL CORD INJURY

ANA CAROLINA CARDOSO DE SOUSA

ORIENTADOR: PROF. ANTONIO PADILHA LANARI BÓ, DR, ENE/UNB

TESE DE DOUTORADO EM ENGENHARIA DE SISTEMAS ELETRÔNICOS E DE AUTOMAÇÃO

FICHA CATALOGRÁFICA

ANA CAROLINA CARDOSO DE SOUSA

Methods for electrical stimulation control of lower limbs in individuals with spinal cord injury [Distrito Federal] 2019.

xiv, 210 p., 210 x 297 mm (ENE/FT/UnB, Doctor, Engenharia Elétrica, 2019).

Tese de Doutorado - Universidade de Brasília, Faculdade de Tecnologia.

Departamento de Engenharia Elétrica

1. Functional electrical stimulation	2. Controllers
3. Electromyography	4. Orthoses
I. ENE/FT/UnB	II. Título (série)

REFERÊNCIA BIBLIOGRÁFICA

SOUSA, A. C. C. (2019). *Methods for electrical stimulation control of lower limbs in individuals with spinal cord injury*. Tese de Doutorado, Publicação: PGEA.TD 161/2019, Departamento de Engenharia Elétrica, Universidade de Brasília, Brasília, DF, 210 p.
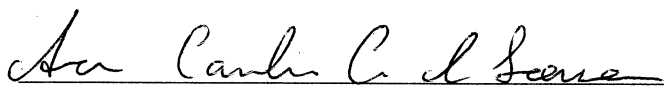
CESSÃO DE DIREITOS

AUTOR: Ana Carolina Cardoso de Sousa

TÍTULO: Methods for electrical stimulation control of lower limbs in individuals with spinal cord injury.

GRAU: Doctor in Electronic Systems Engineering and Automation   ANO: 2019

Ana Carolina Cardoso de Sousa

Depto. de Engenharia Elétrica (ENE) - FT

Universidade de Brasília (UnB)

Campus Darcy Ribeiro

CEP 70919-970 - Brasília - DF - Brasil

AGRADECIMENTOS

Finalizar um doutorado foi uma jornada, e muitas pessoas passaram na minha vida e contribuiram para essa realização.

Meu primeiro agradecimento precisa ser para aquela companhia que eu considero não só minha melhor amiga, mas também o amor da minha vida. Pati, você me entende de uma forma que ninguém mais consegue. Eu te amo por cada contribuição que você deu, seja apontando o que você considerava errado (sem nenhum pudor!) ou ainda me ouvindo e me dando suporte e apoio. A sua opinião (e aprovação) é a primeira que eu busco porque eu sei que, a partir dela, eu consigo constantemente me tornar uma pessoa melhor.

Eu também gostaria de agradecer imensamente aos meus pais. Desde criança, vocês confiaram em mim. E, mesmo não concordando (ou não entendendo minhas decisões), continuaram fornecendo todo apoio que conseguiam me dar. Sempre confiando que eu estava fazendo o meu melhor. Se minha vida é mais fácil, é porque vocês fizeram questão de sempre me fornecer tudo que eu precisava.

Obviamente, eu também gostaria de agradecer a orientação do Prof. Antônio Bó. Não só pela supervisão que sempre buscou um trabalho de excelente qualidade, mas também por ser um modelo de líder, de professor e de orientador. O seu jeito de ver o mundo, de se entregar ao trabalho e de simplesmente fazer acontecer (independente das limitações) são características que serão um modelo pra minha vida.

Agradeço também a supervisão, sugestão, revisão e avaliação de todos pesquisadores que acompanharam meu trabalho, especialmente ao Thomas, Roberto, Adriano, Cristiano e Geovany.

Tive o imenso prazer de trabalhar com colegas fantásticos no EMA e no LARA, pessoas sempre motivadas a realizar trabalhos excelentes (mesmo com tantas limitações). Nosso trabalho envolve errar muito e ser pouco recompensado, o que é frustrante. Mas mesmo assim, acredito que nós compartilhamos valores que vão além da participação em congressos ou publicações em periódicos. A gente compartilha o desejo de usar nossas habilidades pra experimentar novas soluções pro mundo. Dentre essas pessoas, gostaria de agradecer especialmente ao Estevão, essa tese foi realizada graças a sua disponibilidade e dedicação ao projeto.

Por fim, mas não menos importante, gostaria de agradecer às amizades que me acompanharam durante esse tempo. Ao nosso grupinho do bate-papo diário, Ethel, Natália e Aline. Aos nossos encontros de imenso valor e carinho, Horty, Raquel, Manu,

Camila. Aos meus amigos mais antigos que fizeram parte de tantas etapas da minha vida, Dan, Lores, Ju. Ao Carlos e à Danusa pelo companheiro e suporte. Ao casal-20 (que deveria ser mais que 20), Carol e Lucas. Enfim, a todos aqueles que trocaram ideias, carinho, suporte no meu dia a dia: obrigada.

ABSTRACT

Spinal cord injury (SCI) is one of the most severe injuries from motor disabilities. Therefore, there are sets of rehabilitation exercises for muscle strengthening, circulation, pressure release, and improvement of bone density. Advanced technologies may provide rehabilitation improvements for functional movements. Some of these routines use traditional methods with functional electrical stimulation (FES), which produces nerve stimulation through electrical signals, allowing the contraction of paralyzed muscles to produce torque. For feedback control, it is necessary to perform the mathematical modeling of the plant, followed by the controller design based on the available measurement units. Some of FES control challenges include nonlinearities of operation, which requires sophisticated feedback control techniques. We might increase the number of FES rehabilitation studies with patients with complete SCI if we diminish the difficulty to generate a safe and controllable system. In this work, we propose new techniques for FES control of lower limbs of a patient with complete SCI. More precisely, for this document, we intend to develop and evaluate three features of the lower limb rehabilitation to improve FES control. Each of these traits occurs in different perspectives of the control system: (1) the sensor estimation, (2) the control algorithms, and (3) the plant.

For the sensor estimation (1), we used electromyography (EMG) to estimate the voluntary (vEMG) and the evoked (eEMG) activities. We developed methods for detecting stimulation artifacts for two-channel stimulation on the same limb to estimate vEMG and eEMG. These methods are not hardware-synchronized to a stimulator and presented a success higher than 95%.

For the control algorithms (2), we created simulation environments and studied FES control strategies for gait and cycling. Using the FES gait environment, we simulated four trajectory controllers (bang-bang (BB), proportional-integral-derivative (PID), PID iterative learning (PID-ILC), and PID tuning using extremum seeking (PID-ES) controller) to track knee movement during low-speed gait. The PID-ES presented slightly higher correlation coefficients and lower maximum and standard deviation errors. Furthermore, using the FES cycling environment, we simulated a detailed musculoskeletal model and simulated speed controllers to track crankset speed during cycling. The FES cycling environment allowed the investigation of passive knee orthoses parameters, which usually presented lower muscle excitation.

For the plant (3), we compared how adding passive elements in knee orthoses could change the cadence during an FES bike training with an individual with SCI. We performed two days of experiments with and without springs and found that the average cycling speed was higher than 10% on both days.

SCI poses a heavy burden on the quality of life, and the investigation of stimulation protocols for rehabilitation varies significantly. These approaches intended to complement the literature, taking into account the security of the volunteer and the effectiveness of the control system, which may improve rehabilitation for people with complete spinal cord injury.

Keywords: functional electrical stimulation, controllers, electromyography, orthoses.

TABLE OF CONTENTS

LIST OF FIGURES

xiii

xvi

LIST OF TABLES

LIST OF ABBREVIATIONS AND ACRONYMS

ACL	Anterior Cruciate Ligament
ADL	Activities of daily living
AFO	Ankle-foot-orthosis
API	Application programming interface
ASIA	American spinal cord injury association
ATP	Adenosine triphosphate
BB	Bang-bang
BWS	Body weight-supported
CA	Co-activation
CNS	Central nervous system
CoM	Center of mass
CPG	Central pattern generator
DC	Direct current
DOF	Degrees-of-freedom
DSP	Double support phase
EEG	Electroencephalography
EMG	Electromyography
FES	Functional electrical stimulation
FLC	Fuzzy logic control
FNS	Functional neuromuscular stimulation
FSC	Finite state control
FSM	Finite state machine
FSR	Force-sensing resistor
GA	Genetic algorithm

GUI	Graphical User Interface
HNP	Hybrid neuroprosthesis
IEEE	Institute of Electrical and Electronics Engineers
ILC	Iterative learning control
IMU	Inertial measurement unit
IPI	Inter-pulse-intervals
ISNCASIA	International standards for neurological classification of spinal cord injury
KAFO	Knee-ankle-foot-orthosis
LFF	Left foot-flat
LHC	Left heel contact
LHO	Left heel-off
LTO	Left toe-off
MAD	Median absolute deviation
MAP	Muscle action potentials
MFE	Muscle fatigue estimator
MPC	Model predictive control
MR	Magnetorheological
NMES	Neuromuscular electrical stimulation
PID	Proportional–integral–derivative
PID-ES	Proportional–integral–derivative with extremum seeking
PID-DC	Proportional–integral–derivative with delay compensation
PNS	Peripheral nervous system
PO	Overshoot
PW	Pulse width
PWM	Pulse-width modulation

RFF	Right foot-flat
RHC	Right heel contact
RISE	Robust integral of the sign of the error
RMSE	Root-mean-square deviation
ROS	Robot operating system
RTO	Right toe-off
SBO	Spring break orthosis
SCI	Spinal cord injury
SSP	Single support phase
TCP/IP	Transmission control protocol/Internet protocol
WSO	World stroke organization

LIST OF SYMBOLS

°	degree
rad	radian
m	meter
mm	millimeter $(0.001\,m)$
s	seconds
μs	micro second $(0.001\,ms)$
g	gram
kg	kilogram $(1000\,g)$
Hz	hertz
kHz	kilo hertz $(1000\,Hz)$
V	volts
mV	mili volt $(0.001\,V)$
A	ampères
mA	milliampere $(0.001\,A)$
N	Newton
%	percentage
$<$	less than
$<$	larger than
Δ	rate of change
m/s	meter per second
°/s	degrees per second
Nm/rad	Newton meter per radian
mV/V	millivolt per volt

1 INTRODUCTION

The World Health Organization considers an individual with some disability when his or her interaction with the environment is impaired, limited, or restricted (The Lancet, 2011). The definition considers not only physical health but also the social context, as a biopsychosocial model: the same physiological impairments can express different degrees of restriction, depending on the context. Disabilities also present themselves in various forms (visual, hearing, mental, and motor) and ratings (mild, moderate, severe, and extreme). Specifically, motor disability has devastating effects on quality of life, particularly during Activities of Daily Living (ADLs), and affects millions worldwide (e.g., 14 million Brazilian people mentioned some difficulty in walking or climbing stairs (Instituto Brasileiro de Geografia e Estatística - IBGE, 2010)). In addition to these motor difficulties, individuals with diminished mobility are also more susceptible to other health complications. The disuse syndrome of lower limbs (e.g., the dependency of a wheelchair) causes muscle weakness, a decrease in joint motion range, joints ossification, deterioration of peripheral circulatory function, and so on (Thomas Jefferson University Hospital and Magee Rehabilitation, 2009).

Spinal cord injury (SCI) is one of the most severe injuries that affect individuals, with substantial physical, psychic, and social repercussion. However, current disability data in Brazil dates back to the 2010 IBGE census and do not allow differentiation among motor disabilities, or their causes (Instituto Brasileiro de Geografia e Estatística - IBGE, 2010). The next IBGE census in 2020 will follow the same methodology, with only one question about motor disabilities, "Do you experience permanent difficulties to walk or to climb stairs, even using prostheses, clutches or assistive devices?"[1]. Therefore, the incidence coefficient of traumatic SCI in Brazil is unknown, and no precise data on its incidence and prevalence are available, as this condition is not subordinate to a notification to the government (Ministério da Saúde, 2013). Today, we have only some estimations, such as 10 thousand new cases per year, in which 80% of the victims are men, and 60% are between 10 to 30 years old (Ministério da Saúde, 2013).

Beyond the motor and sensory impairment, an SCI individual may present loss of physiological function of the bladder and intestines, edemas due to circulation impairments, spasticity, pressure ulcers, breathing difficulties, difficulty in regulating body temperature, and heterotopic ossification (Ministério da Saúde, 2013; Thomas Jefferson University Hospital and Magee Rehabilitation, 2009). The cause of some of these complications is the lack of use of limbs. Therefore, there are a set of rehabilitation exercises

---

[1] Question 35 of the sample questionnaire in `https://www.ibge.gov.br/media/com_mediaibge/arquivos/ee88a6181125873a8acd7b8c7ab9ad3c.pdf`.

for muscle strengthening, circulation, pressure release, and improvement of bone density. Physiotherapists focus on specific muscles and joints, adapting the program to the patient restrictions, limitations, and advances (Thomas Jefferson University Hospital and Magee Rehabilitation, 2009).

It is essential to understand the differences between spinal cord injuries to predict recovery in rehabilitation. After a complete neurological examination, the physician describes the level of injury (e.g., cervical, thoracic, lumbar, and sacral) and determine if the injury is complete or incomplete (KIRSHBLUM et al., 2011). Complete spinal cord injury occurs when the spinal cord is fully compressed or severed, eliminating the brain's ability to send signals below the point of injury. An incomplete injury occurs when the brain still can send signals below the site of injury.

For lower limbs, researchers already presented numerous wearable assistive devices with sensors to increase the efficiency of the rehabilitation (RIEK, 2017). The measurements units provide a real-time response, not only for patients but also for physicians (examination, diagnostics, or direct interference in movements). Widely used in rehabilitation and ADL assistance, functional electrical stimulation (FES) produces nerve stimulation through electrical signals, allowing contraction of paralyzed muscles to produce torque (LYNCH; POPOVIC, 2012; MARTIN et al., 2012). Today, physiotherapists already use FES in SCI rehabilitation due to its advantages, such as enhancement of muscle strength, decrease of bone loss, cardiovascular and respiratory improvement, and quality of life (THOMAZ et al., 2019).

The complete absence of motor and sensory function below the injury area does not necessarily mean no remaining intact nerves, just that they are not functioning appropriately as a result of the trauma. Therefore, FES is still possible to be used in both complete and incomplete injuries. The spinal cord uses a set of sensory information to generate an appropriate motor response; a property called central pattern generator (CPG) (RAINE; MEADOWS; LYNCH-ELLERINGTON, 2009). The FES success in SCI rehabilitation relates to this property, although muscles may be atrophied after injury, they may still be able to produce muscle contraction with FES. This technique is simple, inexpensive, and non-invasive, already indicated for several therapeutic purposes (RAINE; MEADOWS; LYNCH-ELLERINGTON, 2009).

1.1   CONTEXT

There is a notable trend in the study of the benefit of FES programs with complete SCI individuals (BAPTISTA, 2014). Clinical knowledge states that subjects with complete SCI do not gain many advantages of FES rehabilitation without functional movement (NAKI et al., 2011). This functional movement for complete SCI should

be a control system, i.e., a set of equipment and devices that manage the behavior of physical systems. For this, it is necessary to perform the mathematical modeling of the plant, followed by the controller design based on the available measurement units. We could increase the number of FES rehabilitation studies with complete SCI patients if we diminished the difficulty to generate a safe and controllable system in the clinics. FES control includes nonlinearities of operation (POPOVIĆ; SINKJÆR, 2000), which requires sophisticated feedback control techniques, according to the goals and costs involved. In this work, we focus on volunteers with remaining trunk and upper limbs movements (i.e., bellow T8 injury (KIRSHBLUM et al., 2011)).

Feedback control (or closed-loop) is an operation that, in the presence of disturbances, tends to reduce the difference between the output of a system and some reference input (OGATA, 2010). An everyday example is the temperature control; where the site may alter the desired set temperature. A mathematical algorithm in the controller restores the actual temperature of the desired room optimally by controlling the intensity of an air conditioning. Figure 1.1 illustrates a closed-loop FES control with a controller (e.g., bang-bang or proportional–integral–derivative controllers) that changes the pulse parameters (e.g., current or pulse width) of the stimulator based on sensors response (e.g., inertial or force sensors) to achieve a desired response (e.g., trajectory or speed) of the plant. A plant is any physical object to be controlled; in our case, the lower limb muscles through surface stimulation.
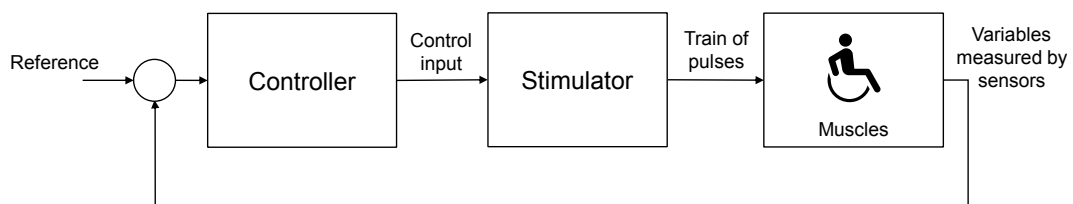
Figure 1.1: Example of a block diagram of a closed-loop FES control. Based on the reference and the variables measured by sensors, the controller calculates a control input and send it to the stimulator. The stimulator uses this message to create a train of pulses that will be applied to the muscles of a complete SCI volunteer muscles through surface electrodes.

Source: prepared by the author.

Extensive research work has been carried out for applications of FES systems, such as cycling (COSTE; WOLF, 2018), balance regulation (VETTE; MASANI; POPOVIC, 2007), and other functional exercises (THRASHER; POPOVIC, 2008). Fast muscle fatigue remains the primary limitation on the use of FES control for long periods in rehabilitation (THRASHER; POPOVIC, 2008). Results from controllers attempting to compensate fatigue by applying dynamic models are still insufficient (KIRSCH et al., 2016), limiting the duration of exercises. Other FES complexities also include mul-

tiple muscles coordination and inadequate stimulation response characteristics (i.e., nonlinearity, electromechanical delays, and time-dependency). This thesis aims to contribute to the overall performance and natural interaction between the user and the FES system. Through this document, we carefully explain and justify all of the required statements and terms.

Primary, we need to answer a broad inquiry in the thesis statement: are there new features that we may add to FES control of lower limbs of a complete SCI patient during rehabilitation? This inquiry suggests a clear answer: yes, there are new features that researchers often add to this topic, in our delimited literature review, we found more than ten citations in 2018 and two citations in 2019. These results show an interest by the academic community in these topics.

In this document, we intend then to evaluate three advanced techniques of the lower limb rehabilitation to improve FES control for complete SCI patients. Each of these advances exists in a different perspective of the control system: (1) the **sensor estimation**, (2) the **control algorithms**, and (3) the **plant**. This work proposes answers to three different questions, one for each perspective.

1.2 PROBLEM DEFINITION

Here we define the queries for each perspective: **sensor estimation**, the **control algorithms**, and the **plant**.

1.2.1 Sensor estimation using electromyography

State of the art research of FES control of lower limbs shows that the most common **sensors** in FES control are contact (e.g., (CHANG et al., 2016)), force (e.g., (REN; ZHANG, 2014)), and inertial (e.g., (QIU et al., 2014)) sensors. Contact sensors used are force-sensing resistors (FSR), which allow accurate measurements of contact, but does not provide a high resolution when compared to force or inertial sensors. Moreover, inertial sensors (for angular position and velocity) are more accessible compared to force sensors, as they do not require an external structure, such as force platforms or elastic bands. In FES control, the combination of these sensors may generate an accurate and precise movement compared to the reference (CHANG et al., 2016). However, challenges remain to separate the movement generated by muscle contraction evoked by the stimulation and movement generated by external disturbances (e.g., spasms or a physiotherapist aid). This information is essential to ensure user safety, and to allow a better assessment of the rehabilitation outcome. Along with these concerns, we should note that more equipment (sensors) usually led to higher costs. One type of estimation of muscle activity that some works use with FES is the **electromyography** (EMG)

(e.g., (SCHAUER, 2017)), an electrodiagnostic technique for evaluating and recording the electrical activity produced by muscles (KAMEN; GABRIEL, 2010). The EMG is the detection of the electric potential generated by muscle fibers when electrically or neurologically activated.

As EMG-FES systems are inexpensive, physicians could use these systems in clinical practice (MONTE-SILVA et al., 2019). To extract the evoked information from EMG signals, we need first to find the inter-pulse-intervals (IPIs), the EMG signal between stimulation artifacts. Many previous projects synchronized the EMG amplifier and the stimulator during stimulation to reduce (e.g., (THORSEN, 1999)) or even altogether remove (e.g., (KNAFLITZ et al., 1988; SHALABY et al., 2011)) artifacts by custom-made hardware interfaces. However, this hardware that combines FES and EMG are not commercially available. Additional signal processing steps are required to detect the onset of the stimulation artifacts precisely. (SOARES; COELHO; NADAL, 2013) and (KLAUER; RAISCH; SCHAUER, 2012) calculated the cross-correlation function between the EMG signal and an artifact template to locate potential artifact onsets. Moreover, finding a suitable artifact template is a challenge when stimulating more than one channel on a limb. Most stimulation devices possess only one current source and generate the pulses on the different channels time-multiplexed in a fast sequence. Threshold-based artifact detection serves as another possible approach to find stimulation artifacts but requires a manual adaptation. In this context, this thesis aims to answer the first inquiry:

How can threshold-based methods automatically detect stimulation artifacts for two channels of electromyography, and how much would be the success rate?

1.2.2 Simulation environments for control algorithms

Fast muscle fatigue limits the use of stimulation for extended periods, and FES is a non-linear system that requires sophisticated controllers that usually demands numerous trials. These adverse circumstances often require specific simulation environments for FES control (e.g., (YAHAYA et al., 2018), (ABDULLA; SAYIDMARIE; TOKHI, 2014) and (BAO; KIRSCH; SHARMA, 2016)). Most of these environments create non-linear musculoskeletal models based on Hill-type principles (HILL; B, 1938): recruitment, frequency, calcium dynamics, and muscle fatigue. Still, the **simulation** results are not entirely comparable, as most researchers do not provide either the environment, the complete model, or parameters used.

In rehabilitation, FES has been used to produce lower limbs movement for subjects with SCI in exercises such as gait (e.g., (CHANG et al., 2016)) and cycling

(e.g., (COSTE; WOLF, 2018)). Today, literature is unable to provide a scenario in which we may compare between **controllers** in similar conditions adequately. Experimental systems demand an abnormally high cost, and there is no detailed musculoskeletal model for this type of exercises until now. In this context, this thesis aims to answer the second inquiry:

> **What simulation environment can we use to compare and evaluate errors of trajectory controllers for FES gait? What simulation environment can we use to compare and evaluate cadence of controllers for FES cycling?**

1.2.3 Plant changes adding passive knee orthoses

In 2016, the Swiss Federal Institute of Technology in Zurich organized the first Cybathlon[2](COSTE; WOLF, 2018), an international competition in which people with physical disabilities compete against each other to complete everyday tasks using start-of-the-art technical assistance systems. One of its disciplines is the FES Bike race, in which SCI cyclists (or pilots) perform pedaling movements with FES. It is a long run since the first demonstration of **FES cycling** (GLASER, 1986). In the last 30 years, people with SCI have been practicing this activity in rehabilitation to achieve a range of physiological benefits, such as enhancement of muscle strength, the decrease of bone loss, cardiovascular and respiratory improvement, and quality of life (POPOVIĆ; SINKJÆR, 2000). Several commercial systems are now available for stationary exercise[3] and mobile cycling[4]. At the University of Brasilia in Brazil, the Empowering Mobility and Autonomy (EMA) holds extensive experience with FES cycling in rehabilitation and Cybathlon competition (BÓ et al., 2017).

Even after this progress, there are outstanding challenges with FES cycling related to the low efficiency and low power output (BERRY et al., 2012; HUNT et al., 2013). Early works (GLASER, 1986; GLASER, 1991) have suggested that the unfavorable biomechanics may be a contributory factor to this low efficiency. These biomechanics include imperfect recruitment of muscle groups, non-optimal timing of muscle activation, and lack of synergistic and antagonistic joint control. Most researchers focus on optimizing recruitment of muscle groups (e.g., (DOLBOW; HOLCOMB; GORGEY, 2014)) and timing the muscle activation (e.g., (WATANABE; TADANO, 2018)), which have the most effect on the overall cycling performance. However, when

---

we consider the competition environment, other details should also be considered for better performance. Researchers have not yet explored the use of energy storage devices to support FES cycling in real experiments. **Passive orthoses** may store kinetic energy as potential energy, and released it when needed without any external power supply (MASSOUD, 2012). In this context, this thesis aims to answer the last inquiry:

> **Is it possible to change crankset cadence in FES cycling with similar quadriceps stimulation when a complete SCI volunteer uses passive knee orthoses?**

1.3 GOALS

In the sensor perspective, we propose a SIMULINK® (The Mathworks Inc., USA) toolbox for EMG processing during FES for two-channels-non-synchronized stimulator and EMG hardware. This toolbox implements methods to separate EMG evoked through stimulation and EMG generated by voluntary contraction (for various EMG sampling frequencies and stimulation rates). The substitution of force sensors with EMG in FES control for rehabilitation should impact the community searching for the muscle response caused by FES. As EMG does not require an external structure, such as force platforms or elastic bands, we could access measurements of the muscle contraction with just a few surface electrodes.

In the controller perspective, we expect to develop one simulation environment for comparison of controllers for low speeds in gait, and one simulation environment for comparison of controllers for cycling. The software provides kinematics and dynamics tools to understand and analyze motions. Using a graphical interface, users can generate simulations with default models or develop new models and controllers. Moreover, it is possible to develop additional functions to simulate the effects of fatigue and disturbances.

In the plant perspective, the present work intends to experiment with passive knee orthoses for FES cycling assistance, changing the cycling cadence during the cycle. To our knowledge, no previous experiments used mechanical passive orthoses in a similar approach for FES cycling. With passive orthoses, the volunteer with SCI could cycle farther with similar stimulation.

1.4 OUTLINE OF THE THESIS

Our goal is first to introduce fundamental elements of FES control. Hence, after this introduction, Chapter 2 presents theoretical foundations for a complete understanding of this thesis, defining essential terms in physiology for human movement,

pathologies, and restoration of lower limbs movements. Subsequently, Chapter 3 inspects the literature on EMG record during stimulation on the same limb, FES knee trajectory controllers and energy storage devices to support functional movements.

To answer the first inquiry related to the EMG perspective, Chapter 4 presents an overview of the proposed threshold-based methods to automatically detect stimulation artifact and estimate EMG evoked by stimulation (eEMG) and volitional EMG (vEMG). Then, we applied this automatic detection and showed a comparison with force sensors.

For the simulation environments, Chapter 5 and Chapter 6 describe in detail our methods for FES gait and FES cycling, respectively. Chapter 5 describes a hybrid neuroprosthesis (HNP) composed of a hip orthosis and FES-controlled knee motion for FES gait. We then compared four controllers in this scenario: bang-bang (BB), proportional-integral-derivative (PID), PID with iterative learning control (PID-ILC), and PID tuning using extremum seeking (PID-ES). Chapter 6 proposes a new detailed musculoskeletal platform to test and develop control strategies for FES cycling. Using this environment, we compared the cycling cadence and quadriceps excitation using an FES cycling simulation platform for different spring torques and ranges.

Afterward, we present the experimental results of passive knee orthoses in FES cycling (Chapter 7). Based on studies from previous chapters, we built and tested two passive knee orthoses in a complete SCI volunteer during FES cycling training.

Lastly, in Chapter 8, we recapitulate significant findings of the thesis focusing on the three perspectives.

2 THEORETICAL FOUNDATIONS

Various pathologies limit lower limbs motor skills, which justify long lines of investigation to improve not only locomotion but also the general quality of life of patients. To to try and improve in the performance of patients, researchers first need to understand the movements physiology, how a disorder changes it, and, finally, in which ways we can use artificial techniques to restore or substitute standard functions of the body. The following sections introduce theoretical foundations and common challenges in this area. Section 2.1 describes both nervous and muscular systems and how anatomy and organization guide natural movements. Section 2.2 presents some gait pathologies and their leading causes. And, finally, Section 2.3 reviews neurorehabilitation aspects and neuroprostheses technologies (devices that can substitute a motor ability damaged by an injury) for restoring or substituting natural control of lower limbs functions.

2.1 PHYSIOLOGY OF HUMAN MOVEMENT

Physiology is the scientific study of living systems' functioning, focusing on organisms, organ systems, organs, cells, and biomolecules (definition from (HALL; GUYTON, 2015)). Our interest resides in the human motor system comprised of three interrelated anatomical systems: skeletal, muscular and nervous. The following concepts serve as an essential guide for understanding simple components and their standard integration in both nervous (Section 2.1.1) and muscular (Section 2.1.2) systems and finally how they interact to provide natural movements (Section 2.1.4 and Section 2.1.5). To avoid extrapolating the thesis outline, we summarized some concepts of nervous and muscular systems for movement control. We consider this a scientific field of its own, and then, for more detailed reading, we recommend the following books: (CORR, 2006), (HALL; GUYTON, 2015) and (POPOVIĆ; SINKJÆR, 2000) and (PERRY, 1992).

2.1.1 Nervous system

The nervous system controls voluntary and involuntary actions, transmitting signals to and from different parts of the body. From the nervous system context, the voluntary control is a complex hierarchical structure with separate neural circuits: premotor cortical area, motor complex, brainstem, and spinal cord. Both brain and spinal cord compose the central nervous system (CNS), and the nerves from CNS divide and distribute to smaller units, forming the peripheral nervous system (PNS). More detailed information about the nervous system physiology can be found in (CORR,

2006), (HALL; GUYTON, 2015) and (POPOVIĆ; SINKJÆR, 2000).

Neuron stands for the electrically excitable cell of the nervous system that processes and transmits information through electrical and chemical signals. Researchers categorize neurons by functions: sensory, motor, and interneurons. Sensory neurons collect data from different energy excitations through chemical, thermal, mechanical, or electromagnetic changes. Motor neurons carry signals from the brain and spinal cord to cause muscle contractions. Interneurons connect neurons, possibly linking distant brain regions.

All neurons are electrically excitable through action potentials, a short-lasting event in which the electrical membrane potential of a cell rapidly rises and falls, following a consistent trajectory (Figure 2.1). These channels close when the membrane potential is near the resting potential of the cell (usually $-70\,mV$). If the voltage increases to a precisely defined threshold value (between $-40\,mV$ to $-55\,mV$), the channels open, allowing the flow of sodium ions to the inside of the cell, which changes electrochemical gradient and increases the membrane potential. This electrical change eventually causes the polarity of the membrane to reverse and the ion channels rapidly close. The repolarization occurs when the sodium ions can no longer enter the neuron and are actively transported back out of the plasma membrane. After the re-polarization, there is a recovering period, called refractory period, in which the neuron cannot be re-stimulated. Because of the refractory period, action potentials remain separate and discrete, and the neurons conduct impulses at rates lower than the absolute refractory periods.
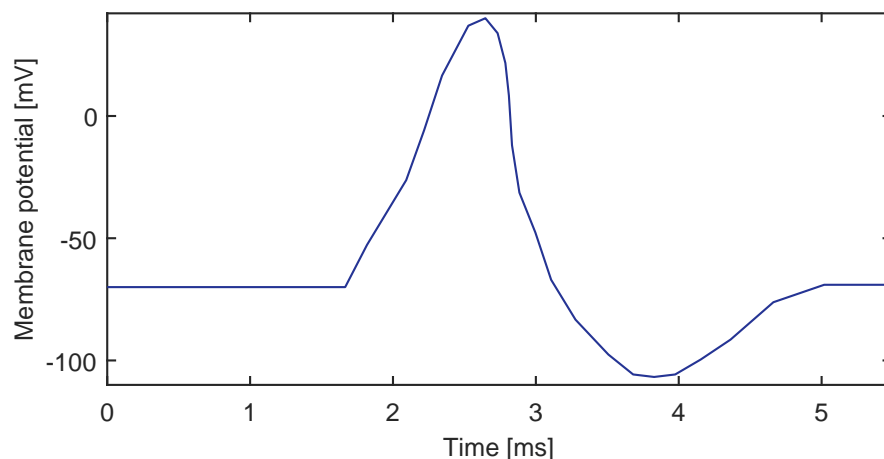
Figure 2.1: The action potential rapid rises and subsequently falls in voltage across a cellular membrane with this characteristic pattern. Sufficient current is required to initiate a voltage response in a cell membrane; if the current is insufficient to depolarize the membrane to the threshold level, the action potential does not fire.

Source: prepared by the author.

2.1.2   Muscular system

Humans have about 330 pairs of skeletal muscles of many shapes and sizes that are situated across more than 300 joints, being attached at two or more points to bones via tendons. Humans generate movement by shortening and broadening muscles, which brings their ends closer to each other, moving our limbs over joints. The following sections describe the individual units of muscles, the fibers (Section 2.1.2.1), and how nerves transmit information to muscles (Section 2.1.2.2). More detailed information about the muscular system physiology can be found in (CORR, 2006), (HALL; GUYTON, 2015) and (POPOVIĆ; SINKJÆR, 2000).

2.1.2.1   Fibers

Fiber is the individual contractile unit in a muscle. There are two general types of skeletal muscle fibers: **slow twitch muscle fiber** (Type I) and **fast twitch muscle fiber** (Type II), further categorized into Type IIa and IIx. The distinctions are related to how muscle respond to contraction. Slow fibers are red due to the presence of large volumes of myoglobin, efficiently producing large amounts of Adenosine triphosphate (ATP, energy). Aerobic metabolic cycles can hold contractions over a long time until fatigue, but they fire more slowly than fast fibers. Postural muscles (e.g., neck and spine) are composed mainly of slow fibers. Type IIa (also known as intermediate fast-twitch fibers) are hybrids between slow and fast fibers, using both aerobic and anaerobic metabolism cycles to produce energy equally. This hybrid feature produces rapid, intense muscle contractions, with quicker fatigue than slow fibers. Finally, Type IIx fibers are white due to a low level of myoglobin, therefore use anaerobic metabolism to produce energy. This results in short, fast bursts of power and rapid fatigue. Fast fibers generally provide the same amount of force per contraction as slow fibers, but with a more immediate firing.

2.1.2.2   Transmission of information from nerves to fibers

A **sensorimotor nerve** is an enclosed cable-like bundle that carries information between CNS and muscles. It consists of both efferent (motor) and afferent (sensory) nerve fibers, which branches and divides to distribute information to tissues. In physiology, it is helpful to recognize which muscles relates to motor nerves because usually the same motor nerves activate muscles that share the same embryological origin.

A **neuromuscular junction** is the site in which muscle activation occurs: the motor nerve stimulates fibers to cause muscular contraction. A single motor neuron can innervate multiple muscle fibers, causing more fibers to contract at the same time. The sliding filament theory (HUXLEY; NIEDERGERKE, 1954) explains how the protein filaments within each skeletal muscle fiber slide past each other to produce contraction.

Each fiber contains a series of basic units called **sarcomeres**, formed by parallel actin (thin) and myosin (thick) filaments. When a muscle activation occurs, it stimulates a reaction between the threads of the sarcomere. The zone containing filaments of myosin (A band) remain relatively constant in length during contraction, while the zone containing filaments of actin (I band) slides through the A band, causing the shortening of the fiber. Specifically, ATP binds to myosin, which attaches to actin with calcium, and pulls the I band towards the center of the sarcomere. This process occurs in all sarcomeres, causing muscle contraction, but as cycles are asynchronous, the force reflects the average number of sarcomeres activated.

It is possible to correlate **artificial stimulus** (e.g., electrical stimulation) with quantified variables, allowing control of muscles. The fibers respond to an all-or-none stimulation from the motor neuron, i.e., increasing intensity does not increase the magnitude of the fiber response. A **twitch** is a response to a single pulse applied to a muscle. It causes a quick contraction, followed by relaxation. Its magnitude varies along the number of muscle fibers stimulated and the response to the stimulus. If the person repeatedly applies an adequate stimulus to a fiber at a rate rapid enough for each stimulus reactivate the contractile elements before the relaxation, the responses summate until a maximal level. If the person continues, the contraction peak remains at the maximal level, and this response is known as tetanus or tetanic contraction. Ultimately, fatigue will cause the peak level to decline progressively. This can be seen in Figure 2.2.
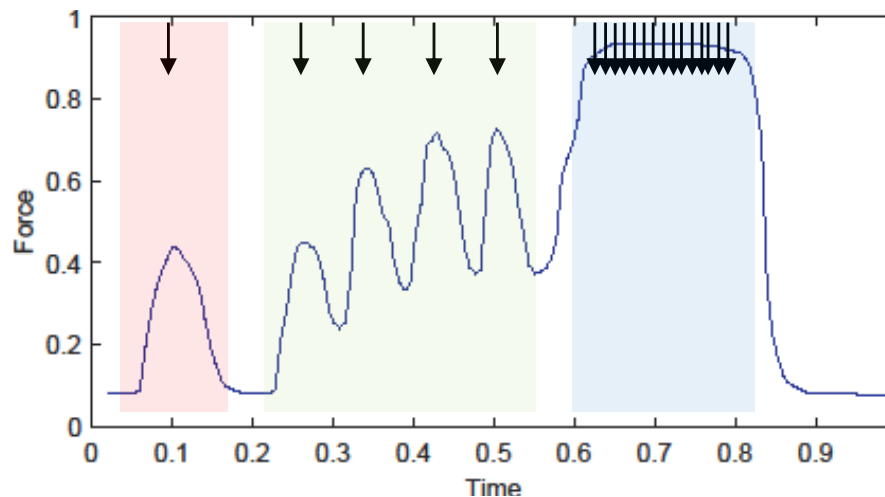
Figure 2.2: The effect of the frequency of stimulation on the force developed in isometric conditions. First stimulus is a twitch ($0.3\,Hz$, light red), followed by $5\,Hz$ (light green) and $50\,Hz$ (light blue) stimulation. Both time and force are normalized.

Source: adapted from (POPOVIĆ; SINKJÆR, 2000).

The relation between internal and external forces defines **isometric** and **iso-**

tonic contraction. In an isometric contraction, the internal force is not sufficient to exceed the external resistance, not changing the size of the muscle. If the internal force exceeds the external resistance and the muscle length changes, literature calls it an isotonic contraction (HALL; GUYTON, 2015; CORR, 2006). A concentric isotonic contraction is when the muscle shortens, and an eccentric isotonic contraction is when the muscle lengthens as it resists the load. Maintaining a constant force characterizes this isotonic contraction.

2.1.2.3 Muscle model

A muscle can neither generate force nor relax instantaneously. The development of force is a complex sequence of events that begins with the firing of motor units and culminates in the formation of actin-myosin cross-bridges within the myofibrils of the muscle. In biomechanics, Hill's muscle model is one of the most classical models to represent muscle contractions (HILL; B, 1938). With adaptations, simulation platforms still implement the model (e.g., OpenSim (DELP et al., 2007)).

The Hill-type principle is that the force-producing properties of muscle are complex and nonlinear. For simplicity, the tetanic contraction relates tension to the velocity concerning internal thermodynamics. Therefore, the higher the load applied to the muscle, the lower the contraction velocity. Similarly, the higher the contraction velocity, the lower the tension in the tissue. This hyperbolic form has been found to fit the empirical constant only during isotonic contractions near resting length.

2.1.3 Lower limb muscles

Figure 2.3 illustrates some muscle group of lower limbs. As the physiology of muscles contains several details, we decided to just describe the most presented muscles in gait studies.

Quadriceps The quadriceps is a group of four muscles (**vastus medialis**, **vastus intermedius**, **vastus lateralis** and **rectus femoris**) that form a single tendon attached to the upper pole of the patella. When the quadriceps contracts, it pulls the knee cover and extends the knee joint. Usually, quadriceps is the most significant muscle targeted by physiotherapy to restore optimum knee function in rehabilitation.

Hamstrings The hamstrings are a group of three muscles (**semitendinosus**, **semimembranosus**, and **biceps femoris**) at the back of the tight. These muscles have a proximal attachment deep to the **gluteus maximus**. Besides, the biceps femoris has an additional attachment to the body of the femur. These muscles
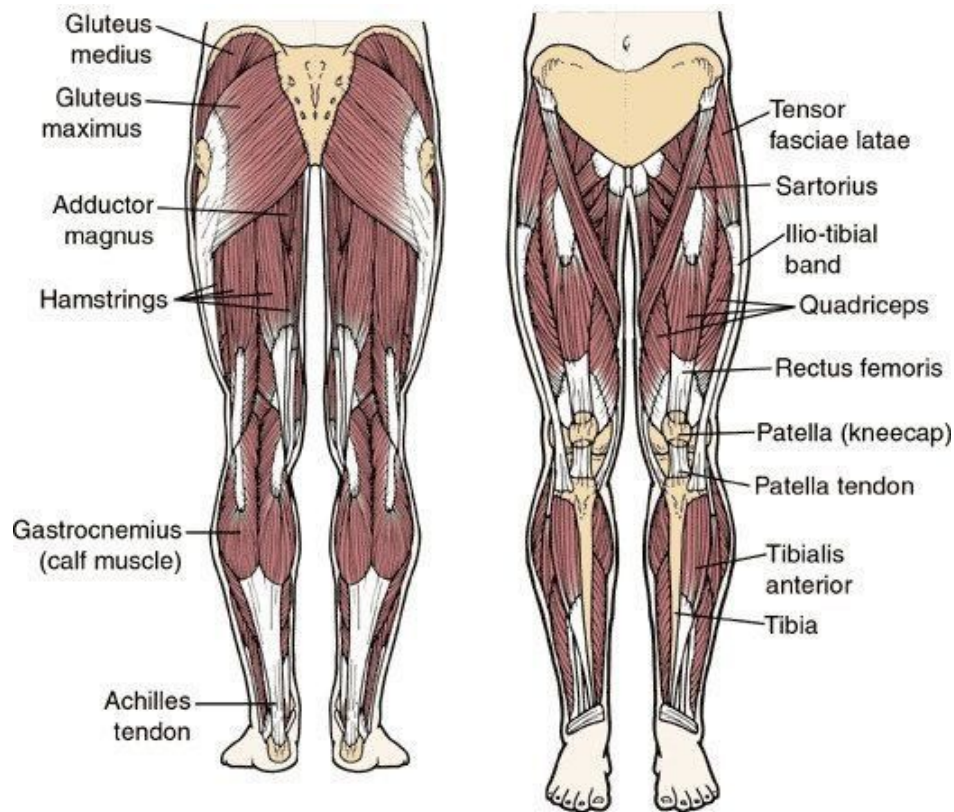
Figure 2.3: Details of lower limbs main muscles.

Source: Digital Repository of Quora in the post accessed in June 2019.

also have the same nerve supply from the sciatic nerve. As the hamstrings span the hip and knee joints, they extend the thigh and flex the knee.

Gluteus maximus The gluteus maximus is the main extensor muscle of the hip. It is the largest and most superficial of the three gluteal muscles.

Gastrocnemius The gastrocnemius is responsible for the curvey shape of the **calf**. It contains two heads originating from the femoral condyles and joining the **soleus** muscle to form the Achilles tendon. The gastrocnemius passes over the knee and ankle, coordinating with other muscles to move each of these joints. Along with the hamstrings, the gastrocnemius flexes the knee, while, along with the soleus muscle, it flexes the ankle.

Tibialis anterior The tibialis anterior locates near the shin, originating in the lateral surface of the tibia. This muscle is responsible for dorsiflexing and inverting the foot. It also allows the ankle to be inverted, giving the horizontal movement of the ankle, which allows a specific cushion if the ankle rolls.

Iliopsoas The iliopsoas is a group muscle formed by three muscles (**psoas major**, **psoas minor** and **iliac**). It is responsible for hip flexion, and flexion of the

14

lumbar spine.

Erector spinae The erector spinae is a set of muscles that straighten and rotate the back.

For a straightforward reading of tables and figures later presented in this document, from this point of the text, we will name the muscle groups as presented in Table 2.1.

Table 2.1: Muscle group labels.

Muscle group	Label
Quadriceps	QUAD
Hamstrings	HAMS
Gluteus maximus	GLUT
Gastrocnemius	GAST
Tibialis anterior	TA
Iliopsoas	ILIOP
Erector spinae	ERECTOR
Calf	CALF
Soleus	SOLEUS
Biceps femoris	BICFEM
Rectus femoris	RECFEM
Vastus lateralis	VASTLAT

2.1.4   Biomechanical aspects of walking

Bipedal walking is an essential characteristic of human locomotion. Before understanding complex gait models, the reader should understand some principles of posture and stability. A classical approach to modulate posture is anatomically defining body segments positions or functional and anatomical information from segments and how its musculoskeletal structures work to support distal segments. In addition to these classical approaches, (POPOVIĆ; SINKJÆR, 2000) also discussed the body capacity to anticipate perturbations during the movement. The first and most important function in posture stability is to build up the body against gravity. A second important function is making an interface between the environment and the body. (POPOVIĆ; SINKJÆR, 2000) presented more detailed information about the biomechanical aspects of walking.

Posture follows a hierarchical model with two levels of control. The first level relates to body segments positions, and the second, to kinematics and force. The nervous system takes advantage of our natural biomechanical constraints to coordinate and control the musculoskeletal system. During standing, for example, gravity, ground

reactions forces and swaying inertial forces are in equilibrium. The result gravity force acts on the **center of mass** (CoM) and maintaining posture is a process of continuous oscillating the body around the stability position. The CNS continually adjusts the relative position of segments to prevent falling, controlling muscles excitation per dynamic equilibrium.

All these basic stability concepts increase complexity during bipedal walking. When walking, our primary goal is moving forward towards a location at the desired speed. For this, humans tend to perform repeated movements that use the least amount of energy and causes the least discomfort due to pain or walking limitations. For research purposes, gait cycle is classified based on what happens to each foot. By observing just one leg, the cycle contains two distinct phases: stance and swing. The stance period occurs when the foot is on the ground, which comprises about 60% of the walking cycle. And the swing happens when the foot is off ground moving forward.

The following explanation organizes gait movements with detailed classifications of gait divide stance and swing into specific phases. (POPOVIĆ; SINKJÆR, 2000) recognized four support phase: first double support phase (DSP), first single support phase (SSP), second DSP and second SSP (Figure 2.4). The first DSP, first SSP and second DSP are the stance phases, while the second SSP is the swing phase.

The gait description begins when the heel first touches the ground (**right heel contact (RHC)**) to start the first DSP. The hip flexes, and the knee fully extends. Several muscles allows flexion and extension of joints, tibialis anterior is responsible for plantar flexion, quadriceps for knee and hip extension, hamstrings for ankle flexion, and rectus femoris for hip flexion.

The single-limb stance starts when the left toe moves out (**left toe-off, LTO**), followed by the right foot on the ground in a flat position (**right foot-flat, RFF**). The main purpose of the early flat stage is to allow the foot to serve as the shock absorber, decreasing body weight force landing on the foot. The hip moves slowly into extension, caused by *adductor magnus* and gluteus maximus muscles.

Subsequently, in the **mid-stance**, the leading leg hits the ground, and muscles work to manage the force passing through a single support leg phase (SSP), i.e., the right leg propels forward. Quadriceps keeps the leg extended, and gluteus maximus, *medius* and *tensor fascia lata* abduct the lower limb, keeping the pelvis leveled. Next, the left heel hits the ground (**left heel contact, (LHC)**). The result forces pass in front of the knee and acts to extend the joint. The biarticular gastrocnemius prevent hyperextension of the knee.

Right toe-off (RTO) starts the second SSP, i.e., the swing phase right after. Hamstrings extend the leg at the hip, quadriceps maintains the extended position of

the knee, and the posterior compartment of the leg plantarflexes the ankle.

Finally, the raised leg is propelled forward in the **swing phase**. In early swing, the hip extends and then flexes due to iliopsoas contraction, resisting gravity as it tries to pull the leg down with the **left foot flatted (LFF)**. In mid-swing, hip flexes and then extend due *sartorius* contraction, causing also the **left heel-off (LHO)**. The knee extension is caused by the quadriceps, positioning the right foot for landing. Finally, in late swing, the heel prepares for landing with hip flexion, a locked extension of the knee and a neutral position of the ankle. When the right heel hits the ground again (RHC), the whole cycle repeats.
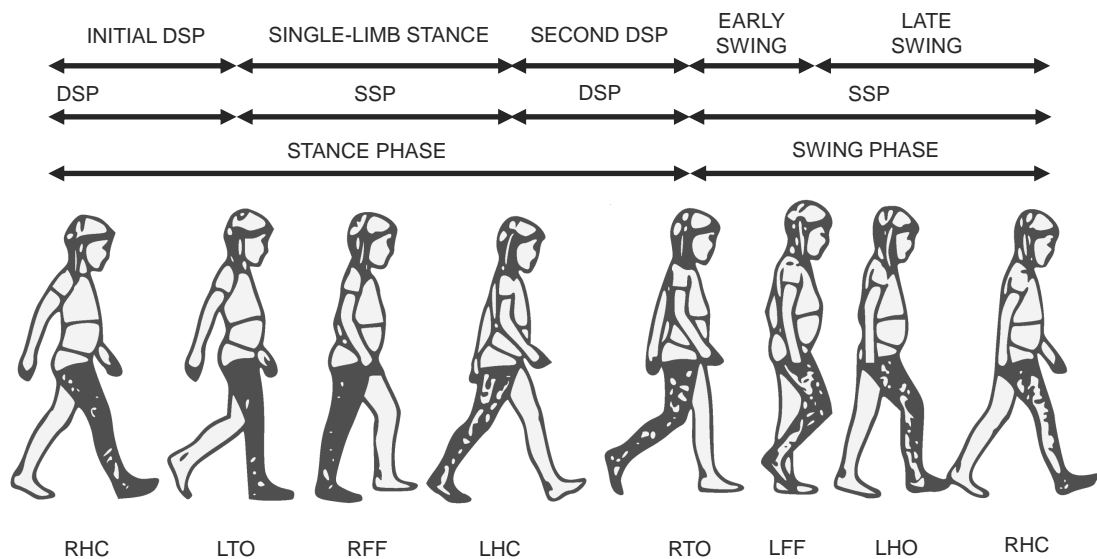
Figure 2.4: Phases of the gait cycle. DSP - Double Support Phase, SSP - Single Support Phase, RHC - Right Heel Contact, LTO - Left Toe-Off, RFF - Right foot-Flat, LHC - Left Heel Contact, RTO - Right Toe-Off, LFF - Left Foot-Flat, LHO - Left Heel-Off.

Source: adapted from (POPOVIĆ; SINKJÆR, 2000).

2.1.5 Biomechanical aspects of cycling

Cycling remains the primary means of transportation in many countries (e.g., Germany and the Netherlands) and, as a recreational and competitive sport, it continues to grow increasingly popular. As a rehabilitation exercise, cycling is a relatively low impact activity that requires both aerobic and anaerobic power (FARIA; PARKER; FARIA, 2005a; FARIA; PARKER; FARIA, 2005b). Ergometers are used in rehabilitation to restore range of motion, muscular strength, and cardiovascular fitness. There are two types of ergometers: **upright** (the seat and crank spindle are aligned nearly vertically) and **recumbent** (the seat and crank spindle are aligned nearly horizontally). Recum-

bent ergometers also characterize by large seats with backrests to provide support for the upper body and are low to the ground, permitting access for wheelchair users and individuals with mobility impairments (LOPES; ALOUCHE; HAKANSSON, 2014). Previous work found no statistically significant differences in the electromyography (EMG) activity of the primary muscles for cycling (rectus femoris, semitendinosus, tibialis anterior, and medial gastrocnemius) between standard recumbent and upright ergometers (LOPES; ALOUCHE; HAKANSSON, 2014).

To each foot, there are two main phases of the pedal cycle: the **power phase** and the **recovery phase** (TIMMER, 1991). The power phase corresponds to the period when the cyclist pushes the pedal to propel the bike forward. The recovery phase is a more passive phase, in which cyclists do not contract all muscles at higher power. The phases are symmetrical; therefore, when the right foot is at the recovery phase, the left foot is at the power phase. Many factors influence muscle activity during cyclings, such as height, positioning of the feet on the pedals, cadence, workload, and rider experience (JORGE; HULL, 1986). In general, the muscles common to this exercise are the quadriceps, hamstrings, tibialis anterior, iliopsoas, gluteus maximus, and the gastrocnemius. We will present the most common description of the roles of lower limb muscles in cycling. In these scenarios, the individuals are high-performance cyclists riding upright ergometers (JORGE; HULL, 1986; TIMMER, 1991; FARIA; PARKER; FARIA, 2005b).

Figure 2.5 illustrates the anatomy of the cycling movement for the following description. The initiation of the pedal cycle starts with the gluteus maximus (12 o'clock), taking the hip (A) from a flexed position through the power phase to an extended position. Then, at approximately 3 o'clock, the quadriceps (B) starts extending the knee — the quadriceps work with the gluteus maximus producing the highest amount of torque in cycling. The primary role of hamstrings (E) is to assist the knee flexion up through the back part of the pedal stroke, and also to assist hip extension.

At the lower leg, the gastrocnemius (C) and tibialis anterior (D) muscles do not add much power; however, it stabilizes the lower leg to enable an efficient transition of the force generated by the upper leg to the pedal. The tibialis anterior (D) dorsiflexes the foot, while the gastrocnemius plantarflexes the food and flexes the knee. The iliopsoas (F) assists the hip flexion.

2.2 PATHOLOGIES

In this research, we focus on pathologies that cause loss of lower limbs motor skills. Depending on the cause and intensity, different bodily functions may be affected (e.g., weakness, partial or total paralysis), therefore different symptoms may occur.
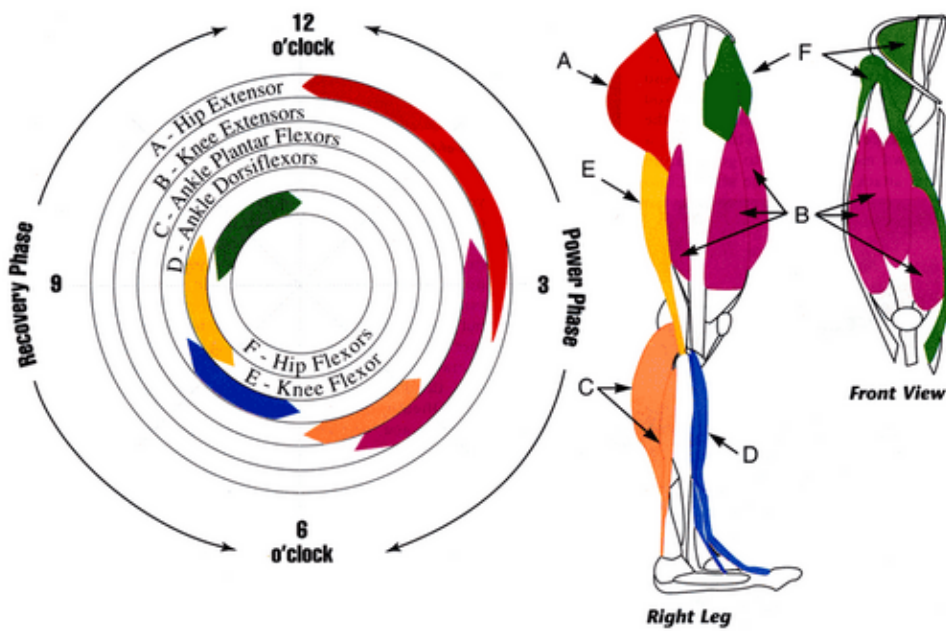
Figure 2.5: Anatomy of cycling movement. The figure illustrates the following muscles in both power and recovery phases: A - quadriceps, B - gluteus maximus, C - gastrocnemius, D - tibialis anterior, E - hamstrings and F - iliopsoas.

Source: from (Nikki, 2014).

The following sections summarize some leading causes of lower limbs motor skill loss (Section 2.2.1) and a few gait pathologies (Section 2.2.2). More detailed information about these pathologies can be found in (POPOVIĆ; SINKJÆR, 2000), and in public information provided by their specific organizations or associations (e.g., World Stroke Organization (WSO)[1] and American Spinal Cord Injury Association (ASIA)[2]).

2.2.1 Main causes

The category of neurological disease traditionally separates clinical rehabilitation aiming to improve motor function. Parkinson disease, cerebrovascular infarction (stroke) and spinal cord injury (SCI) have remained the top causes of partial or total loss of motor function. We only briefly describe **stroke** (Section 2.2.1.1) and **SCI** (Section 2.2.1.2), considering out our thesis outline, in which we focus on rehabilitation solutions for populations that suffered neural damages.

---

[1]   World Stroke Organization: http://www.world-stroke.org/
[2]   American Spinal Cord Injury Association: http://asia-spinalinjury.org/

2.2.1.1 Cerebrovascular infarction (stroke)

Stroke is one of the leading medical problems, remaining the principal cause of disability worldwide. It happens when a part of the brain is deprived of oxygen, ending in cell death, which can cause different sequelae. There are several risk factors causing stroke: high blood pressure, tobacco smoking, obesity, high blood cholesterol and diabetes mellitus. There are two main types of stroke: **hemorrhagic**, due to aneurysm burst or a weakened blood vessel leak, and **ischemic**, due to lack of blood flow by a blood clot. A hemorrhagic stroke is caused by bleeding either directly into the brain or into the space surrounding the brain, which may occur due to a brain aneurysm. Blockage of a blood vessel typically causes an ischemic stroke.

Abilities controlled by that area of the brain (e.g., muscle control) are lost when brain cells die. How a person is affected depends on where the stroke occurs and how much the brain is damaged. Signs and symptoms include the inability to move or feel on one side of the body, problems understanding or speaking or loss of vision to one side. The World Stroke Organization provides reports (e.g., (The Lancet, 2011)) and a global set of stroke guidelines to reduce the global burden of stroke.

2.2.1.2 Spinal cord injury (SCI)

The spinal cord is a bundle of nerves that carry signals through the brain to the body. When a spinal cord is damaged, and these signals are disrupted, this may cause temporary or permanent changes in muscles function. These changes may appear as loss of sensation or voluntary muscles movements. Injuries can occur at any level of the spinal cord and can be classified as a clinically **complete** injury, a total loss of sensation and muscle function, or a clinically **incomplete**, meaning some nervous signals are preserved. These remained signals may facilitate rehabilitation. Besides, depending on location and severity of damage, the symptoms vary widely. Therefore, the prognosis ranges from full recovery to permanent tetraplegia.

In most cases, the damage results from physical trauma such as car accidents, falls, gunshots, or sports injuries. However, it can also result from non-traumatic causes such as infection, insufficient blood flow, and tumors. At each level of the spinal cord, spinal nerves branch off to innervate a specific part of the body. The American Spinal Injury Association (ASIA) defined international standards for neurological classification of spinal cord injury (ISNCSCI). The section of the spinal cord that was damaged corresponds to the spinal nerves at that level and bellow. Lesions can be cervical (C1-C8), thoracic (T1-T12), lumbar (L1-L5), or sacral (S1-S5), as illustrated in Figure 2.6.

SCI is also classified by the degree of impairment, based on neurological responses and motor impairments. Muscle strength scores on a scale of 0-5, the sensation
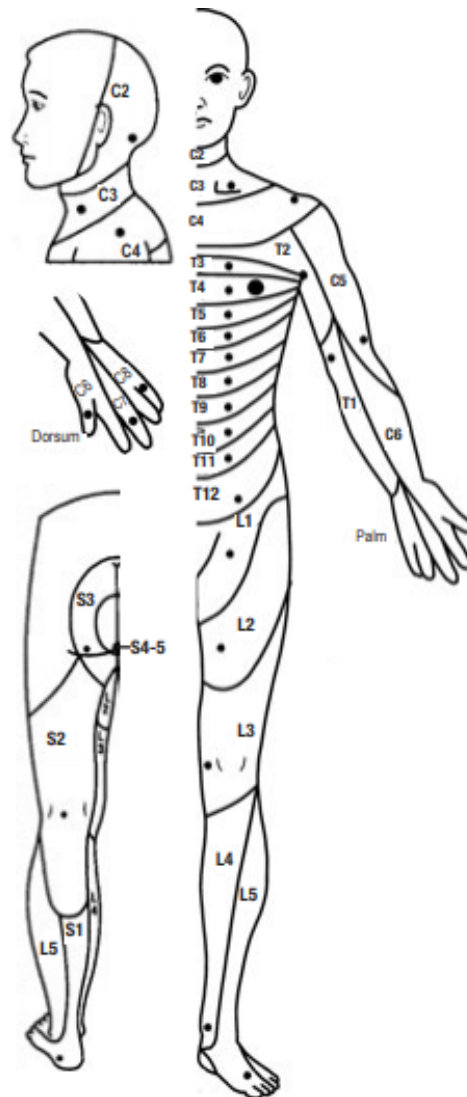
Figure 2.6: Illustration of the international standards for neurological classification of spinal cord injury (ISNCSCI) defined by the American Spinal Injury Association (ASIA). The black dots illustrates the key sensory points for diagnosis.

Source: Digital Repository of ASIA available in the worksheet accessed in April 2018.

is graded on a scale of 0-2 (0 is no sensation, 1 is altered or decreased sensation, and 2 is full sensation) (KIRSHBLUM et al., 2011).

Along with motor difficulties, other complications can occur in short or long term after injuries, such as muscle atrophy, pressure sores, infections, and respiratory problems. Later treatment usually includes medication and rehabilitation therapy. Mobility aids and assistive devices may help to perform activities of the daily life (ADLs).

2.2.2 Gait pathologies

As a contrast of total natural control of movements (Section 2.1.4), pathological motor conditions may include several symptoms, such as balance problems, decreasing in movement precision, muscle fatigue, lack of coordination and sensory deficits. (POPOVIĆ; SINKJÆR, 2000) classified some of these conditions as:

Hemiparesis A weakness of the entire left or right side of the body. Usually, it happens on the side of the body opposite the side of the brain that was damaged.

Hemiplegic Gait A complete paralysis of half of the body. The upper limb is in a flexed position, adducted and internally rotated at the shoulder. The lower limb is internally rotated, knee extended and the ankle inverted and plantarflexed. Usually, the gait is slow with circumduction or hip hitching of the affected limb to aid floor clearance. Hemiplegia can also lead to the pusher syndrome (clinical disorder in which patients actively push their weight to the hemiparetic side).

Diplegic Gait A spasticity in the lower half of the leg resulting in plantarflexed ankles presenting in tiptoe walking and often toe dragging. Excessive hip and knee flexion are required to overcome this.

Parkinsonian Gait Often associated with Parkinson's disease. There is joints rigidity that results in reduced arm swing for balance. A stooped posture and flexed knees are a common presentation. There may be occurrences of freezing or short rapid bursts of steps.

Ataxic Gait Uncoordinated steps with a wide base of support and staggering and variable foot placement, usually associated with cerebellar disturbances. They present with high steps and slapping of feet on the floor to gain some sensory feedback.

Neuropathic Gaits High stepping gait to gain floor clearance often due to a weakness or paralysis that limits the patient ability to raise the front part of their foot (foot drop).

2.3 RESTORATION OF LOWER LIMBS MOVEMENTS

Unfortunately, medical management and rehabilitation engineering are unable to reverse pathologies presented in Section 2.2. Therefore, much has been done to improve health and restore functions. The investigation of new rehabilitation technologies and treatments has received much attention, including the integrated, neuroscience-based research leading to an improved rehabilitation service. Neurorehabilitation com-

prises methods and technologies for maximizing the efficiency of preserved neuro-muscular structures in a human with motor disability. (POPOVIĆ; SINKJÆR, 2000) based the neurorehabilitation on four elements: (1) assessing the difference between the motor-performance of humans without any disability and humans with some disability; (2) designing rehabilitation methods aiming to maximize the use of the preserved neuromusculoskeletal system; (3) assessing the contributions that this rehabilitation is functioning and improving the quality of life; and (4) revising the rehabilitation accordingly.

One of the **limitations** of rehabilitation technologies and treatments for walking retraining remains the full weight bearing conditions, balance, and stepping. The patient uses parallel bars and walking aids to alleviate the load on the legs while they maintain balance during complex gait movements to generate a step. Furthermore, although standing is a prerequisite for walking, it is essential to separate rehabilitation techniques between these movements. Standing provides medical benefits to the human body by itself and is distinct depending on the type of gait impairment. In principle, paretic subjects can potentially stand with no arms, while paralyzed subjects need some extra joints fixation.

Paralyzed subjects may improve walking capacity mainly by augmenting hip flexion, knee extension, and balance on a treadmill training. Moreover, this rehabilitation enhances muscle strength and enhances cardio-respiratory fitness. Therefore spastic paraplegic subjects with different degrees of paralysis can benefit from this rehabilitation. Individuals with complete paralysis in one limb with an also improve walking after weeks of training. (POPOVIĆ; SINKJÆR, 2000) presented more detailed information about this restoration of lower limbs movements concepts.

A crucial aspect of rehabilitation is **repetitive training**, which led to the development of more advanced mechanized equipment, e.g., treadmills and active orthoses. Some of this equipment provide body relief while other provide the movement itself by some actuation. Another technology improvement for the balance challenge is sensory feedback to decrease the risk of instability leading to falls, such as special instruments measuring gait temporal and distance parameters, walkers and auditory feedback. Sections 2.3.1, 2.3.2 and 2.3.3 describe some instruments that can be used to substitute or augment motor and sensory modalities.

2.3.1 Functional electrical stimulation (FES)

Some researchers and physicians also refer to functional electrical stimulation (FES) as functional neuromuscular stimulation (FNS) or neuromuscular electrical stimulation (NMES). In the rehabilitation context, the term most commonly used is FES. The NMES term is often used just for just activation, e.g., in an isometric exercise.

For a straightforward reading, we will use the term FES for an overall application. In addition to rehabilitation, we may also include FES include in the context of neuroprostheses, a series of devices that can substitute a motor ability damaged by an injury (POPOVIĆ; SINKJÆR, 2000). These devices increase independence by restoring the person ability to perform a functional movement in the absence of external adaptive modifications, making it more transparent to the user.

FES activates motoneurons by stimulating nerve fibers or provides sensory feedback by stimulating sensory nerve fibers. As a motor activator, the stimulator delivers a monopolar or bipolar signal configuration. In monopolar, a single active electrode is positioned near the muscle while a common electrode is positioned relatively distant to the stimulated structure, yet somewhere along the neural pathways to the CNS. In bipolar, two electrodes are positioned at the muscle to be stimulated, and the electrical circuit is closed.

The stimulator delivers trains of electrical charge pulses, modeled with a relatively simple electric circuit: generator, electrodes, and tissue. The neuro-muscular structure receives an electrical charge determined by **amplitude** (current) and **stimulus pulses duration** (pulse width), generator output impedance, and electrodes impedance. Current controlled stimulators usually are more efficient to control the charge transmitted for different impedances (POPOVIĆ; SINKJÆR, 2000). However, the voltage controlled stimulator is safer, especially when something causes electrodes displacement. In this case, there is a current density increase and the patient may suffer a skin burn. Usually, for safety, commercial stimulators deliver constant current, regardless of changes in the system.

(POPOVIĆ; SINKJÆR, 2000) presents some electrodes and stimulus waveforms that excite the tissue. However, fundamental physiological properties favor one over the other. The selected waveform is generally rectangular and may be monophasic or biphasic. Biphasic stimulus (Figure 2.7) is recommended because it is more comfortable and with implanted electrodes the potential for tissue damage is lower. Either amplitude modulation or pulse width modulation may govern the level of muscle recruitment. The threshold of fibers excitation is proportional to the diameter of the tissue, and since the nerve is a mixture of afferent and efferent fibers with a spectrum of fiber diameters, short pulses of constant amplitude will excite large afferent and efferent fibers. Longer pulses may also stimulate smaller fibers, including afferent frequently carrying information of other stimuli, and sometimes may be painful to the subject.

Motor response strength is regulated by the number of active motor nerve fibers and the action potentials trigger rate (cf. Section 2.1.2.2). During voluntary control, these mechanisms are called recruitment and temporal summation, respectively. When
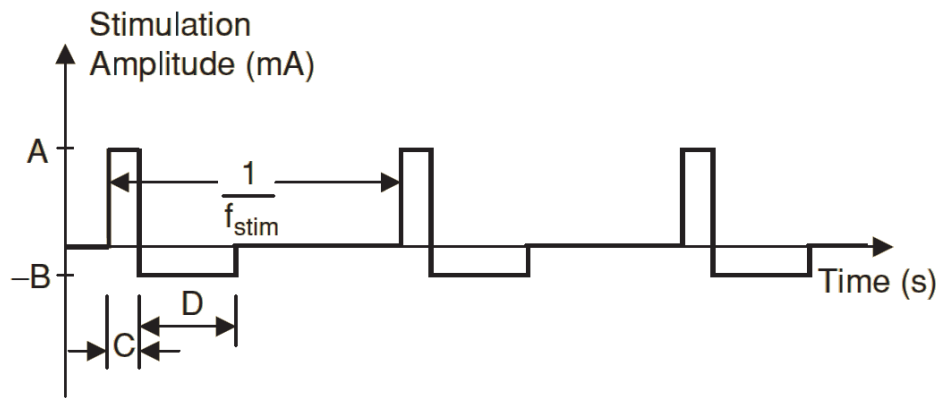
Figure 2.7: Stimulation pulse train. Example of a typical stimulation waveform used for transcutaneous FES: a biphasic square-wave pulse train with a frequency of 20–40 Hz, an amplitude of 0–120 mA, and a pulse duration of 0–300 μs.

Source: from (POPOVIĆ; SINKJÆR, 2000).

the stimulus is sufficiently large, an action potential will be provoked in the nerve and will propagate in both directions (up and down). The minimum stimulus level to achieve the action potential response is known as a threshold. A single muscle action potential generates a twitch response in all muscle fibers innervated by the same nerve. The magnitude and time course of the twitch contraction depends on the number and type of muscle fibers in the motor unit and recent stimulation history (e.g., potentiation, muscle fatigue). FES systems activate several motor units, regulated by the electrical charge injected (integral of the current over the duration of the stimulus). In the rectangular pattern, the electrical charge per pulse is calculated by multiplying the stimulus pulse amplitude and the pulse duration.

In a **voluntary** contraction, the recruitment is fixed: first slow then faster fiber units. In an **artificial stimulation**, this recruitment order inverts because larger faster fibers are more easily excited compared to small slow fibers (cf. Section 2.1.2.1). Also, stimulus pulses applied in rapid succession to the nerve produce a mechanically additive effect of the twitch response. Lower frequencies are unfused, and variations of the muscle force are noticeable. As mechanical responses sum with increasing frequency, the forced variability ceases, and the force increases.

Compared to surface electrodes, implanted electrodes improve stability, forward progression of step with more delicate control of movements during walking (KOBE-TIC; MARSOLAIS, 1994). It also reduces donning time and provide better repeatability. However, for clinical rehabilitation exercises, surface electrodes are more straightforward to handle.

2.3.1.1 Electromyography (EMG) and FES

Electromyography is a technique for monitoring the electrical activity of excitable membranes in muscle cells, representing the action potentials triggered by reading the electrical voltage over time (voltage versus time) (KAMEN; GABRIEL, 2010). The electromyographic signal (EMG), or electromyogram, is the algebraic sum of all signals detected within the range of the electrodes and may be affected by muscular, anatomic and physiologic properties, as well as by the control of the peripheral nervous system and the instrumentation used for signal acquisition. As an alternative to the mechanical control systems, several authors have proposed to use the EMG-signal for controlling neural prostheses with FES (e.g., (SCHAUER et al., 2016) and (WANG et al., 2018)).

During stimulation, two types of artifacts usually exist in the EMG-signal, as illustrated in Figure 2.8, the stimulation artifacts, and muscle responses (DURFEE; DENNERLEIN, 1989). After a stimulation pulse, a typical EMG response starts with the stimulation artifact, a spike lasting between less than a millisecond and a couple of milliseconds, followed by an excitation curve, called M-wave. The latter is formed by the synchronous muscle action potentials (MAP) of all motor units that have been fired by the stimulation pulse. The magnitude of the superposition of MAPs caused by volitional muscle activation is often smaller than the artifact and M-wave (SENNELS et al., 1997).

2.3.2 Passive orthoses

Orthoses are the rehabilitation devices that straighten, correct, protect, support, or prevent musculoskeletal deformities. The orthosis is a functional substitute (augmentation), in contrast to the prosthesis that is both a morphological and functional replacement of the body part and its function. There are several challenges applying orthoses, such as interface, weight, size, and control that preserves the user's natural mechanisms. Therefore, the orthosis must be robust, yet light and cosmetically attractive.

A lower-limb orthosis is an external device applied to a lower-body segment to interfere in function by controlling motion. (POPOVIĆ; SINKJÆR, 2000) classified orthoses based on which joints are encumbered. An ankle-foot-orthosis (AFO) encumbers the ankle and foot, which are externally applied and intended to control position and motion of the ankle, compensate for weakness, or correct deformities. AFOs can be used to support weak limbs or to position a limb with contracted muscles into a more normal position. They are also used to immobilize the ankle and lower leg in the presence of arthritis or fracture, and to correct foot drop. On the other hand, a knee-ankle-foot-orthosis (KAFO) provides stabilization of the knee along with stabilization of the ankle and foot. Motions at all three of these lower limb areas are affected by
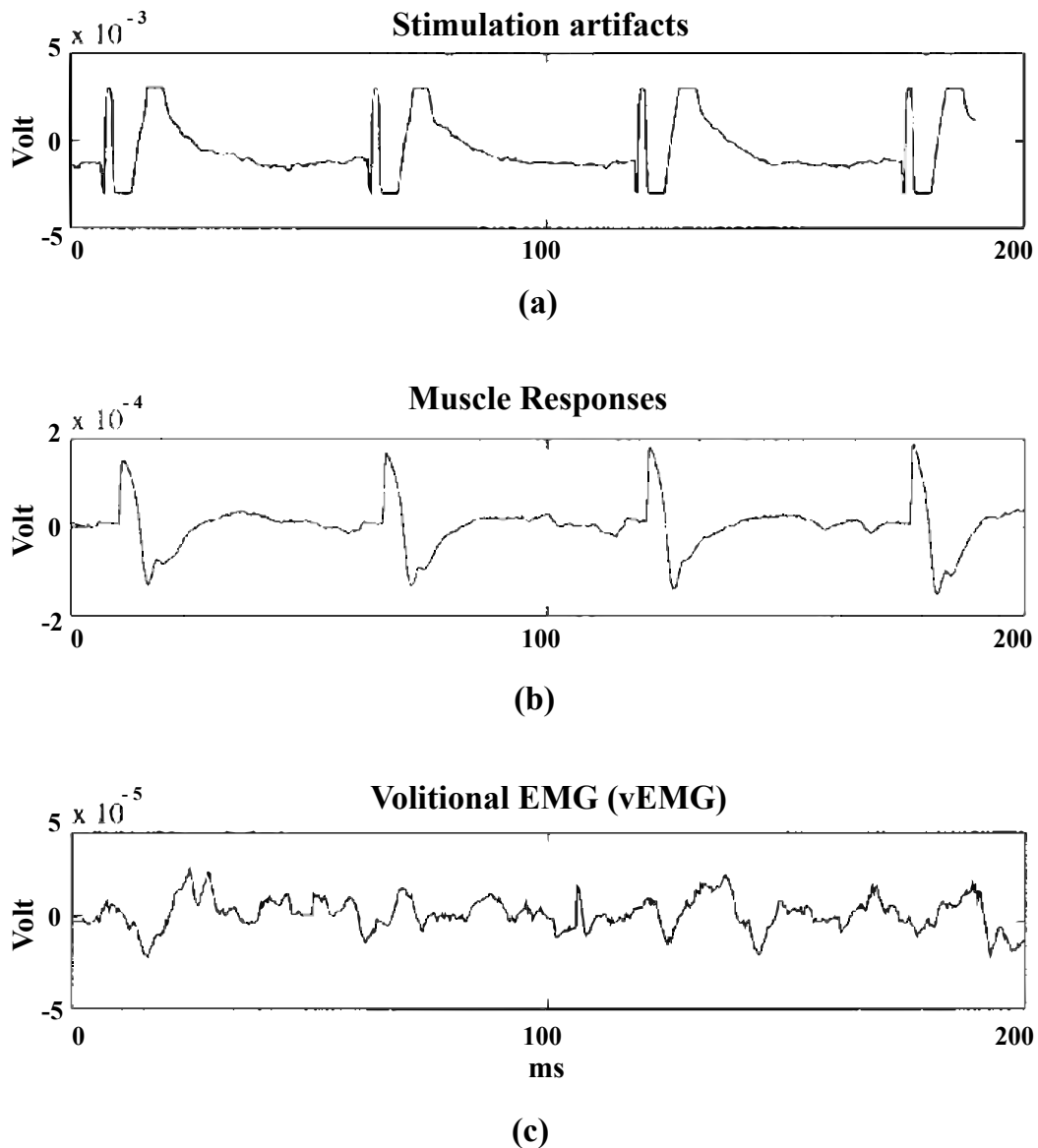
Figure 2.8: Typical time courses of the signal components in EMG-recordings from the wrist extensor muscles of a tetraplegic individual presented in (SENNELS et al., 1997). (a) EMG-recording during 20 Hz stimulation of the wrist extensor muscles with no volitional muscle activity. Stimulation artifacts dominate this signal. The amplifier is saturated and does not fully recover during the interpulse interval. (b) Blanked EMG-recording during 20 Hz stimulation of the wrist extensor muscles with no volitional activity. Muscle responses dominate this signal. (c) EMG from the volitional activated wrist extensor muscles with no stimulation applied.

Source: from (SENNELS et al., 1997).

a KAFO and can include stopping, limiting, or assisting. A KAFO provides stabilization of the knee along with stabilization of the ankle and foot. Motions at all three of these lower limb areas are affected by a KAFO and can include stopping, limiting, or assisting motions.

Often a simple addition of passive mechanisms improves outcomes among patients. The **passive orthosis** reduces muscle fatigue effects, lowering the gait metabolic cost by providing a more natural and stable gait. It reduces the load on a user's arms and decreases the stimulation duty cycle of FES, which achieves better control of movements during training (ALIBEJI; KIRSCH; SHARMA, 2017).

2.3.3 Active orthoses

An **active orthosis** can be used to control some degrees of freedom (e.g., the knee cage provides stability in the lateral direction and allows flexion and extension). Considering actuator energy, (YOUNG; FERRIS, 2016) divided active orthoses into two categories: **full** and **semi-active**. A full-active orthosis depends on portable power sources and actuators to convert electric, pneumatic or hydraulic energy into mechanical work, inserting energy in lower limbs joints. Alternatively, semi-active orthoses use passive elements, such as springs, dampers or ambulatorial assistive devices, to improve the energy stored during the movement.

Another category that (YOUNG; FERRIS, 2016) provides considers intended use: **strength increasing**, **assistive devices** and **rehabilitation**. The first category is a human performance increase of strength, endurance and other physical capabilities by individuals without disability. The second category considers assistive devices for individuals with disabilities. Assistive robotic orthoses allow users to complete movements they could not achieve on their own. The third category is for rehabilitation only. These devices can assist, resist, or perturb user's movements to improve therapeutic exercises. Active orthosis increase activity during rehabilitation (e.g., stationary treadmill-based robots as the Lokomat (HIDLER, 2004)). These devices provide for patients enough safety, support and balance to walk.

3 RELATED WORK

Motor disabilities have devastating effects on the quality of life and affect millions worldwide. Hence, there is an immediate urge to improve rehabilitation techniques for patients to achieve the best possible functional outcome. In general, the repetitive and intensive movement of physiotherapy provides real physiological benefits (NENE; HERMENS; ZILVOLD, 1996). These benefits include prevention of osteoporosis, reduced incidence of fractures, reduced incidence of urinary calcinosis, reduced spasticity, prevention of pressure ulcers, and prevention of heterotopic ossification. This thesis focuses on advances in physiotherapy techniques and equipment for lower limbs rehabilitation using functional electrical stimulation (FES).

Section 2.3.1 already introduced FES as a widely used technique for driving movements of muscles in rehabilitation. Moreover, extensive research work has been carried out for rehabilitation enhance. For instance, pathologies that cause a lack of heel strike and decrease floor clearance (i.e., foot drop), FES has been used to this correction in cases of hemiplegia for over fifty years (POPOVIC, 2008; CORR, 2006). Furthermore, exercises assisted by FES provide rehabilitation advantages, such as muscles strength, prevention of atrophy, balance, regulation of spasticity, cardiovascular fitness, and improvement of function.

This chapter presents the state of the art of some features of control of FES. Although some work focuses on both individuals with SCI or hemiplegia, we delimited our studies on exercises used for lower limb rehabilitation for subjects with SCI (ASIA A or B). Therefore, the mechanical and electrical control system is responsible for the entire lower joints movements, which makes the controller an essential feature. First, we present the state of the art combination between electromyography (EMG) and FES (Section 3.1). Second, we present the studies of FES controllers (Section 3.2), specifically for knee trajectory. At last, Section 3.3 present studies on energy storage devices to support functional movements, focusing on FES cycling.

3.1 ELECTROMYOGRAPHY (EMG) AND FES

Often the use of FES is still possible in the rehabilitation of individuals who have suffered from a complete SCI. FES control implementations proposed in the literature are numerous; however, it is still a challenge to separate the movement generated by muscle contraction evoked by the stimulation and movement generated by external disturbances (e.g., spasms or a physiotherapist aid). Several authors proposed the use of EMG for controlling neural prostheses (e.g., (SENNELS et al., 1997; SCHAUER et

al., 2016)). In our literature review, we look for works that combined surface EMG and FES with electrodes at the group muscles (Section 3.1.1); therefore excluding articles based on another limb without disabilities (e.g., (SEHNDKAR et al., 2017)).

A typical EMG response to FES starts with the stimulation artifact due to the electric field in the tissue and skin generated by the stimulation current (DURFEE; DENNERLEIN, 1989). After the stimulation, the muscle response (M-wave) appears as many motor units respond to the pulses. Early work mostly adapted the EMG hardware to reduce artifacts (DURFEE; DENNERLEIN, 1989; TEPAVAC; NIKOLIC, 1992; MIZRAHI et al., 1994), shutting down the EMG amplifier while the stimulator sends the pulse. A typical application of these early works is the estimation of fatigue, (DURFEE; DENNERLEIN, 1989; MIZRAHI et al., 1994) compared the EMG evoked by stimulation (eEMG) with the torque generated by the quadriceps stimulation in isometric exercises. As for other exercises, such as cycling, the acquirement of joint torque is more complicated to obtain. Therefore, (Jia-Jin Chen et al., 1995) calculated the estimated joint torque to compare with the eEMG.

Naturally, researchers also applied this type of signal processing for incomplete SCI and stroke patients, which may still have some residual movements. To our knowledge, (SENNELS et al., 1997) was the first work that created algorithms to separate the eEMG from the voluntary EMG (vEMG) to enhance grasping. The adaptive filters successfully selected the M-wave, allowing this separation; however, it was computationally demanding since it involves complex processes, such as QR decomposition and forward/backward substitution. Moreover, the digital filtering also removed components of the M-wave, as the spectrum may overlap (O'KEEFFE et al., 2001).

3.1.1 State of the art

In the presented work, we intend to evaluate the software algorithms that combine EMG and FES on the same limb. To find previous research in this signal processing topic, we investigated the most recent papers ($\leq$ 20 years) published in PubMed and IEEE databases using the following combination of terms within the title and abstract:

- ((electromyography) OR (EMG)) AND ((stimulation) OR (FES)),

- ((electromyography) OR (EMG)) AND ((artifact detection)) .

After rejecting duplicate articles and carefully reading the title, keywords, and abstract, we identified three features that related to our work:

- if the artifact detection was done via hardware or software,

- if the measurements were done in the upper or lower limbs,

- if the measurements were from subjects with or without disability.

From Tables 3.1 and 3.2, we observe that most works until 2010 used hardware solutions to remove artifacts and syncronize FES and EMG. For real-time applications, (WIDJAJA et al., 2009) considered that hardware blanking performed better, because of its faster response when compared to software blanking. However, the hardware solution fixed time intervals using potentiometers, which may lead to clipping or blanking out of subsequent M-waves. The hardware approach also fails to take into account the dynamic effect of stimulation, whereby the tail of the stimulus artifact may survive the blanking pulse. Section 3.1.1.1 presents these hardware solutions.

Nowadays, we can achieve higher software speeds; therefore, it seems that the tendency of the newest research is software blanking techniques, presented in Section 3.1.1.2.

3.1.1.1 Hardware blanking

In 2000, (PEASGOOD et al., 2000) described a blanking circuit for artifacts. They incorporated a blanking circuit where the gain was reduced to unity just before, during, and after the stimulation pulse. They found that the M-wave could breakthrough into the sampled signal at high stimulation levels.

Also using blanking filter to remove artifacts, (MANDRILE et al., 2003) focused on an extensive investigation of the effect of stimulation waveform, detection system, current amplitude, and distance of stimulation electrodes to EMG electrodes in the artifacts. The results indicated that artifact amplitude increases monotonically with the stimulation current and decreases when increasing the distance of the recording system from the stimulation electrode. Artifact amplitude depended on the stimulation waveform, interelectrode distance, and the spatial filter used for artifact detection.

After the first trials treating data offline to find volitional activity during grasping (BESIO et al., 1999), the group studied skin-electrodes impedance to decrease artifacts (BESIO; PRASAD, 2006). The work analyzed how electrode material, electrode size, skin preparation, and surface pressure affect the skin-to-electrode impedance. They developed a protocol as a guide for researchers to minimize impedance and artifacts in experimenting with electrodes. Works that obeyed this guide focused on electrocardiogram electrodes.

In 2013, (MURAOKA et al., 2013) developed a pocket-sized stimulator to estimate volitional movement. The device isolates the EMG signal when the stimulator generates pulses. However, ordinary users still find it difficult to operate the system because of the manual adjustments of the gain of the EMG-amplifier and the setting of the threshold voltage of the stimulation output.

Table 3.1: Summary of recent projects that used hardware solutions for artifact blanking.

System project	Upper or lower limbs	Subjects
(PEASGOOD et al., 2000)	Lower	1 without
(MANDRILE et al., 2003)	Upper	11 without
(BESIO; PRASAD, 2006)	Upper	20 without
(MURAOKA et al., 2013)	Upper	1 without

3.1.1.2 Software blanking

Researchers have modified different software approaches to extract EMG information. (O'KEEFFE et al., 2001) developed a two-stage peak detection algorithm that does not require estimation of the artifact shape or duration and does not require any external hardware synchronization. The results show artifacts removal of 95% to 100%, with EMG sampling higher than 4kHz to ensure optimum fidelity, and with careful electrode placement to avoid saturation of the artifacts.

In the context of assistive devices to suppress pathological tremor of the forearm using FES, (ZHANG; ANG, 2007) presented a signal processing technique to estimate sensing information to regulate FES. The first stage removes the artifacts using the blanking window, setting the EMG signal to zero during a fixed blanking window period. There is a compromise regarding the width of the blanking window. If the period is too long, it can ensure the complete elimination of artifacts, but the natural EMG will also be lost. If the period is too low, the artifacts remain at the signal. The ideal range for the blanking window width depends on the stimulation intensity and electrodes positioning. In the second stage, filters remove the M-wave and separate the tremor frequency from vEMG. Later, they implemented these algorithms in a real-time data acquisition system (WIDJAJA et al., 2009), with the same restriction of manually selecting the threshold for artifact detection.

In 2016, (SCHAUER et al., 2016) combined FES and EMG for gait therapy after stroke, demonstrating the feasibility of their real-time EMG filter algorithm to estimate vEMG. The estimation corresponded to the expected response for all subjects and walking styles (normal walking, emphasized push-off, emphasized dorsiflexion) at different stimulation levels ((sub)sensory, sensory, and motor). They searched for local maxima (peaks) in the signal with fixed thresholds.

Recently, (FANG et al., 2018) presented a real-time FES-induced torque estimation system based on EMG. Kalman filter and RNN are used online to identify and then predict torque output based on eEMG recordings only. The real-time FES-induced torque estimation system can contribute to personalizing quantitative evaluation of muscle response under FES, which is first useful for clinical diagnostics to estimate the exact mechanical response by using eEMG signal. In this work, they also used a fixed blanking window period for artifact detection.

Other works presented more sophisticated tools for software artifact detection (YOCHUM et al., 2014; QIU et al., 2015; PILKAR et al., 2017). These sophisticated methods provide effective results for artifact detection for one-channel EMG and FES systems; however, they still require a high computation effort, which limits the use in real-time scenarios in embedded systems. (YOCHUM et al., 2014) used continuous wavelet transforms to remove artifacts for both monophasic or biphasic stimulation pulses. Moreover, (QIU et al., 2015) designed an adaptive matched filter via genetic algorithm optimization to remove FES artifact and preserve volitional EMG (vEMG).

When exploring for methods more straightforward than wavelets or genetic algorithm optimization, (PILKAR et al., 2017) investigated the use of empirical mode decomposition (EMD) methods to remove the artifacts from EMG. By comparison, the EMD based decompositions are simpler to perform and do not need prior knowledge about signal properties such as artifact durations or instances as the data itself drive the methods. Hence, instead of trying to distinguish between the artifact and EMG frequencies and then filtering them, EMD algorithms separate the signal into the artifact and EMG components in a way that preserves the intrinsic properties of each. However, the work still requires further investigation into the eEMG and vEMG results, as some data at specific harmonic frequencies were lost (PILKAR et al., 2017).

3.2 FES KNEE TRAJECTORY CONTROLLERS

The majority of patients prefer FES for being more natural to use and provide augmented propulsion when compared to orthotic systems (NIGHTINGALE et al., 2007). During standing and walking, the activation paralyzed muscles can stabilize the body against collapse and provide power for forwarding progression with different FES configurations (CYBULSKI; PENN; JAEGER, 1984; NENE; HERMENS; ZILVOLD, 1996). For instance, (NENE; HERMENS; ZILVOLD, 1996) presented a configuration that uses up to 48 invasive electrodes channels on hips, knees, and ankles. In clinical rehabilitation scenarios, invasive electrodes are not usually viable, while noninvasive surface electrodes are unable to adequately recruit the hip flexors muscles (psoas major and iliacus muscle). Therefore, FES gait exercises usually recruit muscles for knee and/or ankles extension and/or flexion. This literature review looks

Table 3.2: Summary of recent projects that used software solutions for artifact blanking.

System project	Upper or lower limbs	Subjects
(O'KEEFFE et al., 2001)	Lower	10 without
(ZHANG; ANG, 2007)	Upper	1 without
(WIDJAJA et al., 2009)	Upper	1 without
(YOCHUM et al., 2014)	Upper	5 without
(QIU et al., 2015)	Lower	7 without
(SCHAUER et al., 2016)	Lower	4 without
(PILKAR et al., 2017)	Lower	6 without 1 SCI
(FANG et al., 2018)	Lower	3 without 3 SCI

for gait locomotion considering only the FES knee trajectory control and noninvasive surface electrodes (Section 3.2.1). Subsequently, we present a few aspects of hybrid neuroprostheses (HNP) (Section 3.2.2) at similar conditions.

3.2.1 FES-only

In 1989, (MCNEAL et al., 1989) described and tested the first described FES knee trajectory control on subjects with SCI. Using surface electrodes on quadriceps muscles, the authors found the input-output pairs (stimulation current and angles) and designed a feedforward controller to track a trajectory. They tested this controller on four subjects with SCI for eight weeks and found low errors along the weeks. The first closed-loop was described in (VELTINK, 1991) with tests on individuals without disability using a discrete-time proportional-integrator-derivative (PID) controller. Between each cycle, they changed the current based on the controller performance on the previous cycle.

Although the system is nonlinear, (QUINTERN; RIENER; RUPPRECHT, 1997) showed that it is possible to use the PID controller for knee tracking and isometric torque tracking on an volunteer with SCI using both antagonist muscles, hamstrings, and quadriceps. In this work, the authors also compared PID and PID combined with feedforward control and concluded that for the isometric control, the changes were not

relevant. However, the errors for the angle tracking were higher without feedforward control. Moreover, for the knee extension movement, there is a good agreement between the reference and the measured angle, and, for the knee flexion, the measured angle was always higher than the desired value.

In 1997, (Gwo-Ching Chang et al., 1997) presented the first neuro-PID, in which they trained a network to find possible input-output relationships. Using the neuro-PID, they improved the tracking error when compared to just PID or just neural. They addressed some limitations to the training; it must be representative of the whole space of possible input-output relationships; and the network depends on the accuracy of the modeled plant, the neural network approximation, and the variations with time and input of the plant dynamics. Therefore, it is necessary to implement neural controllers combined with other conventional control strategies, e.g., PID, and the control demands several trials.

In 2002, (FERRARIN et al., 2002) tested the first rehabilitation application; they used a PID controller to track the knee trajectory to assist an volunteer with SCI to stand up and sit down. The goal was to decrease the superior limb effort to perform these movements. The FES control decreased the stimulation required to maintain the standing posture, increased the stimulation strength in real-time when the knee starts to flex (i.e., prevents the fall), and slow down the sitting-down movement (i.e., smoother knee trajectory).

3.2.1.1 State of the art

To describe and compare the FES knee trajectory state of the art, we investigated the most recent papers (≤ 15 years) published in PubMed and IEEE databases using the following combination of terms within the title and abstract:

- ((Functional Electrical Stimulation OR FES) AND (knee) AND (trajectory).

After rejecting duplicate articles and carefully reading the title, keywords, and abstract, we identified works with more repercussion factors on FES control. Projects differ from the target population (e.g., SCI or hemiplegic), electrodes (e.g., surface and intramuscular), control (e.g., PID and RISE), among other features. As efforts and results differ from the type of experiment, we present the systems in order of experimental effort. Therefore, we first present projects that only evaluated HNPs in a simulation environment. (Table 3.3). Second and third, projects that developed and evaluated FES knee control on subjects without disability (Table 3.4) and subjects with disability (Table 3.5), respectively.

From state of the art, this project intends to recognize gaps in FES trajectory control. Therefore, Tables 3.3, 3.4 and 3.5 highlight the following characteristics:

- stimulated group muscles (Table 2.1 describes the labels used in this text),

- type of controller (e.g., PID only or PID with neural network), and

- number of different volunteers for experiments.

Table 3.3: Summary of recent projects that only evaluated FES knee trajectory control in a simulation environment.

System project	Muscles stimulated	Controller used
(MOHAMMED et al., 2005)	QUAD and HAMS	HOSM
(MOHAMMED; POIGNET; GUIRAUD, 2006)	QUAD and HAMS	MPC
(IBRAHIM et al., 2011)	QUAD	FLC
(BOUDVILLE et al., 2013a)	QUAD	PID
(BOUDVILLE et al., 2013b)	QUAD	FLC-GA
(QIU et al., 2014)	QUAD	PID-GA

Simulation projects showed strategies to control the amount of stimulation into a musculoskeletal knee joint model with one or two muscles for subjects with SCI. In 2005, (MOHAMMED et al., 2005) presented a state-space model of the knee with quadriceps and hamstrings. The study aimed to increase joint stiffness and force the model to behave as a first-order system dynamically. Due to the nonlinearity and the presence of a two-degree order system, they adopted a high order sliding mode controller (HOSM) to ensure robust control. Later, the group implemented the model predictive control (MPC) technique in a similar musculoskeletal knee joint model (MOHAMMED; POIGNET; GUIRAUD, 2006). They again concluded that the controller handled the multivariable nonlinear system, improving the tracking control. However, there was no comparison between these or with other controllers.

Other efforts concentrated on only quadriceps muscle during actuation of the knee joint (IBRAHIM et al., 2011; QIU et al., 2014). (IBRAHIM et al., 2011) implemented a cycle-to-cycle fuzzy logic controller (FLC) to compensate for the time dependency

Table 3.4: Summary of projects that evaluated FES knee trajectory control on subjects without disability.

System project	Muscles stimulated	Controller used	# subjects
(CHENG et al., 2009)	QUAD	Neural PID	5
(SHARMA et al., 2009)	QUAD	RISE	5
(DOWNEY et al., 2015; DOWNEY et al., 2017)	QUAD	RISE	4
(KAWAI; EJIRI; KAWAI, 2015; DOWNEY et al., 2017)	QUAD	Neural RISE	4
(BOUDVILLE et al., 2019)	QUAD	PID-GA	1

Table 3.5: Summary of projects that evaluated FES knee trajectory control on subjects with disability.

System project	Muscles stimulated	Controller used	# subjects
(PREVIDI et al., 2004)	QUAD	VRFT	1
(AJOUDANI; ERFANIAN, 2007)	QUAD	Neuro-SMC	3

of the system, with no comparison between other controllers. In contrast, (QIU et al., 2014) compared three-parameter optimization methods for the PID controller. In this work, the authors implemented (1) the PID based on backpropagation (BP) neural network, (2) the PID based on genetic algorithm (GA), and (3) the traditional Ziegler-Nichols method. The PID tuned by BP neural network presented lower errors, while the GA-PID, a lower delay (both strategies improved the traditional method).

Specifically for application with hemiplegic volunteers, (BOUDVILLE et al., 2013a; BOUDVILLE et al., 2013b) modeled and simulated the control of a structure in which the non-paretic leg may assist the paretic leg during knee tracking. The assistance may, consequently, improve tracking control and decrease fatigue as less stimulation is required. They first implemented a PID controller (BOUDVILLE et al., 2013a) and later an FLC controller (BOUDVILLE et al., 2013b), with no comparison between

them. Later, they developed and tested this equipment in one subject without disability (BOUDVILLE et al., 2019). The paper used particle swarm optimization (PSO) genetic algorithm (GA) as an optimizing strategy to determine the optimal PID controller parameters for the FES knee exercise. They compared the PID-PSO-GA system with the traditional PID, showing that PSO reduced the RMSE.

(SHARMA et al., 2009) implemented the nonlinear controller robust integral of the sign of the error (RISE) in people without disabilities. The controller did not require a muscle model, and they affirm that it yields asymptotic stability for a nonlinear muscle model in the presence of bounded nonlinear disturbances (e.g., spasticity, delays, fatigue). However, the authors did not present a comparison with other controllers. In 2009, (CHENG et al., 2009) combined the PID with a neural network to ensure robust control over a nonlinear system. The experiments used an FES system tuned by the radial basis function (RBF) neural network-based PID model. Results showed lower errors with the RBF neural network-based PID model when compared to the traditional Ziegler-Nichols tuning PID model. Further, the system adapted to time dependencies caused by FES.

We should note that not all projects aimed to develop and compare controllers. Some projects designed and compared new features or methods for the tracking control, such as asynchronous stimulation (DOWNEY et al., 2015; DOWNEY et al., 2017), and co-activation of antagonist muscles (KAWAI; EJIRI; KAWAI, 2015).

Switched stimulation is a method that uses multiple stimulation channels to segregate and switch between different sets of recruited motor units. They conducted experiments in six individuals without disability using the RISE controller. Compared to the standard set of electrodes, the developed controller yields longer durations of successful tracking (DOWNEY et al., 2017). Similar to the co-activation simulations from Table 3.3, (KAWAI; EJIRI; KAWAI, 2015) compared the results with and without co-activation of antagonist muscles. They noted that, with the co-activation, the overshoot decreases, probably due to the opposite force applied to the joint.

In (PREVIDI et al., 2004), the authors designed and tested the virtual reference feedback tuning (VRFT) on one subject with SCI. Their strategy avoided the modeling step, reducing the time required for controller design, and simplifying the rehabilitation protocol. They also affirmed that linear controllers are capable of FES tracking control when applied on a small range of knee joint angle. However, for large ranges, the nonlinear static mapping considerably improved the tracking performances. Moreover, (AJOUDANI; ERFANIAN, 2007) designed and tested a nonlinear controller in 3 subjects with SCI. The neural controller results, when compared to conventional sliding mode control (SMC), reduced the chattering effect while simultaneously decreased the tracking path error. Moreover, the experimental results demonstrated a rapid

convergence speed for trajectory tracking.

3.2.1.2 FES limitations

There are still limitations when we intend to control knee trajectories only using FES, primarily because of the accelerated muscle fatigue. Some of the controllers and features attempt to compensate it; however, results remain insufficient to enable achieving similar force when compared to the natural recruitment of muscle fibers. Additionally, when we consider the gait context, systems generally only provide stimulation for the sagittal plane, which can result in one foot crossing in front of the other, i.e., scissoring (FARRIS et al., 2009). Consequently, FES walking in paraplegia would require high levels of metabolic energy. Collapse is unacceptable in any viable gait restoration system; the user needs to maintain trunk stability via upper-body forces on an assistive device, such as a walker (KOBETIC et al., 2009).

Furthermore, for some pathological conditions, such as muscle atrophy and spasticity, the response to electrical stimulation is strongly altered. Time-varying behavior also occurs on neurologically intact subjects, particularly before proper training with FES. People without disabilities are instructed to relax their muscles as far as possible when using stimulation; however, they often voluntarily contract in reaction to FES, much disturbing total torque at the joint. All these complexities increase when using surface electrodes; it is hard to achieve precise selectivity using discrete surface electrodes, mainly since motor points may displace below electrodes for different positions. Moreover, for stronger stimulation levels, the induced current may diffuse to other muscles, producing erratic behavior. Other technical challenges to achieve robust FES control also include multiple muscle coordination and unreliable muscle force generations created by stimulation response characteristics (i.e., nonlinearity, electromechanical delays, and time-dependency). All of these limitations increase energy consumption and reduces walking time and distances, implying on a search for new controllers, especially for complex movements (e.g., gait).

3.2.2 Hybrid neuroprosthesis (HNP)

Several technological developments enabled a variety of mechanical orthoses to be viable, which vary from cable structures for standing to complete wearable active orthoses. For consistency, we use the same definitions as (DOLLAR; HERR, 2008) for exoskeletons and active orthoses. Exoskeletons are anthropomorphic active mechanical devices, which fits the operator's body and works in concert with his or her movements. Usually, this term describes a device that augments the performance of a volunteer without disability. For our thesis, we focus on the term active orthosis, which typically

describes a device used to increase the ambulatory ability of a person suffering from a leg pathology.

We categorize active orthoses as Body weight-supported (BWS) treadmill training with robotics, full-limb active orthoses, and modular active orthoses. BWS treadmill training is a robotic system assisting the user during gait, entirely dependent on the treadmill. Contrary to BWS systems, full-limb and modular active orthoses have the technical achievements of portability (although these systems are commonly used in treadmills). We differ full-lower-limbs and modular active orthoses based on the modularity. A full-lower-limb active orthosis should thoroughly assist both legs (and sometimes part of the trunk), making it possible for a person with paraplegia to take some steps. On the other hand, a modular active orthosis actuates on specific limbs or joints, allowing some types of rehabilitation movements, but usually not the complete gait movement.

Mechanical orthosis gives support, stability, and constraining of unwanted motion. Hence, researchers proposed hybrid neuroprosthesis (HNP), which combined FES and lower limb orthoses to increase safety and rehabilitation efficiency (the achievement of rehabilitation potential and duration of exercise). The AMOLL project (RABISCHONG et al., 1979) was the first published work on modular active orthoses with actuation for both hip and knee components in flexion and extension. The modular nature of these devices allows each patient only to use the components necessary for his ambulation. Researchers continued with devices similar to the AMOLL project (RABISCHONG et al., 1979), and this work advanced to the first description of an HNP, in which they substitute one module with FES (POPOVIĆ; SINKJÆR, 2000).

Other early HNPs proposals (PEREZ-ORIVE; MAYAGOITIA, 1994; OHASHI et al., 1993) described simple robotics control techniques with an open-loop control of FES. (POPOVIĆ; SINKJÆR, 2000) confirmed with experiments that active orthosis provides effective control of movement, and stimulation reduces energy requirements. More recent works evaluated energy limitations of the mechanical orthosis, and then combined FES to benefit from muscle power (HA; MURRAY; GOLDFARB, 2016), as well as the other way around (JAILANI et al., 2011), which, consequently, leads to lighter and better controllable systems.

3.2.2.1 State of the art

To describe and compare the HNPs state of the art, we investigated the most recent papers (≤ 15 years) published in PubMed, IEEE or ScienceDirect databases using the following combination of terms within the title and abstract:

- (Hybrid Exoskeleton),

- (Hybrid AND Orthosis),

- ((Functional Electrical Stimulation OR FES) AND exoskeleton).

After rejecting duplicate articles and carefully reading the title, keywords, and abstract, we identified the groups with more repercussion factors on HNPs, focusing on control developments. Projects differ from actuators (e.g., DC motors and friction brakes), measurement variables (e.g., angle and torque), electrodes (e.g., surface and intramuscular), control (e.g., PID and fuzzy), application (e.g., assistive gait and rehabilitation), among other features. Although these designs vary widely, we can still describe and compare specific features (e.g., type of electrodes and muscles stimulated)[1].

From the state of the art, this project intends to recognize for which application the HNPs were applied (e.g., rehabilitation exercise for one leg). We also intend to identify stimulation and actuators features (e.g., surface electrodes on QUAD combined with knee DC motors). Therefore, Tables 3.6, 3.7 and 3.8 highlight the following characteristics:

- type of movement tested (e.g., rhythmic swinging of the leg or complete gait),

- single or double legs tested,

- type of electrodes (e.g., noninvasive surface or invasive intramuscular electrodes),

- which variables were measured for control and evaluation,

- stimulated group muscles (Table 2.1 describes the labels used in this text),

- type of actuators (e.g., DC or breaks), and

- number of different volunteers for experiments.

From the literature search, we identified two simulation projects that evaluated HNPs for rehabilitation exercise for one leg (Table 3.6). Most projects that conducted experiments with individuals were able to complete gait trials (Tables 3.7 and 3.8), even though designing, developing and experimenting demand more funds, security checks and time. This context indicates an inclination to employ HNPs for gait assistance. Even trials that experimented with only one leg or even with simple rehabilitation exercises expressed the intention to also employ HNPs for gait in the future. We also

---

[1] As efforts and results differ from the type of experiment, we present the systems in order of experimental effort. Therefore, we first present projects that only evaluated HNPs in a simulation environment (Table 3.6). Second and third, projects that developed and evaluated HNPs on subjects without disability (Table 3.7) and on subjects with disability (Table 3.8), respectively.

recognized fewer trials with subjects with disability (Table 3.8) compared to without (Table 3.7). The lack of trials with individuals with disability indicates the difficulty to find individuals available for tests, in addition to the responsibility of security checks for this population to use the HNP. The lack of this kind of analysis also probably indicates immature technologies, as most authors explicitly expressed the intention to apply HNPs to individuals with SCI.

In terms of stimulation, Tables 3.7 and 3.8 show essentially the use of surface electrodes on HNPs. Although intramuscular electrodes provide more selectiveness and require a lower pulse intensity, surface electrodes are still simpler to implement on experiments with different subjects. Tables 3.7 and 3.8 also show that most studies use one (JAILANI et al., 2010; DEL-AMA et al., 2012; OBINATA et al., 2007), two (REN; ZHANG, 2014; HA; MURRAY; GOLDFARB, 2016) or three (ALIBEJI; KIRSCH; SHARMA, 2015) pairs of surface electrodes on each lower limb. The only HNP with a more complex and invasive technique was presented by CWRS, with 16 channel intramuscular electrodes (Gwo-Ching Chang et al., 1997) tested in one individual with mid-thoracic paraplegia. Tables 3.7 and 3.8 also highlight QUAD and HAMS as the most used muscle groups (even in the simulation environments from Table 3.6), because these are the stronger and most essential muscles for knee flexion and extension, showed to be essential to gait.

As for actuators, there are two types: semi (spring or brakes) and fully active (DC motors or hydraulics). Probably because of their lower cost and high torque, Tables 3.6, 3.7 and 3.8 show that both types of activation usually uses uses DC motors.

Usually, stimulation controllers are feedforward, and actuators controllers consider offline predetermined trajectories based on application (e.g., rhythmic swing or gait). For feedback, most used variables are position (JAILANI et al., 2011; ALIBEJI; KIRSCH; SHARMA, 2015; BULEA et al., 2014; REN; ZHANG, 2014; HA; MURRAY; GOLDFARB, 2016), torque (VALLERY et al., 2005) or even the relationship of both (CHEN et al., 2013). Also, HNPs tested on volunteers with and without SCI (Tables 3.7 and 3.8) used an FSM at a high level and cooperative combined stimulation and actuators at a lower level. Most projects focus on the first-actuator approach and use stimulation as a way to reduce motor torque (REN; ZHANG, 2014; HA; MURRAY; GOLDFARB, 2016). However, (Gwo-Ching Chang et al., 1997) explicit presented a muscle-first approach, in which actuators just adjusted the trajectory or providing movement that stimulation is unable to.

3.3 ENERGY STORAGE DEVICES TO SUPPORT FUNCTIONAL MOVEMENTS

Rapid muscle fatigue is a notable limitation for FES muscle contractions in individuals with SCI. Consequently, some adjustments aim to diminish this effect. The simple addition of energy storage devices (usually elastic with mechanical springs) may reduce muscle fatigue effects and lower the metabolic cost by providing a more natural and stable movement (HUSSAIN; TOKHI; JAILANI, 2009; IBRAHIM et al., 2008). Passive knee orthoses, e.g., store kinetic energy as potential energy, and released it when needed without any external power supply (MASSOUD, 2012). From this point to facilitate reading, we will often use the general term passive orthoses also for passive orthoses with an energy storage device, unless we explicitly declare otherwise.

In a simulation environment, some authors have already combined this type of passive knee orthoses in rehabilitation exercises, e.g., in FES rowing, FES elliptical stepping, and FES gait. For rowing, (HUSSAIN; TOKHI; JAILANI, 2009) simulated a knee torque storing energy during the driving phase (knee extension) and releasing energy during the recovery phase (knee flexion). Results showed that the addition of passive orthoses reduced the overall level of QUAD excitation. For elliptical stepping exercise, (YAHAYA et al., 2018) simulated a linear extension spring as the energy storage element. The spring resistance reduced the excessive cadence, and the assistance boosts the cadence at the starting of every cycle. This actuation led to lower average cadence errors when compared with the system without passive orthoses.

Moreover, other authors have designed and experimented with passive knee orthoses to regulate FES. (GHAROONI; HELLER; TOKHI, 2001; FARRIS et al., 2009) used a spring to flex the knee during swing phase. The passive orthoses took advantage of the fact that the bi-articular muscles link knee and hip, and reduced the number of stimulation channels. In a different joint, (DEL-AMA et al., 2012) designed lightweight and compact design passive ankle orthoses to avoid foot drop. The spring stiffness allows plantar and dorsal flexion during stance phases of gait with a low interference with the movement.

In the presented work, we intend to evaluate the combination of passive orthoses and FES cycling. Therefore, to find previous research in this topic, we investigated the most recent papers (≤ 15 years) published in PubMed and IEEE databases using the following combination of terms within the title and abstract:

- ((cycling) AND (orthoses)),

- ((cycling) AND (spring)),

- ((cycling) AND (energy storage)),

- ((cycling) AND (exoskeleton)).

After rejecting duplicate articles and carefully reading the title, keywords, and abstract, we identified three simulation studies (IBRAHIM et al., 2008; MASSOUD, 2012; ABDULLA; SAYIDMARIE; TOKHI, 2014) and two experimental studies in subjects without disability (CHAICHAOWARAT et al., 2017; CHAICHAOWARAT; KINUGAWA; KOSUGE, 2018). To our knowledge, no previous experiments combined passive orthoses with FES cycling in either volunteers with and without disability. Section 3.3.1 and Table 3.9 summarizes the state-of-art of the combination of passive elastic elements in cycling in chronological order.

3.3.1 State of the art

The first work on elastic elements in cycling (IBRAHIM et al., 2008) discussed the use of an energy storage device to assist FES-cycling, while eliminates the dead points of the pedal cycle. They added elastic cables to the bicycle, where the spring stores and releases elastic potential energy during the knee flexion in cycling. The simulation results of a bang-bang quadriceps controller led to the conclusion that passive orthoses could reduce the number of stimulation channels required in FES cycling. Moreover, the released energy could eliminate the dead points of the pedal cycle.

Also adapting the bicycle, (ABDULLA; SAYIDMARIE; TOKHI, 2014) described a flywheel and an electrical clutch mechanism at the crank intending to maintain cycling cadence. The clutch engaged and disengaged a flywheel to assist or retard the cycling when necessary, while the fuzzy logic control (FLC) stimulates the quadriceps. The flywheel engages with the crank to absorb the surplus energy produced by stimulating the leg, store it as kinetic energy and slow down the movement. Also, it engages again to use the same stored energy to assist the leg and speed up the cycling. In a simulation environment, they compared the results with and without the assistance mechanism. Results showed that the quadriceps stimulation intensity increased, but the mechanism delayed muscle fatigue. We should note that (ABDULLA; SAYIDMARIE; TOKHI, 2014) uses an electronic controller that actuates the elastic device at the bicycle; therefore, it is not entirely passive.

Moreover, we should note that (IBRAHIM et al., 2008) and (ABDULLA; SAYIDMARIE; TOKHI, 2014) added elastic elements to the bicycle, changing its mechanical structure. Therefore, we do not classify these items as orthoses.

In 2012, (MASSOUD, 2012) described the first energy storage passive knee orthoses for FES-cycling. They identified that the cycling performance depended on the spring position and parameters (spring constant and spring natural length). Therefore, they evaluated efficiency (work accomplished over the energy expended) for three

44

spring positions and ten spring constants. Only the quadriceps are excited (bang-bang control) to drive a stationary bicycle, and the spring released energy during flexion. The simulation results led to the conclusion that when the spring constant (stiffness) increases, the efficiency also increases.

In an environment without FES, (CHAICHAOWARAT et al., 2017; CHAICHA-OWARAT; KINUGAWA; KOSUGE, 2018) designed and experimented with passive knee orthoses for cycling assistance. In their concept validation (CHAICHAOWARAT et al., 2017), the spring stored energy from knee flexion and released during knee extension. They based their approach on the unbalanced effort required from the quadriceps (knee extensor) and hamstrings (knee flexor) during the same cycling cadence (JORGE; HULL, 1985). They tested the system on a cycling trainer with a subject without disability wearing the orthoses on both legs. With the torsion spring support, the surface electromyography recorded from some major leg muscles shows the decrease of knee extensor muscle activity as the leg is moving around the pedal crank top dead center.

After concept validation, in (CHAICHAOWARAT; KINUGAWA; KOSUGE, 2018), they compared the EMG over the quadriceps of three participants without disability performing constant power cycling with and without the orthoses. At the same cycling power, less quadriceps activity was observed in all participants when using the spring support. Although these results were the first that compared cycling performance with and without passive orthoses, the system intends to help cyclists hamstring training, not FES rehabilitation. They propose that the torsion spring support gradually works out the hamstrings, enhancing cycling with the same quadriceps effort of athletes.

Table 3.6: Summary of recent projects that only evaluated HNPs in a simulation environment.

System	Movement	Legs	Variables	Muscles	Actuators
TUM	Swing	1	Knee θ and τ	QUAD, HAMS	DC
CAS	Leg press	1	Hip and knee θ, τ and EMG	QUAD, GLUT	DC

Table 3.7: Summary of projects that evaluated HNPs on subjects without disability.

System	Movement	Legs	Variables	Electrodes	Muscles	Actuators	Subjects
FEXO Knee	Swing	1	Knee θ, τ and F	Surface	QUA HAMS	DC	4
SBO	Gait	1	Hip and knee θ and $\dot{\theta}$	Surface	QUAD	Spring break	1
Kinesis	Gait	2	Knee θ and τ, and FSRs	Surface	QUAD	DC and springs	4
HyPO	Gait	1	Hip and knee θ and $\dot{\theta}$	Surface	QUAD	DC	1
SEAHO	Leg extension	1	Hip and knee θ	Surface	QUAD	DC	4
	Gait	2	Hip θ	Surfacee	GAST, QUAD, HAMS	DC and springs	1
Vanderbilt University	Gait	1	Hip and knee θ	Surface	QUAD	Spring break	1

Table 3.8: Summary of projects that evaluated HNPs on subjects with disability.

System	Movement	Legs	Variables	Electrodes	Muscles	Actuators	Subjects
Vanderbilt University	Gait	2	Hip and knee θ and τ	Surface	HAMS	Spring break	1
	Leg Lift	1	Knee θ and τ	Surface	QUAD	DC	1
	Gait	2	Hip and knee θ and τ	Surface	QUAD, HAMS	DC	3
CWRU	Sitting, standing and gait	2	Hip, knee and ankle θ, and FSRs	Intramuscular	ERECTOR, GLUT, HAMS, ADDUC, QUAD, ILIOP, GRAC, TENSOR	Hydraulics	1

Table 3.9: Summary of recent projects that combined passive elastic elements in cycling.

System project	Target population	Elastic element	Energy released	Subjects
(IBRAHIM et al., 2008)	SCI	Bicycle	Flexion	Simulation
(MASSOUD, 2012)	SCI	Knee (orthoses)	Flexion	Simulation
(ABDULLA; SAYIDMARIE; TOKHI, 2014)	SCI	Bicycle	Flexion	Simulation
(CHAICHAOWARAT et al., 2017)	Athletes	Knee (orthoses)	Extension	1 without
(CHAICHAOWARAT; KINUGAWA; KOSUGE, 2018)	Athletes	Knee (orthoses)	Extension	3 without

4 DETECTION OF STIMULATION ARTIFACTS TO ISO-LATE EMG ACTIVITY

The real-time FES-induced torque estimation based on EMG have provided good performance (FANG et al., 2018). Myocontrolled neuroprostheses use EMG for timing and intensity control of stimulation applied to these exercises, estimating not only the volitional activity (from the patient, vEMG) but also the evoked activity (from FES, eEMG). Some results even suggest that myoneuroprostheses can replicate the muscular strategy adopted by subjects without disability (FERRANTE et al., 2012).

To extract components from EMG signals, we need first to find the inter-pulse-intervals (IPIs), i.e., the EMG signal between stimulation artifacts. Therefore, we developed methods for detecting stimulation artifacts for two-channel stimulation artifact detection on the same lower limb segment to estimate vEMG and eEMG described in Section 4.1) and previously published in (SOUSA et al., 2018). Figure 4.1 summarizes the entire method for extracting volitional and evoked EMG information. Section 4.2) describes the experiments to evaluate the success of artifact detection in two different hardware setup.

The application of closed-loop FES control strategies still faces several technical challenges related to the design, such as (1) the variety of uncertainties in muscle physiology among different patients, and (2) the difficulties related to the prediction of the exact contraction force exerted by the muscle. These difficulties are mainly related to the unknown mapping between the stimulation input parameters and the generated muscular force (ALOUANE et al., 2018). However, we know that the force and the
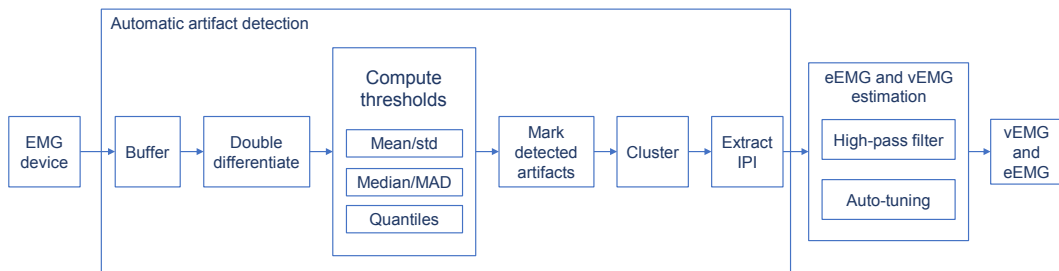
Figure 4.1: From the signal measured by the EMG device, the automatic artifact detection buffers the signal, then double differentiates it. From this result, the method uses one of the three threshold methods to compute the maximum and minimum values to identify possible artifacts. These points are marked and then clustered for later extraction of the IPI. To estimate volitional and evoked EMG (vEMG and eEMG), the method uses one of two filter methods.

Source: Prepared by the author.

EMG signal may be correlated (FANG et al., 2018). Therefore, we present a proof of concept of one method in subject with complete SCI in Section 4.3. In this experiment, we compared the normalized force with the normalized eEMG estimation.

4.1 VOLITIONAL AND EVOKED EMG ESTIMATION

The stimulation artifact detection is executed at stimulation frequency. It must consider that poor cable connection, and movements also generate EMG artifacts. Depending on the hardware, even noise may cause artifacts. Section 4.1.1 presents the artifact detection method. This method takes into account that most stimulators have one current source that generates pulses on two channels sequentially in a short period. Besides, the method foresees that pulses of each stimulation channel will be visible in both EMG channels due to the proximity of all electrodes at one limb segment. To evaluate the applicability of the EMG extraction, we also implemented two methods for filtering eEMG and vEMG, as described in Section 4.1.2.

4.1.1 Artifact detection

The method that starts buffering two vectors with M raw EMG samples (one buffer for each channel). The buffer size should be $M > L$ for searching the last incomplete IPI and $M > 2L$ for searching the last complete IPI. Here, L corresponds to the expected number of EMG samples between two stimulation pulses. L is defined by the sampling frequency of EMG ($f_e = \{1\text{kHz}, 2\text{kHz}, 4\text{kHz}\}$) and stimulation ($f_s = \{25\text{Hz}, 40\text{Hz}, 50\text{Hz}\}$) as

$$L = \left\lceil \frac{f_e}{f_s} \right\rceil {}^1.$$ (4.1)

Note that we choose M in a way that we know the number of expected stimulation pulses inside the buffer (synchronization of FES and EMG). As illustrated in Figure 4.2, for a buffer that contains $M = \lceil 3.1L \rceil$ samples we expect at least three stimulation artifacts during active FES (even larger buffer sizes might be chosen if the computational power allows it). At each stimulation instant k, the EMG amplifier transmits EMG vectors with up to L samples to the artifact detection for both EMG-channels. The built raw EMG buffer vectors are

$$\mathbf{b}_c[k] = \begin{bmatrix} b_{c,1}[k] & \dots & b_{c,M}[k] \end{bmatrix}^T,$$ (4.2)

where $c \in \{1, 2\}$ stands for the EMG channel, $b_{c,M}[k]$ represents the most recent EMG samples available.

During execution, the method considers that EMG and stimulator frequencies are constant and hardware dependent. Beforehand, the user declares both frequencies,

---

[1] In mathematics, the ceiling function $\lceil x \rceil$ maps x to the least integer greater than or equal to x.

also considering the application. To improve the volitional and evoked estimation, we should keep a high relation between EMG and stimulation, which leads to large samples between two stimulation pulses (c.f., Equation 4.1). With more samples, we could more easily separate the vEMG and eEMG. The user also chooses which potential artifact detection algorithm will be applied, and which the output IPI, the last complete or the recent incomplete one (see Figure 4.2(a)). The method returns the corresponding IPI when stimulation is active (stimulation intensity (charge) of any channel $q_i > 0, i \in 1, 2$) or the most recent L EMG samples when the stimulation is off ($q_i = 0, i \in 1, 2$). The most recent L EMG samples are useful for estimation of only volitional activity without FES. The stimulation intensities are, therefore, additional inputs to the artifact detection method.

When stimulation is active, the method marks all potential artifacts by one of the three algorithms available based on some EMG signal properties (mean/standard deviation, median/median absolute deviation (MAD) or quantiles). To remove offsets and to amplify the high-frequency signal components, we compute the second-order differences in each EMG channel buffer. Thus, for $\mathbf{b_1}$ and $\mathbf{b_2}$ at each instant k, we obtain

$$
\begin{aligned}
\mathbf{B_1} &= \Delta^2 \mathbf{b}_1, \\
\mathbf{B_2} &= \Delta^2 \mathbf{b}_2.
\end{aligned}
\tag{4.3}
$$

From $\mathbf{B_1}$ and $\mathbf{B_2}$, we compute two thresholds ($p_{\mathrm{max,c}}$ and $p_{\mathrm{min,c}}$) for each channel $c \in \{1, 2\}$, depending on one of the three methods explained in Sections 4.1.1.1, 4.1.1.2 and 4.1.1.3. Afterward, we cluster the results between the thresholds, as described in Section 4.1.1.4.

4.1.1.1   Mean-standard deviation

The most intuitive method considers the means $\overline{B_1}$ and $\overline{B_2}$ and standard deviations σ_1 and σ_2 of the vectors $\mathbf{B_1}$ and $\mathbf{B_2}$, respectively. Then, the maximum and minimum thresholds are defined as

$$
\begin{aligned}
p_{max_c} &= \overline{B_c} + \alpha \sigma_c, \\
p_{min_c} &= \overline{B_c} - \alpha \sigma_c,
\end{aligned}
\tag{4.4}
$$

where $\alpha > 0$ is a tuning parameter. Red lines in Figure 4.3 illustrate an example of maximum and minimum thresholds using mean and variance for $\alpha = 3$.

4.1.1.2   Median-median absolute deviation (MAD)

Since both the mean and the standard deviation are particularly sensitive to outliers, the median value median may become a more suitable estimator than the

mean (LEYS et al., 2013). The median absolute deviation (MAD) is also a considerable estimation of the variability of a signal. The MAD for both channels is determined by

$$B_{\text{MAD},c} = \text{median}\left(\left|B_{c,1} - \text{median}_{\mathbf{B},c}\right|, \ldots, \left|B_{c,M} - \text{median}_{\mathbf{B},c}\right|\right), \qquad (4.5)$$

where $\text{median}_{\mathbf{B},c}$ corresponds to the median of $\mathbf{B}_c$. The thresholds are then defined as

$$
\begin{aligned}
p_{max_c} &= \text{median}_{\mathbf{B},c} + \alpha B_{\text{MAD}_c}, \\
p_{min_c} &= \text{median}_{\mathbf{B},c} - \alpha B_{\text{MAD}_c},
\end{aligned}
\qquad (4.6)
$$

where $\alpha > 0$ is again a tuning parameter. Green lines in Figure 4.3 illustrate an example of maximum and minimum thresholds using median and MAD for $\alpha = 3$.

4.1.1.3 Quantiles

The previous methods set the thresholds symmetrically concerning the mean and median, and do not take asymmetries in the possibly time-varying artifact into account. The following method bases on quantiles, which are the cut points dividing the probability distribution into contiguous intervals with equal probabilities. By defining the maximum and minimum thresholds as

$$
\begin{aligned}
p_{max_c} &= \alpha\text{-quantile}(\mathbf{B}_c), \\
p_{min_c} &= (100 - \alpha)\text{-quantile}(\mathbf{B}_c),
\end{aligned}
\qquad (4.7)
$$

we properly consider the asymmetry of the stimulation artifacts. Here, α is usually set between 90% and 98.5%. Larger values would only return the maximal and minimal values of the raw EMG inside the buffer. Blue lines in Figure 4.3 illustrate an example of maximum and minimum thresholds using quantiles for $\alpha = 95\%$.

4.1.1.4 Clustering

After calculating the thresholds, we mark all EMG sampling instances i for of buffers that fulfill the criterion

$$B_{c,i} > p_{max,c} \text{ or } B_{c,i} < p_{min,c}, \qquad (4.8)$$

and join the resulting sets of time points from both channels. $B_{c,i}, i = \{1, \ldots, M\}$ are the elements of the vector $\mathbf{B}_c$ for channel $c \in \{1, 2\}$.

To identify the last complete or incomplete IPI during active FES, we cluster the detected potential stimulation artifacts. If two artifacts are less than $\lceil 0.1L \rceil$ samples apart, then the samples between them are also marked, creating the vector $\mathbf{v}_r$ of detected potential stimulation artifacts as seen in Figure 4.2(b). The number of clusters should relate to the number of expected stimulation artifacts during the period of the buffer. However, noisy signals can increase or even decrease the number of

detected clusters. Therefore, we use a base vector $\mathbf{v}_b$ of expected clusters to compare with the vector $\mathbf{v}_r$. We construct the base vector with the knowledge of the stimulation frequency and the individual channel state of pulse generation (on/off).

Figure 4.2(c) shows the base vector construction; we expect three clusters, which are L samples apart. The duration of each predicted cluster is set to the average duration of the clusters present in $\mathbf{v}_r$. To reject wrong clusters and to reconstruct missing clusters, the cross-correlation between $\mathbf{v}_r$ and $\mathbf{v}_b$ is determined. Afterward, we align the base vector to $\mathbf{v}_r$, and the corresponding IPI is extracted based on the shifted base vector.

The parameter α is continuously adjusted online by comparing the number of found and expected clusters in the buffer. For the mean/standard deviation and median/MAD method, α is decreased by 10% if fewer clusters are found than expected, and increased by 10% if more clusters are found. For the quantiles, α will be adapted by $\pm$ 1% and will be limited to the range [90%,98.5%]. For all methods, the adaption only increases α if we find a difference greater than two between the present and expected clusters.

The final extracted IPIs are checked for plausibility. As the artifact should occur at the beginning of the vector, we considered the artifact detection and IPI extraction as correct when the maximum or minimum peak of the double differentiated EMG is located in the first 3 ms of the IPI.

4.1.2 Evoked and volitional estimation

To evaluate the applicability of the EMG extraction, we also designed and implemented a filtering block in SIMULINK to estimate volitional and evoked EMG activity during active FES from the returned IPI vectors. We select (1) the stimulation and EMG frequencies, and (2) the intervals within the IPI for assessing the volitional and evoked EMG activity. As illustrated in Figure 4.3, after the artifact the M-wave usually contains information about the evoked EMG signal (the medium gray area), and the M-wave tail includes information on the volitional EMG (the light gray area). For these subintervals, the method estimates volitional and evoked EMG activity, respectively. We implemented two filter methods, a high-pass filter (AMBROSINI et al., 2014) (described in Section 4.1.2.1), and the auto-tuning procedure (KLAUER et al., 2016) (described in Section 4.1.2.2). The purpose of both methods is to estimate some frequency component from the EMG. However, the comparison of both filters is out of this thesis scope; our intention remains only to demonstrate a real-time use of these filters with our algorithm.
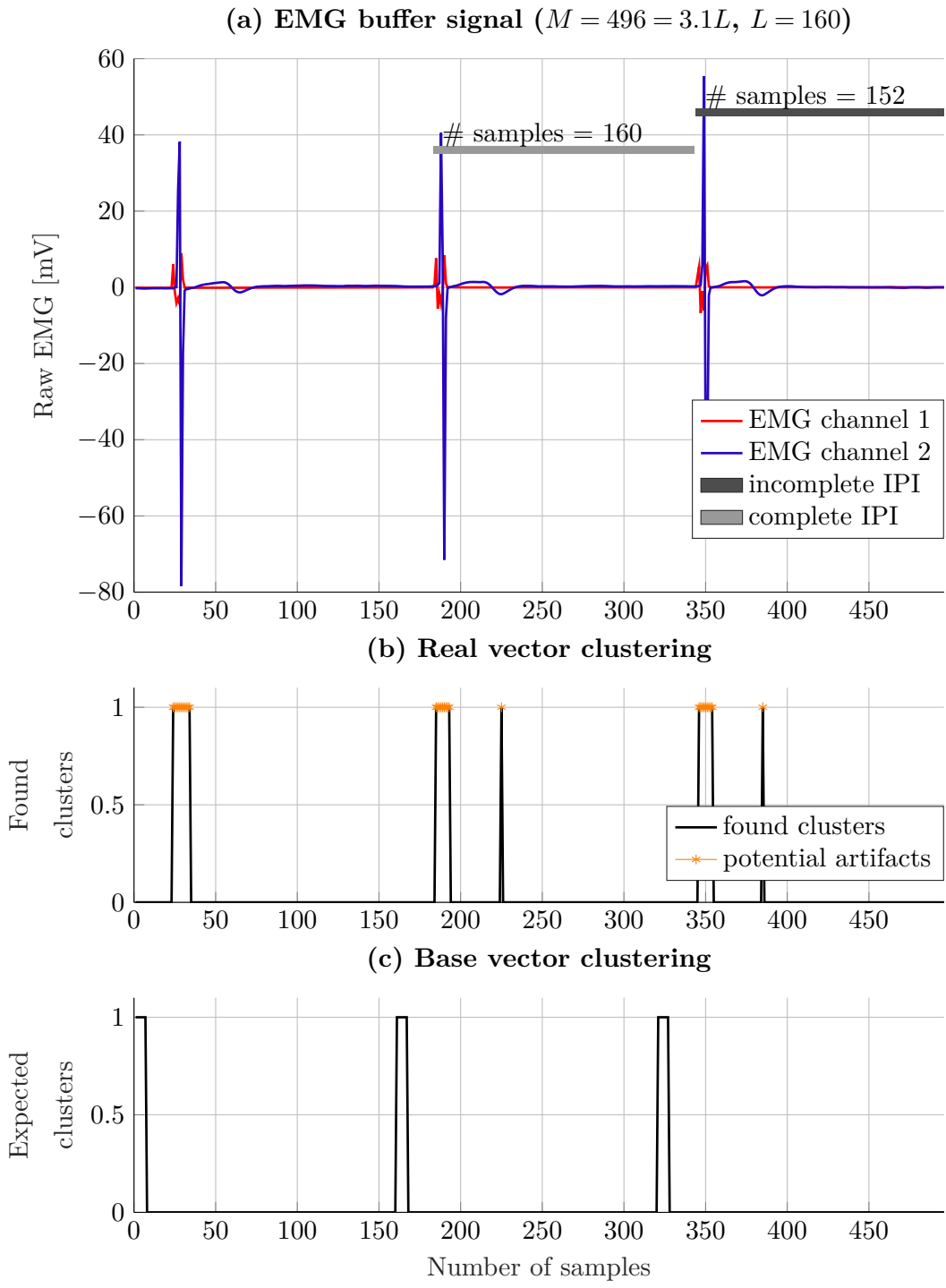
Figure 4.2: Clustering potential artifacts. (a) EMG buffer with complete and incomplete EMG vectors marked. (b) Potential artifacts clustering yields the real vector v_r. (c) Base vector with expected stimulation artifacts.

Source: Prepared by the author for (SOUSA et al., 2018).
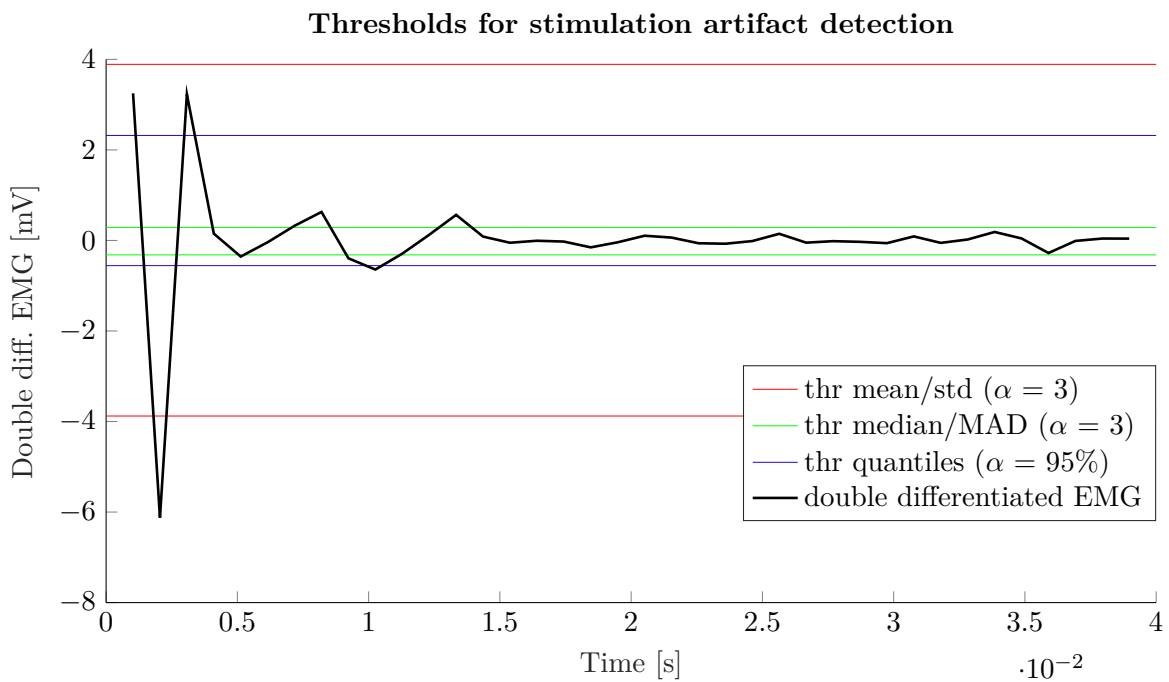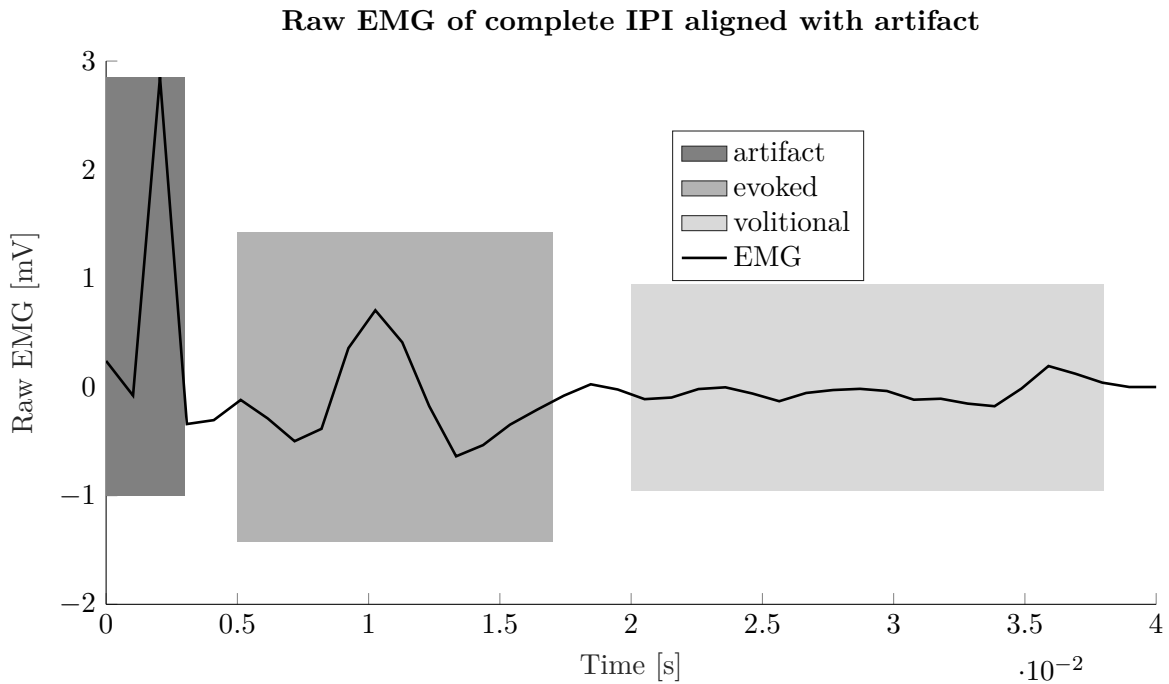
Figure 4.3: Extracted IPI of EMG with the (dark gray), region of M-wave (medium gray) and the volitional activity (light gray). We also show maximum and minimum thresholds using mean/standard deviation (red lines, $\alpha = 3$), median/MAD (green lines, $\alpha = 3$) and quantiles (blue lines, $\alpha = 95\%$).

Source: Prepared by the author for (SOUSA et al., 2018).

4.1.2.1 High-pass filter

The high-pass filter considers that only low-frequency electrically-induced components affect the measured EMG signal (AMBROSINI et al., 2014). They eliminated

these components by applying a non-casual digital high-pass filter with a cut-off frequency of 200Hz to the windowed EMG of each stimulation period. We used an infinite impulse response Butterworth filter (2nd order).

4.1.2.2   Auto-tuning procedure

The auto-tuning assumes that the FES-evoked EMG component (M-wave) is a time-variant signal in the mV-range while the volitional EMG signal part is band-limited Gaussian noise in the μV-range (KLAUER et al., 2016). The estimation of the vEMG requires the removal of the M-wave from the EMG signal; in this approach, we record the EMG vectors of the last six stimulation periods. The algorithm predicts the currently measured EMG vector by a linear combination of the old stored EMG vectors.

With this linear combination, the method estimates the current M-wave. Then, we optimize the corresponding weight parameters by a linear least-squares approach at each stimulation period. The obtained estimate of the M-wave is subtracted from the currently measured EMG vector to determine the vEMG component, which is then evaluated employing the 1-norm. This separation approach works better for the second half of the stimulation period, where only the tail of the M-wave appears.

Similarly, for eEMG, we obtain an estimate of the M-wave by a linear combination of the six previous EMG vectors. Then, the 1-norm is taken to obtain the intensity of the estimated M-wave in a sub-window of the inter-pulse interval.

4.2   EXPERIMENTS AND RESULTS OF ARTIFACT DETECTION

We aimed to develop and provide a SIMULINK® (The Mathworks Inc., USA) toolbox for EMG processing during FES that can be used with different non-hardware-synchronized stimulators and EMG amplifiers for various EMG sampling frequencies and stimulation rates[2]. For testing the volitional and evoked EMG estimation, we used two different hardware setups (stimulators and EMG amplifiers) during walking.

4.2.1   Experimental setup

In this experiment, the control is closed-loop; i.e., we use the inertial sensor as feedback. We applied stimulation at specific parts of gait while measuring EMG and inertial information. The system required a robust environment to guarantee the comparison between both hardware setups, which is described in Section 4.2.1.1.

---

[2]   It is being developed and maintained in `https://github.com/lara-unb/ema_emg_simulink`.
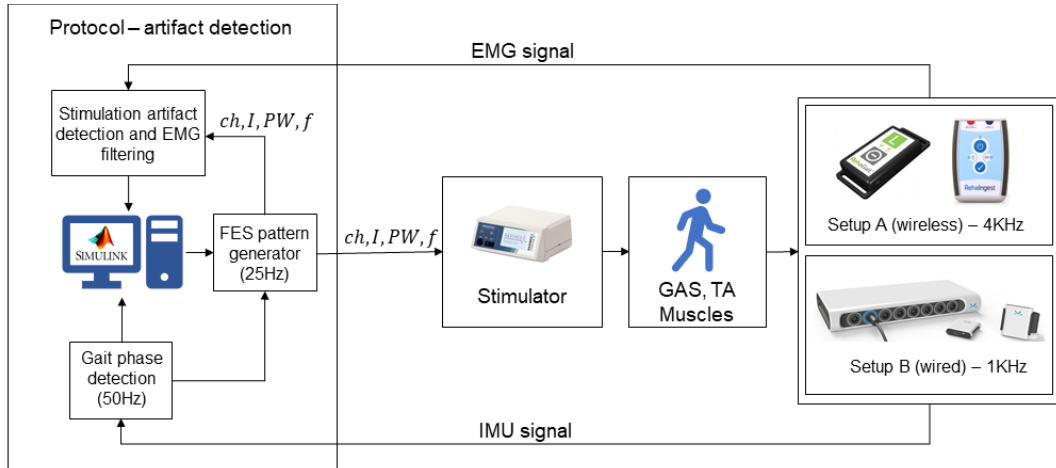
Figure 4.4: Diagram of the EMG artifact detection protocol. This protocol provides a signal u_x based on the gait phase detection timed by an inertial measurement unit (IMU). The protocol translates u_x to the stimulator, sending the channel to stimulate (ch), current (I), pulse width (pw) and frequency (f). Through surface electrodes on the subject, the stimulator applies the corresponded signal to tibialis anterior (TA) and gastrocnemius (GAS). During the experiment, the system measures EMG and IMU sensors.

4.2.1.1   Setup and equipment

We conducted the experiments with two subjects without disability[3], each one using a different hardware setup (Figure 4.4 illustrates the general configuration). We only stimulated one leg at the tibialis anterior, gastrocnemius, placing the reference EMG electrode over a bony prominence at the knee or ankle joint of the same leg.

There are two different arrangements for the pair of EMG electrodes: longitudinally, or latitudinally (ZHANG; ANG, 2007). For longitudinal arrangement, the electrodes are placed along with the potential propagating path of the muscle. Thus the high amplitude raw EMG signals can be picked up. In this position, the effects of artifacts and M-waves are also relevant. For latitudinal arrangement, the EMG electrodes cross over the muscle. Although the raw EMG signal is slightly weaker, it can reduce the effects of the artifacts and M-wave. In our experiments, we placed the EMG electrodes latitudinal to minimize the size of the M-wave induced by FES.

For hardware Setup A, we used one inertial sensor (RehaGait) and one two-channel EMG recording device (RehaIngest) with Galvanically isolated USB interface. We measured the EMG at 4000 Hz, and the IMU accelerations and angular rates at 50 Hz.

For hardware Setup B, we used one system that combines one wireless inertial

---

[3]   The performed trials have been approved by the ethics committee of the Berlin Chamber of Physicians.

sensor and one wireless EMG sensor with an average transmission latency of 50 ms (MUSCLELAB). The EMG sensor features two bipolar measurement channels. We measured the EMG at 1000 Hz, and the IMU accelerations and angular rates also at 50 Hz.

For stimulation, we used the same current-controlled multi-channel stimulator (RehaMove3) with a galvanically isolated USB interface.

Appendix A presents more detail about the equipment.

4.2.1.2 Protocol

The FES was administered in synchronization with the gait cycle using a velocity-adaptive real-time gait phase detection (GPD) (MULLER; SEEL; SCHAUER, 2015) based on an inertial sensor at the foot to trigger the stimulation. Four gait phases (foot flat, pre-swing, swing phase, loading response) and four gait events (full contact, heel-rise, toe-off, initial contact) are detected. The tibialis anterior is activated shortly before the toe-off (10% of the estimated gait cycle duration) and until heel strike to support the lifting of the foot during the swing phase. The gastrocnemius is stimulated to support push-off before the heel off (20% of the estimated gait cycle duration) until toe-off. We set stimulation frequency to 25 Hz, while adjusting the pulse width pw and current amplitude I in real-time for the biphasic pulses. To enable robust detection of stimulation pulse instants and IPIs, we also stimulate the muscles at a sub-sensory level ($I = 6$mA, $pw = 50\mu$s), i.e., when no functional stimulation at a sensory or motor level occurs.

The volunteers walked on a treadmill at slow walking speed (2 km/h) first without sensory or motor level stimulation. Then the pw and I were both linearly increased for both channels until the subject reported the sensation of stimulation pulses (sensory level stimulation). In setup A, we manually increased the intensities until visible muscle contraction (motor level stimulation). For all levels of stimulation intensity the subjects walked (1) normally, (2) with emphasized push-off (more gastrocnemius activity expected), and (3) with emphasized dorsiflexion (more tibialis anterior activity expected). The different gait patterns caused changes in the form and in the amplitude of the stimulation artifacts to challenge the artifact detection.

For EMG estimation, we employed the artifact detection on the tibialis anterior from both gait experiments, and then evaluated the percentage of complete IPIs that passed the plausibility check for both tibialis anterior and gastrocnemius channels.

4.2.2 Experimental results of the artifact detection

Table 4.1 resumes the performance of the mean/standard deviation, median/MAD and quantiles for different values of α. For mean/standard deviation and median/MAD, we set $\alpha = 3$ as suggested by (LEYS et al., 2013) as a very conservative value. For the quantiles, we set α to 95%, 96%, 97% and 98% to compare performance on different α. We also evaluated the α-adaptation of the three methods. All results refer to the last complete IPIs, yet the incomplete IPIs showed very similar results. We should observe that the incomplete IPI is only trustable if it contains enough datibialis anterior to evaluate the M-wave (for eEMG) and the M-wave tail (for vEMG).

The artifact detection and EMG filtering methods were real-time capable, i.e., no real-time error occurred, and we were able to obtain vEMG and eEMG at 50 Hz. The filtering results showed that the visually observed volitional muscle activity of the tibialis anterior and gastrocnemius concerning the detected gait phases were as described in (PERRY, 1992).

4.2.2.1 Setup A vs Setup B

Setup A with RehaIngest exhibited slightly higher success rates when compared to MUSCLELAB. This difference is most likely due to the lower EMG frequency of MUSCLELAB (1000 Hz) and wireless connection. Hence, the artifacts are sometimes not sampled at their maximal or minimal values and appear therefore smaller that negatively affects the detection. Even with this discrepancy, the mean/standard deviation and the quantiles with $\alpha = 97\%$ accomplished success rates higher than 95% for both systems without the α-adaptation. For the median/MAD method, the low success rate at $\alpha = 3$ indicates that this default setting is inappropriate for EMG signals during FES. The green lines from Figure 4.3 confirm the too small thresholds for the median/MAD method. Likewise, the α-adaptation reinforce this argument, by settling on a much higher average α ($\overline{\alpha} = 75.82$ for RehaIngest, and 18.11 for MUSCLELAB).

4.2.2.2 Automatic adaptation

Also, the divergent results from the quantiles indicate that each system has its own optimal α value ($\alpha = 98\%$ for RehaIngest, and $\alpha = 97\%$ for MUSCLELAB). All three threshold-selection methods exhibited success rates higher than 95% for both systems with α-adaptation. The quantiles presented a slightly lower result for the MUSCLELAB due to a higher sensitivity to adjustments compared to the mean/standard deviation and median/MAD. Furthermore, the α-adaptation avoids manual calibration and also reacts to unexpected signal behavior during online execution. Therefore, independently of the method chosen, we recommend the α-adaptation.

60

Table 4.1: Gait experiment: Artifact detection success rate for gastrocnemius and tibialis anterior (complete IPI).

	RehaIngest	MUSCLELAB
Mean/std	$\alpha = 3$	$\alpha = 3$
gastrocnemius	98.93%	94.92%
tibialis anterior	98.57%	94.48%
Mean/std α-adaptation	$\overline{\alpha} = 1.37$	$\overline{\alpha} = 2.01$
gastrocnemius	99.75%	96.09%
tibialis anterior	99.69%	96.21%
Median/MAD	$\alpha = 3$	$\alpha = 3$
gastrocnemius	54.86%	87.32%
tibialis anterior	52.55%	90.08%
Median/MAD α-adaptation	$\overline{\alpha} = 75.82$	$\overline{\alpha} = 18.11$
gastrocnemius	99.83%	97.88%
tibialis anterior	99.79%	97.50%
Quantiles	$\alpha = 95\%$	$\alpha = 95\%$
gastrocnemius	74.21%	96.53%
tibialis anterior	69.33%	97.36%
Quantiles	$\alpha = 96\%$	$\alpha = 96\%$
gastrocnemius	91.74%	97.50%
tibialis anterior	87.03%	97.85%
Quantiles	$\alpha = 97\%$	$\alpha = 97\%$
gastrocnemius	98.22%	97.59%
tibialis anterior	96.34%	97.62%
Quantiles	$\alpha = 98\%$	$\alpha = 98\%$
gastrocnemius	99.89%	84.96%
tibialis anterior	99.81%	85.37%
Quantiles α-adaptation	$\overline{\alpha} = 98\%$	$\overline{\alpha} = 97\%$
gastrocnemius	99.69%	95.54%
tibialis anterior	99.60%	96.46%

4.2.2.3 Thresholds

Contrary to advise from the literature (LEYS et al., 2013), the mean/standard deviation, and median/MAD methods present similar success rates for suitable α. Considering the planned implementation of the artifact detection into a wireless EMG sensor with ARM Cortex M4 microcontroller, we must acknowledge that the median/MAD and quantiles methods demand vector sorting, which critically depends on the buffer size M. Therefore, the mean/standard deviation method with the cross-correlation and α-adaptation seems more suitable for the requirements of automatically detecting stimulation artifacts within EMG signals on a microcontroller.

4.3 EXPERIMENTS AND RESULTS OF EVOKED EMG ESTIMATION

As a proof-of-concept of the artifact detection use for this application, we established a robust mechanical and electronic experimental environment, described in Section 4.3.1. The results from this experimental environment serve as the first step for mapping the EMG and force signals.

4.3.1 Experimental setup

In this experiment, the control is open-loop; i.e., there is no feedback. We applied a predefined set of stimulation parameters, and measured EMG and force. As we performed experiments with subject with complete SCI, the system required a robust environment, described in Section 4.3.1.1.

4.3.1.1 Setup and equipment

To provide the experimental setup, we integrated the force sensor information with the stimulator signal using the Robot Operating System (ROS[4]) and Python scripts. With the ROS platform, we may develop a modular system, which enables a faster transition to other applications. For EMG, we used the Simulink® (The Mathworks Inc., USA) toolbox described in Section 4.1.

Figure 4.5 presents the basic ROS structure used in these experiments. A package is a folder with files regarding one or multiple parts of a system. These parts are named ROS nodes (elliptical shapes), described in an executable file (usually there is one node per package). Nodes may communicate with each other by publishing (sending data) or subscribing (receiving data) to a specific ROS topic (channel for message exchanges, arrows).
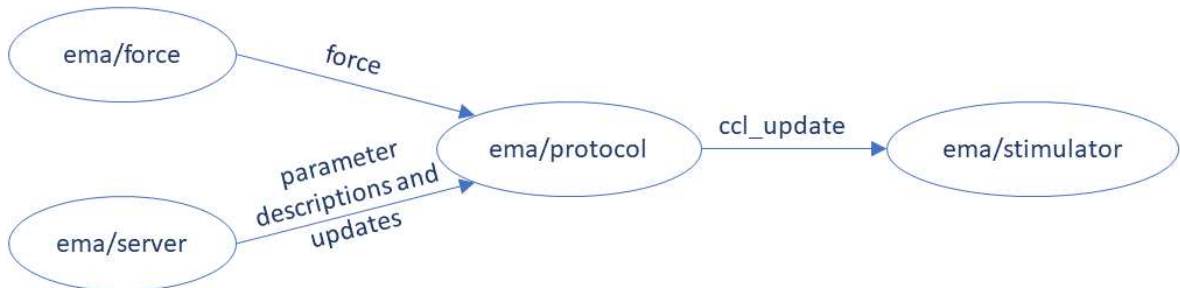
Figure 4.5: Diagram of nodes and topics of the EMG-force experiment. ROS nodes are illustrated by elliptical shapes, and ROS topics are illustrated by arrows (inward and outward arrows represent subscribing and publishing, respectively).

Source: prepared by the author.

---

[4] Detailed explanation is available at http://wiki.ros.org/ROS/Introduction.

The **server node** establishes the communication between the interface, in which the user determines the current and pulse width. The ROS system collects this information and guarantees the communication between all topics. The **force node** works as a driver, measuring and publishing the current force to the **protocol node**. Based on these messages, the protocol node creates the set of channels, current, pulse width, and frequency to send them to the **stimulator node**.

In addition to the computer running the ROS system[5], the experimental setup also contains the stimulator, and a mechanical setup with the force sensor. Figure 4.6 incorporates the interface, the equipment (stimulator, force sensor and EMG), and the musculoskeletal system of the volunteer (muscles).
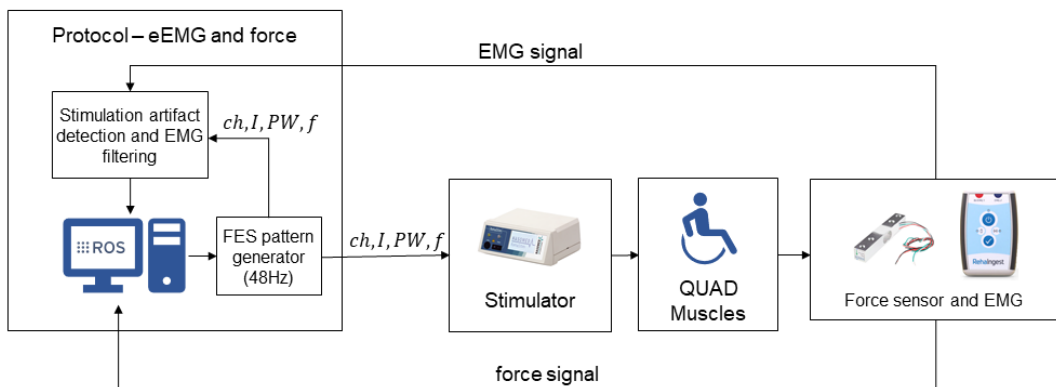
Figure 4.6: Diagram of the EMG protocol for evoked EMG estimation. This protocol provides a signal u_x based on the predetermined set of stimulation. The protocol translates u_x to the stimulator, sending the channel to stimulate (ch), current (I), pulse width (pw) and frequency (f). Through surface electrodes on the subject, the stimulator applies the corresponded signal to the quadriceps (QUAD) muscles. During the experiment, the system measures EMG and force sensor.

Source: prepared by the author.

We used the RehaStim (Hasomed, Germany), an 8-channel stimulator that provides biphasic current pulses and enables online update of stimulation amplitude and pw. The stimulation frequency is $48\,Hz$. In this experiment, we used the current modulation as it did not require a high resolution, and applied the stimulation to generate contraction to the quadriceps (QUAD) muscle through $4.8 \times 9.6\,cm$ rectangular electrodes. During stimulation, we measured EMG using the RehaIngest (Hasomed, Germany) with Galvanically isolated USB interface at $4000\,Hz$. We estimated the eEMG offline using the artifact detection and filtering tools developed in Section 4.1.

To measure force, we used equipment composed of a load cell and a chair. The force cell contains an amplifier that extends the Wheatstone bridge from a load

5   It is being developed and maintained in `https://github.com/lara-unb/ema_stim_matrix`.

cell (LC Straight Bar 50Kg, Sparkfun, USA) calibrated between 1kg and 10kg. The sensor was attached to the subject's ankle through a velcro strap, providing real-time information on the knee force related to an initial position at approximately $20\,Hz$. Figure 4.7a presents the mechanical design of the chair, in which several regulations allow the coupling and fixation of the torso and the leg during the tests. Figure 4.7b presents a volunteer during setup with electrodes, IMU (not used in this experiment), force sensor, and stimulator.

Appendix A presents more detail about the equipment.
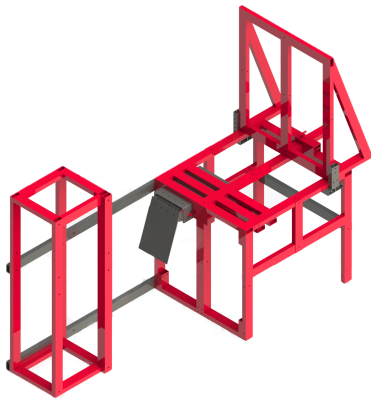
(a) Mechanical design of the chair.

(b) Volunteer during setup.

Figure 4.7: Setup system for isometric exercise with the knee locked at 45º.

Source: (a) prepared by Miguel E. G. Paredes and (b) prepared by Lucas M. Pinheiro.

4.3.1.2 Subject

Our volunteer with SCI was a 41-year-old male, with American Spinal Injury Association Impairment Scale designation A (AIS A), level T9, injured seven years earlier. This volunteer already uses FES daily and presents a normal cardiovascular response to stress and physical exercise, along with healthy skin. As a subject with AIS A SCI, our volunteer has no sensitivity at the lower limbs. There are two points of contact of his lower limbs in this experiment: the pelvis on the chair and the elastic bend at the ankle. During stimulation, the team is always aware of these areas, so the system does not apply excessive pressure and compression, causing injuries. A local ethical committee[6] approved the experimental tests, and the subject provided written consent (Appendix B).

---

[6] Presentation Certificate for Ethical Appreciation (Certificado de Apresentação para Apreciação Ética, CAAE): 11717119.3.0000.0030.

4.3.1.3 Protocol

Before starting the stimulation set, the subject was comfortably seated in the chair described in Section 4.3.1.1, where we fixed the ankle for the isometric exercise. We positioned the leg at 45º and placed the electrodes over the quadriceps muscles. In this position, we set the current I fixed at 40 mA and increased the pulsed width pw until we found the limit for the volunteer. We selected a pw that generates an evident contraction of the quadriceps without exposing the participant to harm. For a volunteer with complete SCI, we understand this limit as subjective, as the torque is different between subjects, legs, and even daily health conditions. After setting I and pw, we let the volunteer rest for five minutes. We based the protocol on (LAUBACHER et al., 2019).

Then, we applied a set of stimulation composed of 36 stimulation sequences with the previously selected pw. Each sequence is characterized by a 0.5s climb ramp to increase I from 0 to 40mA, 4s at 40mA, a 0.5s descent ramp decreasing from 40 to 0mA, and 5s rest. During the entire set, the load cell and EMG recorded the responses. In this application, we used only one channel for EMG and FES to limit interferences between M-waves from co-activated muscles.

4.3.2 Proof of concept of the force-EMG relation

The vEMG of the volunteer with complete SCI remains close to zero; therefore, Figure 4.8 presents the estimated eEMG (after artifact detection and filtering) and force response from the volunteer's left leg. For eEMG estimation, we first found the artifacts using the quantiles methods with automatic $\alpha = 98\%$, and then we filtered the window between 5ms and 10ms (samples 20 to 41) with the high-pass filter described in Section 4.1. In eEMG, we observe values over 40mA, which are related to the artifact detection. In these cases, the filtering calculates eEMG considering the artifact detection incorrectly.

Although the number of peaks seems notable when we observe the graph, the algorithm only found 0.8% of incorrect artifacts, which can be easily removed by additional filters during real-time control. As we did not connect the software for measuring EMG and the software for setting FES, the artifact detection has no information when the stimulation was on or off. If we set the stimulation off, the software is unable to find artifacts. Therefore, to estimate eEMG, we set the stimulation as 'on' during the entire trial. Most of the artifact detection errors relate to the periods of transitions between off-to-on stimulation, as the artifact clusters may be incorrect, as there were no pulses before (c.f., Figure 4.8).

The isometric exercise intends to estimate muscle fatigue, which we may observe
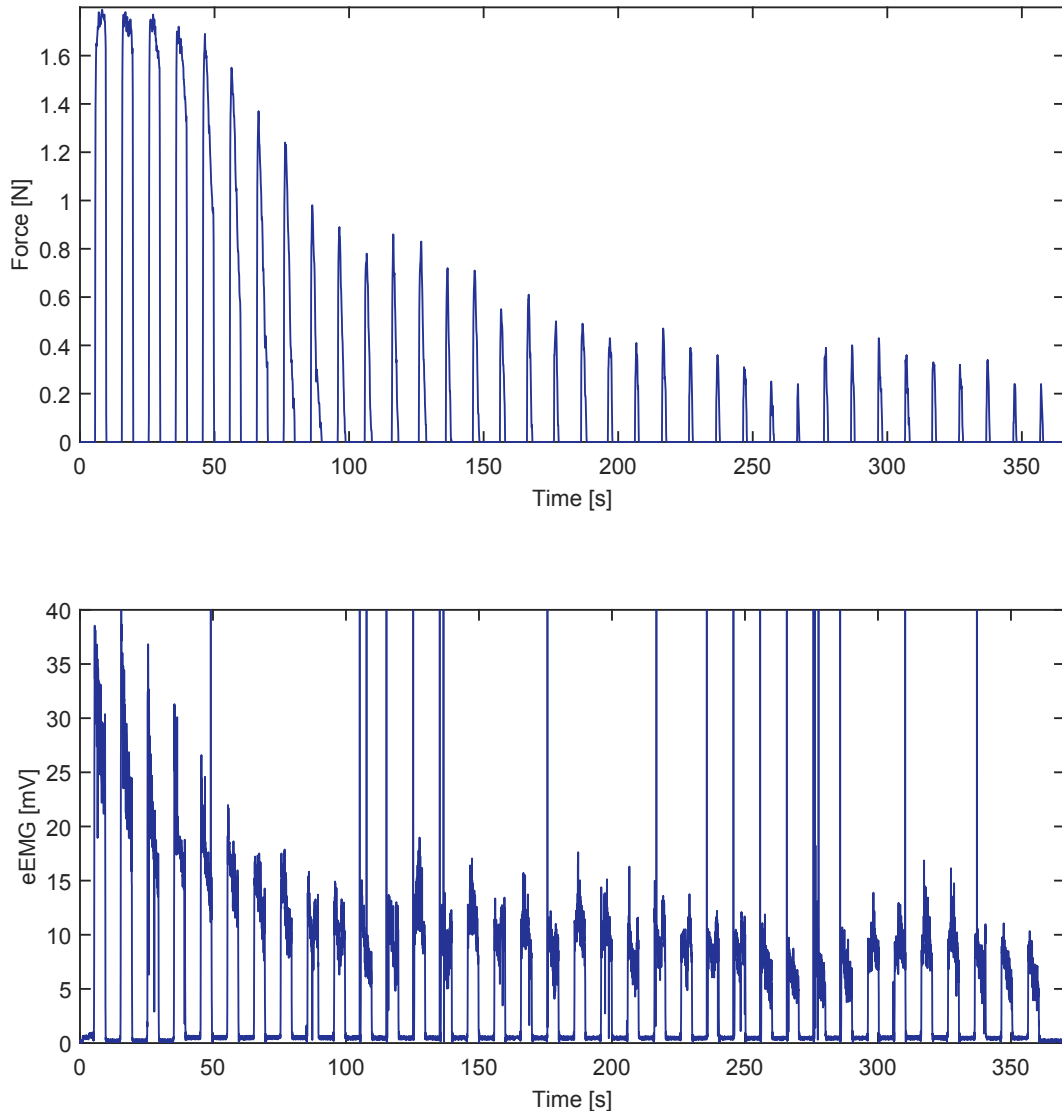
Figure 4.8: Plots of the force and eEMG response during the isometric exercise period for the volunteer with complete SCI. We may observe incorrect artifacts as values higher than 40mV.

Source: prepared by the author.

the force decreasing over time. We observed that eEMG also decreases over time. For better visualization, we normalized the results with the highest measurement for force and the highest measurement for eEMG in Figure 4.9. As the incorrect artifact detection could lead to higher values than the maximum eEMG (mostly represented in peaks higher than 40mV), we removed the incorrect artifacts before normalizing. We also marked the first and last highest measurement for force and eEMG. Even with apparent differences, the signals similarities from Figure 4.9 relate force and eEMG.
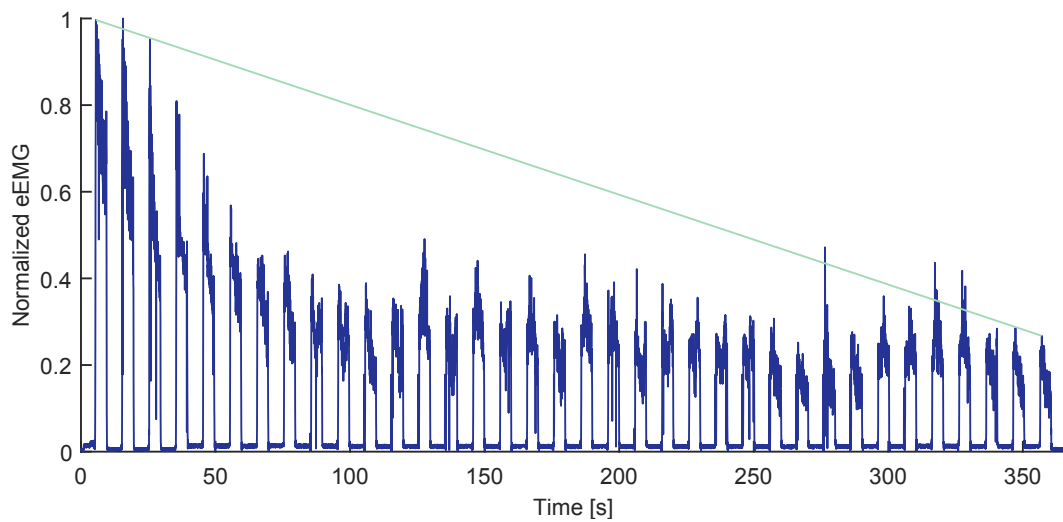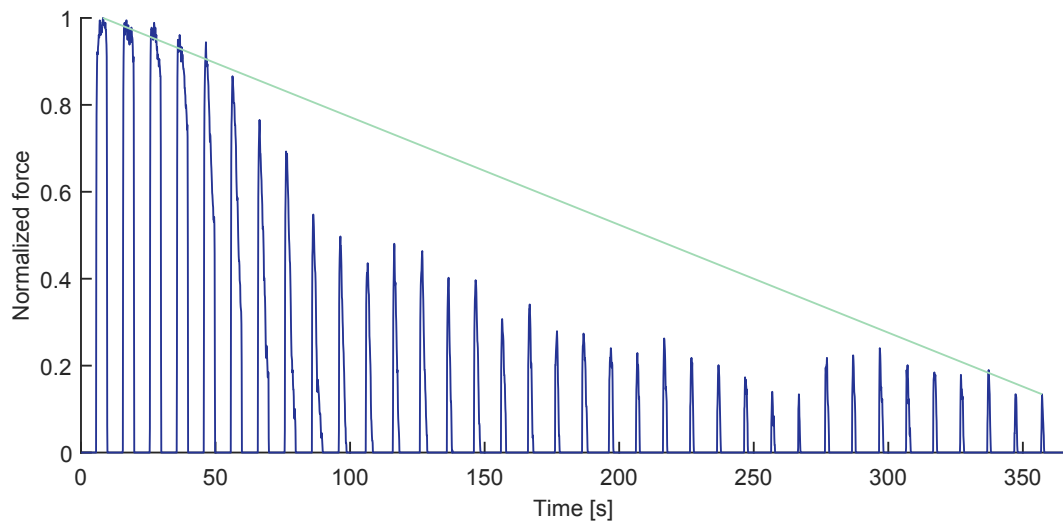
Figure 4.9: Observation of the force and eEMG normalized signals. We excluded incorrect artifact detection and marked the first and last highest measurement for force and eEMG to show the decrease of power during the procedure.

Source: prepared by the author.

5 SIMULATION STUDIES ON CONTROL STRATEGIES FOR FES GAIT

Gait training is a set of activities aimed to acquire walking skills in physiotherapy. These exercises may include (1) balance training, to help the body to maintain its balance in static or dynamic positions; (2) posture training, to intervene at the alignment and position of the body to gravity, the center of mass and support base; (3) and motor learning, to intervene to perform qualified actions. It is common to use FES with patients with complete SCI to increase muscular tonus (SZECSI; STRAUBE; FORNUSEK, 2014). As the accelerated fatigue generated by FES limits the duration of experiments, we developed the simulation environment for initial gait tests (SOUSA; FREIRE; BÓ, 2019) presented in Section 5.1. In this environment, we studied four FES control strategies combined with active orthoses (SOUSA; FONSECA; BÓ, 2019), presented in Section 5.2.

5.1 SIMULATION ENVIRONMENT FOR FES GAIT

This work aims to provide a simulation environment to compare hybrid neuroprosthesis (HNP) controllers at low speeds. Some applications have produced hip extension through surface electrodes on the gluteus maximus muscles, e.g., in FES cycling (BÓ et al., 2017). Surface FES is unable to adequately recruit the hip flexors muscles (psoas major and iliacus muscle). Therefore, the system combines FES knee control with an active hip orthosis. Other works used a similar configuration, e.g., (OBINATA et al., 2007; KIRSCH et al., 2014; FARRIS et al., 2009; KOBETIC et al., 2009).

We implemented the FES gait in the Opensim platform, an open-source software that simulates highly detailed musculoskeletal models (DELP et al., 2007; HILL; B, 1938)[1]. The software provides kinematics and dynamics tools to understand and analyze motions. To implement FES gait in OpenSim, we require a musculoskeletal model containing the lower limbs and muscles (Section 5.1.1), as well as the active orthoses (Section 5.1.2). Figure 5.1 illustrates the resulting model developed for this study, presenting the active orthoses into the one leg OpenSim model[2].

---

[1] Developed in maintained in https://simtk.org/projects/opensim.
[2] It is being developed and maintained in https://simtk.org/projects/fes-gait.
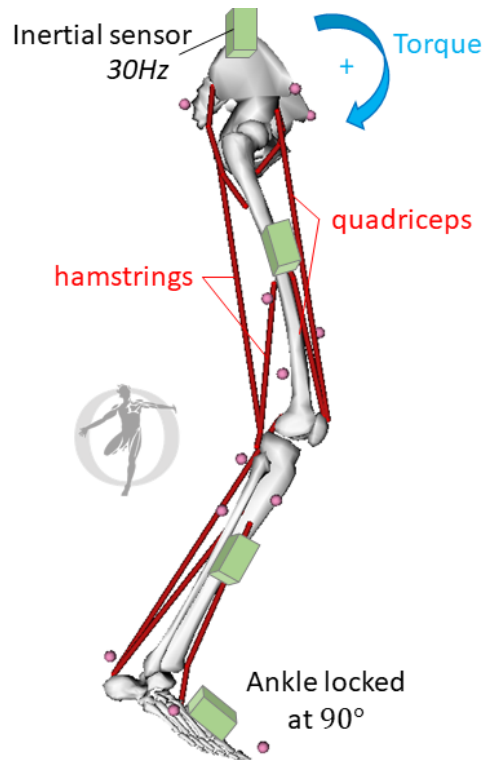
Figure 5.1: The complete model for knee FES control and hip orthosis control. Red lines represent the excitable quadriceps and hamstrings muscles. We locked the ankle joint at 90 degrees and let the hip runs freely through torque PID control, and knee, through FES PID control. Green cubes represent the inertial sensors (on the trunk, upper leg, lower leg, and foot).

Source: adapted from the figure prepared by the author for (SOUSA; FREIRE; BÓ, 2019).

5.1.1 One leg model

The one-leg design starts with a default OpenSim model[3]. We locked the pelvis translation and let hip and knee joints run free to simulate a person's gait. We also constrained the ankle at 90°, simulating the effect of a passive orthosis. This configuration represents a subject with SCI in weight support with contact forces from the treadmill during a gait training scenario. Table 5.1 shows the locked positions. Although limited, the simple model of the one-leg corresponds to rehabilitation scenarios where patients should perform single-joint exercises in function training since multi-joint exercises seem to favor specific muscle groups at the expense of others and lead to muscle imbalance and may cause a higher risk of a lower-body injury (BOUDVILLE et al., 2019).

State variables of the model are the hip and knee position and speed. Moreover,

---

[3] The simplified standard model for fast simulations is called *leg6dof9musc*, and is available at simtk-confluence.stanford.edu/display/OpenSim/Musculoskeletal+Models.

Table 5.1: Parameters of the locked degrees of freedom for FES gait.

DOF	Value
Pelvis x-axis	0 mm
Pelvis y-axis	0 mm
Ankle angle	90°

the available muscles in the model are hamstrings, vastus lateralis, biceps femoris, rectus femoris, gluteus maximus, iliopsoas, gastrocnemius, soleus, and tibialis anterior (cf. Table 2.1).. As we are not stimulating the ankle and trunk, we do not excite iliopsoas, gastrocnemius, soleus, and tibialis anterior. Note that vastus lateralis and biceps femoris form the quadriceps.

5.1.2 Active hip orthosis

It is also possible to simulate the mechanical orthosis by coupling objects to the lower limb model. However, for faster simulations, we decided to model the torque applied directly at the hip. This simplification requires less computational effort and leads to more precise results in OpenSim. The mechanical orthosis actuator performance is also out of the scope of this work; our primary focus is to discuss the FES controllers for repetitive gait movements.

Accordingly, we employed the OpenSim Torque Actuator API to add an external torque between the pelvis and the thigh. The actuator control signal u_a sets the torque magnitude of the active orthosis τ_a[4] as

$$\tau_a = 100u_a, \tag{5.1}$$

in which $0 < \tau_a < 1$. In this model, the maximum active orthosis torque is 100Nm, and the torque controller controls this torque intensity and direction, i.e., hip extension and flexion (blue arrow from Figure 5.1).

5.1.3 Muscle fatigue

Muscle fatigue is a temporary reduction in the capability of muscle to generate force. In this work, we simplified the fatigue model presented in (POTVIN; FUGLE-VAND, 2017) as a first-order model with a time constant F. At each sample time, we update the duration of activation t_{a_x} of each muscle ($x = \{QUAD, HAMS\}$) and calculate the level of fatigue of a specific muscle as

$$u_{fat_x} = 1 - e^{-t_{a_x}/F}. \tag{5.2}$$

---

[4]   When creating torques in OpenSim, we define a maximum value, in this case, 100Nm, and set a variable to represent the proportional magnitude [0,1].

Afterward, we calculate the actual excitation that OpenSim applies to each muscle

$$u_{f_x} = u_x - u_{fat_x}, \tag{5.3}$$

where u_x is the signal from the FES controller, in which x represents the muscle ($x = \{QUAD, HAMS\}$). This signal is saturated between the range $[0,1]$. Although the muscles are relieved and restore its capability of producing force after resting, we did not include this characteristic in this model. In this way, we may quickly visualize the effect of fatigue.

5.2 FES AND ACTIVE ORTHOSES GAIT CONTROL

To simulate the one-leg gait movement, we integrated the hip and knee joints with two independent tracking controllers. Therefore, we actuated the torque on the hip and excited the muscles to generate movement. We employed the PID controller for hip extension and flexion for the active hip orthosis. The knee angle position is controllable by an FES controller actuating on quadriceps to generate knee extension or on hamstrings to generate knee flexion. During gait, this integration should consider that different gait speeds generate different joint movement patterns. Also, the control architecture must combine actuators and FES, considering the specificities of the musculoskeletal system and even the complexity of gait.

Figure 5.2 illustrates the musculoskeletal dynamics, the predefined trajectories, and the chosen controllers. The control architecture is composed of: (1) a torque proportional-integral-derivative (PID) controller (Section 5.2.1) that represents an active orthosis to generate hip movement, and (2) an FES (2a) bang-bang (BB), an FES (2b) PID, an FES (2c) PID iterative learning (PID-ILC), or an FES (2d) PID tuning using extremum seeking (PID-ES) controller. Section 5.2.2 describes each of these four controllers and Section 5.2.3 describes the methods to measure joint movements and determine the predefined trajectories.

5.2.1 Active orthosis proportional-integral-derivative (PID) control

The PID controller manipulates the intensity of the active hip orthosis torque, tracking the hip trajectory. We parametrized the controller as

$$u_a = u_a(t), \tag{5.4}$$

in which $u_a(t)$ changes accordingly to the error

$$e_\alpha(t) = \alpha_{ref}(t) - \alpha(t) \tag{5.5}$$

and the cumulative error $\int_0^t e_\alpha(\tau)d\tau$ as

$$u_a = K_p e_\alpha(t) + K_i \int_0^t e_\alpha(\tau)d\tau + K_d \frac{de_\alpha(t)}{dt}, \forall t \geq 0. \tag{5.6}$$
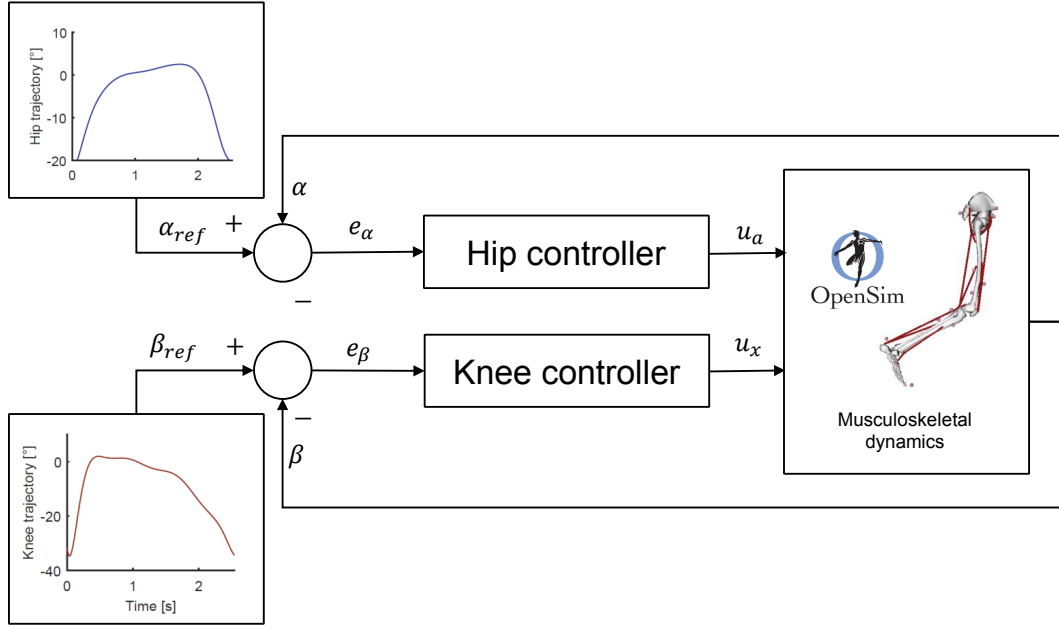
Figure 5.2: In this gait control architecture, the knee controller provides an excitation signal for the muscles u_x based on the error (e_β) between the reference knee joint angle β_{ref} and the measured angle β. The hip controller provides a signal u_a based on the error (e_α) between the reference hip joint angle α_{ref} and the measured angle α. Both controllers consider the predefined hip and knee trajectories. With the control signals (muscles excitation and torque), OpenSim calculates the musculoskeletal dynamics.

Source: adapted from the figure prepared by the author for (SOUSA; FREIRE; BÓ, 2019).

The active orthosis actuates on both directions. Therefore, a negative u_a indicates an counter-clockwise direction (cf. Figure 5.1).

5.2.2 FES control

For a forward dynamic simulation, the OpenSim Excitation Editor allows the specification of excitation patterns to muscles (excitation control signal: from 0 to 1). Therefore, we controlled the knee angle position by one of the FES controllers (described in Sections 5.2.2.1 to 5.2.2.4) actuating on the quadriceps to generate knee extension or on hamstrings to generate knee flexion. Moreover, OpenSim also simulates neuromuscular delays, the delay between a motor unit action potential, and the development of muscle force. Therefore, we use the reference knee position from the reference trajectory β_{ref} at the next iteration, as a correction factor.

5.2.2.1 Bang-bang (BB) controller

The BB controller manipulates the intensity of the quadriceps and hamstrings muscles with the control signal u_x ($x = \{QUAD, HAMS\}$), tracking the knee trajec-

tory. We parametrized the controller accordingly to the error

$$e_\beta = \beta_{ref} - \beta, \tag{5.7}$$

where β is the measured knee angle, and β_{ref} is the knee trajectory reference. The control signal for the quadriceps muscle is

$$u_{QUAD} = \begin{cases} h, & e_\beta > 0 \\ 0, & e_\beta \leq 0 \end{cases} \tag{5.8}$$

and the signal for the hamstrings muscle is

$$u_{HAMS} = \begin{cases} 0, & e_\beta > 0 \\ h, & e_\beta \leq 0 \end{cases}, \tag{5.9}$$

where h is the intensity of the muscle excitation ($[0,1]$).

5.2.2.2 Proportional-integral-derivative (PID) controller

The PID FES controller manipulates the intensity of the hamstrings and quadriceps excitation, tracking the knee trajectory. We parametrized the control signal u accordingly to the error e_β (Equation 5.7) as

$$u = K_p e_\beta(t) + K_i \int_0^t e_\beta(\tau)d\tau + K_d \frac{de_\beta(t)}{dt}, \forall t \geq 0. \tag{5.10}$$

To limit the number of parameters to be tuned, we simulated only the PI controller. Therefore, we set $K_d = 0$.

Then, the control signal for the quadriceps muscle is

$$u_{QUAD} = \begin{cases} u, & e_\beta > 0 \\ 0, & e_\beta \leq 0 \end{cases} \tag{5.11}$$

and the signal for the hamstrings muscle is

$$u_{HAMS} = \begin{cases} 0, & e_\beta > 0 \\ u, & e_\beta \leq 0 \end{cases}. \tag{5.12}$$

5.2.2.3 PID controller with iterative learning control (PID-ILC)

The ILC is a method of tracking control for systems that work in a repetitive mode (FREEMAN et al., 2012; PEDRO; SMITH, 2017). At each iteration i, the controller may improve the tracking accuracy learning the required input needed to track the reference accurately. Therefore, the system is consistently recording the control signals and errors in its memory. At each step j, the controller first calculates the PID control signal $u_{j_{PID}}$ as described in Equation 5.10.

Then, the system calculates the learning control signal as

$$u_{j_{ILC}} = u_{(j-1)} + e_{(j-1)} K_{ILC}, \qquad (5.13)$$

where $u_{(j-1)}$ and $e_{(j-1)}$ were the control signal and error from the previous step $(j-1)$, and K_{ILC} is a proportional gain.

The PID-ILC controller calculates the weighted average

$$u_j = u_{j_{PID}}(1-\gamma) + u_{j_{ILC}}(\gamma), \qquad (5.14)$$

where γ is the weight for each part of the controller. The control signal for the quadriceps and hamstrings muscles are calculated as Equations 5.11 and 5.12, respectively.

5.2.2.4   PID tuning using extremum seeking (ES)

Manual tuning of the controller parameters is difficult because the dynamics is nonlinear and has a high degree of inter-segmental coupling (DAVOODI; ANDREWS, 1999). To avoid this manual tuning of the PID parameters, we implemented the extremum seeking (ES) control similarly to (KILLINGSWORTH; KRSTIĆ, 2006; PAZ; OLIVEIRA, 2019), keeping the ES conventional with sinusoidal perturbations, not stochastic signals. This controller automatically tunes the PID parameters ($\boldsymbol{\theta}(t) = \{K_p, K_i, K_d\}$) based on perturbations on input control signal. For that, we assume that the output equilibrium map $u = f(\boldsymbol{\theta})$ has a maximum peak at $\boldsymbol{\theta} = \boldsymbol{\theta}^*$ (DAVOODI; ANDREWS, 1999).

Figure 5.3 represents the ES controller implemented to the gait simulations. We employ the sum of the estimated parameters with the slow periodic perturbation sinusoidal as inputs for the PID controller, i.e.,

$$\boldsymbol{\theta} = \hat{\boldsymbol{\theta}} + \boldsymbol{A}\sin(\boldsymbol{\omega}t + \boldsymbol{\Phi}), \qquad (5.15)$$

where $\boldsymbol{A} = \{A_{K_p}, A_{K_i}, A_{K_d}\}$, $\boldsymbol{\omega} = \{\omega_{K_p}, \omega_{K_i}, \omega_{K_d}\}$ and $\boldsymbol{\Phi} = \{\Phi_{K_p}, \Phi_{K_i}, \Phi_{K_d}\}$ are design parameters for the sinusoidal equation, and $\hat{\boldsymbol{\theta}}$ are the estimated parameters $\{\hat{K}_p, \hat{K}_i, \hat{K}_d\}$. When the perturbation is slow, the plant dynamics do not interfere with the peak seeking scheme (KRSTIĆ; WANG, 2000).
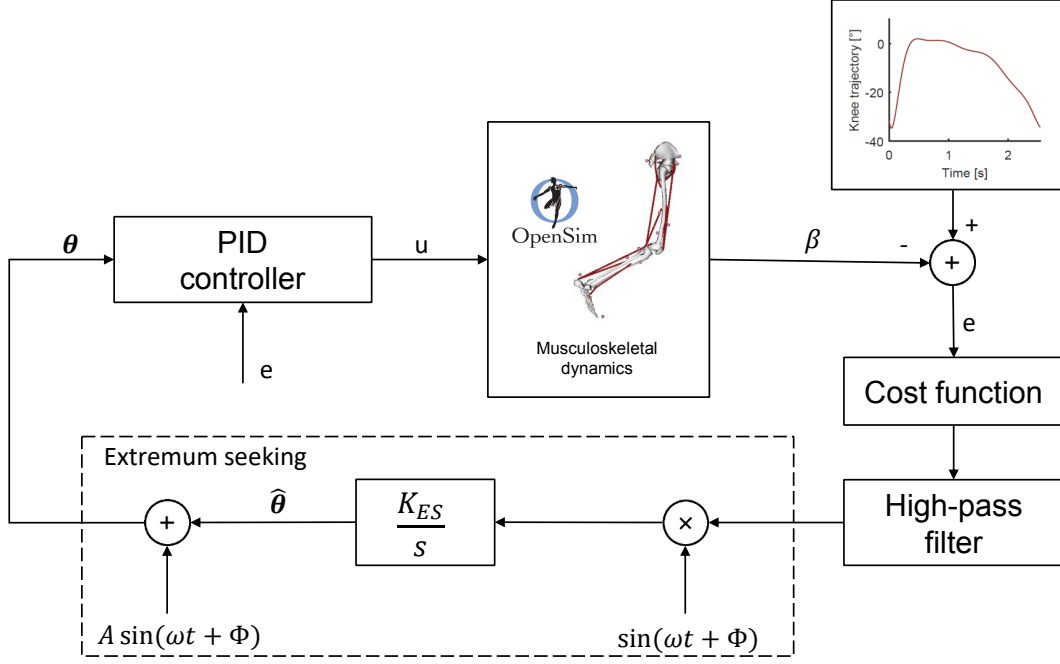
Figure 5.3: Detailed diagram of the closed-loop system for PID-ES.

Source: prepared by the author.

Similarly to (PAZ; OLIVEIRA, 2019), we calculate the cost function over the time interval $[t_0, T]$ of the error to estimate the parameters $\hat{\boldsymbol{\theta}}$ as

$$J(\boldsymbol{\theta}) = \frac{1}{T - T_0} \int_{t_0}^{T} e_\beta^2(t, \boldsymbol{\theta}) dt. \tag{5.16}$$

This equation quantifies the performance of the PID controller to reach the maximum $\boldsymbol{\theta}^*$

The high-pass filter (HP filter) - with a cut-off frequency of f_{HP} - eliminates the DC component from u and avoids high overshoots (KRSTIĆ; WANG, 2000). Thus, $A \sin(\boldsymbol{\omega} t + \boldsymbol{\Phi})$ and $s/(s + \omega_h)$ (HP filter) will be approximately two sinusoids, which are in phase for $\hat{\boldsymbol{\theta}} < \boldsymbol{\theta}^*$ and out of phase for $\hat{\boldsymbol{\theta}} > \boldsymbol{\theta}^*$.

In the either case, the product of the two sinusoids $(J(\boldsymbol{\theta})_{HP}$ and $\sin(\boldsymbol{\omega} t + \boldsymbol{\Phi}))$ will have a DC component, which is extracted by integrating these values with K_{ES}/s. To calculate the excitation u to be applied at the OpenSim model, the controller calculates the PID control signal u from $\boldsymbol{\theta}(t)$ as described in Equation 5.10 with the updated PID parameters $\hat{\theta}_i(k+1)$. The control signal for the quadriceps and hamstrings muscles are calculated as Equations 5.11 and 5.12, respectively.

5.2.3 Hip and knee trajectories for gait

For the kinematic gait trajectories, a volunteer walked on a treadmill (Jog Forma, Technogym, Italy) for 120 seconds at two speeds. For the first 60 seconds,

the treadmill maintained the slowest possible speed reported by the subject ($0.1\,m/s$), and, after, it maintained a conservative rehabilitation speed ($0.3\,m/s$). 3-space IMUs (described in Appendix A.5) measured the joint angles from the trunk, upper leg, lower leg, and foot (cf. Figure 5.1) at 15Hz. We chose these speeds because previous work (ODERBERK; INBAR, 1991) concluded that the measured angular trajectories are similar for different subjects but different for different walking speeds. They compared slow (0.2m/s) and average speed (0.8m/s) walking, concluding that the slow walking had a higher demand for stabilizing each separate phase of the walking cycle.

Before generating simulations, we imported the four-position datasets (trunk, hip, knee, and ankle angles) into an OpenSim model. OpenSim allows the visualization of musculoskeletal data or simulation results within the GUI. The volunteer reported struggle to maintain balance at $0.1\,m/s$, and we could visualize this in the OpenSim GUI, observing that the leg appears to be dragging the foot at this speed. Although this speed is not ideal, considering an SCI rehabilitation gait, the speed, and its struggles remain realistic for a rehabilitation scenario.

For each joint dataset, we also calculated polynomials approximation with an error-based filter and averages to create unique averaged regression functions (ROBBI et al., 2019). For both speeds, even at a low sample frequency and the dragging foot, the polynomials approximation was able to create the gait trajectories functions. These curves are the step trajectories to be followed by the controllers during gait. Figure 5.4 illustrates hip and knee trajectories for $0.1\,m/s$ $0.3\,m/s$ and shows the positive angular reference for knee and hip (yellow arrows).

5.2.4 Comparative studies on control strategies for FES gait

To compare the controllers applied to the gait simulation environment, we simulated different configurations for each FES controller. For all simulations, the final time T_f is ten times the gait period T_{step} ($T_{step} = 1.76s$ for $0.3\,m/s$ and $T_{step} = 2.54s$ for $0.1\,m/s$), the control frequency f is 50Hz, and the hip and knee joint initial position were the values at the start of the trajectories (to avoid high overshoots at the beginning of control).

To evaluate the controllers on similar conditions, we simulated each controller for both gait speeds g_s ($0.1\,m/s$ and $0.3\,m/s$). Furthermore, we simulated these systems with and without the effect of fatigue. Table 5.2 summarizes all 32 simulations initial parameters (4 controllers, 2 gait speeds, and 4 fatigue time constants).

To evaluate the results, we plotted the hip and knee tracking trajectories results over time, and calculated performance parameters: standard deviation of the knee error (σ_β), maximum knee error (e_{max_β}) and Pearson correlation coefficient ($corr_\beta$).
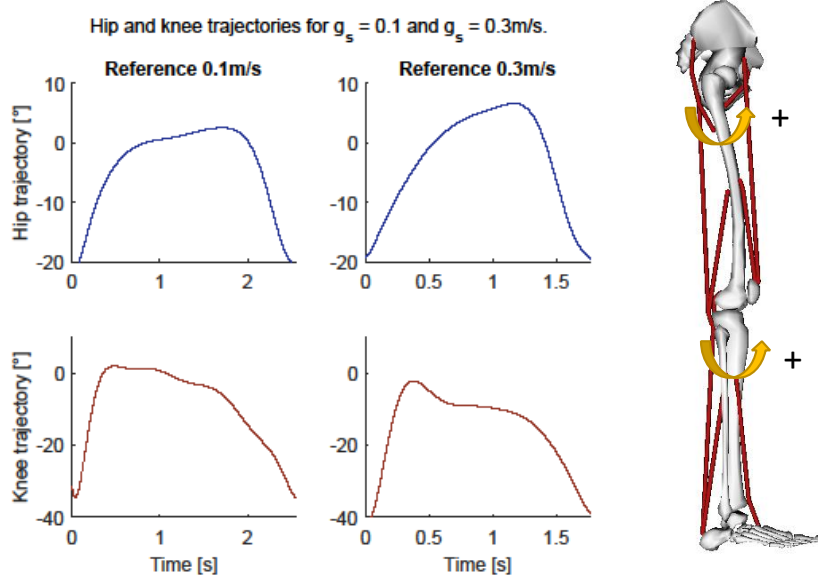
Figure 5.4: Hip and knee reference trajectories for $0.1\,m/s$ and $0.3\,m/s$. At right, the model also illustrates the angular references.

Source: prepared by the author.

Table 5.2: Initial parameters for the different configurations for simulating the BB controller.

Controller	g_s [m/s]	F
BB, PID, PID-ILC, PID-ES	$\{0.1, 0.3\}$	$\{\infty, 1250, 312.5, 78.125\}$

5.2.4.1 Controller parameters

Before starting simulations, the system requires the definition of each controller specific parameters:

- BB: h (1 parameter);

- PID: K_p, K_i and K_d (3 parameters);

- PID-ILC: K_p, K_i, K_d, γ and K_{ILC} (5 parameters);

- PID-ES: K_p, K_i, K_d, f_{HP}, A, ω, Φ and K_{ES} (7 parameters).

It should be noted that parameters optimization is out of the scope of this document. We decided to implement basic steps to define all initial parameters to keep the results consistent:

1. Set $K_p = K_i = K_d = 0$ and manually adjust the ES parameters f'_{HP}, A', ω', Φ' and K'_{ES} to simulate 5 steps of the gait trajectory with $g_s = 0.1$ m/s.

77

2. For BB, calculate the average excitation of both muscles during the last step of simulation and set h as this result.

3. For PID, PID-ILC and PID-ES, set K_p, K_i and K_d (for PID and PID-ILC) as the final adjustment of the ES at the last step of simulation.

4. For PID-ILC, set $K_{ILC} = 2K_p$ and manually adjust K_{ILC}.

5. For PID-ES, set $f_{HP} = f'_{HP}/10$, $A = K'_p/10$, $\omega = 1.6\omega'$, $\Phi = \Phi'$ and $K_{ES} = K'_{ES}$.

Figure 5.5 shows the results for the 5-steps simulations with the ES controller. We set the PID parameters $K_p = K_i = K_d = 0$, and $f'_{HP} = 0.0080$, $A' = 0.0120$, $\omega' = 8$, $\Phi' = 0$ and $K'_{ES} = 400$. For the parameters K_i and K_d, we also adjusted A', ω' and Φ' to guarantee that the values are lower and the perturbation is out of phase with each other. The system has not yet converged, but the knee already has enough torque to perform movement. The Pearson correlation at the fifth step was 0.8830. With these results, Table 5.3 presents the initial parameters for all controllers.
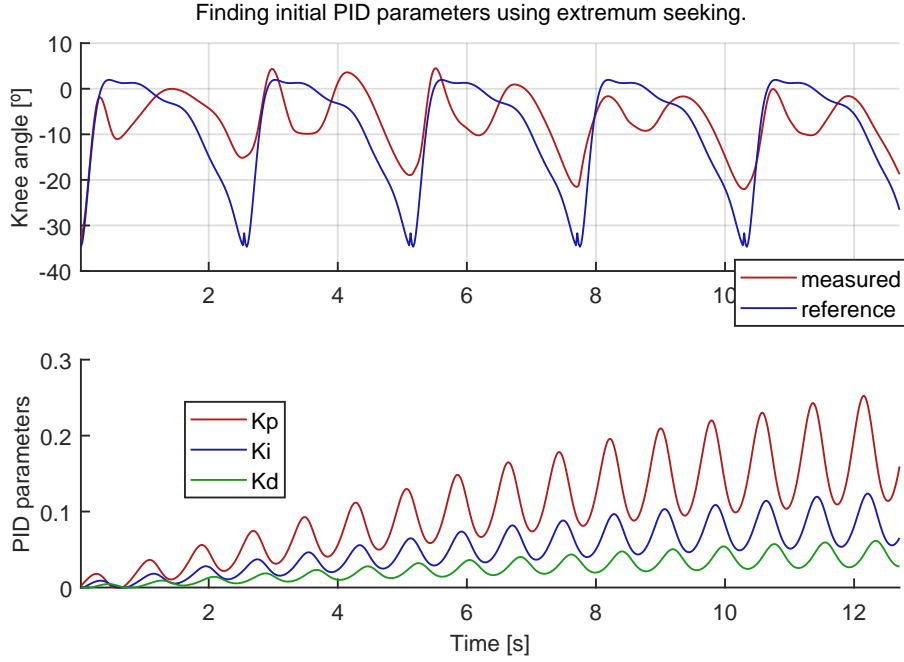
Figure 5.5: Simulation to define the initial parameters of the controllers. We simulated five steps using the extremum seeking with $K_p = K_i = K_d = 0$.

Source: prepared by the author.

Table 5.3: Initial parameters for all controllers.

Controller	Parameters
BB	$h = 0.0148$
PID	$K_p = 0.1488$, $K_i = 0.0619$, $K_d = 0.0289$
PID-ILC	$K_p = 0.1488$, $K_i = 0.0619$, $K_d = 0.0289$, $K_{ILC} = 0.2976$, $\gamma = 0.2$
PID-ES	$K_p = 0.1488$, $K_i = 0.0619$, $K_d = 0.0289$, $f_{HP} = 0.00080$, $A = 0.01488$, $\omega = 16$, $\Phi = 0$, $K_{ES} = 400$

5.2.4.2 Results

Figures 5.6 and 5.7 present the knee trajectory simulations without the effect of the fatigue for each controller, while Figures 5.8 and 5.9 present the results with the fatigue constant $F = 78.125$. In most configurations, the system was able to simulate the knee movement similar to the desired trajectory, especially for the gait speed $g_s = 0.3m/s$. However, the controllers presented lower correlations at the slowest speed, probably due to the lack of inertia during movement, which was a similar condition reported by the volunteer without disability. Figure 5.8 shows that the muscles reached a point of complete fatigue, not contributing to the movement at the configuration $F = 78.125$ and $g_s = 0.1m/s$. The knee trajectory movement was passive and caused

79

by the orthosis actuation on the hip. Appendix D presents the trajectory simulations with the effect of the other fatigue (Figures D.1 to D.4).
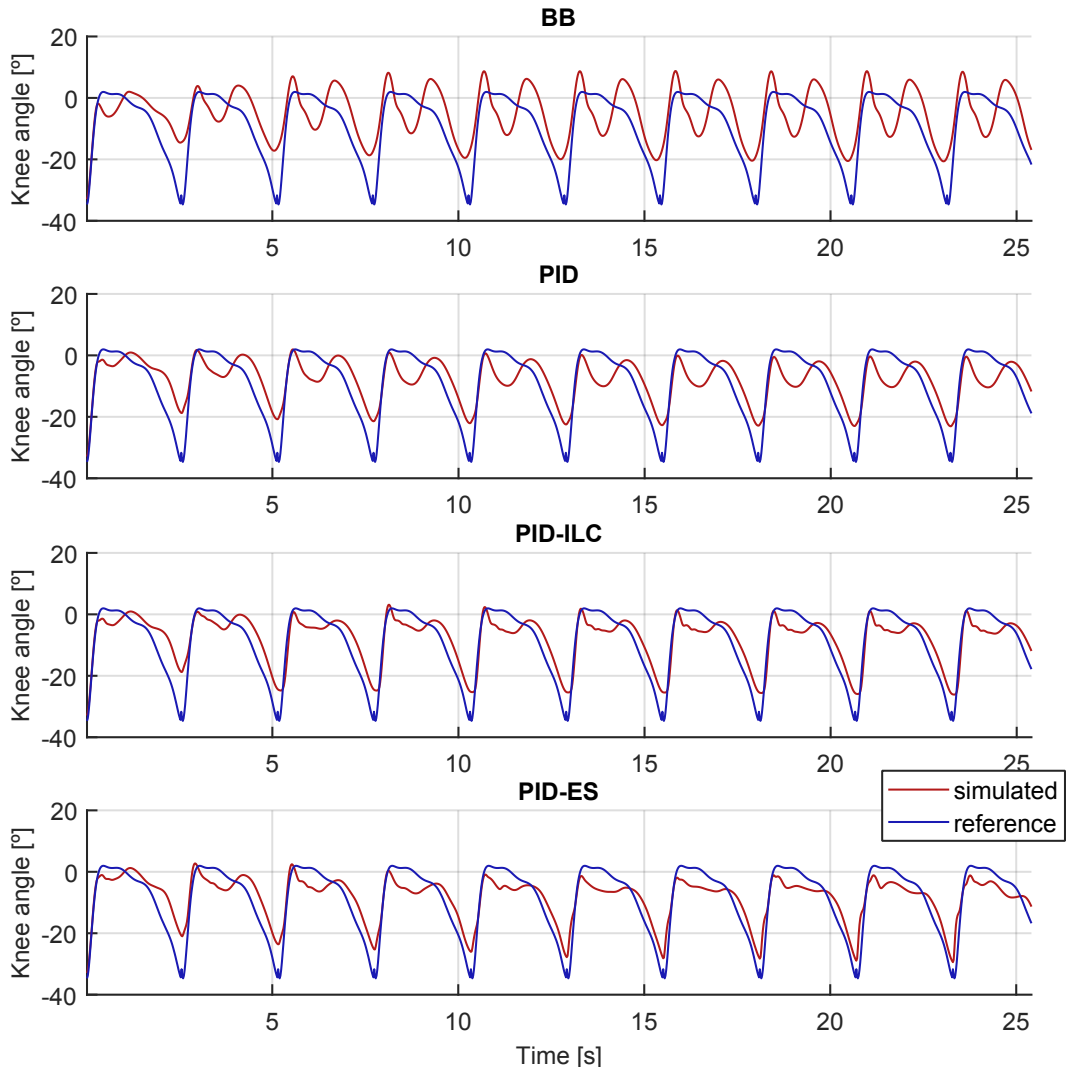
Figure 5.6: Knee trajectory through 10-gait steps of the four controllers for the gait speed $g_s = 0.1 m/s$. In this simulation, there is no effect of fatigue.

Source: prepared by the author.
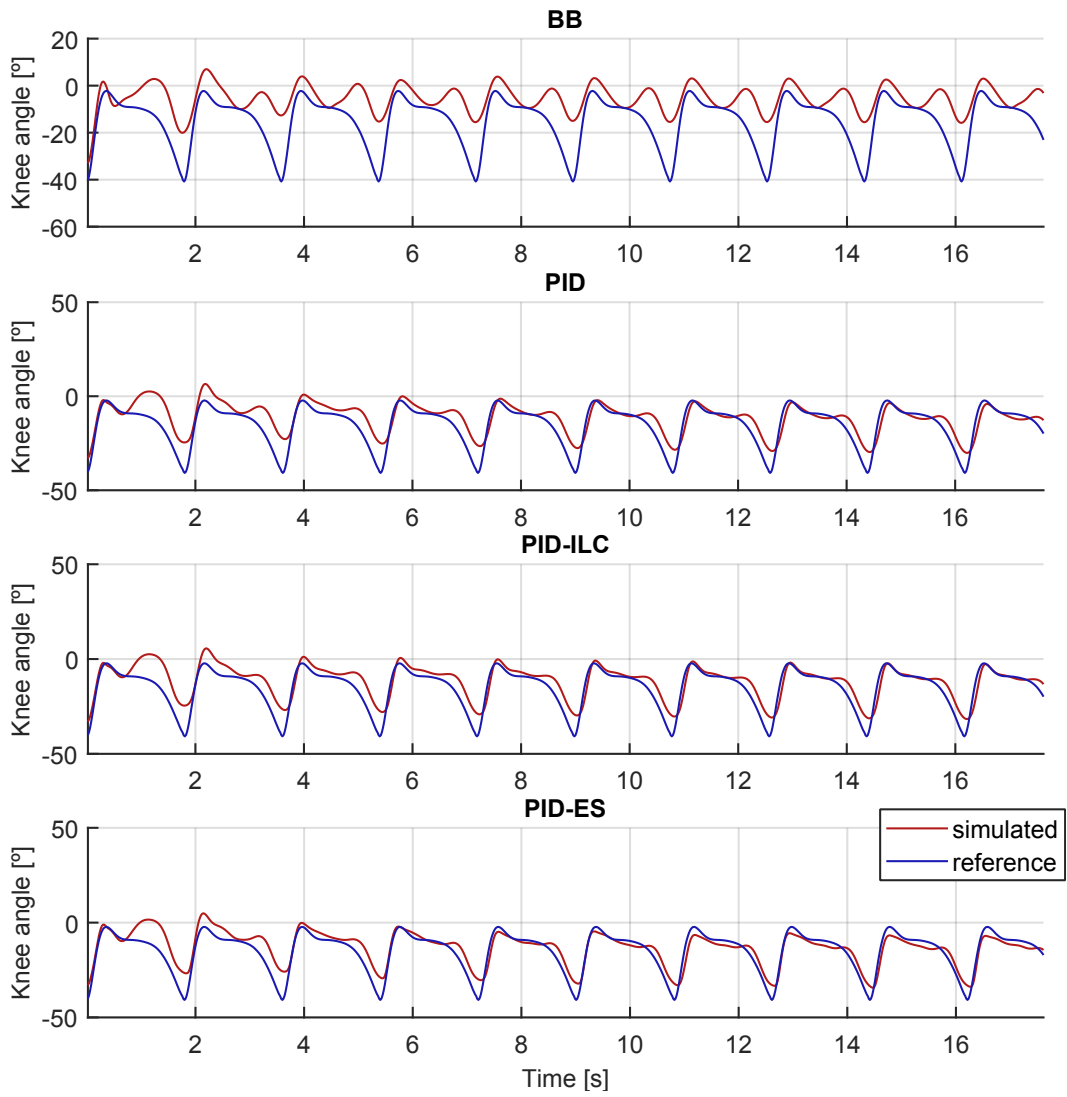
Figure 5.7: Knee trajectory through 10-gait steps of the four controllers for the gait speed $g_s = 0.3 m/s$. In this simulation, there is no effect of fatigue.

Source: prepared by the author.
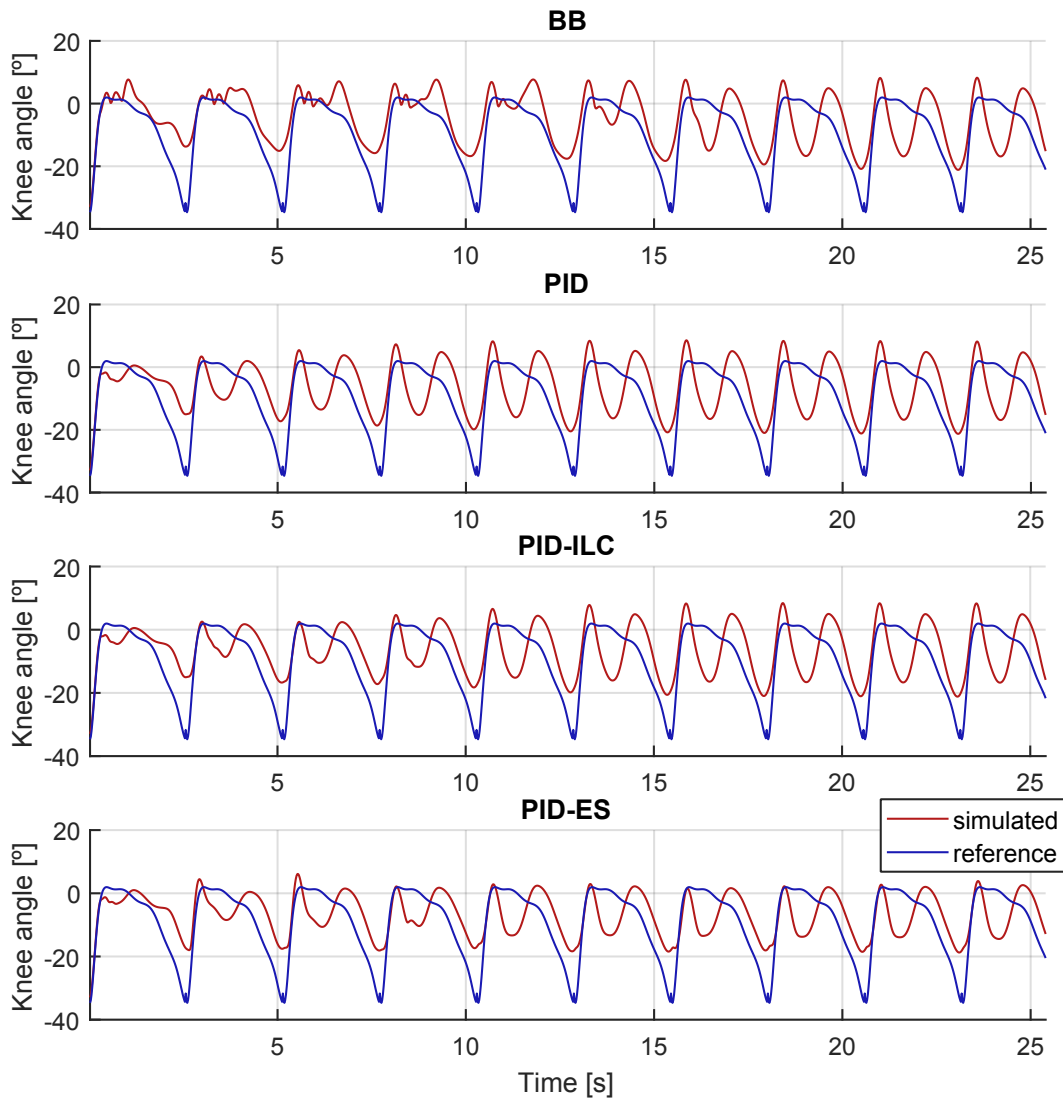
Figure 5.8: Knee trajectory through 10-gait steps of the four controllers for the gait speed $g_s = 0.1m/s$. In this simulation, the fatigue constant was $F = 78$, we may observe the fatigue on, e.g., step 7 for the BB control.

Source: prepared by the author.
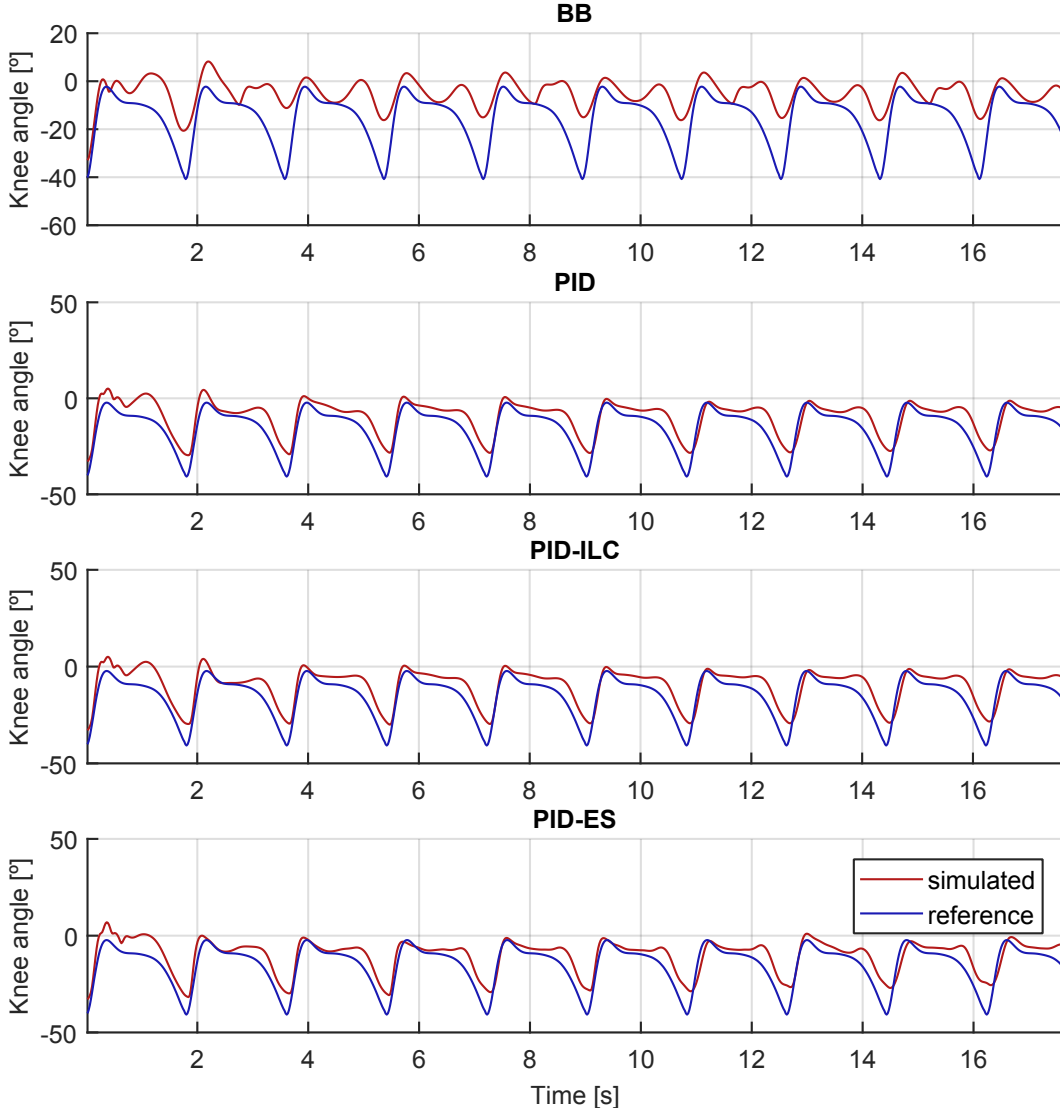
Figure 5.9: Knee trajectory through 10-gait steps of the four controllers for the gait speed $g_s = 0.3m/s$. In this simulation, the fatigue constant was $F = 78$.

Source: prepared by the author.

5.2.5 Discussion

After calculating the Pearson correlation coefficient at each step for all simulations, we plotted the results at Figure 5.10. Each subplot presents correlations for the four controllers at each step (from 1 to 10). The first column (left) presents the configurations with the slow speed ($g_s = 0.1m/s$), and the second column (right) presents the configurations with the faster speed. Each of the four lines presents results for each fatigue constant, respectively $F = 0$, $F = 1250$, $F = 312.5$ and $F = 78.125$ for lines 1 to 4. Similarly, we plotted the maximum error and the standard deviation calculatios in Figures 5.11 and 5.12. Appendix D presents Tables D.1 and D.2, in which we show $corr_\beta$, e_{max_β} and σ_β at the last step.
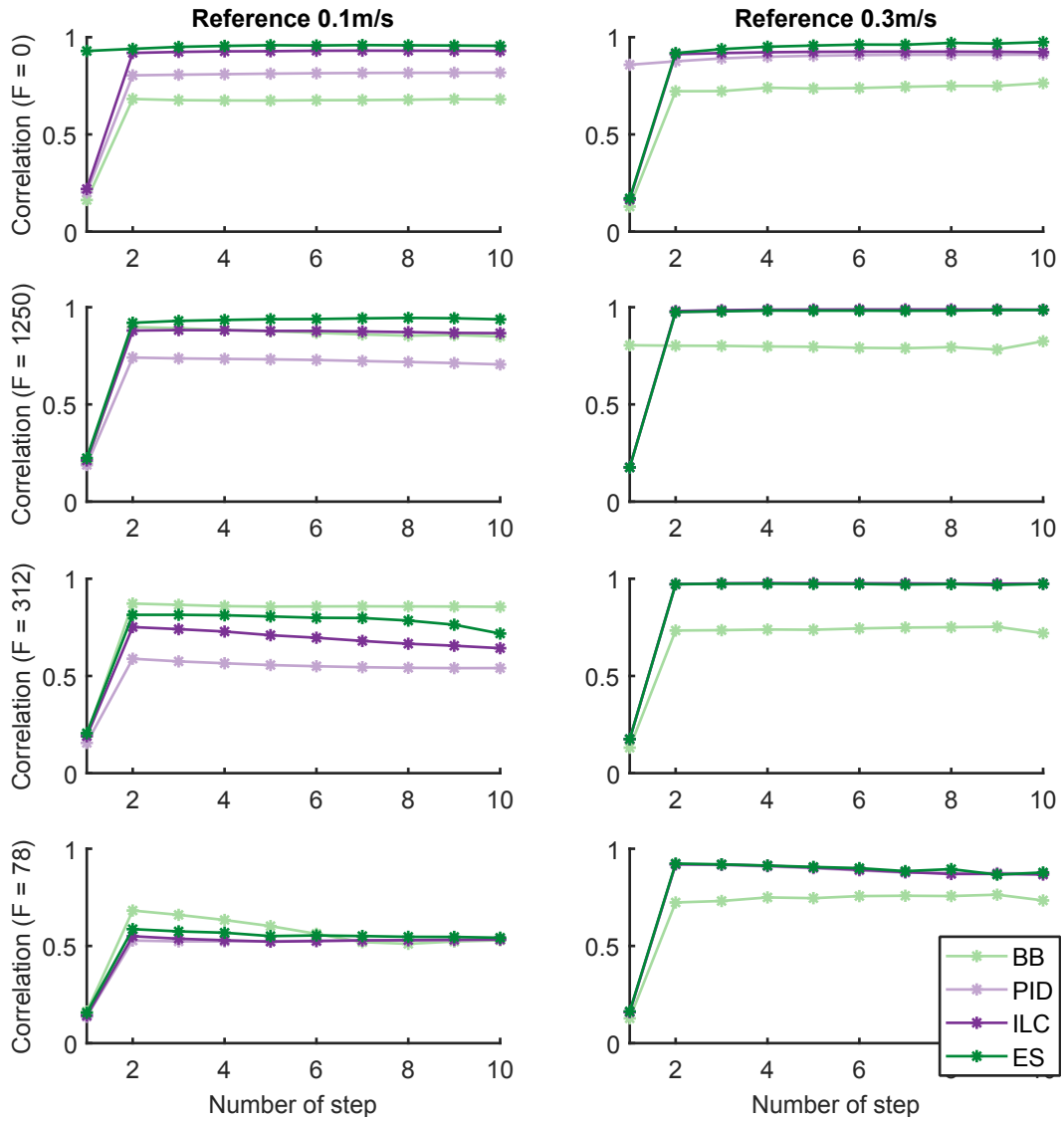
Figure 5.10: Pearson correlation coefficients at each of the 10 steps simulated for each controller. At left we present the results for $g_s = 0.1m/s$, and at right, for $g_s = 0.3m/s$. Each line shows the results for the fatigue constant ($F = 0$, $F = 1250$, $F = 312.5$ and $F = 78.125$).

Source: prepared by the author.
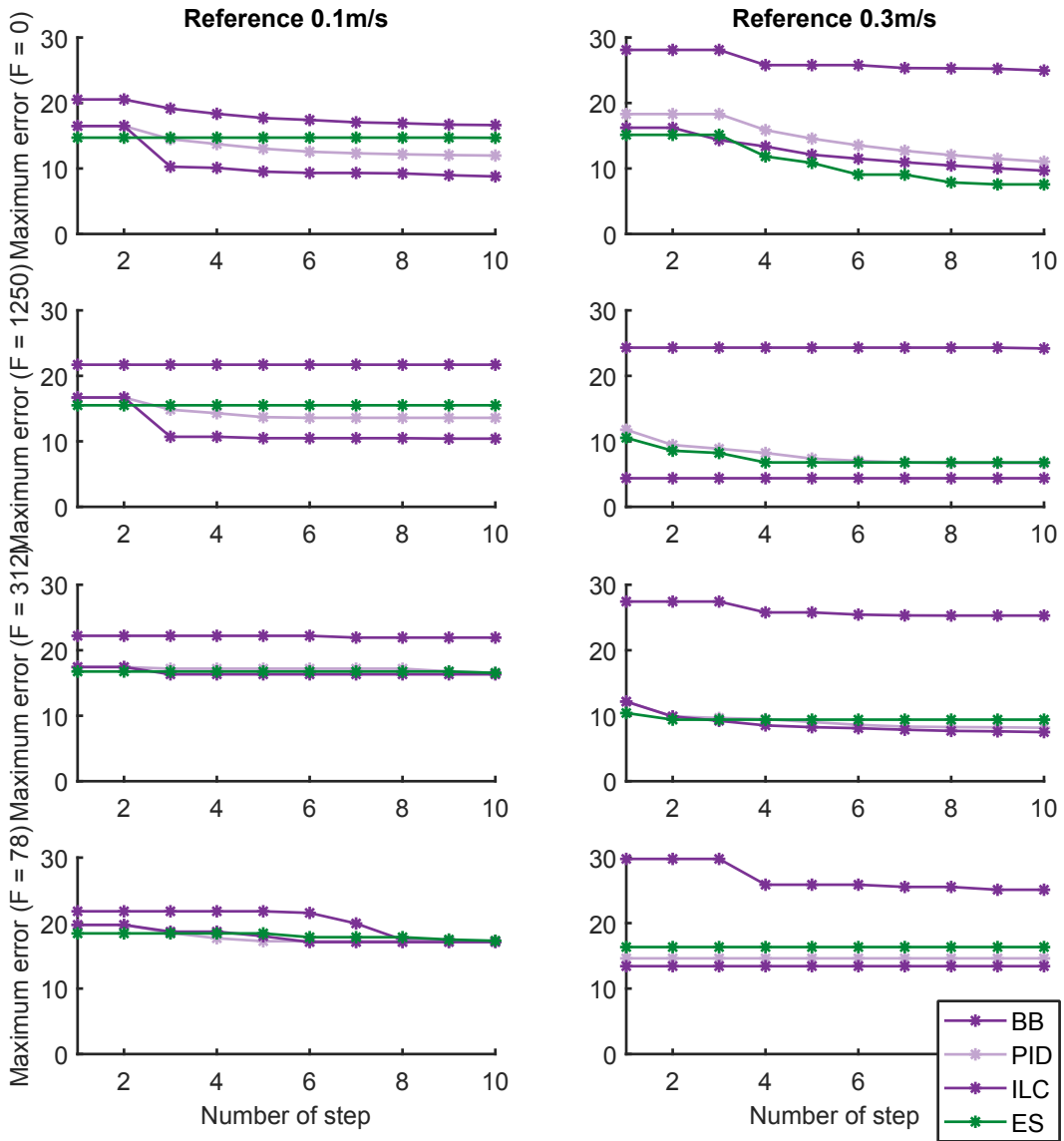
Figure 5.11: Maximum absolute errors at each of the 10 steps simulated for each controller. At left we present the results for $g_s = 0.1m/s$, and at right, for $g_s = 0.3m/s$. Each line shows the results for the fatigue constant ($F = 0$, $F = 1250$, $F = 312.5$ and $F = 78.125$).

Source: prepared by the author.
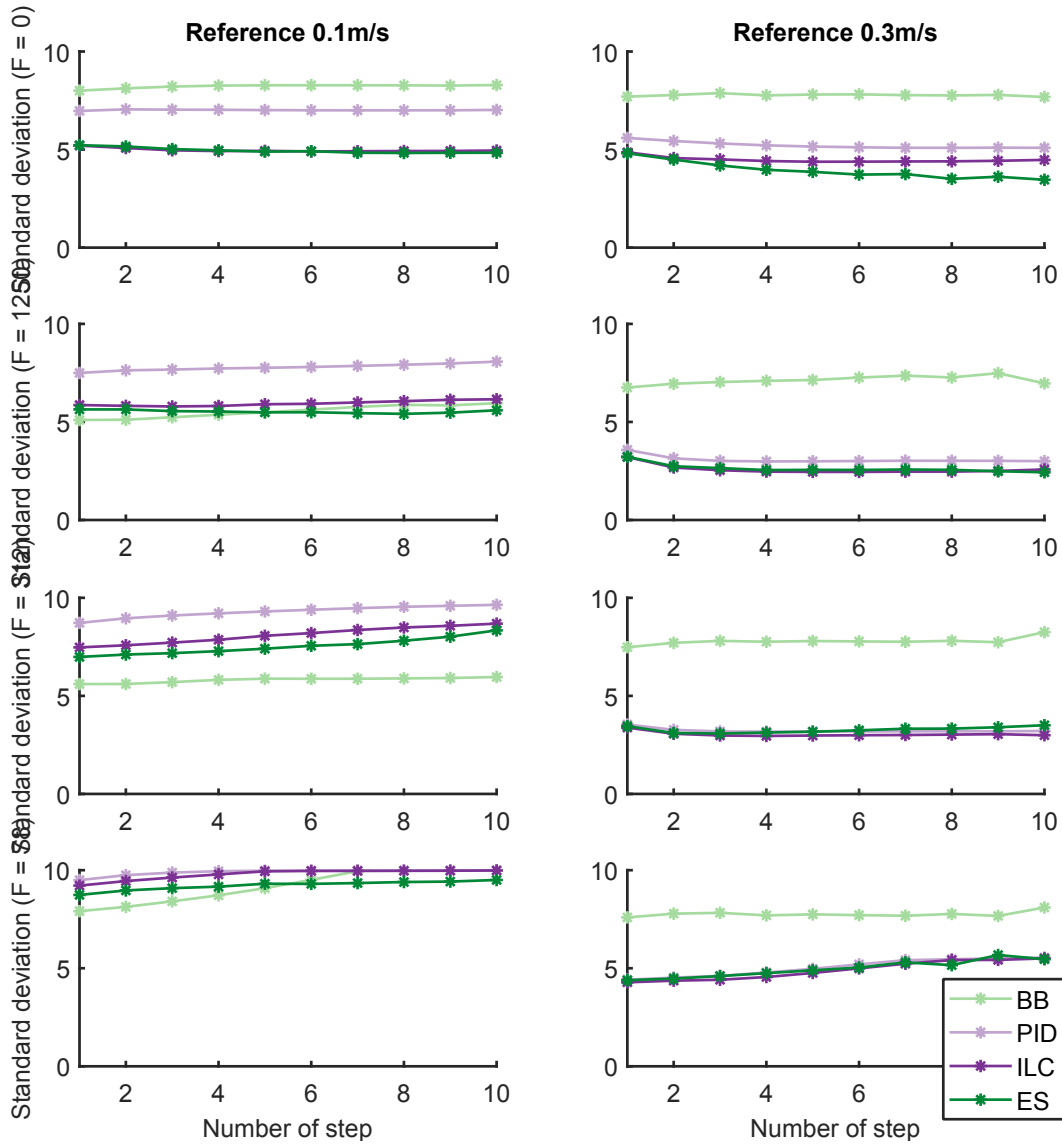
Figure 5.12: Standard deviation errors at each of the 10 steps simulated for each controller. At left we present the results for $g_s = 0.1m/s$, and at right, for $g_s = 0.3m/s$. Each line shows the results for the fatigue constant ($F = 0$, $F = 1250$, $F = 312.5$ and $F = 78.125$).

Source: prepared by the author.

For both speeds, the knee flexes while the hip extends (i.e., the knee pushes against the hip) because the hamstrings constitute of a biarticular muscle-group which limits the hip flexion, and OpenSim simulates this muscle nature. Without any external observer of the musculoskeletal model (i.e., modeling this particular state and redesigning the controller), the controllers are unable to fully keep the trajectory with this perturbation, which justifies the permanent error between the reference and the measured trajectory even in the higher correlation results (e.g., Figure 5.6 at lower peaks), similarly to the observations from (KAWAI; EJIRI; KAWAI, 2015).

In FES, there are additional problems with delivering consistent stimulation energy to the muscle due to a variety of factors, including muscle fatigue (SHARMA et al., 2009). The results show that, without fatigue, the correlations were usually higher, as there is no reduction in efficiency. For $g_s = 0.1m/s$, the correlation stayed constant at the last cycles and with $g_s = 0.3m/s$, it remained either constant or slightly higher for the four controllers. At $g_s = 0.1m/s$, the controllers reached steady states faster due to the parameters found in Section 5.2.4, also indicated by the maximum and standard errors decrease. When added the effect of fatigue (specifically for $F = 312.5$ and $F = 78.125$), the results tend to present lower correlation coefficients, and higher errors as the muscles provide less torque when fatigated, a result expected due to the loss of efficiency.

As an alternative visualization of the overall performance of the controllers, we averaged all correlations, standard deviations, and maximum errors of the last steps (values presented in Tables D.1 and D.2) for both speeds (i.e., there are 16 values for each speed). Since the correlation is a result that, by definition, ranges from 0 to 1, we considered these as final results (Table 5.4), and we plot them at Figures 5.13(a) and 5.13(b). For the correlation, 1 means the highest possible correlation (a perfect performance or the reference). For the maximum errors and standard deviations, we normalized these values related to the higher result given at Tables D.1 and D.2 (i.e., maximum error, 25.09, and standard deviation, 10.03). Consequently, these results range from 0 to 1; however, 0 means lower errors (better performance), and 1 means higher errors (worst performance). To keep the same pattern as the correlation, we decreased these values by 1 and plotted them at Figures 5.13(a) and 5.13(b) (values from Adjust from Tables 5.5 and 5.6). Therefore, the final plots illustrate more high-grade performances (higher correlation, and lower standard deviation and maximum errors) as far as possible from the center of the circle.

Table 5.4: Mean correlation ($corr_\beta$) results at the last step for $g_s = 0.1m/s$ and $g_s = 0.3m/s$.

	$0.1m/s$	$0.3m/s$
Controller	Mean	Mean
BB	0.73	0.74
PID	0.65	0.94
PID-ILC	0.74	0.94
PID-ES	0.79	0.95

As previously repported (VELTINK, 1991), the BB controller presented low correlation coefficients and high errors when compared to other controllers. As the controller does not adjust the magnitude of excitation, the muscles also fatigue faster. The lack of error quantification may cause high overshoots, decreasing the correlation

Table 5.5: Mean maximum error (e_{max_β}) results, normalization and adjustments at the last step for $g_s = 0.1m/s$ and $g_s = 0.3m/s$.

| Controller | 0.1m/s | | | 0.3m/s | | |
	Mean	Norm	Adjust (1-norm)	Mean	Norm	Adjust (1-norm)
BB	19.37	0.77	0.23	22.80	0.91	0.09
PID	14.84	0.59	0.41	10.13	0.40	0.60
PID-ILC	13.16	0.52	0.48	13.16	0.52	0.65
PID-ES	16.01	0.64	0.36	8.74	0.35	0.53

Table 5.6: Mean standard deviation (σ_β) results, normalization and adjustments at the last step for $g_s = 0.1m/s$ and $g_s = 0.3m/s$.

| Controller | 0.1m/s | | | 0.3m/s | | |
	Mean	Norm	Adjust (1-norm)	Mean	Norm	Adjust (1-norm)
BB	7.56	0.75	0.25	7.90	0.79	0.21
PID	8.68	0.87	0.14	4.21	0.42	0.58
PID-ILC	7.45	0.74	0.26	7.45	0.74	0.26
PID-ES	7.07	0.70	0.30	3.89	0.39	0.61
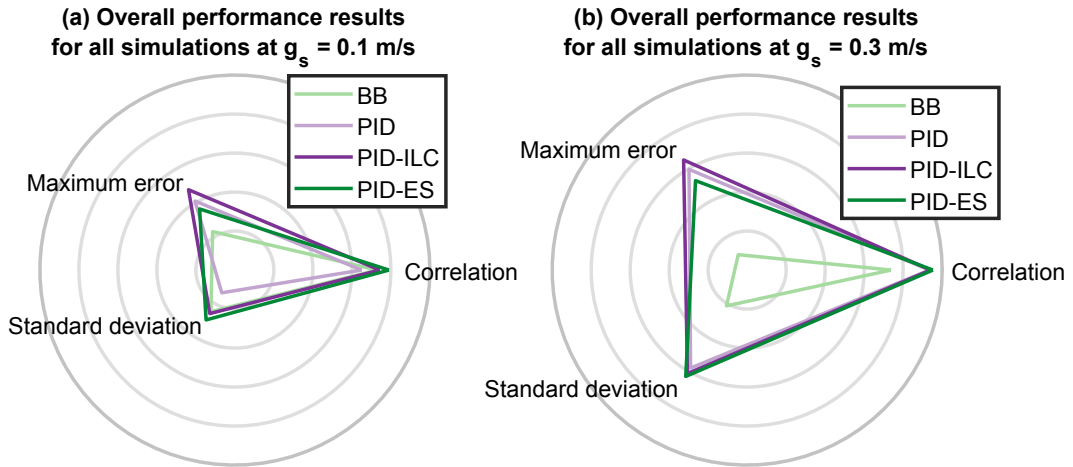
Figure 5.13: Avaliation of the controllers (BB, PID, PID-ILC, PID-ES) performace. These polar plots show the mean maximum error, mean standard deviation and mean correlation results of all simulations at (a) $g_s = 0.1m/s$ and (b) $g_s = 0.3m/s$. Higher results (outside of the circle) presented better performance.

Source: prepared by the author.

between the reference and actual movement. The only configuration that presented better results (when compared to other controllers) was $F = 312.5$ and $g_s = 0.1$, at this configuration, the initial PID parameters probably required a more refined tuning. In a real scenario, the BB controller could lead the system to unstable responses,

which may be dangerous for a subject without SCI. When compared to BB, the PID control presented a high correlation at the last step (> 0.9) to the reference in several conditions. Nevertheless, for lower speeds, PID control presented inadequate response even in a scenario without fatigue (0.82 correlation). These results match the previous claim that PID control is not good enough in FES applications due to the non-linearities of physiological based muscle behavior (POPOVIĆ; MALEŠEVIĆ, 2009).

In some configurations, especially for $g_s = 0.1m/s$, there is an improvement between correlation coefficients of the PID controller and the PID-ILC and PID-ES. PID-ILC and PID-ES controllers maintained higher coefficients and lower errors through steps. Except for the maximum error for $g_s = 0.3m/s$, results between PID, PID-ILC, and PID-ES are similar, yet, PID-ILC and PID-ES still maintained a slightly lower maximum and standard deviation errors. Moreover, observing only the PID-ILC and PID-ES results, the PID-ES presented slightly higher correlation coefficients and lower maximum and standard deviation errors. Further, even with slightly better performance, we should note that the chattering effect presented in the ES control is undesirable because it can excite unmodeled and high-frequency plant dynamics in experiments with subjects, as already mentioned for the sliding mode controller from (AJOUDANI; ERFANIAN, 2007).

6 SIMULATION STUDIES ON CONTROL STRATEGIES FOR FES CYCLING

FES cycling training presents some advantages for individuals with SCI, such as enhancement of muscle strength, the decrease of bone loss, cardiovascular and respiratory improvement, and quality of life (POPOVIĆ; SINKJÆR, 2000). The international community considers FES cycling so relevant that one of the disciplines in the Cybathlon competition was the FES bike race(COSTE; WOLF, 2018). Our group at the University of Brasilia, the Empowering Mobility and Autonomy (EMA), also holds extensive experience with FES cycling control, participating in the first edition of the competition in 2016 (BÓ et al., 2017).

As the accelerated fatigue generated by FES limits the duration of experiments, we developed the simulation environment for cycling (SOUSA et al., 2016), presented in Section 6.1[1]. In this environment, we studied control strategies with and without passive orthoses assistance to the model (Sections 6.2 and 6.3).

We must emphasize that each cycling geometry and muscle torques would lead to different nominal results, and we did not evaluate the optimal muscle ranges for our system. Therefore, the actual values in which the orthoses may only be able to assist the system would be dependent on the musculoskeletal, geometrical, and dynamic systems. The biomechanical evaluation is extensive and out of the scope of this thesis.

6.1 SIMULATION ENVIRONMENT FOR FES CYCLING

In our work, we intend to generate movement from joint excitation control. Towards a similar solution to ours, OpenSim provides an education teaching material for cycling. The goal is to create an interactive biomechanics teaching tool that allows students to examine how muscle excitation impact speed[2]. The ergometer however, is upright, nor recumbent.

The environment is similar to the work we present in Chapter 5. To implement FES cycling in OpenSim, we need a musculoskeletal model containing the lower limbs and muscles (Section 6.1.1), as well as its mechanical coupling with pedals and crankset (Section 6.1.2). Figure 6.1 illustrates the resulting model developed for this study, in which we attached a standard OpenSim lower limbs model to the foot support with

---

[1] It is being developed and maintained in `https://simtk.org/projects/fes-cycling`.
[2] OpenSim Teaching Materials – Educational Cycling Model: `https://simtk-confluence.stanford.edu:8443/display/OpenSim/OpenSim+Teaching+Materials+--+Educational+Cycling+Model`.

pedals and crankset[3].
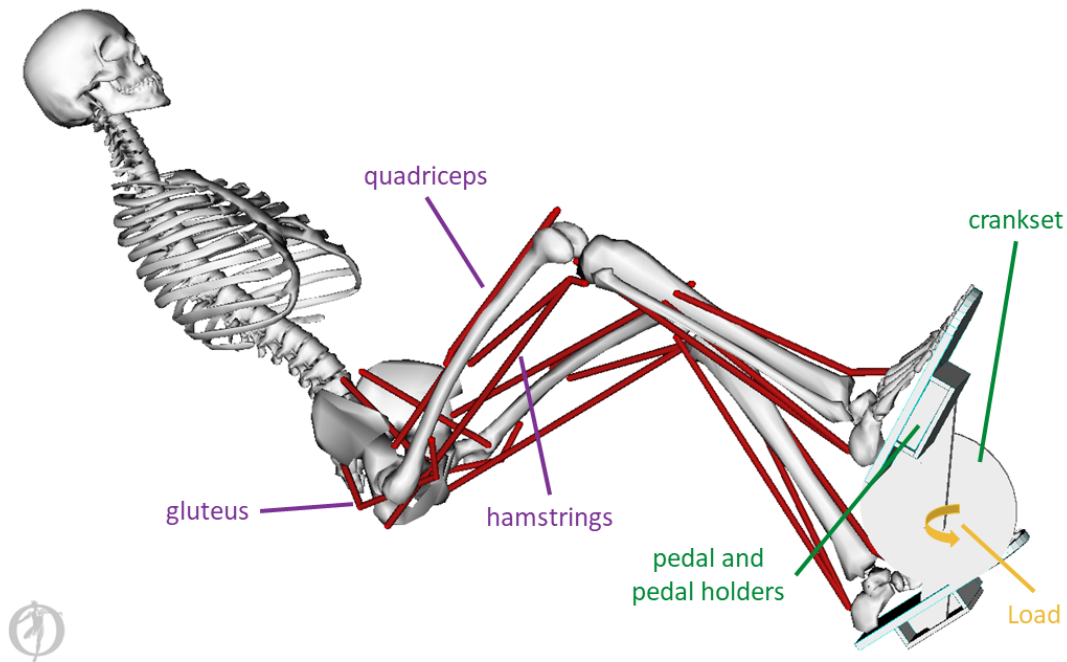
Figure 6.1: Model description for FES cycling similar to the EMA Trike. OpenSim represents muscles (e.g., quadriceps, hamstrings, and gluteus) as red lines. We developed the foot support with pedals and crankset, in which we also included a torque to simulate a crankset load.

Source: adapted from the figure prepared by the author for (SOUSA et al., 2016).

6.1.1 Lower limbs model

The lower limbs design started with a default OpenSim model simplified for fast simulations[4]. We locked lumbar, pelvis and ankles movements and let hips and knees run freely to simulate a person riding a bicycle. Table 6.1 presents the locked positions based on the EMA Trike (BÓ et al., 2017). State variables of the model are the position, speed, and force from hips, knees, crankset, and pedals. Besides, the available muscles in the model are hamstrings, vastus laterali, biceps femoris, rectus femoris, gluteus maximus, iliopsoas, gastrocnemius, soleus and tibialis anterior (cf. Table 2.1). We kept excitation to just muscles on the tights, excluding iliopsoas, gastrocnemius, soleus, and tibialis anterior. Note that vastus laterali and biceps femoris form the quadriceps.

6.1.2 Foot support with pedal and crankset

As there was no promptly available model within OpenSim database for cycling, we designed the mechanical coupling with pedals and crankset. Using the free software

---

[3] It is being developed and maintained in `https://simtk.org/projects/fes-cycling`.
[4] The simplified standard model for fast simulations is called *gait10dof18musc*, and is available at `https://simtk-confluence.stanford.edu/display/OpenSim/Musculoskeletal+Models`.

Table 6.1: Parameters of the locked degrees of freedom for FES cycling.

DOF	Value
Pelvis tilt	45°
Pelvis x-axis	$0\,mm$
Pelvis y-axis	$0\,mm$
Right ankle angle	0°
Left ankle angle	0°
Lumbar extension tilt	0°

Blender, we added to the lower limb model, a *drivetrain* and two *foot supports*. We divided the drivetrain into *crankset* and *pedals*. The crankset can only rotate in the sagittal plane, and cannot move in translation. We attached each pedal to the crankset at the end of the crank arms, allowing rotation along the axes perpendicular to the crank arms. The foot support immobilizes the ankles and connects the foot to the pedals through a box that accommodates the pedal. Consequently, the foot support transfers the force to the pedal using contact geometries (physical shapes that allow collisions in OpenSim). Figures 6.1 and 6.2 illustrate the resulting model developed for this study, in which we attached the lower limbs to the foot support.
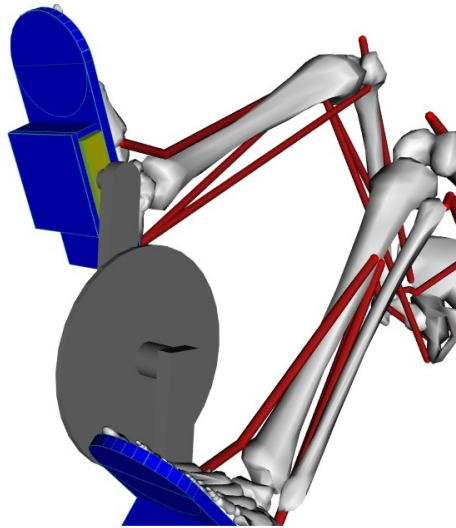
Figure 6.2: Detail from the complete model focused at the foot support with pedal and crankset for FES cycling.

Source: prepared by the author for (SOUSA et al., 2016).

6.1.3 Load at the crankset

During cycling, the ground forms an opposite equal counter-clockwise force allowing for the bicycle to enter forward motion. Therefore, the energy from the bicycle

wheel converts into kinetic energy of the bicycle motion. As well, we lose energy in different forms, thermic, sound, friction, air resistance, and even mechanical structures of the bicycle. Therefore, we modeled a load at the crankset to simulate some of these disturbances. The load acts as a torque in the opposite direction of the movement τ_{load}, i.e., resisting the movement. The torque magnitude τ_{load} [Nm] is set by the variable L[5] as

$$\tau_{load} = \begin{cases} -100L, & \dot{\theta}_c \geq 0 \\ 0, & \dot{\theta}_c < 0, \end{cases} \tag{6.1}$$

where $\dot{\theta}_c$ is the cycling cadence, calculated by the differentiation of the crankset angle during the time.

6.1.4 Muscle fatigue

Muscle fatigue is a temporary reduction in the capability of muscle to generate force. It remains relevant to consider the physiological properties of motor units when attempting to understand and predict muscle fatigue. However, as this topic is out of the scope of this thesis, we simplified the fatigue model presented in (POTVIN; FU-GLEVAND, 2017) as a first-order model with a time constant F. At each sample time, we update the duration of activation t_{a_x} of each muscle ($x = \{QUAD, HAMS, GLUT\}$) and calculate the level of fatigue of a specific muscle as

$$u_{fat_x} = 1 - e^{-t_{a_x}/F}. \tag{6.2}$$

Afterward, we calculate the actual excitation that OpenSim applies to each muscle

$$u_{f_x} = u_x - u_{fat_x}, \tag{6.3}$$

where u_x is the signal from the FES controller. This signal is saturated between the range $[0,1]$. When the muscles excitation level are reduced or activation stops, they usually restore their capability of producing force after resting. However, we did not include this characteristic in this model.

6.2 FES CYCLING CONTROL WITHOUT ORTHOSES ASSISTANCE

While cycling, we contract a set of muscles to provide necessary torques for pedal stroke. For similar cycling movements, we applied coordinated excitation on quadriceps, hamstrings and gluteus maximus muscle groups, based on previous FES controllers (HUNT, 2005; BÓ et al., 2015). During one pedal stroke, quadriceps provides most torque for the pedal stroke through knee extension. The gluteus maximus offers power

---

[5] When creating torques in OpenSim, we define a maximum value, in this case, 100Nm, and set a variable to represent the proportional magnitude [0,1].

for the hip extension after quadriceps extend the knee. Subsequently, hamstrings flex the knee. For efficient and safe cycling, these muscle groups must be excited in specific ranges, depending on crankset angle and speed. Part of the model discussion focused on how the addition of muscles improves cycling performance. Hence, we compared the following set of muscles: (1) quadriceps only (Q), (2) quadriceps and hamstrings (QH) and (3) quadriceps, hamstrings and gluteus maximus (QHG). Also based on (HUNT, 2005; BÓ et al., 2015), we defined ranges to excite each muscle to achieve cycling (illustrated in Figures 6.3a and 6.3b). The control structure in Figure 6.4 incorporates the musculoskeletal dynamics, the predefined range angles, and the chosen controller.

(a) Without phase adjustment.   (b) With phase adjustment.
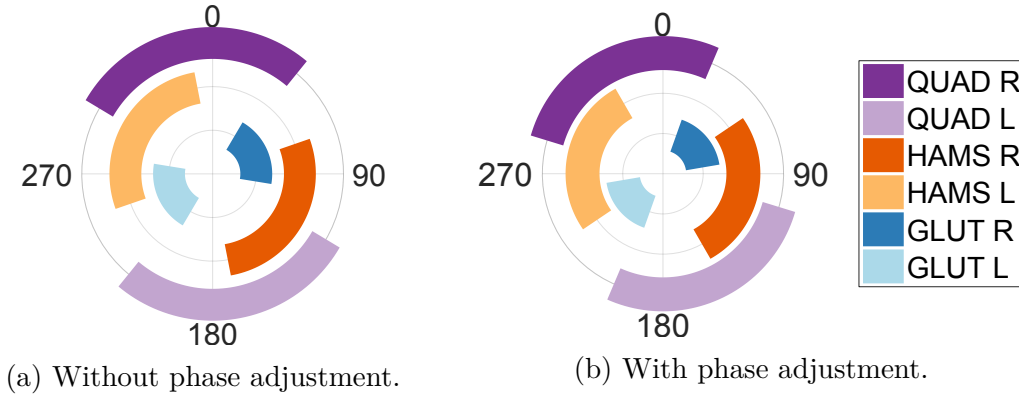
Figure 6.3: Predefined muscles range angles for excitation during one pedal stroke for the right and left legs. Right and left quadriceps (QUAD R and L) in purple, hamstrings (HAMS R and L) in orange, gluteal (GLUT R and L) in blue and right and left orthosis (ORTHOSIS R and L) in green. We represent the left side in light colors and the right side in dark colors. The average crankset cadence $\bar{\dot{\theta}}_c$ is 260°/s.

Source: prepared by the author.

During cycling, the current crankset cadence $\dot{\theta}_c$ also influences the stimulation range due to the controller and neuromuscular delays (HUNT, 2005). OpenSim also simulates the neuromuscular delays. These delays cause a loss of efficiency in the stimulation since the muscle contractions take place in different angle positions. Therefore, we also developed the cadence-based phase adjustment controller, adapting the controller with a counterclockwise shift angle θ_{shift} defined as

$$\theta_{shift} = \frac{K}{\dot{\theta}_{max}} \dot{\theta}_c, \tag{6.4}$$

where K_s is a correction factor and $\dot{\theta}_{max}$ is the maximum speed for the trial. Figure 6.3b presents an example for $K_s = 30°$ and $\dot{\theta}_c = 260°/s$ and $\dot{\theta}_{max} = 500°/s$.

Afterward, we developed the bang-bang (Section 6.2.1) and proportional-integral-derivative controllers (PID, Section 6.2.2). For both controllers, the muscles are excited accordingly to the predefined muscle range illustrated in Figure 6.3a.
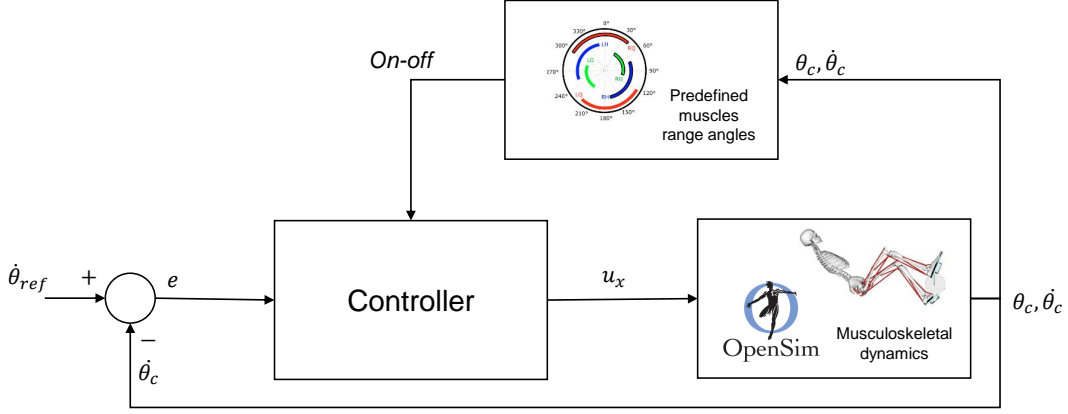
Figure 6.4: In this cycling control architecture, the controller provides a signal (u_x) based on the error (e) between the reference cadence ($\dot{\theta}_{ref}$) and the crankset speed ($\dot{\theta}_c$). The controller also considers the muscle range angles for excitation based on the crankset position (θ_c). With the control signals (muscles excitation), OpenSim calculates the musculoskeletal dynamics (θ_c and $\dot{\theta}_c$).

Source: adapted from the figure prepared by the author for (SOUSA et al., 2016).

6.2.1 Bang-bang (BB) controller

The muscles are excited continuously accordingly to the predefined muscle range after the phase adjustment. For each muscle $x = \{QUAD, HAMS, GLUT\}$, we calculate the signal control

$$u_x = f_x\left(\theta_c, \dot{\theta}_c\right)h, \tag{6.5}$$

where $f_x\left(\theta_c, \dot{\theta}_c\right)$ stands for the phase control muscle range that depends on the crank angle θ_c and the cadence cycling speed $\dot{\theta}_c$.

6.2.2 Proportional-integral-derivative (PID) controller

The PID controller manipulates the intensity of the excitation to achieve the required output-cycling cadence. Hence, this controller not only tries to maintain a cadence reference $\dot{\theta}_{ref}$, but also reacts to changes in muscle response, such as disturbances or muscle fatigue. Therefore, we parametrized the controller as

$$u_x = f_x\left(\theta_c, \dot{\theta}_c\right)h(t), \tag{6.6}$$

in which $h(t)$ changes accordingly to the error $e(t) = \dot{\theta}_{ref} - \dot{\theta}_c$, the cumulative error and the derivative of the error (HUNT, 2005)

$$h(t) = K_p e(t) + K_i \int_0^t e(\tau)d\tau + K_d \frac{de(t)}{dt}, \forall t \geq 0. \tag{6.7}$$

It is possible that the cadence $\dot{\theta}_c$ achieves a value greater than the reference speed $\dot{\theta}_{ref}$, i.e., $e(t) < 0$ and $h(t) < 0$. In our control strategies, we have no intention

to activate the antagonist muscle to avoid unnecessary stimulation of muscles (which cause fatigue). Further, we also do not intend to not excite the muscle, i.e., $h(t) = 0$. Abrupt stimulation may cause unexpected muscle behaviors due to the non-linear characteristics of stimulation. Therefore, we will keep the previously calculated value

$$h_k = h_{k-1}, \tag{6.8}$$

where k is the k-iteration of the controller.

6.2.3 Results

To compare the controllers applied to the cycling simulation environment, we simulated different configurations for each controller (bang-bang and PI). We set the final time T_f as 20 seconds and the control frequency f as $50\,\text{Hz}$. Model initiated with the right foot standing on the top, at $\theta_c = 0°$. Then, we calculated performance parameters: mean cadence ($\bar{\dot{\theta}}_c$), mean cadence acceleration ($\bar{\ddot{\theta}}_c$), standard deviation of the cadence ($\sigma_{\dot{\theta}}$), maximum error

$$e_{max} = max\{\dot{\theta}_{ref}(t) - \dot{\theta}_c(t)\}, \tag{6.9}$$

root-mean-square deviation error (RMSE)

$$e_{RMSE} = \sqrt{\overline{(\dot{\theta}_{ref}(t) - \dot{\theta}_c(t))^2}}, \tag{6.10}$$

rise time (t_r, the time the cycling takes to change from 10% to 90% of $w = 0°/s$ of $\dot{\theta}_{ref}$), muscles excitation levels (Φ_x, where $x = \{QUAD, HAMS, GLUT\}$), and the number of complete cycles (n_c, the number of complete cycles, i.e., every k-iteration that θ_c reaches 360°). As there is no reference for the bang-bang controller, we calculated the $\sigma_{\dot{\theta}}$, e_{max}, and e_{RMSE} related to the average values of the cadence. For each simulation, we calculated these parameters at the last complete cycle of the crankset. That is the most guaranteed pedal cycle within the 20s simulation that achieved a permanent regime (steady-state). We should note that although we focus on the permanent regime, muscle groups and controllers also affect the transient state. We defined that the system achieved permanent regime (steady state) when the acceleration $\ddot{\theta}_c$ was lower than $10°/s^2$.

We also calculated the muscles excitation levels as an estimated measure of energy Φ defined as the cumulative integral of excitations

$$\Phi_x = \sum_{i=1}^{n} \phi_{x_i}, \tag{6.11}$$

where ϕ_{x_i} is the excitation intensity of muscle group $x = \{QUAD, HAMS, GLUT\}$ in iteration i, and n is the number of samples of the simulation. As a cyclic movement with a symmetric model, there was no difference between right and left muscles, therefore Φ_{QUAD}, Φ_{HAMS} and Φ_{GLUT} stand for the sum of the right leg.

6.2.3.1   Results of the BB controller

To compare how the muscle sets interfere at cycling performance, we first simulated the **bang-bang controller** (BB) at three different muscle group sets, only quadriceps (Q), quadriceps and hamstrings (QH), and quadriceps, hamstrings, and gluteus (QHG). For each of this muscle set, we compared the effect of different excitation magnitudes ($h = 1.0$, $h = 0.9$, $h = 0.8$, $h = 0.7$, and $h = 0.6$). Furthermore, we simulated these systems with and without a load at the crankset ($L = 0$ and $L = 0.01$). At last, we simulated with (all muscles fatigue with the same time constant $F = 10$) and without ($F = 0$) the effect of fatigue. Table 6.2 summarizes all 60 simulations initial parameters for the bang-bang (3 muscle group sets, 5 excitation magnitudes, 2 loads and 2 fatigue time constant).

Table 6.2: Initial parameters for the different configurations for simulating the cadence-based phase adjustment bang-bang controller.

Muscles set	h	L	F
{Q, QH, QHG}	{1.0, 0.9, 0.8, 0.7, 0.6}	{0, 0.01}	{0, 10}

Figures 6.5, 6.6, 6.7 and 6.8 present all 60 cycling cadence plots through time. We divided in four figures ({$L = 0, F = 0$}, {$L = 0.01, F = 0$}, {$L = 0, F = 10$} and {$L = 0.01, F = 10$}) with five subplots for each h ($h = \{0.6, 0.7, 0.8, 0.9, 1.0\}$). In each subplot, we plotted three graphs for each muscle set group (Q, QH and QHG).
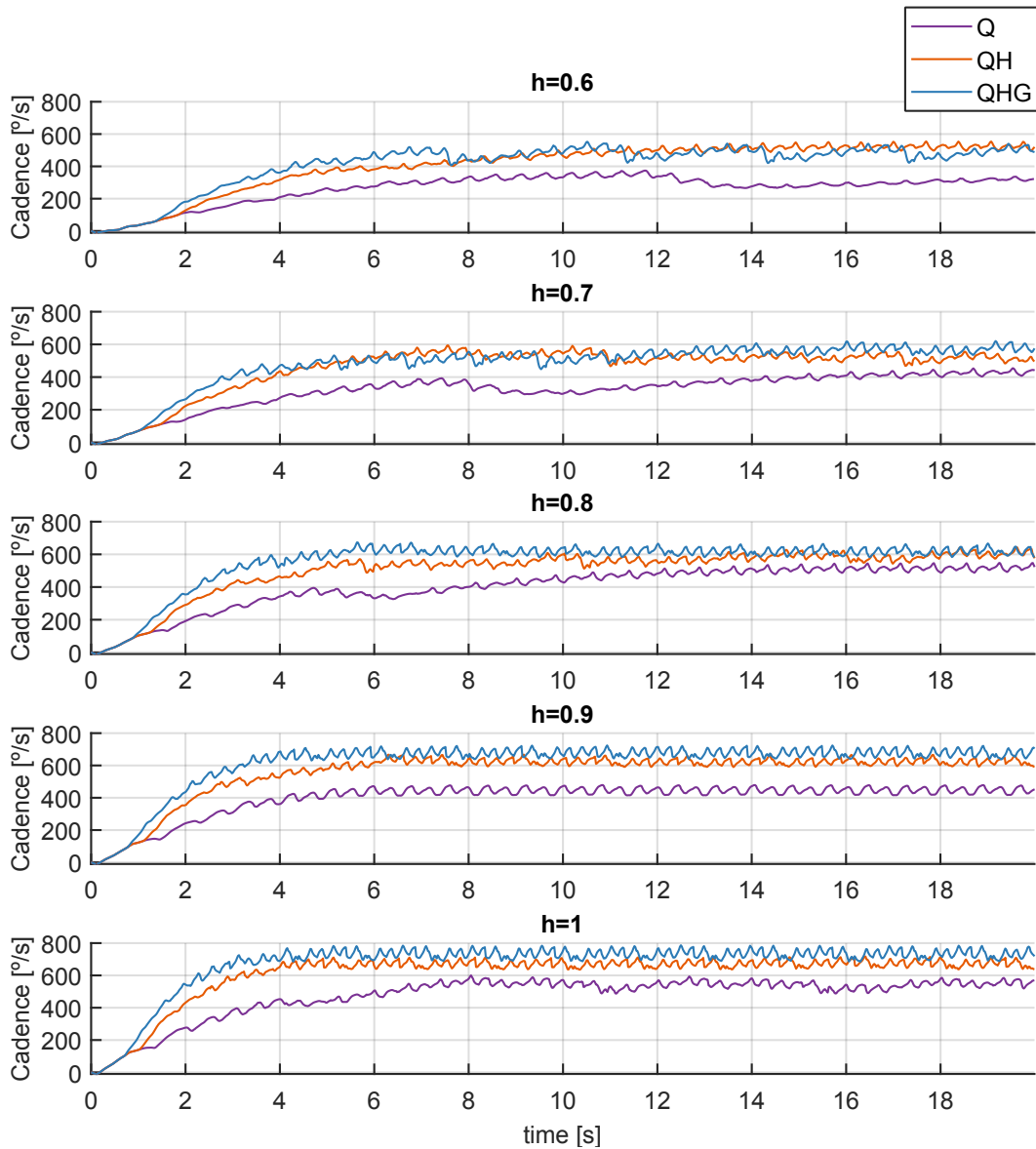
Figure 6.5: Cycling cadence simulations through 20 seconds of bang-bang controller for $h = \{0.6, 0.7, 0.8, 0.9, 1.0\}$. In this simulation, we kept the fatigue as zero, i.e., there is no muscle fatigue effect at the model. We also kept the load crankset as zero, i.e., there is no resistance at the crankset to the movement. Each muscle group set is represented by purple, orange and blue lines, respectively, Q, QH, and QHG.

Source: adapted from the figure prepared by the author for (SOUSA et al., 2016).
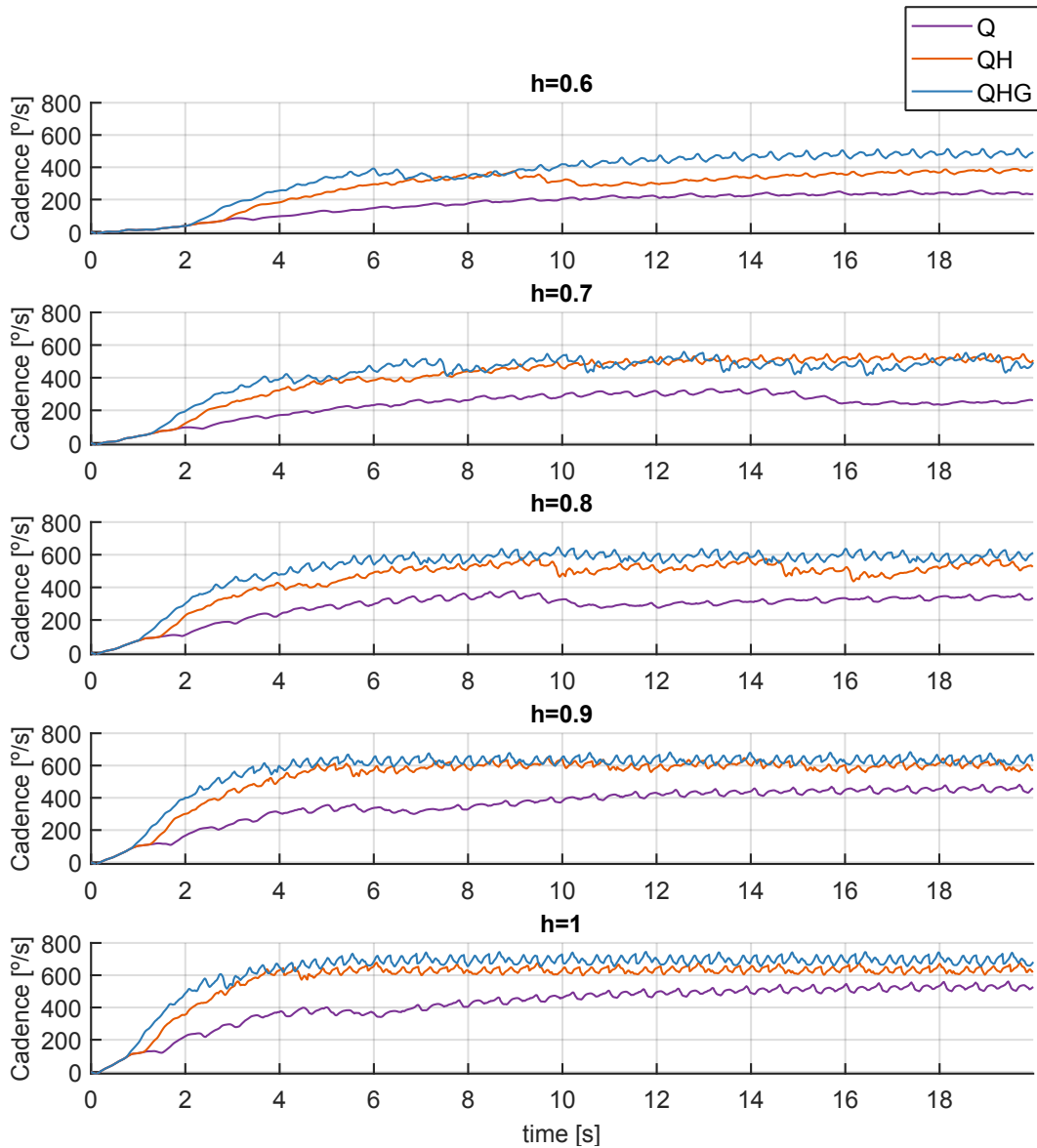
Figure 6.6: Cycling cadence simulations through 20 seconds of bang-bang controller for $h = \{0.6, 0.7, 0.8, 0.9, 1.0\}$. In this simulation, we kept the fatigue as zero, i.e., there is no muscle fatigue effect at the model. We added the load $L = 0.01$ resisting the movement. Each muscle group set is represented by purple, orange and blue lines, respectively, Q, QH, and QHG.

Source: adapted from the figure prepared by the author for (SOUSA et al., 2016).
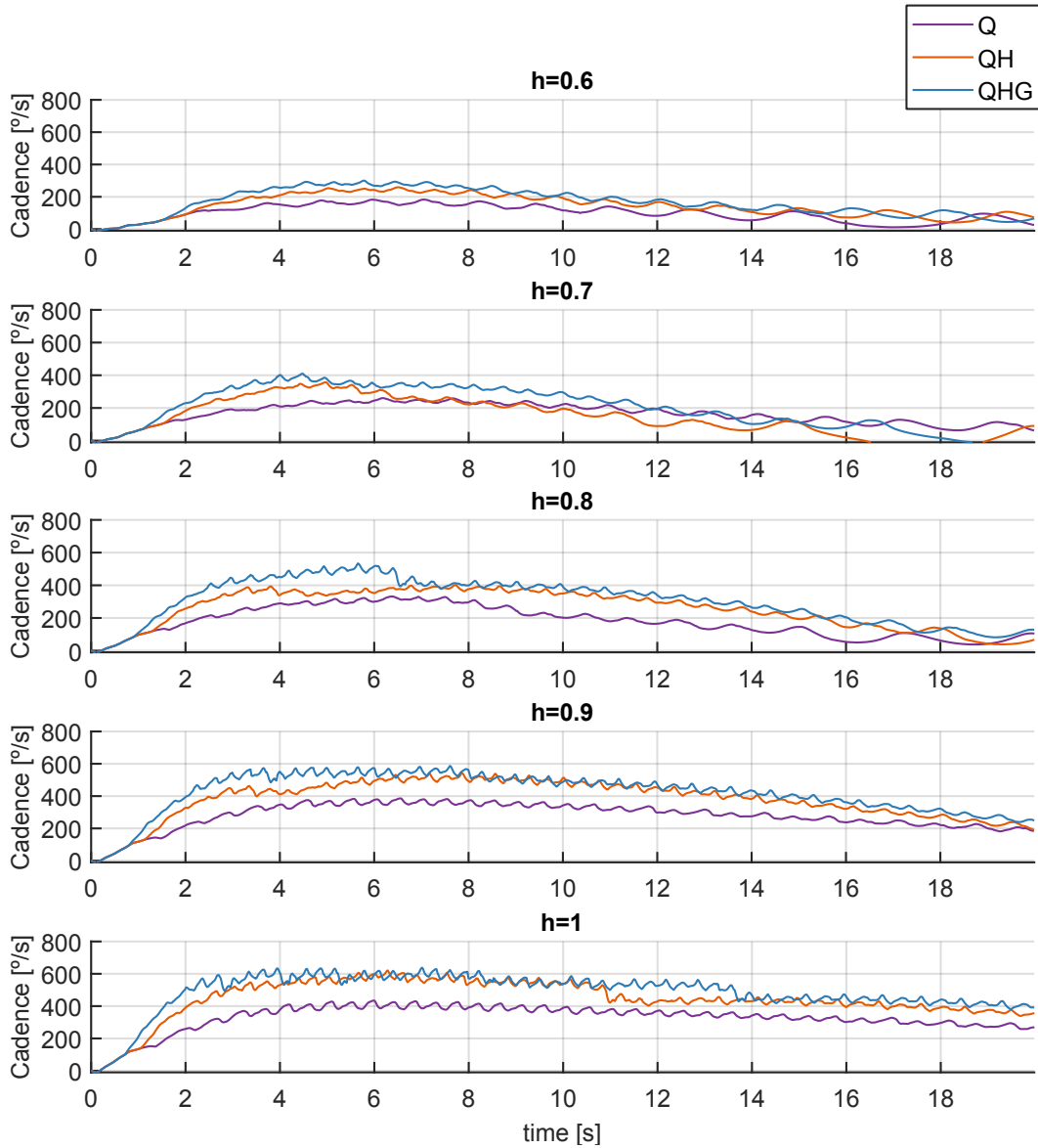
Figure 6.7: Cycling cadence simulations through 20 seconds of bang-bang controller for $h = \{0.6, 0.7, 0.8, 0.9, 1.0\}$. In this simulation, we added the muscle fatigue effect with a constant time of $F = 10$ for each muscle group. We kept the load crankset as zero, i.e., there is no resistance at the crankset to the movement. Each muscle group set is represented by purple, orange and blue lines, respectively, Q, QH, and QHG.

Source: adapted from the figure prepared by the author for (SOUSA et al., 2016).
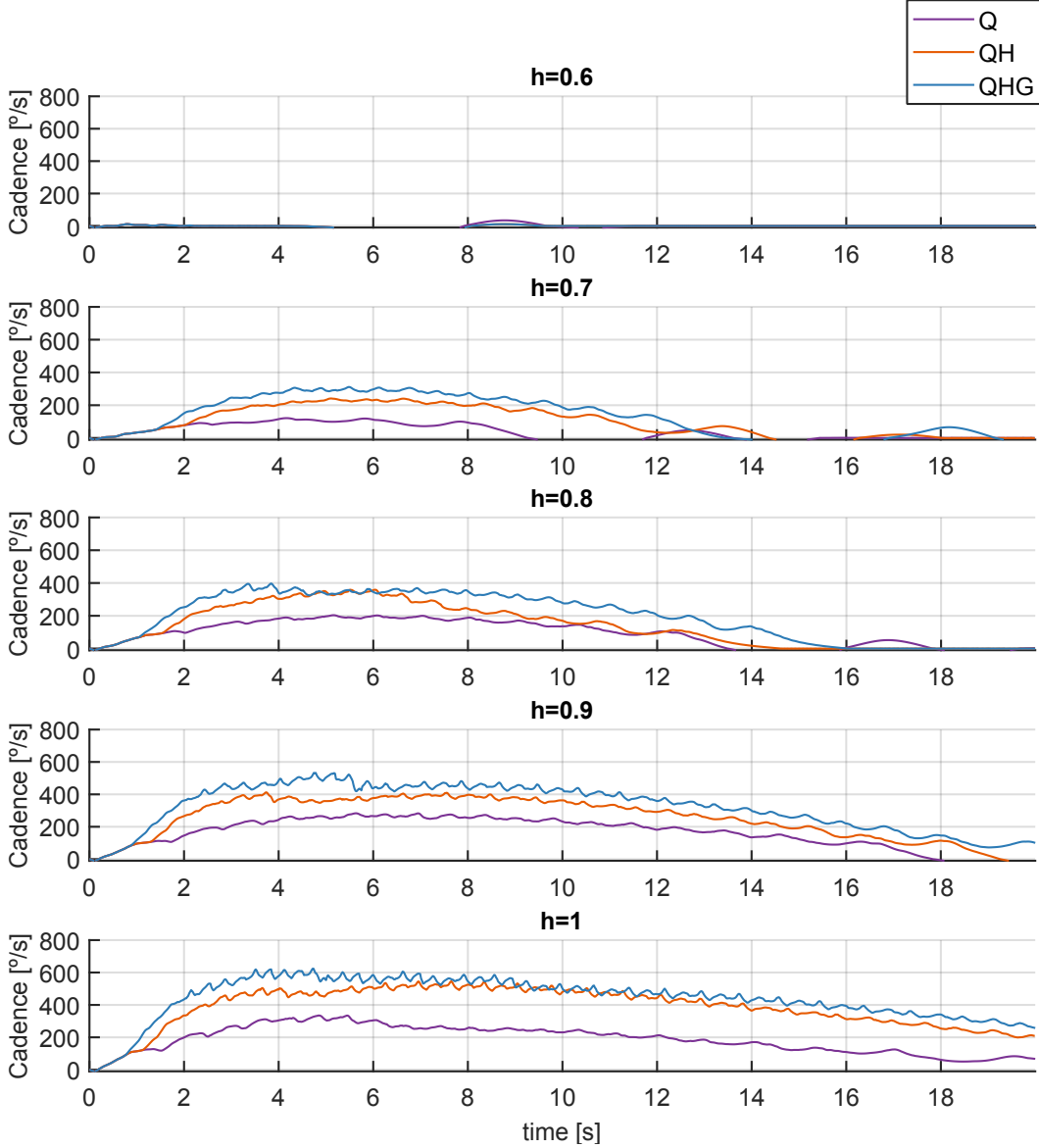
Figure 6.8: Cycling cadence simulations through 20 seconds of bang-bang controller for $h = \{0.6, 0.7, 0.8, 0.9, 1.0\}$. In this simulation, we added the muscle fatigue effect with a constant time of $F = 10$ for each muscle group. We added the load $L = 0.01$ resisting the movement. Each muscle group set is represented by purple, orange and blue lines, respectively, Q, QH, and QHG.

Source: adapted from the figure prepared by the author for (SOUSA et al., 2016).

Appendix C present Tables C.1, C.2, C.3 and C.4, in which we show all performance results. As the bang-bang controller does not reach a reference speed, we calculated t_r, e_{max} and e_{RMSE} considering $\dot{\theta}_{ref} = \bar{\bar{\theta}}_c$.

6.2.3.2 Results of the PID controller

We also simulated the **PID controller** with three different muscle group sets: only quadriceps (Q), quadriceps and hamstrings (QH), and quadriceps, hamstrings,

and gluteus (QHG). We kept the PID controller parameters the same for all simulations, i.e., with $K_p = 1.0$, $K_i = 0.55$ and $K_d = 0$. We simulated these systems with and without crankset load ($L = 0$ and $L = 0.01$), and with and without the muscle fatigue effect ($F = 0$ and $F = 10$). Although the model may cycle faster cadences, we set $\dot{\theta}_{ref} = 360°$ because, in real cycling, our pilot with SCI usually mantains his cadence bellow 360° (BÓ et al., 2017). Table 6.3 summarizes all 12 simulations initial parameters for the PID controller (3 muscle group sets, 2 loads and 2 fatigue time constant).

Table 6.3: Initial parameters for the different configurations for simulating the cadence-based phase adjustment PID controller.

Muscles set	L	F
{Q, QH, QHG}	{0, 0.01}	{0, 10}

Figures 6.9, 6.10, 6.11 and 6.12 present all 24 cycling cadence plots through time. Similarly to the bang-bang controller, we divided in four figures ({$L = 0$, $F = 0$}, {$L = 0.01$, $F = 0$}, {$L = 0$, $F = 10$} and {$L = 0.01$, $F = 10$}). In each figure, we plotted three graphs for the muscle sets (Q, QH and QHG).
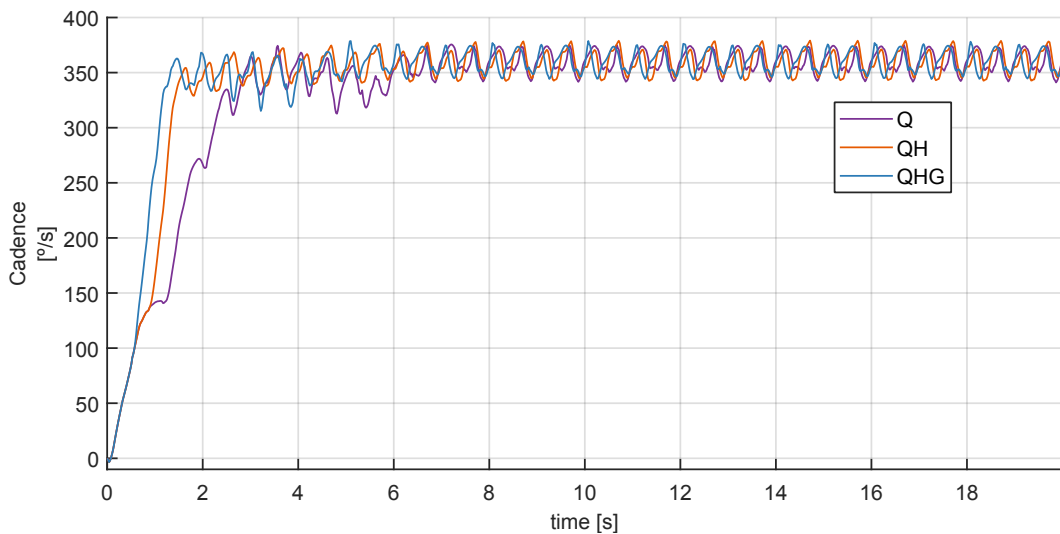
Figure 6.9: Cycling cadence through 20 seconds of simulation for the PID controller. In this simulation, we kept the fatigue as zero, i.e., there is no muscle fatigue effect at the model. We also kept the load crankset as zero, i.e., there is no resistance at the crankset to the movement. Each muscle group set is represented by purple, orange and blue lines, respectively, Q, QH, and QHG.

Source: adapted from the figure prepared by the author for (SOUSA et al., 2016).

Appendix C present Tables C.5, C.6, C.7 and C.8, in which we show all performance results.
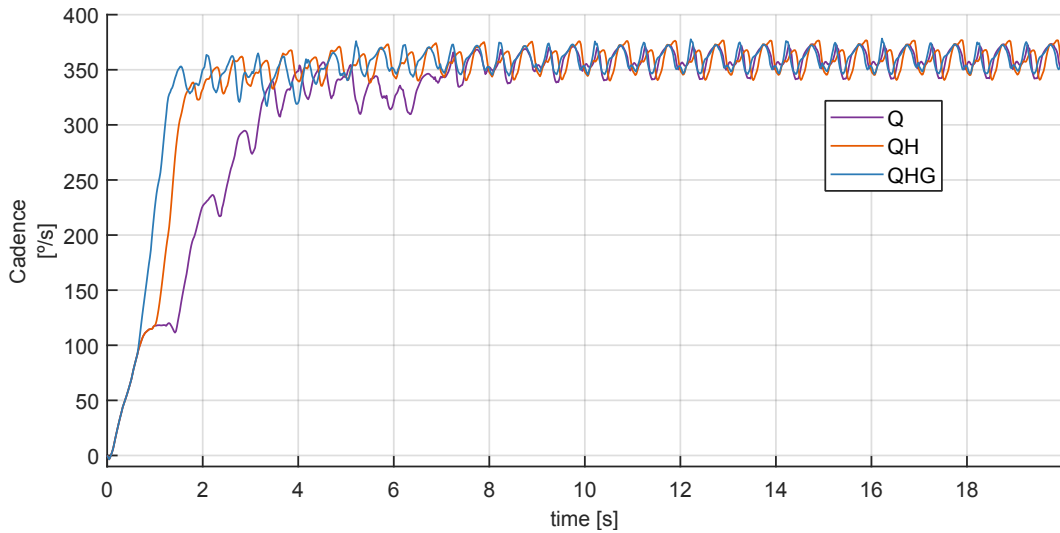
Figure 6.10: Cycling cadence through 20 seconds of simulation for the PID controller. In this simulation, we kept the fatigue as zero, i.e., there is no muscle fatigue effect at the model. We added a load resisting the movement of $L = 0.01$. Each muscle group set is represented by purple, orange and blue lines, respectively, Q, QH, and QHG.

Source: adapted from the figure prepared by the author for (SOUSA et al., 2016).
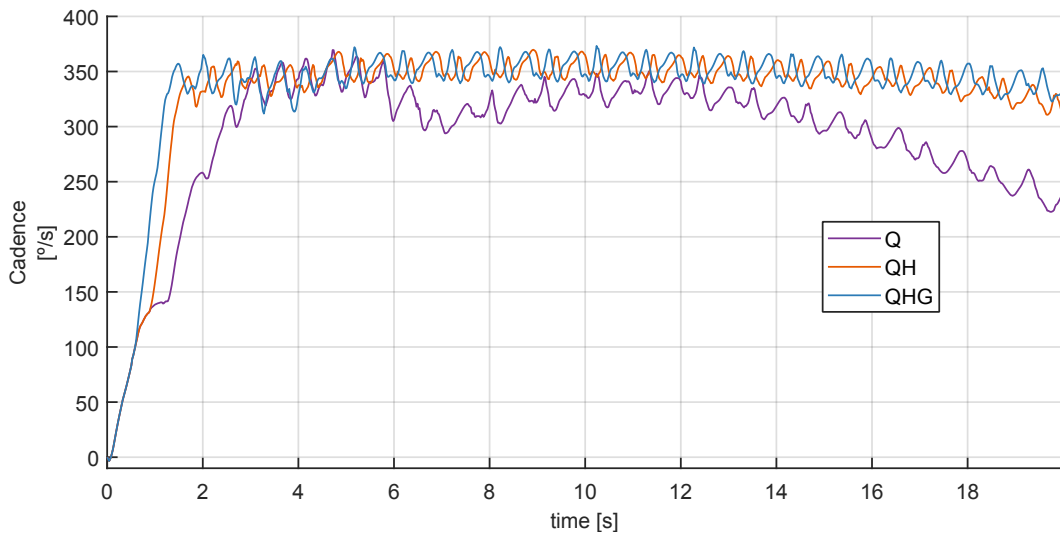
Figure 6.11: Cycling cadence through 20 seconds of simulation for the PID controller. In this simulation, we added the muscle fatigue effect with a constant time of $F = 10$ for each muscle group. We kept the load crankset as zero, i.e., there is no resistance at the crankset to the movement. Each muscle group set is represented by purple, orange and blue lines, respectively, Q, QH, and QHG.

Source: adapted from the figure prepared by the author for (SOUSA et al., 2016).
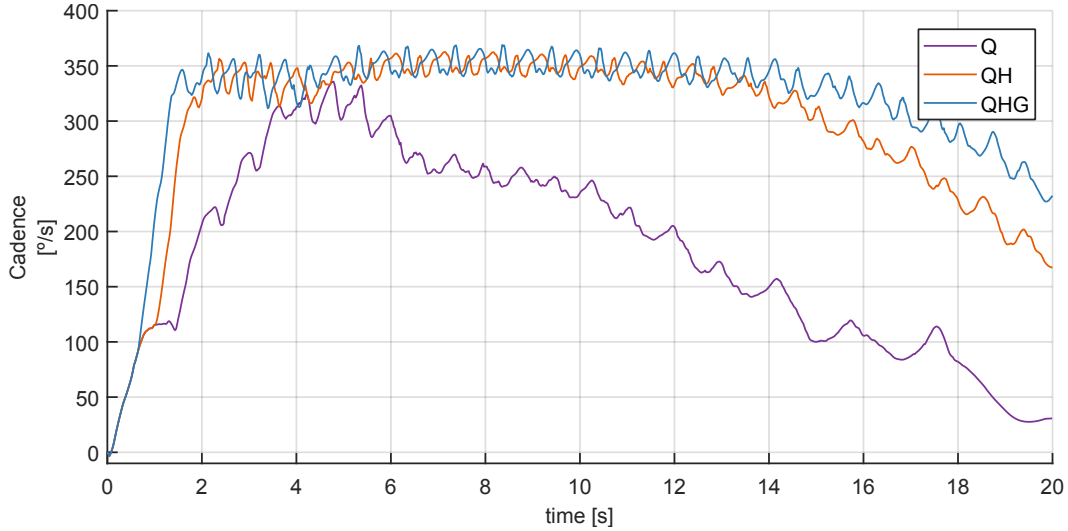
Figure 6.12: Cycling cadence through 20 seconds of simulation for the PID controller. In this simulation, we added the muscle fatigue effect with a constant time of $F = 10$ for each muscle group. We added a load resisting the movement of $L = 0.01$. Each muscle group set is represented by purple, orange and blue lines, respectively, Q, QH, and QHG.

Source: adapted from the figure prepared by the author for (SOUSA et al., 2016).

6.2.4 Discussion

Section 6.2.3 presented the results from the developed cycling simulation environment. This environment offered the possibility to conduct comparisons between different muscle groups, excitations, loads, fatigue effect and controllers. It should be noticed that not all simulations with $F = 0$ achieved steady state in 20 seconds (i.e., the acceleration was $\ddot{\theta}_c >= 10°/s^2$). Moreover, as expected, simulations with $F = 10$ always presented a decrease in the cadence.

Regular cycling movement demands specific muscles at specific points. Considering first the results from the bang-bang controller, Figure 6.5 shows that our model can cycle in scenarios with different muscle sets and different h. Figures 6.5, 6.6, 6.7 and 6.8, and also the $\bar{\dot{\theta}}_c$ and t_r from Tables C.1, C.2, C.3, and C.4, confirm the expectation that, with more muscle sets, the model tends to develop higher cadences in less time, even with loads and/or muscle fatigue. Even for the scenarios still in transient regime, if we observe the acceleration signal, e.g., in Table C.1 for $h = 0.6$, the muscle set QHG still accelerates $\ddot{\theta}_c = 25°/s^2$, therefore, it is likely that the system reaches higher speeds. We may also observe that there are scenarios that the excitation does not produce enough muscle torques to initiate the cycling movement, e.g., $F = 10$, $L = 0.01$ and $h = 0.6$ (Figure 6.8 and Table C.4).

Moreover, the load resists the movement, frequently decreasing $\bar{\dot{\theta}}_c$ and incre-

105

asing t_r, when we compare Figure 6.5 and 6.6, or Figure 6.7 and 6.8 (likewise the $\bar{\dot{\theta}}_c$ and t_r values from Tables C.1, C.2, C.3, and C.4). Further, Figures 6.7 and 6.8 show the cadence decreases over time due to the exponential muscle fatigue effect from Equation 6.2. We notice that the predefined muscles range angles for excitation from Figure 6.3b could be optimized to provide higher cadences or even lower errors ($\sigma_{\dot{\theta}}$, e_{max} and e_{RMSE}). However, the outcome of this optimization would only be for this specific model states (positions, speeds, and torque), yet this effort would escape the scope of the present work.

For the PID, with a variable $h(t)$, the control considers not only specific points in which the muscle should be excited but also the excitation intensity to achieve a reference cadence ($\dot{\theta}_{ref}$). The results from Figures 6.9 and 6.10, and the $\bar{\dot{\theta}}_c$ from Tables C.5 and C.6 show that the controller can keep the reference speed, adjusting $h(t)$ for each muscle.

Figure 6.13 presents a comparison of $h(t)$ between both controllers in the scenario: QHG, $F = 0$ and $L = 0.01$. In Figure 6.13a, we observe a constant $h = 0.6$ for all muscles, which leads to a final average speed $\bar{\dot{\theta}}_c = 486.5°/s$ (Table C.2). The same scenario for the PID controller (Figure 6.13d) shows the variable $h(t)$ that intends to keep $\bar{\dot{\theta}}_c = 360°/s$ (from Table C.6: $\bar{\dot{\theta}}_c = 360.1°/s$). In Figures 6.13c and 6.13f, we may also observe that the variable $h(t)$ from the PID controller, decreased the errors ($\sigma_{\dot{\theta}}$, e_{max} and e_{RMSE}). From the bang-bang controller (Table C.2), $\sigma_{\dot{\theta}} = 13.20$, $e_{max} = 28.31$ and $e_{RMSE} = 13.03$, and from the PID controller (Table C.6), $\sigma_{\dot{\theta}} = 8.80$, $e_{max} = 15.23$ and $e_{RMSE} = 8.7$. Similarly to the predefined muscles range angles, we are aware that the PID parameters (K_p, K_i and K_d) could be optimized. However, this outcome would also be model-specific, out of the scope of the presented work.
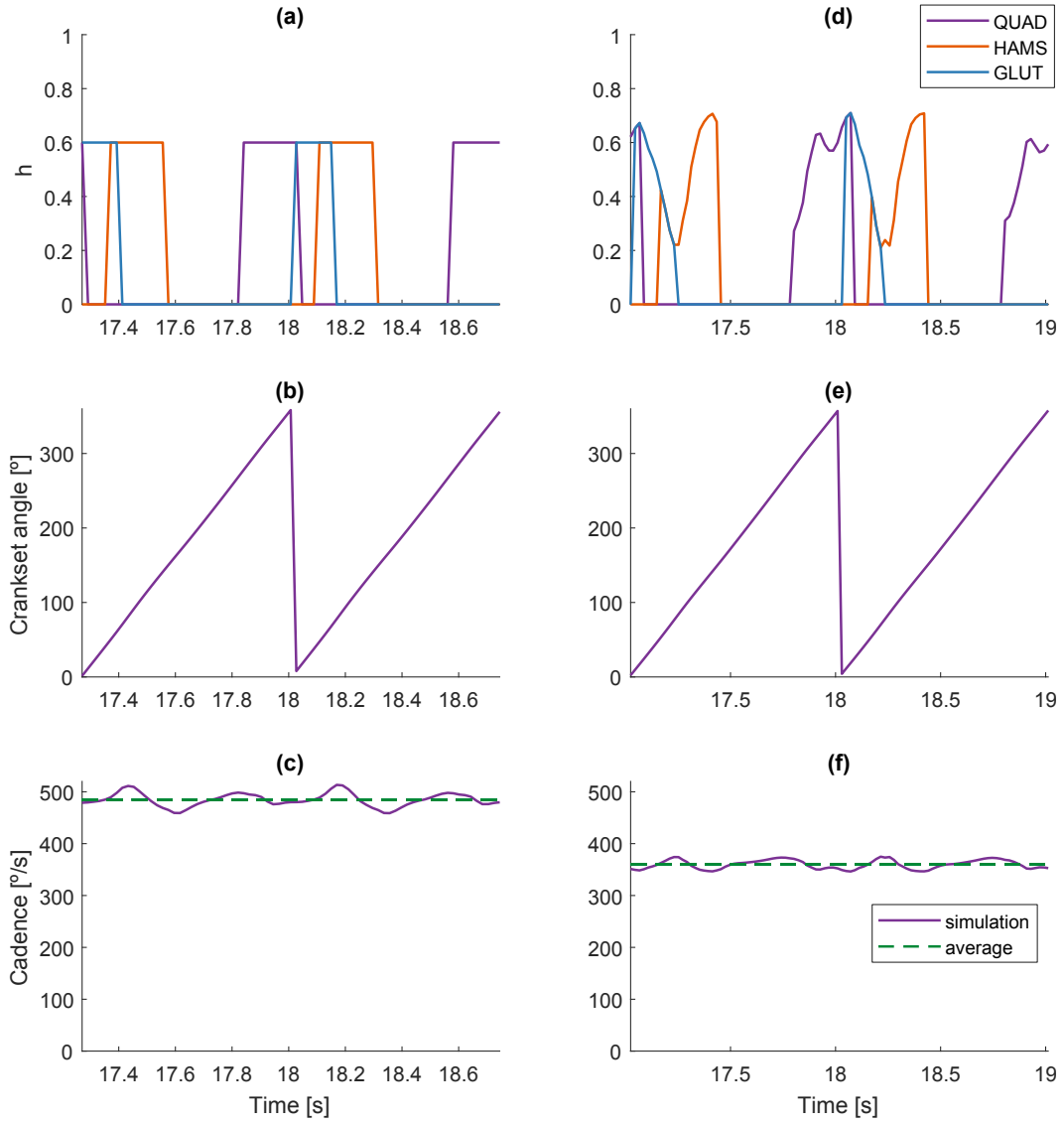
Figure 6.13: Cycling response through the last two complete cycles ($\theta_c = 0°$ to $\theta_c = 360°$) of BB and PID controllers. We kept $F = 0$ and $L = 0.01$. (a) Excitation of quadriceps (purple), hamstrings (orange) and gluteus maximus (blue) muscles for the BB controller with $h = 0.6$. (b) Gear angle in degrees. (c) Cycling cadence $\dot{\theta}_c$ and the average cadence $\overline{\dot{\theta}_c}$. (d) Excitation of quadriceps (purple), hamstrings (orange) and gluteus maximus (blue) muscles for the PID controller. (e) Gear angle in degrees. (f) Cycling cadence $\dot{\theta}_c$ and the reference cadence $\dot{\theta}_{ref} = 360°/s$.

Source: prepared by the author.

As lower excitation leads to slower fatigue effects, it is understandable that cadence-speed closed-loop controllers (e.g., PID controller) provide more efficient levels of stimulation to achieve the reference speed. This is confirmed by the results from the PID controller from Figures 6.11 and 6.12 when compared to the results from Figures 6.7 and 6.8. Although, the last average cadences from PID controller were lower than the target reference $360°/s$ (Tables C.7 and C.8), the closed-loop controller

may prolong the cycling movement.

At this point, we have presented a detailed musculoskeletal simulation environment for FES Cycling studies on control strategies. This environment already offers tools for performance discussion, and its integration with Matlab makes it more familiar to engineers. Next to existing practical efforts, it is relevant to find reasonable ways of estimating the effects of controllers on muscle activation beforehand.

6.3 FES CYCLING CONTROL WITH ORTHOSES ASSISTANCE

As rapid muscle fatigue is a notable limitation for FES control, some adjustments aim to diminish this effect. We hypothesize that the addition of passive orthoses stores energy (elastic with the mechanical springs) to assist movement, reducing muscle fatigue effects and lowering the metabolic cost by providing a more natural and stable movement for cycling. In an environment without FES, (CHAICHAOWARAT et al., 2017) introduced the concept of passive knee orthoses for cycling assistance, in which a spring stores energy from knee flexion to release it as the knee extends. They based the passive assistance on the unbalanced effort required from the quadriceps (knee extensor) and hamstrings (knee flexor) during the same cycling cadence. Further, in (CHAICHAOWARAT; KINUGAWA; KOSUGE, 2018), they performed tests with and without the knee orthoses with three subjects without disability. At the same cycling cadence, the passive knee orthoses decreased the quadriceps effort during cycling trials.

In the presented simulation environment, we modeled passive knee orthoses for FES cycling assistance, determining the spring parameters, and how these parameters relate to the average cycling cadence and muscle excitation. In the following sections, we expect to reduce muscle fatigue effects and lower the metabolic cost by providing a more natural and stable movement for cycling through passive orthoses.

6.3.1 Passive orthoses model

To model the passive orthoses, we adapted the simulation environment by adding passive knee orthoses and a wheel accelerating system illustrated in Figure 6.14. The predefined muscles range angles remain the same as in Section 6.3b. Figure 6.15 illustrates the muscle an orthoses ranges for one cycle.

We modeled the passive orthoses based in (CHAICHAOWARAT et al., 2017). The supporting knee torque (τ_{spr}) operates as a rotational spring

$$\tau_{spr} = \begin{cases} K_s(\theta_j - \theta_s) & ,\theta_j \geq \theta_s \\ 0 & ,\theta_j < \theta_s \end{cases} \tag{6.12}$$

where K_s represents the spring stiffness, θ_j represents the knee joint angle, and θ_s the starting angle. Figure 6.16 illustrates an example of a spring with $\theta_s = 52°$ and
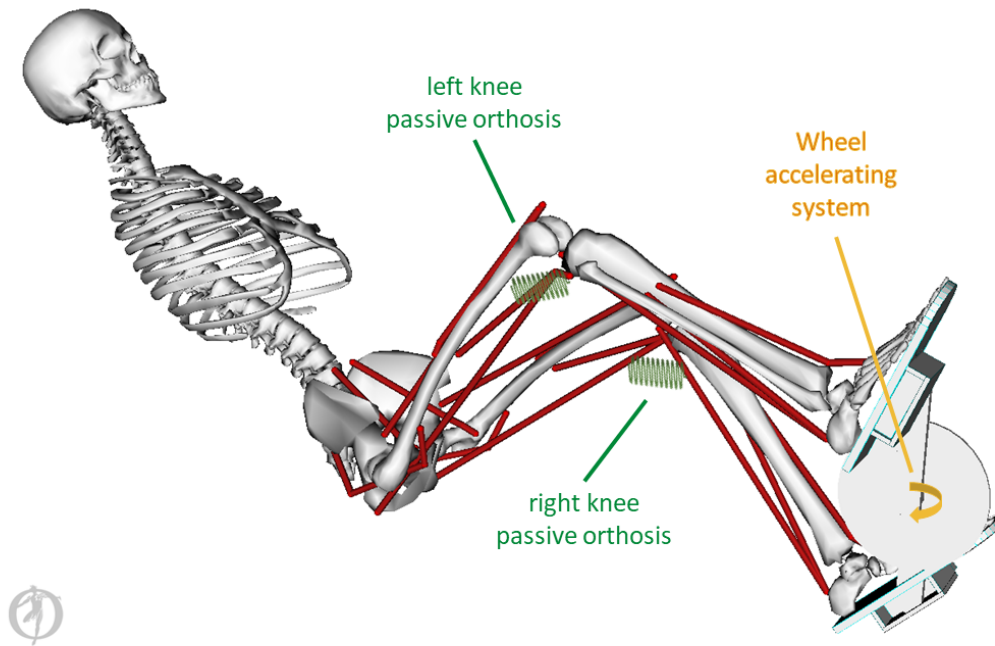
Figure 6.14: Adaptation of the previous system with the addition of left and right passive knee orthoses (green) and a wheel accelerating system at the crankset (orange).

Source: adapted from the figure prepared by the author for (SOUSA; SOUSA; BÓ, 2019).
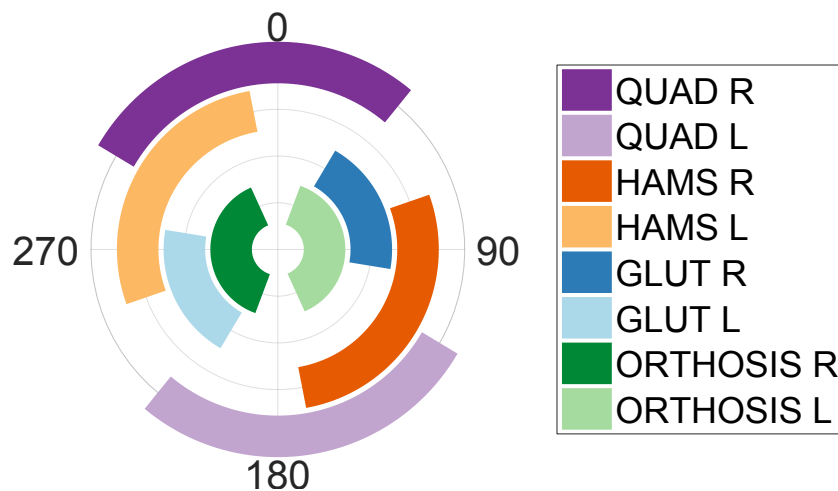
Figure 6.15: Muscles and spring range angles for excitation during a pedal stroke. Right and left quadriceps (QUAD R and L) in purple, hamstrings (HAMS R and L) in orange, gluteal (GLUT R and L) in blue and right and left orthosis (ORTHOSIS R and L) in green. We represent the left side in light colors and the right side in dark colors.

Source: prepared by the author.

$\tau_{max} = 15$ Nm/°. At this representation, 0° refers to the maximum knee extension, i.e., while the knee angle increases, the leg flexes, and while it decreases, the leg extends. In Figure 6.16b, we may observe that the spring provides the maximum torque τ_{max}. We

preferred to explain the property related to the intensity of elasticity (elastic constant) as a maximum torque. Whit this variable, the effect in biomechanics during cycling is more accessible to read.
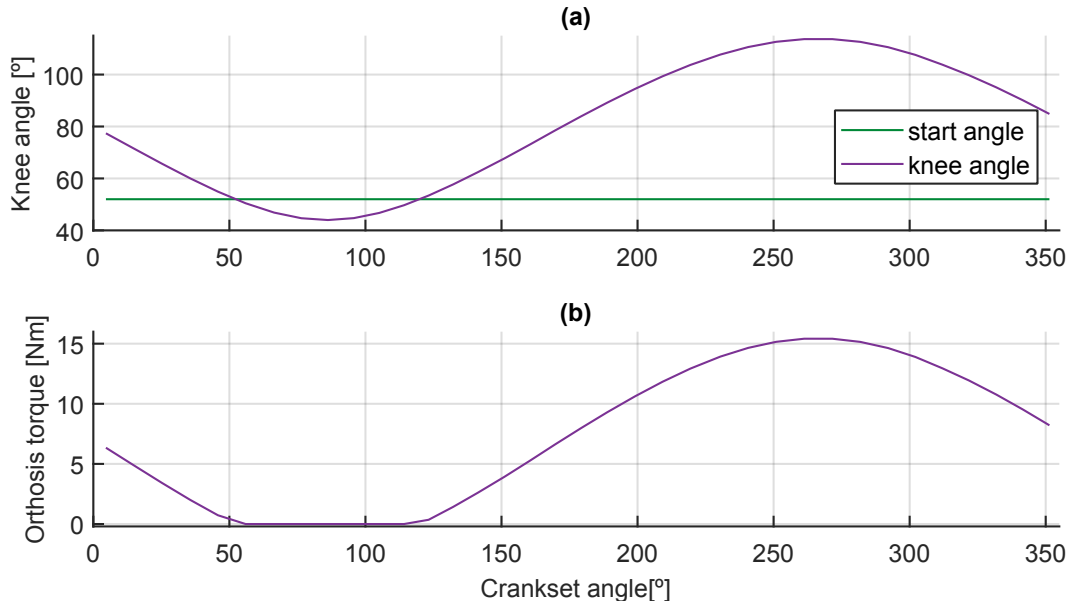
Figure 6.16: Example of the spring with $\theta_s = 52°$ and $\tau_{max} = 15$ Nm/° during a complete crankset cycle. The crankset angle reference is related to the position of the right foot. (a) Right knee (purple line) and spring start angle (green line). (b) Passive orthosis torque (purple line), the torque becomes zeros when the right knee angle is lower than 52°.

Source: adapted from the figure prepared by the author for (SOUSA; SOUSA; BÓ, 2019).

In this model, the spring releases energy (i.e., aids the cycling movement) for half the time, and stores energy (i.e., resists the cycling movement) for the other half. As the spring may resist movement at some states, sometimes the model is unable to cycle without external aid. To compare a wide range of passive orthoses parameters without this effect, we also modeled a wheel acceleration system that guarantees that the system starts cycling by applying the torque

$$
\tau_{acc} = \begin{cases} 15\,Nm & ,\dot{\theta}_c < \dot{\theta}_t \\ 0 & ,\dot{\theta}_c \geq \dot{\theta}_t, \end{cases} \tag{6.13}
$$

where $\dot{\theta}_c$ is the cycling cadence, calculated by the differentiation of the crankset angle during the time. After the cycle achieves the target crankset cadence $\dot{\theta}_t$, the system may keep cycling due to inertia and geometry conditions of the bicycle. An optimal solution is the use of passive orthoses without this wheel acceleration system; however, we are not considering this limitation at this point of the discussion.

From Figure 6.16, we observe that the knee has two inflection angles (θ_i), in which the knee stops flexing and starts extending, or the other way around. For an easier mechanism prototyping in the future, we set the inflection point of the orthosis at the same inflection angle of the knee (i.e., the knee shifts from extension to flexion, or vice versa).

6.3.2 Passive orthoses spring parameters

After modeling the new FES cycling system, we conducted simulations to determine how the spring parameters (τ_{max} and θ_s) affect the cycling movement. In OpenSim, we fixed $f = 50$Hz, $T_f = 20$s. We also kept the initial position with the right foot standing on the top, at $\theta_c = 0°$. The controller was the **bang-bang** (BB) controller with three different muscle group sets, only quadriceps (Q), quadriceps and hamstrings (QH), and quadriceps, hamstrings, and gluteus (QHG). For each muscle set, we also compared the effect of different excitation magnitudes ($h = 1.0$, $h = 0.9$, $h = 0.8$). Furthermore, we simulated these systems with and without a load at the crankset ($L = 0$ and $L = 0.01$). We chose the knee inflection point around 112° (c.f. Figure 6.16), so the orthosis has the same inflection angle of the knee.

To compare the effect of the maximum spring torque τ_{max}, we ranged the τ_{max} from -40 Nm to 40 Nm, in which the negative signal determines that the spring extends the knee, and the positive signal determines that the spring flexes it. A maximum torque higher than $|40|$ Nm could lead to simulations not able to cycle, i.e., the muscles torque are unable to provide movement when the spring is storing energy. We also set $\theta_s = 52°$, therefore, $\Delta\theta = 60°$ (the angular range that the orthosis actuates from its minimum to its maximum torque value i.e., $\Delta\theta = \theta_i - \theta_s$, c.f. Figure 6.16). We chose a value for θ_s that does not overlap the left and right orthoses and actuates long enough so we can guarantee results. Table 6.4 summarizes all 480 simulations for τ_{max} (3 muscle group sets, 5 excitation magnitudes, 2 loads and 16 τ_{max}).

Table 6.4: Configurations for simulations to determine the effect of τ_{max}.

Muscles set	h	L	τ_{max} [Nm]
{Q, QH, QHG}	{1.0, 0.9, 0.8, 0.7, 0.6}	{0, 0.01}	{-40, -35, -30, ..., 30, 35, 40}

After these simulations, we fixed τ_{max} and ranged the θ_s. As the complete range of the knee trajectory is approximate 70°, we ranged $\Delta\theta$ from 10° to 60°. Table 6.5 summarizes all 180 simulations for θ_s (3 muscle group sets, 5 excitation magnitudes, 6 $\Delta\theta$ and 2 loads).

Then, for each simulation, we plotted cadences vs. time graphs, and calculated performance parameters: the average crankset cadence $\bar{\dot{\theta}}_c$ and the standard deviation

111

Table 6.5: Configurations for simulations to determine the effect of $\Delta\theta$.

Muscles set	h	L	$\Delta\theta$ [°]
{Q, QH, QHG}	{1.0, 0.9, 0.8, 0.7, 0.6}	{0, 0.01}	{60, 50, 40, 30, 20, 10}

$\sigma_{\dot{\theta}}$. From these performance parameters, we analyze how τ_{max} and θ_s could increase the average cadence of a complete cycle with similar muscle excitations (h).

6.3.3 Results of spring parameters simulations

To analyze the interference from the passive orthoses, we present a comparisson between results with passive orthoses assistance and without orthoses ($\tau_{max} = 0$), always considering similar h. Sections 6.3.3.1 and 6.3.3.2 present the results for τ_{max} and θ_s.

6.3.3.1 Maximum torque

In Figures 6.17, 6.18, 6.19, 6.20 and 6.21, we marked the baseline results (without orthoses) with black dashed lines for each h. In each figure, we presented six plots, which correspond to the simulation results from the three different muscles sets with and without loads. For each τ_{max}, we plotted the error bars with the mean crankset cadence ($\bar{\dot{\theta}}_c$) and three times the standard deviation ($3\sigma_{\dot{\theta}}$) at the last cycle. If the cadence with the orthoses is greater than without, we marked in blue, and if it was lower, in red.

In Figures 6.17 to 6.21, we observed that positive torques (i.e., the torque that releases energy during leg extension) usually lead to similar or lower cadences, and the negative torques usually lead to higher cadences. We also observed that positive torques lead to higher $\sigma_{\dot{\theta}}$. Moreover, these results imply that we may achieve higher cadence (possibly delaying muscle fatigue) with the same muscle excitation h with springs that flexes the knee at 112°. Appendix C present Tables C.9, C.10, C.11, C.12 and C.13 that summarize the numerical results for $\bar{\dot{\theta}}_c$, $\ddot{\theta}_c$ and $\sigma_{\dot{\theta}}$ (only for positive torques).
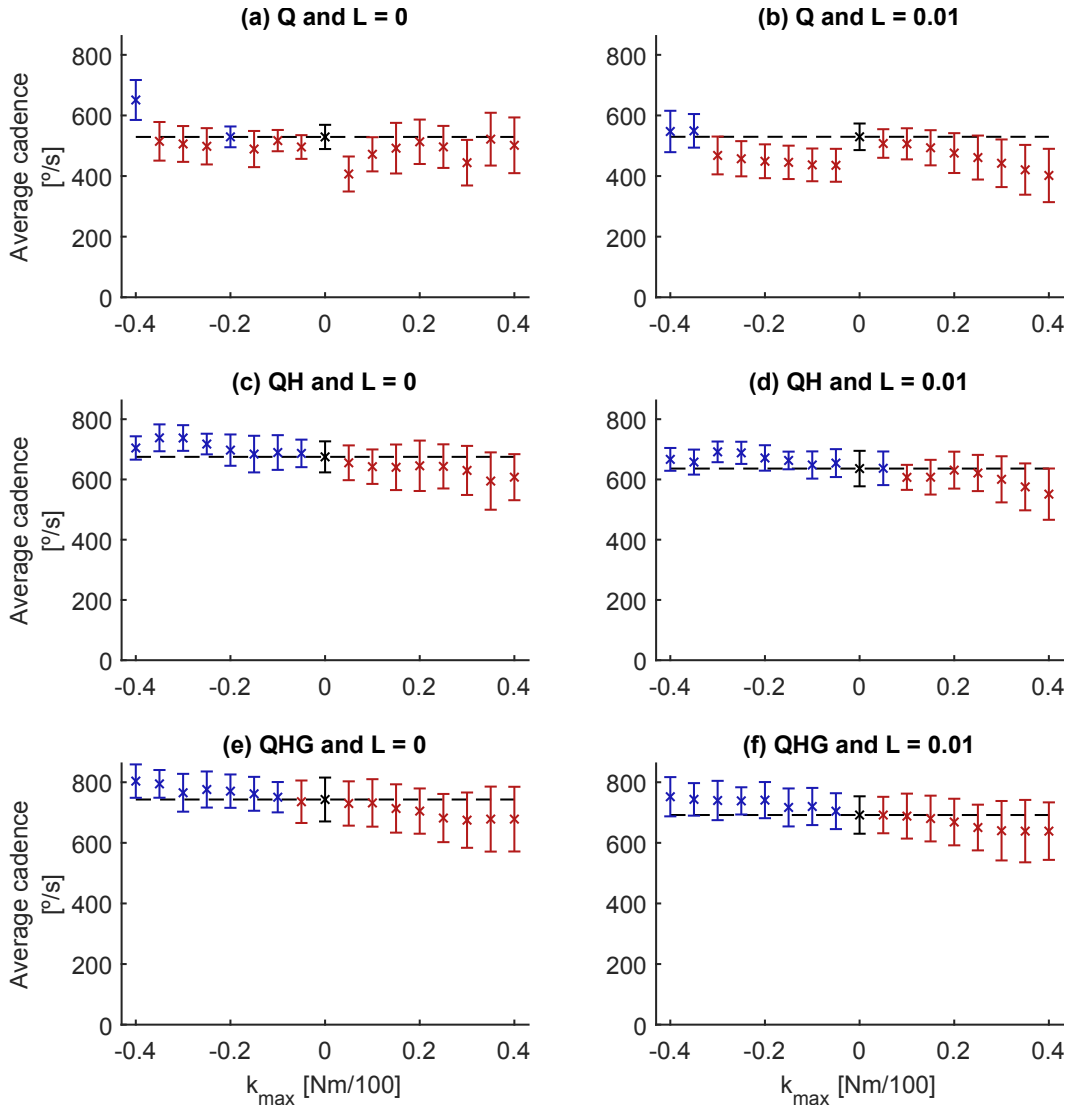
Figure 6.17: Last cycle average cadences with respect to τ_{max}. The dashed black line represents the reference crankset cadence without passive orthoses ($\tau_{max} = 0$). We used the BB controller with $h = 1.0$ and marked cadences greater than the baseline in blue, and the lowers in red.

Source: prepared by the author.
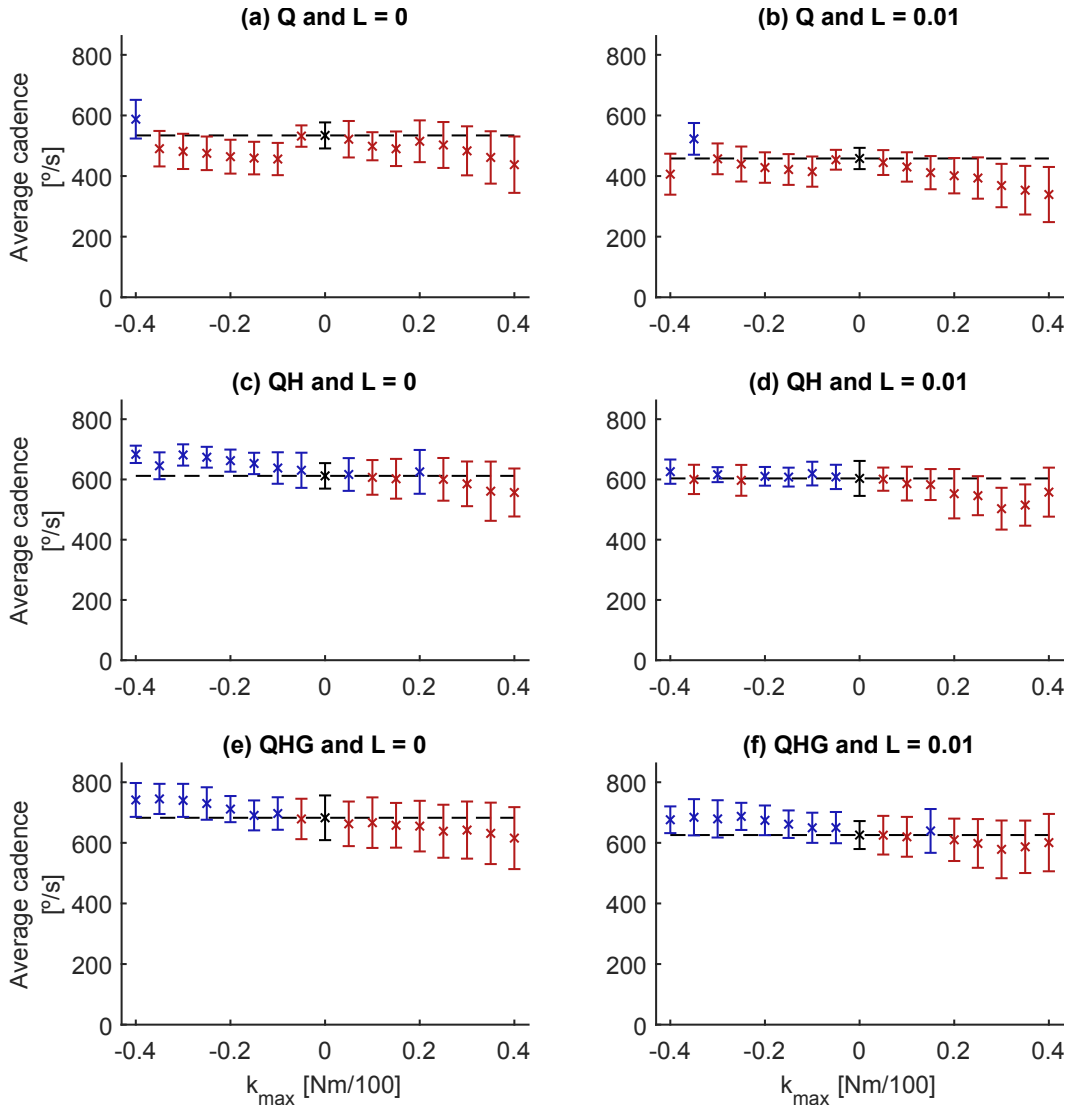
Figure 6.18: Last cycle average cadences with respect to τ_{max}. The dashed black line represents the reference crankset ($\tau_{max} = 0$). We used the BB controller with $h = 0.9$ and marked cadences greater than the baseline in blue, and the lowers in red.

Source: prepared by the author.
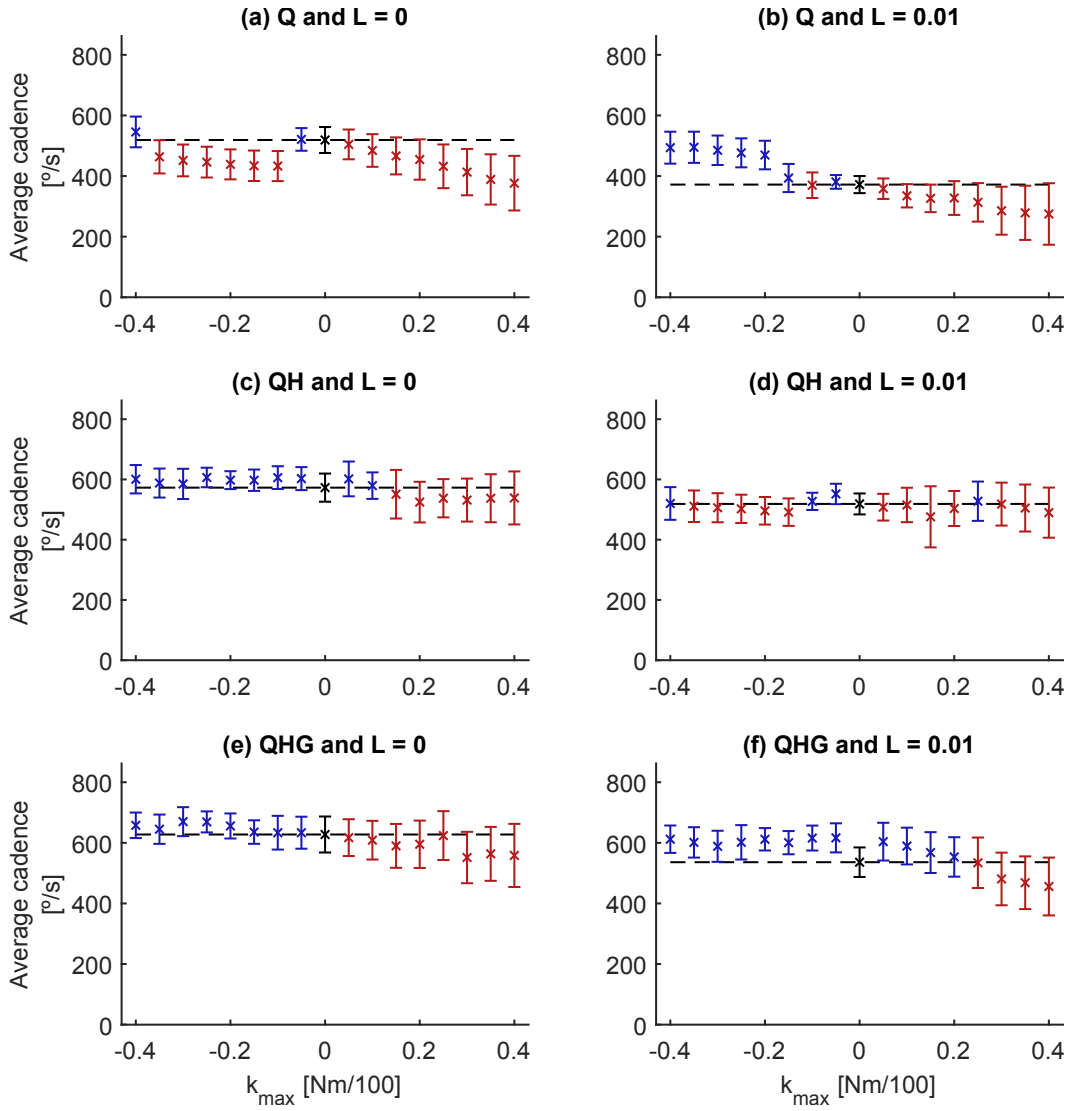
Figure 6.19: Last cycle average cadences with respect to τ_{max}. The dashed black line represents the reference crankset ($\tau_{max} = 0$). We used the BB controller with $h = 0.8$ and marked cadences greater than the baseline in blue, and the lowers in red.

Source: prepared by the author.
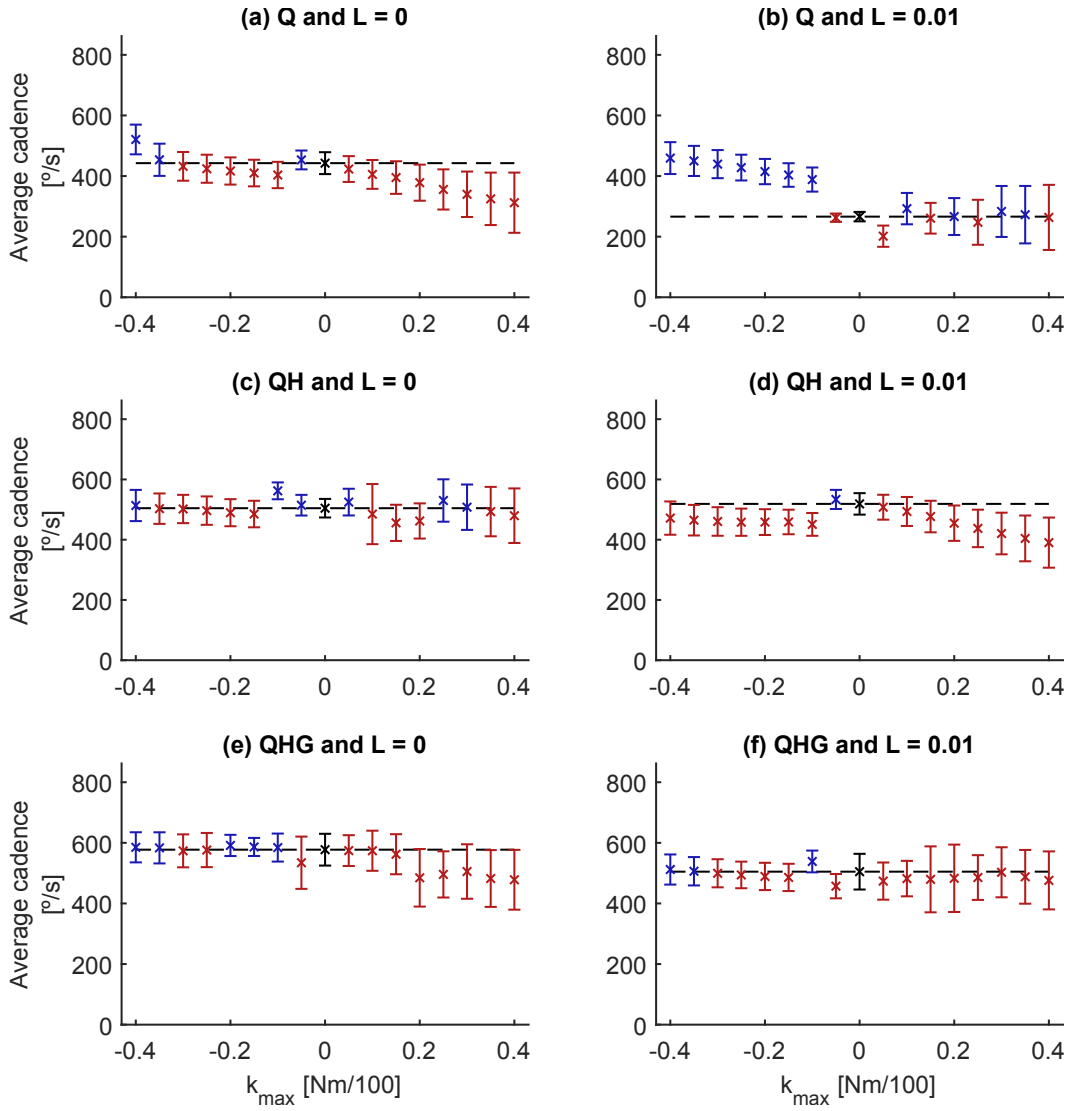
Figure 6.20: Last cycle average cadences with respect to τ_{max}. The dashed black line represents the reference crankset ($\tau_{max} = 0$). We used the BB controller with $h = 0.7$ and marked cadences greater than the baseline in blue, and the lowers in red.

Source: prepared by the author.
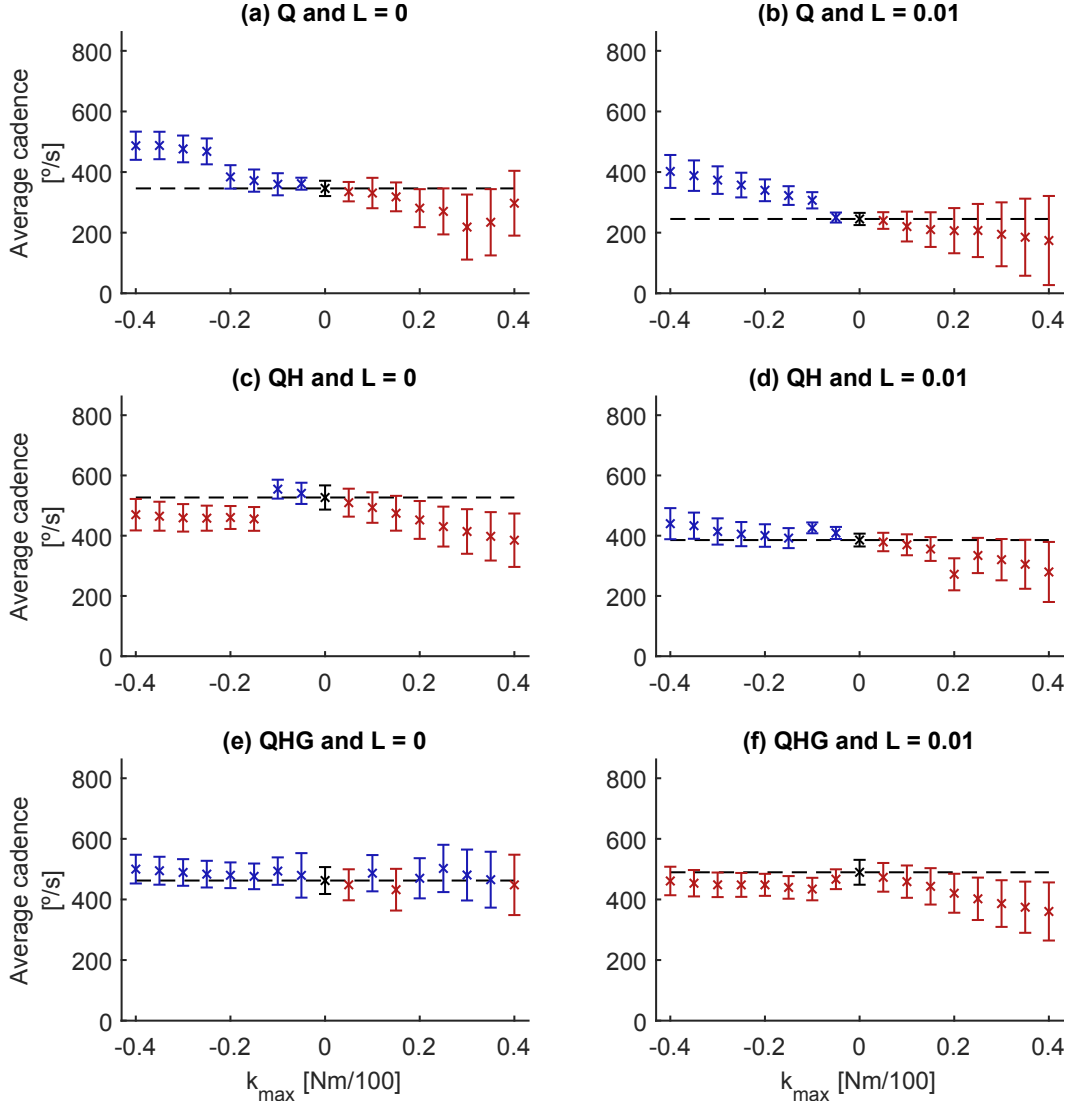
Figure 6.21: Last cycle average cadences with respect to τ_{max}. The dashed black line represents the reference crankset ($\tau_{max} = 0$). We used the BB controller with $h = 0.6$ and marked cadences greater than the baseline in blue, and the lowers in red.

Source: prepared by the author.

Although the spring improves several results, we observed exceptions in Figures 6.17, 6.18, 6.19, 6.20 and 6.21. Some results presented higher $\bar{\dot{\theta}}_c$ and lower $\sigma_{\dot{\theta}}$ for positive τ_{max}, and also lower $\bar{\dot{\theta}}_c$ and higher $\sigma_{\dot{\theta}}$ to negative τ_{max}. From the figures, we notice a relation between τ_{max} and the cycling cadence. For better visualization, we plotted all simulation results in two 3-D graphs. Figure 6.22 presents the simulation performance of the average cycling at the last cycle ($\bar{\dot{\theta}}_c\}$). We define performace as the rate between $\bar{\dot{\theta}}_c\}$ and the baseline $\bar{\dot{\theta}}_B\}$ (i.e., same muscle set, h and L). Blue represents values higher than 100%, i.e., $\bar{\dot{\theta}}_c$ was higher than the baseline.

Similarly, we also presented the performance of the standard deviation of the cycling at the last cycle ($\sigma_{\dot{\theta}}$) in Figure 6.23. Blue represents lower $\sigma_{\dot{\theta}}$ compared to the

(a)

(b)

(c)
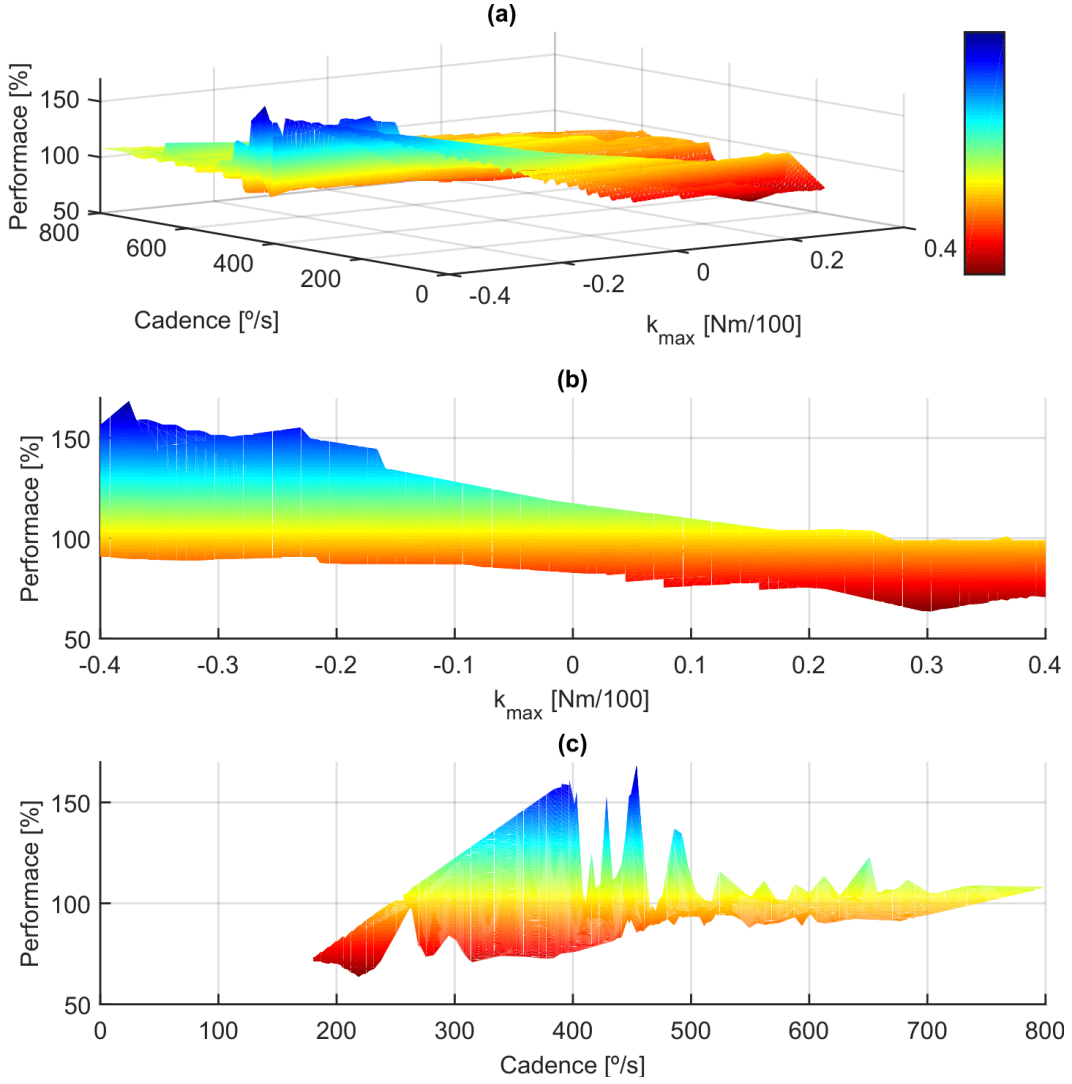
Figure 6.22: Simulation performace of the average cycling ($\bar{\dot{\theta}}_c$) for all τ_{max}. Blue represents higher $\bar{\dot{\theta}}_c$ (compared to the previously simulated baseline that corresponds to the same muscle set, h and L), and red, lower $\bar{\dot{\theta}}_c$. (a) 3-D plot. (b) Detail of performace and τ_{max}. (c) Detail of performace and $\bar{\dot{\theta}}_c$.

Source: prepared by the author.

baseline, i.e., less variability in cadence.

We consider a more efficient cycling, a cycling with higher $\bar{\dot{\theta}}_c$ and lower $\sigma_{\dot{\theta}}$, i.e., color map in blue on both figures. The simulations indicate that most positive torques lead to lower $\bar{\dot{\theta}}_c$ (Figure 6.22(b)) and higher $\sigma_{\dot{\theta}}$ (Figure 6.23(b)), while negative torques lead to higher $\bar{\dot{\theta}}_c$ and lower $\sigma_{\dot{\theta}}$. We also observed an almost a range of higher cadences between 300º/s and 400º/s for negative torques (Figure 6.22(a) and (c)). These results could imply that for specific ranges the spring increases efficient in cycling.

To better explain how the spring actuates on the cycling movement, we also
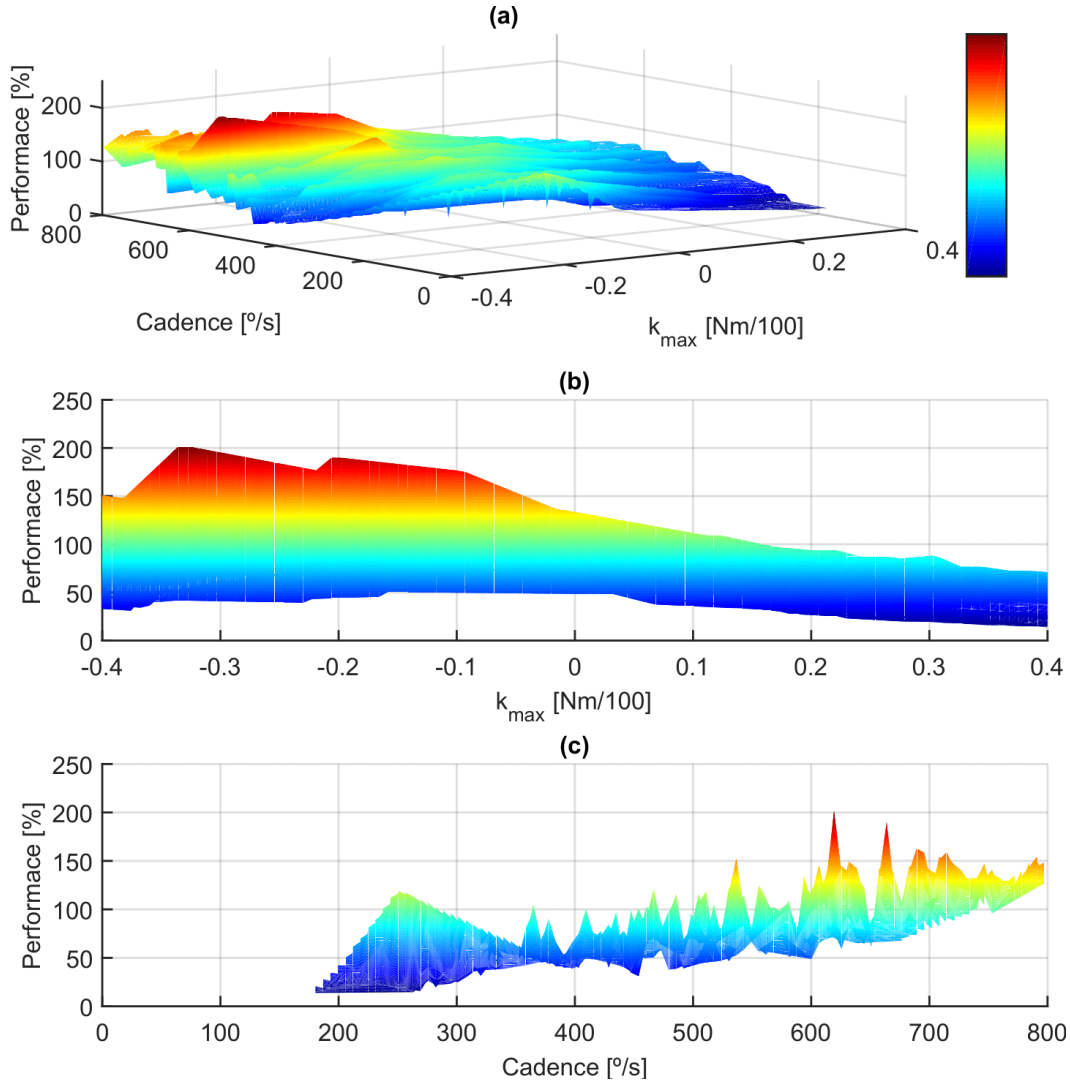
Figure 6.23: Simulation performace of the standard deviation of the cycling cadence ($\sigma_{\dot{\theta}}$) for all τ_{max}. Red represents higher $\sigma_{\dot{\theta}}$ (compared to the previously simulated baseline that corresponds to the same muscle set, h and L), and blue, lower $\sigma_{\dot{\theta}}$. (a) 3-D plot. (b) Detail of performace and τ_{max}. (c) Detail of performace and $\sigma_{\dot{\theta}}$.

Source: prepared by the author.

plotted four results in polar coordinates for $\tau_{max} = 10, 40, -10, -40 Nm$ for the muscles set QHG, $L = 0.01$ and $h = 1$ in Figures 6.24(a), (b), (c) and (d), respectively. We plotted the baseline without passive orthoses in dashed red. Observing the right quadriceps, hamstrings, gluteus maximus, and orthosis in Figure 6.15, we note that the spring interferes between the crankset angles 210° and 330°, approximately. At the beginning of the spring interference (around 210°), the knee is flexing (c.f., Figure 6.16) and there is no muscle activated at this leg. If we consider the negative τ_{max} (Figures 6.24(c) and (d)), the spring is the only feature releasing energy to aid the movement. At the point where the knee starts to extend, and the spring starts to accumulate energy (between 270° and 330°), we start to activate the right quadriceps. This effect increases the cy-

119

cling cadence at this range (c.f. the blue compared to the black line in Figures 6.24(c) and (d)). The same happens when the left leg reaches the opposite side due to cycling geometry.

If we consider positive τ_{max}, between the crankset angles 210° and 270°, the spring extends the knee while it is supposed to flex. Therefore, this effect decreases the cycling cadence in this range. Although after the spring releases the energy (i.e., aiding the movement), the quadriceps torque is sufficiently high to generate the movement at itself. As the gluteus and hamstrings are weaker muscles compared to the quadriceps, the spring does not sufficiently aid the quadriceps when compared to hamstrings and gluteus maximus.
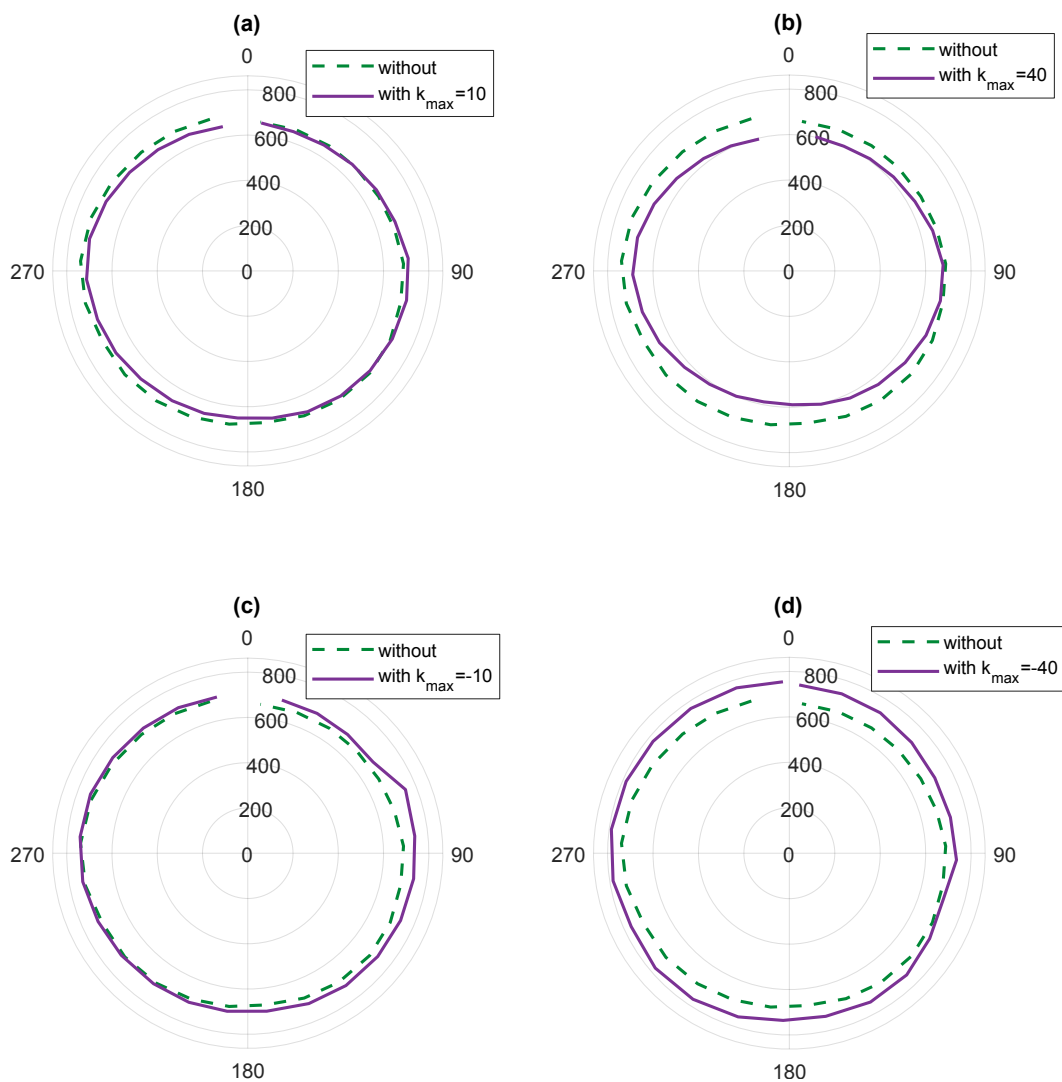
Figure 6.24: Cycling cadence in polar coordinates of the last complete cycles (from $\theta_c = 0°$ to $\theta_c = 360°$) of results with and without springs with $\tau_{max} = \{10, 40, -10, -40\}$ Nm. We kept $F = 0$ and $L = 0.01$. (a) Results for $\tau_{max} = 10$ Nm. (b) Results for $\tau_{max} = 40$ Nm. (c) Results for $\tau_{max} = -10$ Nm. (d) Results for $\tau_{max} = -40$ Nm.

Source: prepared by the author.

120

As our aim is to increase the average cadence, we define a successful result with the orthoses when the mean cycling cadence at the last cycle is higher than the result without orthoses. Table 6.6 presents the percentage for success for each negative τ_{max}.

Table 6.6: Success rates for simulations in which we ranged τ_{max}.

$-\tau_{max}$ [Nm]	Success rate
40	86%
35	70%
30	56%
25	53%
20	63%
15	50%
10	70%
5	66%

6.3.3.2 Actuation range

Similarly to Section 6.3.3.1, in this section we analyze the results in terms of the actuation ranges. In Figures 6.25, 6.26, 6.27, 6.28 and 6.29, we marked the baseline results with black dashed lines. In each figure, we presented the simulation cadences from the three muscle sets with and without loads. In these figures we also plotted the error bars with the mean crankset cadence $(\bar{\theta}_c)$ and three times the standard deviation $(3\sigma_{\dot{\theta}})$ at the last cycle (for each θ_s).
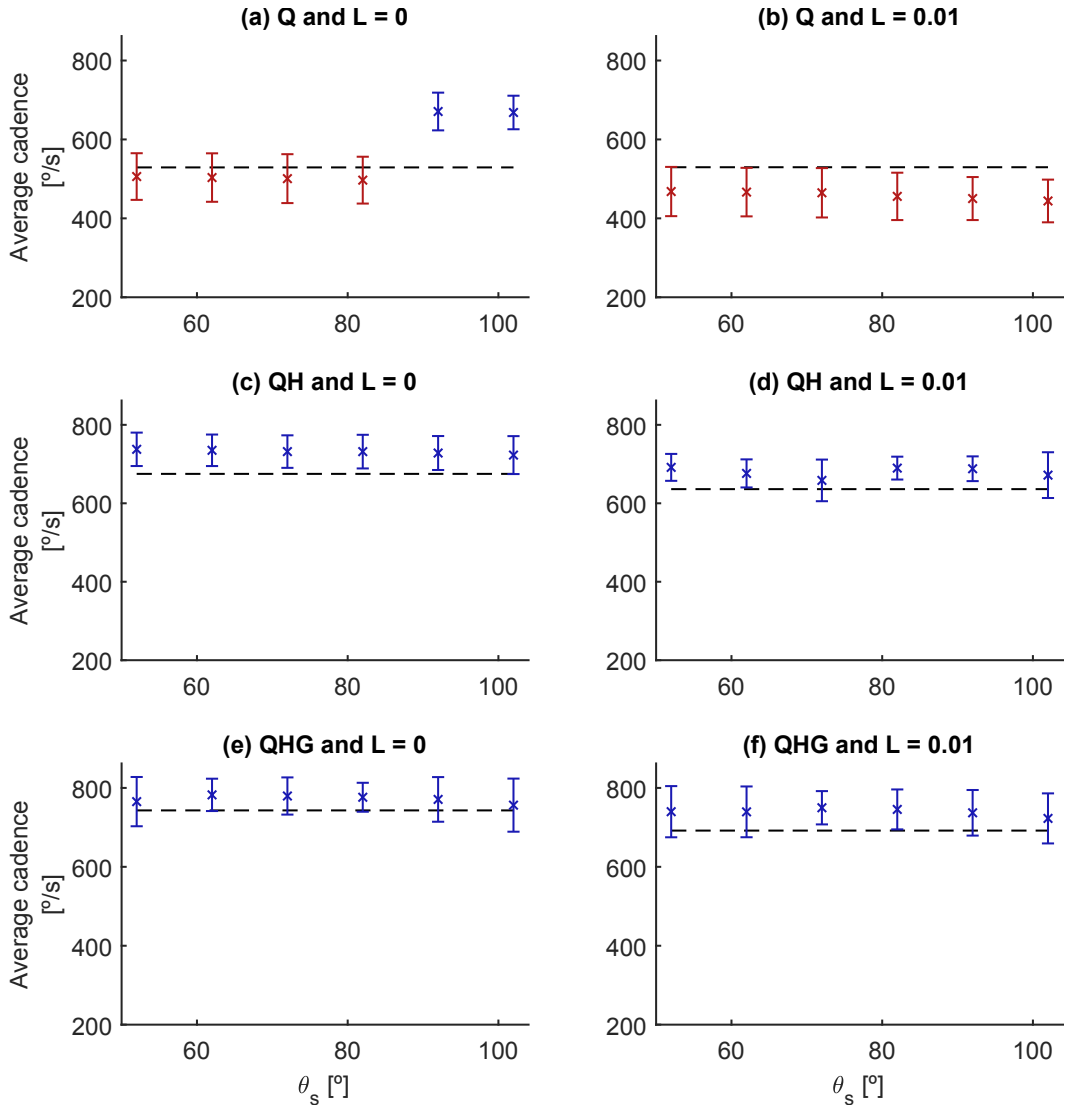
Figure 6.25: Last cycle average cadences with respect to $\Delta\theta$. The dashed black line represents the reference crankset ($\tau_{max} = 0$). In these simulations, we used the BB controller with $h = 1$ and marked all cadences greater than the baseline in blue, and the cadences lower than the baseline in red.

Source: prepared by the author.
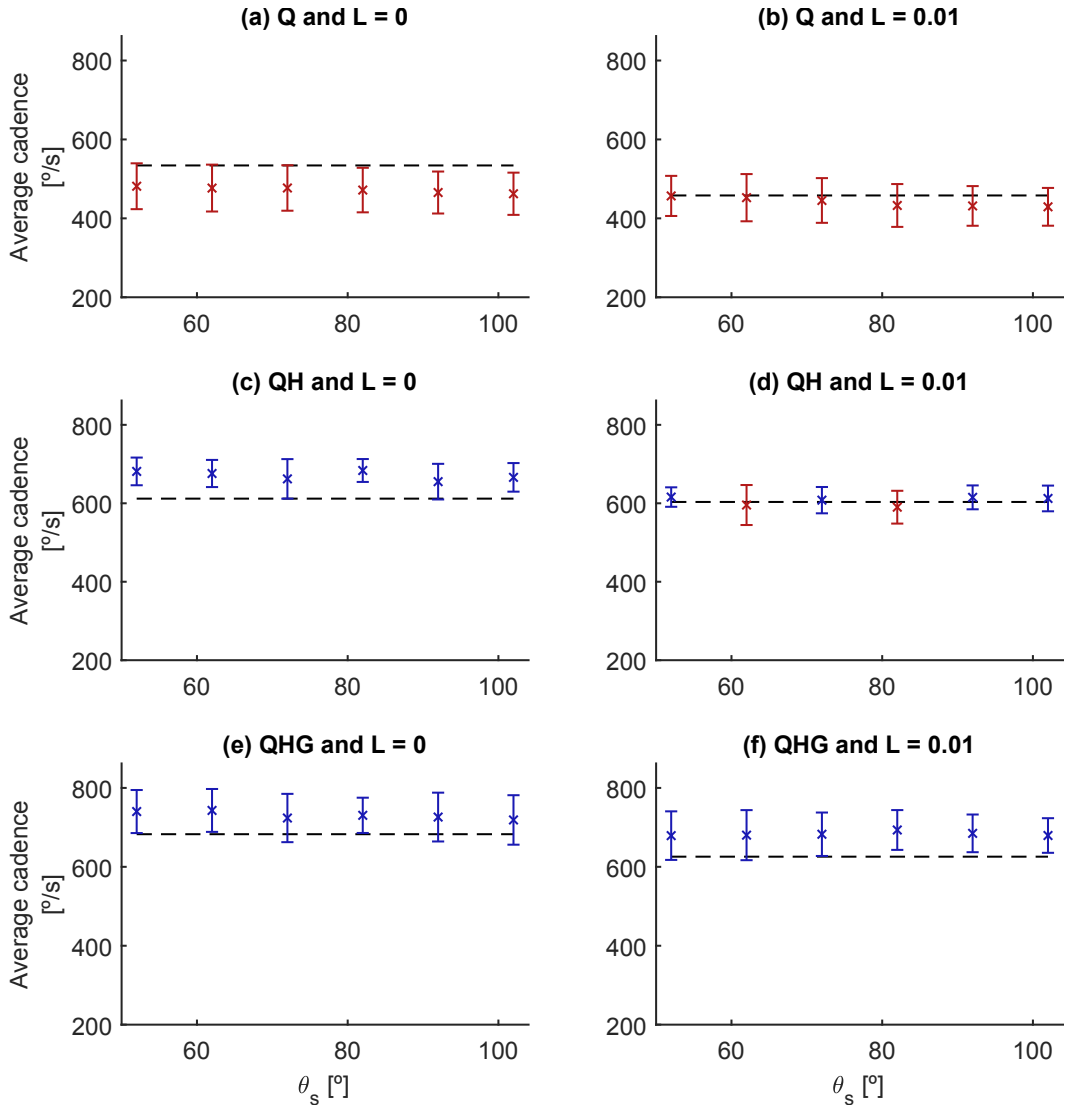
Figure 6.26: Last cycle average cadences with respect to $\Delta\theta$. The dashed black line represents the reference crankset ($\tau_{max} = 0$). In these simulations, we used the BB controller with $h = 0.9$ and marked all cadences greater than the baseline in blue, and the cadences lower than the baseline in red.

Source: prepared by the author.
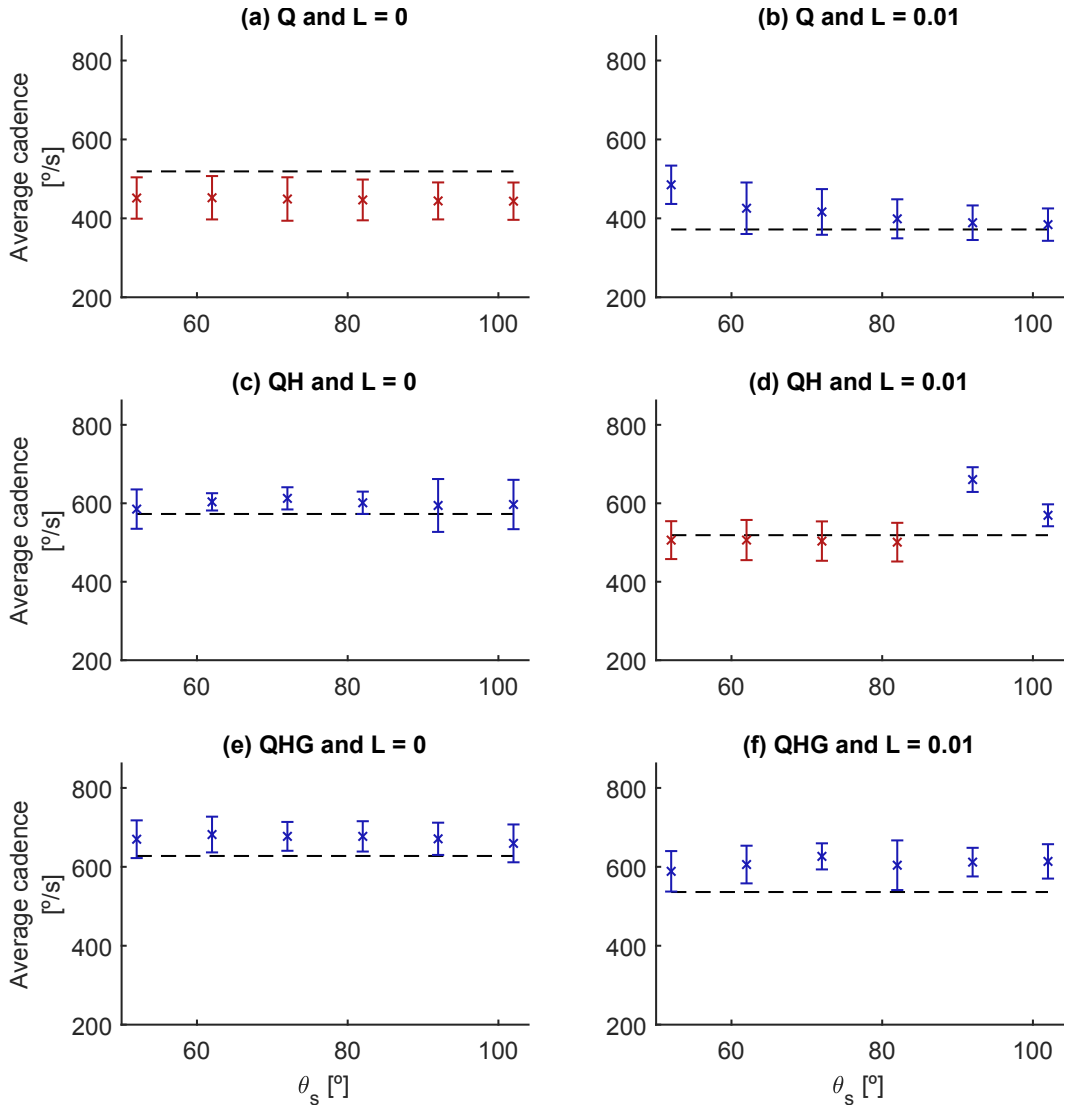
Figure 6.27: Last cycle average cadences with respect to $\Delta\theta$. The dashed black line represents the reference crankset ($\tau_{max} = 0$). In these simulations, we used the BB controller with $h = 0.8$ and marked all cadences greater than the baseline in blue, and the cadences lower than the baseline in red.

Source: prepared by the author.
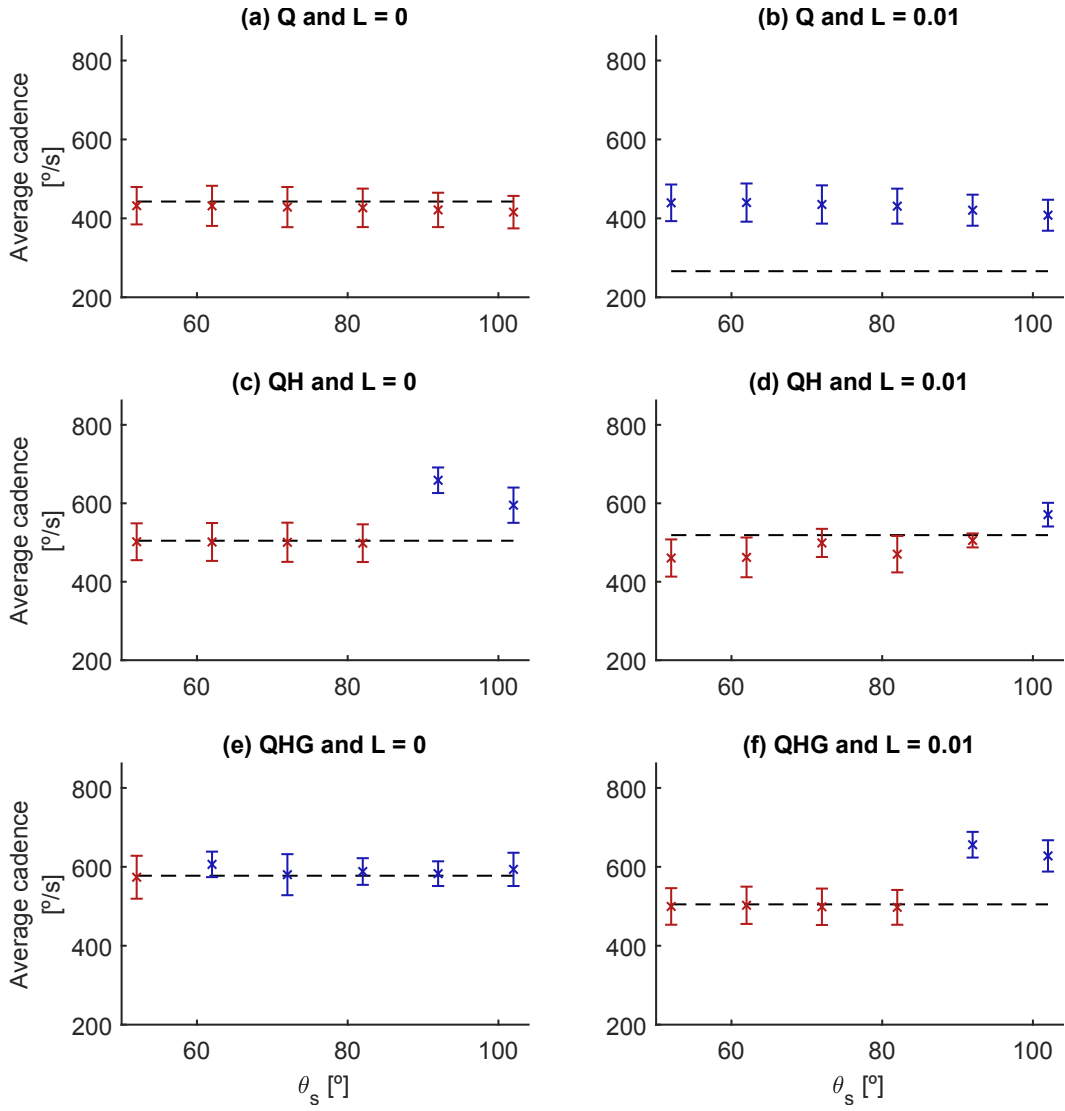
Figure 6.28: Last cycle average cadences with respect to $\Delta\theta$. The dashed black line represents the reference crankset ($\tau_{max} = 0$). In these simulations, we used the BB controller with $h = 0.7$ and marked all cadences greater than the baseline in blue, and the cadences lower than the baseline in red.

Source: prepared by the author.
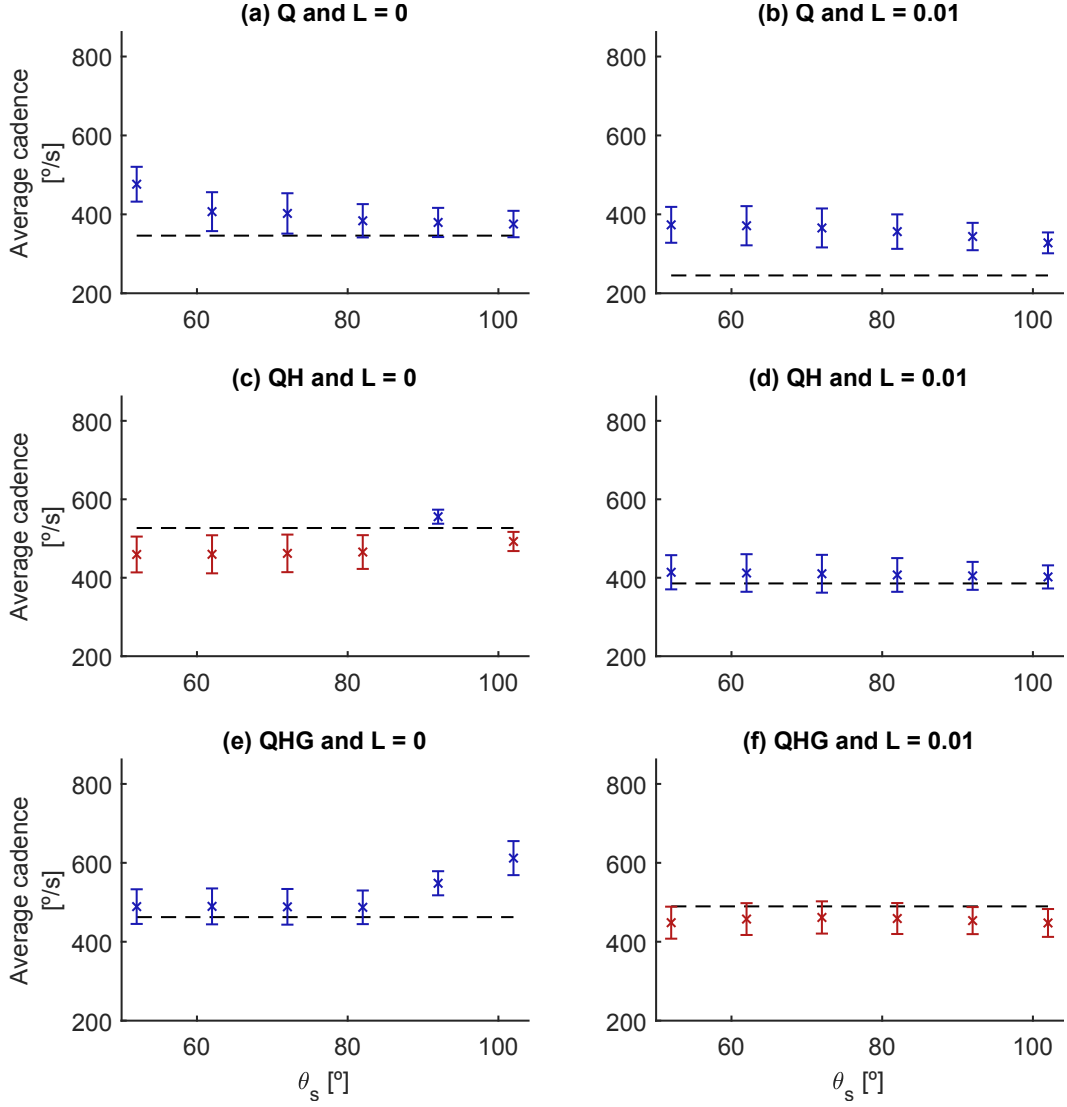
Figure 6.29: Last cycle average cadences with respect to $\Delta\theta$. The dashed black line represents the reference crankset ($\tau_{max} = 0$). In these simulations, we used the BB controller with $h = 0.6$ and marked all cadences greater than the baseline in blue, and the cadences lower than the baseline in red.

Source: prepared by the author.

In Figures 6.25 to 6.29, we observed that most θ_s improved the cycling average speed. The plots also indicate that higher θ_s (i.e., lower ranges 10° and 20°) led to higher cadences and lower standard deviation errors. In this configuration, the right and left springs do not act simultaneously. Therefore, the higher results are probably due to this dynamic actuation of the springs in synchronization only with the knee movements. The actuation of both springs at the same time could likely lead to additional efforts during cycling, decreasing the movement efficiency. Appendix C present Tables C.18, C.17, C.16, C.15 and C.14 that summarize the numerical results for $\bar{\dot{\theta}}_c$, $\ddot{\theta}_c$ and $\sigma_{\dot{\theta}}$.

Similarly to Section 6.3.3.1, we created 3-D plots with the results from all θ_s (Figures 6.30 and 6.31). In Figure 6.30, we observe that between $300°/s$ and $400°/s$ (Figure 6.30(a) and (c)) the use of springs increases the final speed when compared to the baseline. Both results indicate a correlation between the spring actuation and the cycling cadence, not only the spring parameters.
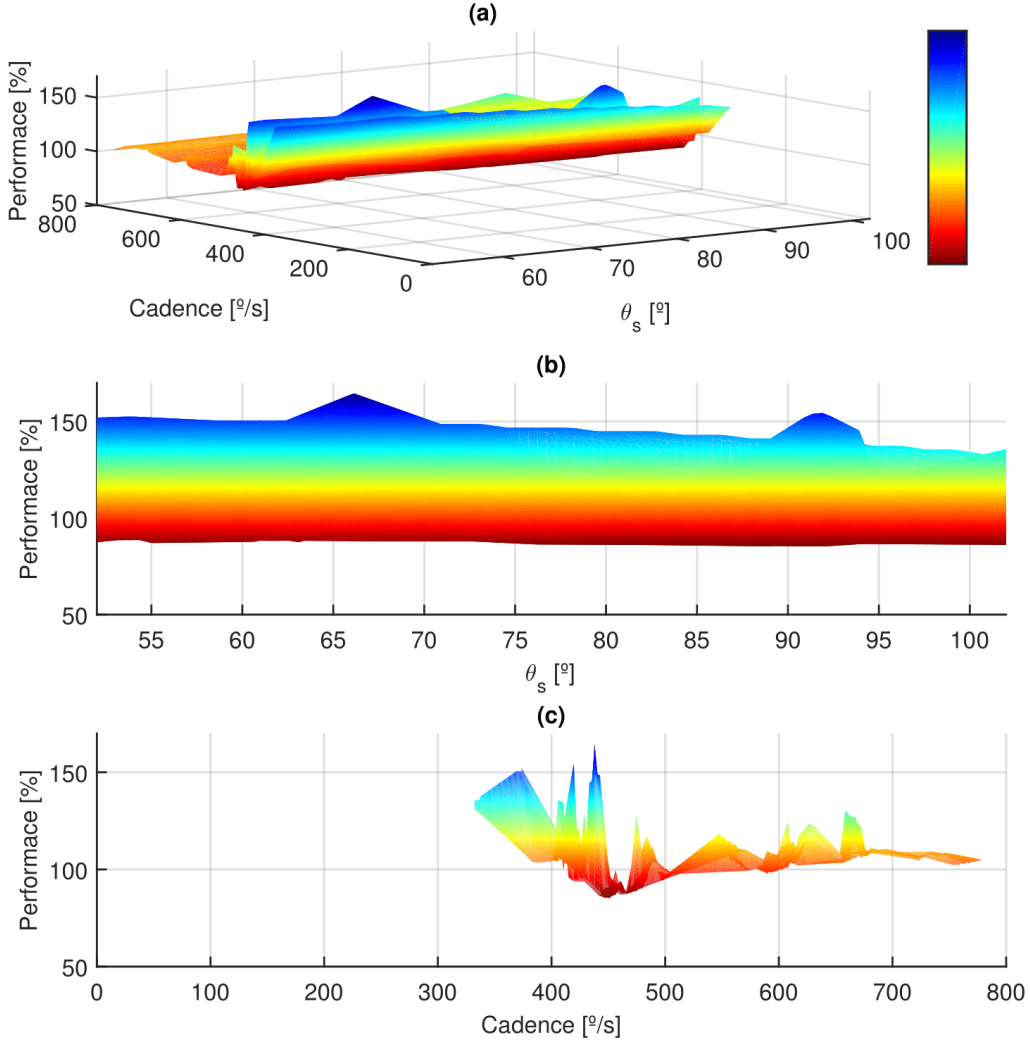
Figure 6.30: Simulation performace of the average cycling ($\bar{\dot{\theta}}_c$) for all θ_s. Blue represents higher $\bar{\dot{\theta}}_c$ (compared to the previously simulated baseline that corresponds to the same muscle set, h and L), and red, lower $\bar{\dot{\theta}}_c$. (a) 3-D plot. (b) Detail of performace and θ_s. (c) Detail of performace and $\bar{\dot{\theta}}_c$.

Source: prepared by the author.

Similarly to τ_{max}, we also performed 30 simulations for each $\Delta\theta$ (three muscle group sets, five excitation magnitudes, two loads) in Section 6.3.3.2. Table 6.7 presents the percentage for success for each $\Delta\theta$.
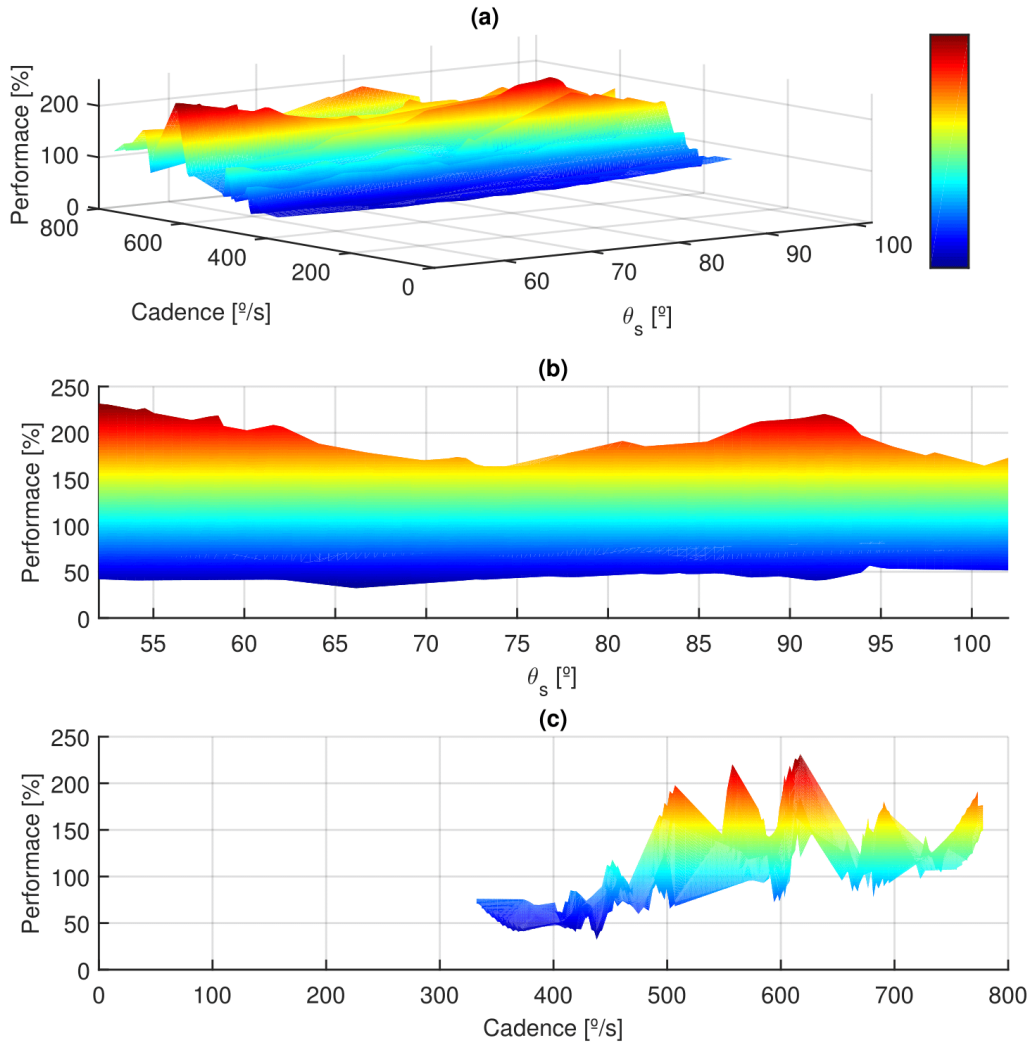
Figure 6.31: Simulation performace of the standard deviation of the cycling cadence $(\sigma_{\dot{\theta}})$ for all θ_s. Red represents higher $\sigma_{\dot{\theta}}$ (compared to the previously simulated baseline that corresponds to the same muscle set, h and L), and blue, lower $\sigma_{\dot{\theta}}$. (a) 3-D plot. (b) Detail of performace and θ_s. (c) Detail of performace and $\sigma_{\dot{\theta}}$.

Source: prepared by the author.

Table 6.7: Success rates for simulations in which we ranged $\Delta\theta$.

$\Delta\theta$ [°]	Success rate
10	76%
20	76%
30	56%
40	60%
50	56%
60	56%

6.3.4 PID controller with passive orthoses

After the spring parameters simulations, we compared the cadence of simulations with and without passive orthoses for different speeds controlled by the PID controller.

6.3.4.1 Spring parameters for PID control

We based our choice for the spring parameters (τ_{max} and θ_s) on the results provided by Section 6.3.3. First, we need to find suitable elastic constant values for manufacturing. As we intend to design the orthoses with rotational springs, we need to calculate the elastic constant K_e related to τ_{max} and θ_s

$$K_e = \frac{\tau_{max}}{\Delta\theta}. \tag{6.14}$$

From the Table 6.6, we observed higher success rates in $\tau_{max} = \{-40, -35\}$ Nm with 86% and 70%. However, these values would demand elastic constants values between 4 and 0.58Nm/°. Although we may develop a system with these spring parameters, in our project, we intend to design more general and cheaper passive orthoses, i.e., use standard spring constants. Therefore, as a design requirement, we limited $K_e <$ 0.5 Nm. Moreover, higher K_e could require motors at the beginning of the movement, and we aim not to interfere with the autonomy of an FES cycling system. From this requirement, the next viable option for τ_{max} is -10 Nm (with 70% success). With this parameter, we could still choose $\Delta\theta$ between 20 and 60, which would lead to K_e between 0.50 and 0.167 Nm/°.

With $\Delta\theta = 10$° and 20°, Table 6.7 show higher success rates (76%). To keep the requirement ($K_e < 0.5$), we choose $\Delta\theta = 20$°. Therefore, we simulated the PID controller with $\tau_{max} = $ -10 and $\Delta\theta = 20$°.

6.3.4.2 Results

To visualize the performance of cycling with this passive orthosis and PID control, we kept $K_p = 1.0$, $K_i = 0.55$ and $K_d = 0$ with the muscle group set QHG. We fixed $f = 50$ Hz, $T_f = 20$s and the initial position with the right foot standing on the top, at $\theta_c = 0$°. To analyze the start of cycling, we kept the accelerating torque as zero (i.e., no motor at the beginning $\tau_{acc} = 0$). Based on cadence references from real FES cycling with subjects with SCI (BÓ et al., 2017), we simulated the three cadence references 260°/s, 300°/s, and 360°/s.

For each cadence reference, we simulated these systems with and without a load at the crankset ($L = 0$ and $L = 0.01$). Further, we simulated with and without the effect

of fatigue ($F = 0$ and $F = 10$). Table 6.8 summarizes all 12 simulations (3 references, 2 loads and 2 fatigue time constant).

Table 6.8: Configurations for simulations to determine the effect of a specific passive orthosis and the PID control.

Reference [°/s]	L	F
{260, 300, 360}	{0, 0.01}	{0, 10}

Figures 6.32, 6.33, 6.34 and 6.35 present all 12 cycling cadence plots through time. We divided in 4 figures ($\{L = 0, F = 0\}$, $\{L = 0.01, F = 0\}$, $\{L = 0, F = 10\}$ and $\{L = 0.01, F = 10\}$) with three subplots for each reference ($\{260, 300, 360\}$°/s). We present all performance results in Tables 6.9 to 6.11.
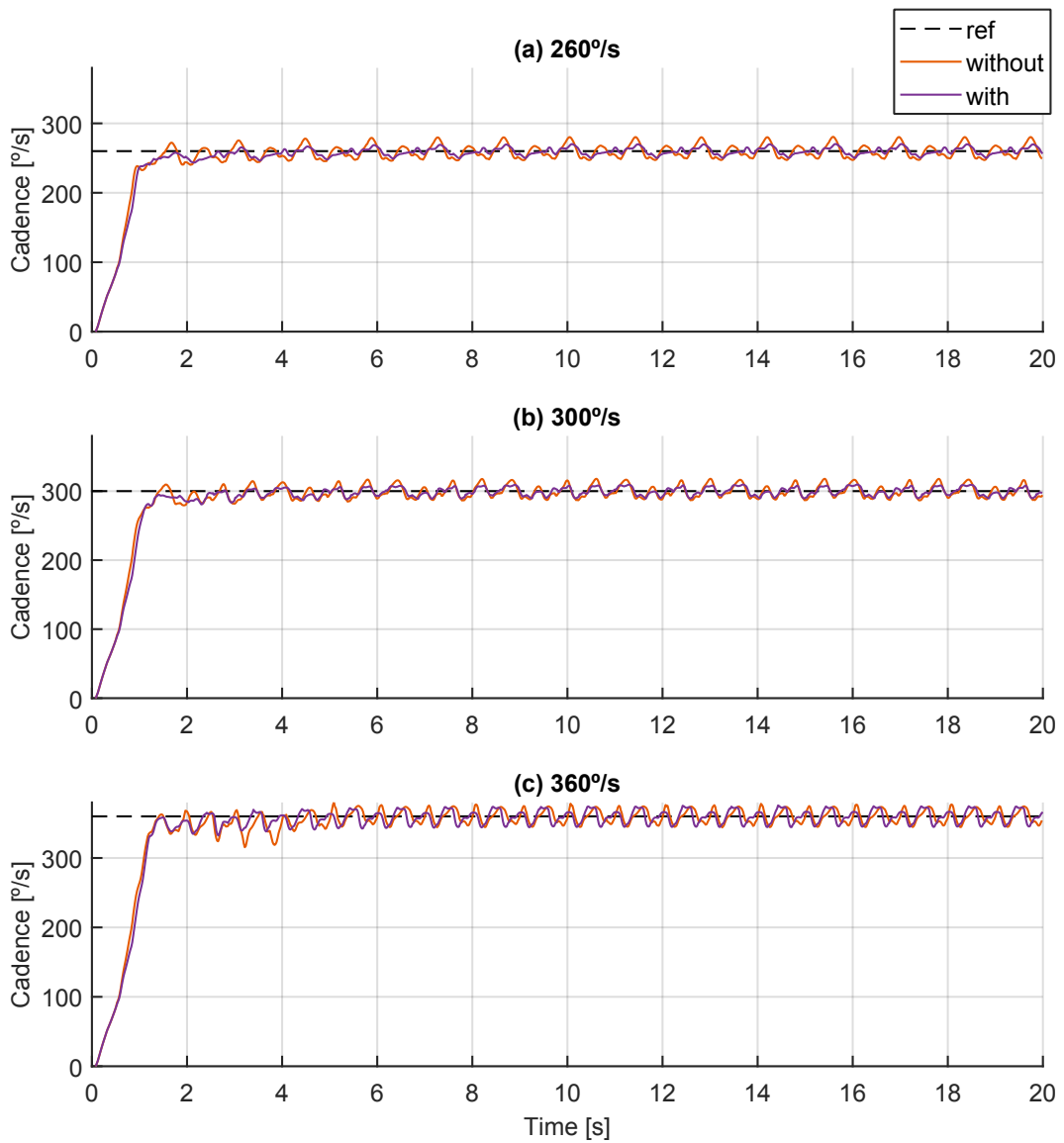
Figure 6.32: Cycling cadence simulations through 20 seconds of PID controller with orthoses. In this simulation $L = 0$ and $F = 0$.

Source: prepared by the author.
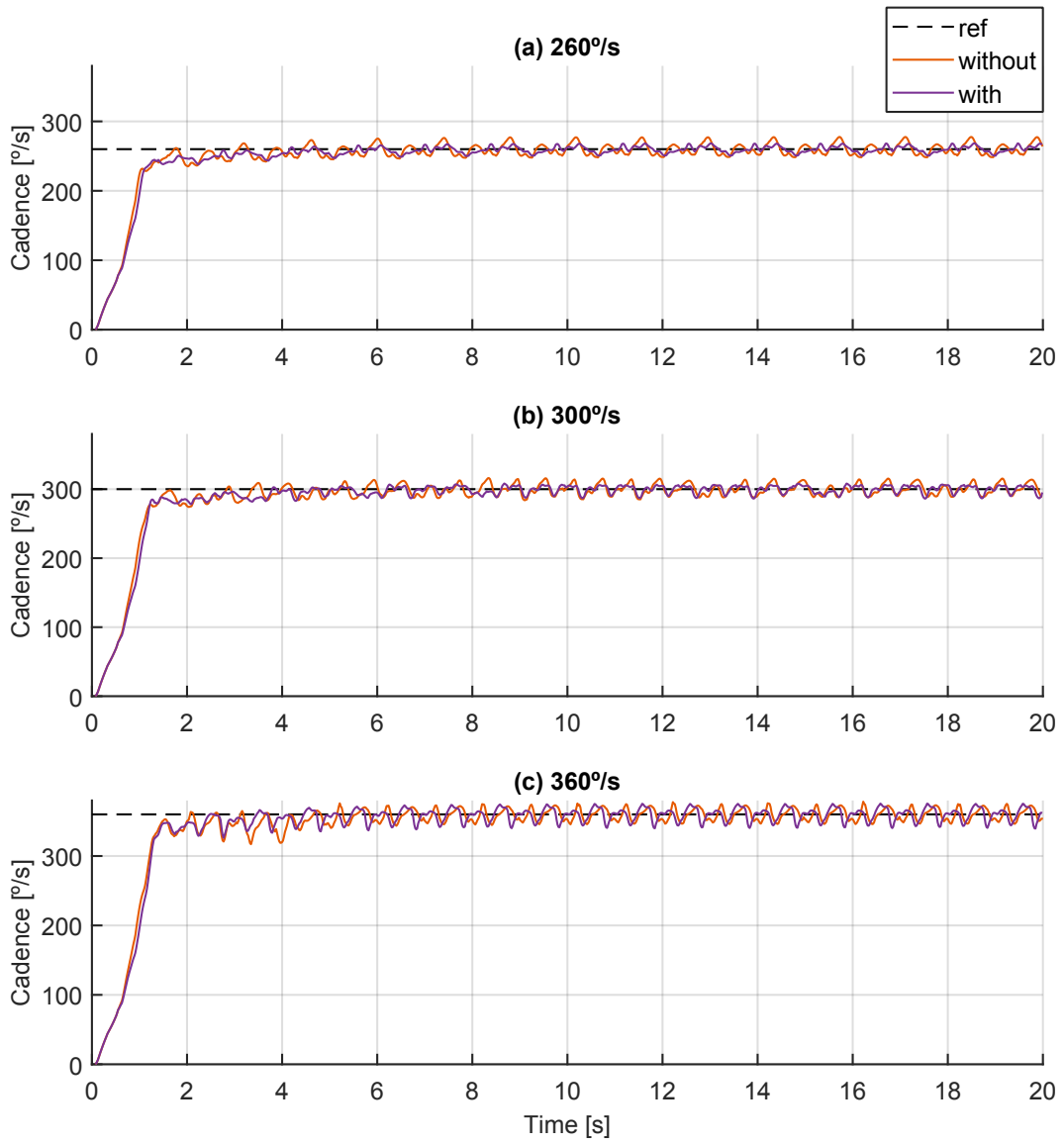
Figure 6.33: Cycling cadence simulations through 20 seconds of PID controller with orthoses. In this simulation $L = 0.01$ and $F = 0$.

Source: prepared by the author.
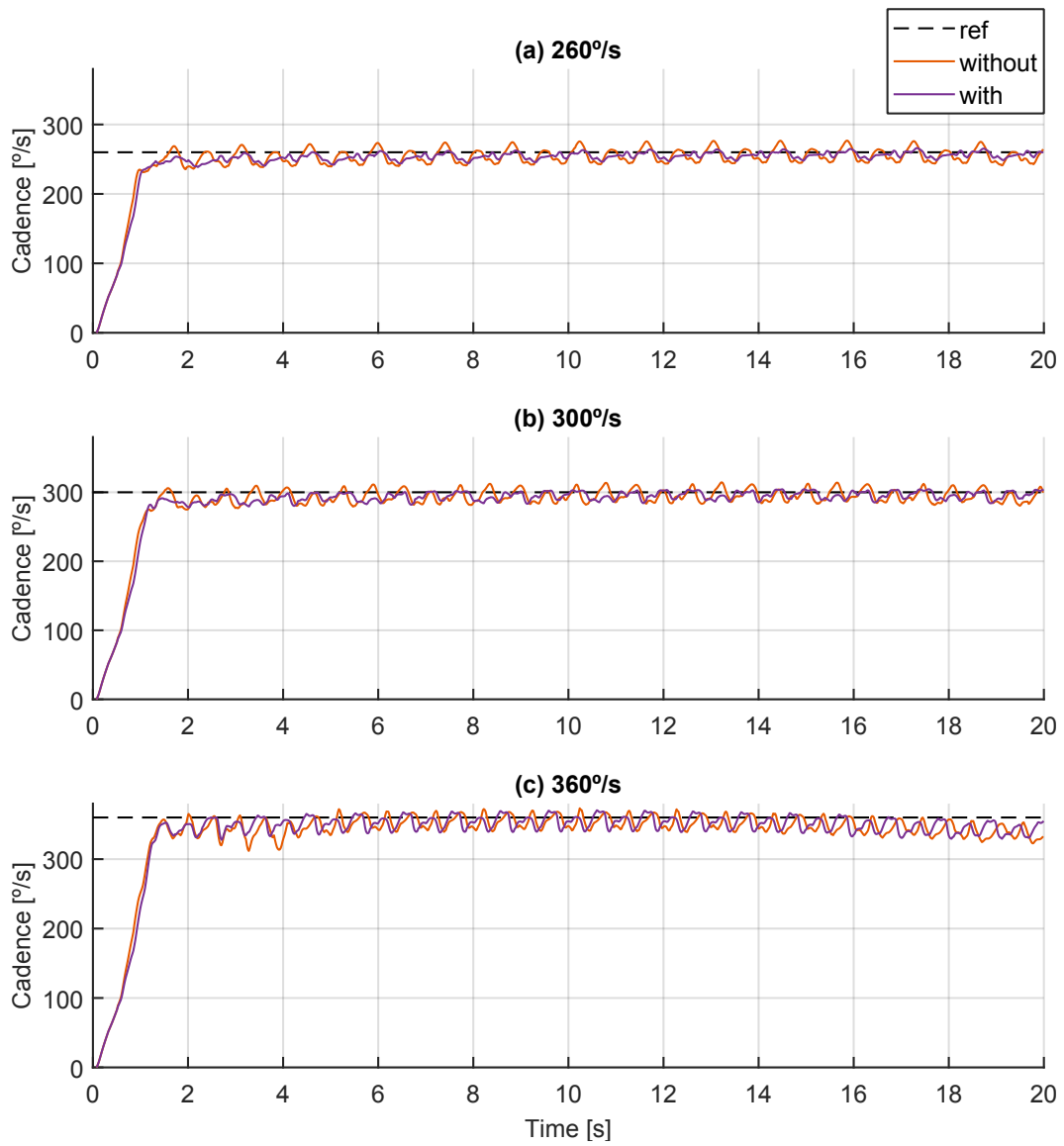
Figure 6.34: Cycling cadence simulations through 20 seconds of PID controller with orthoses. In this simulation $L = 0$ and $F = 10$.

Source: prepared by the author.
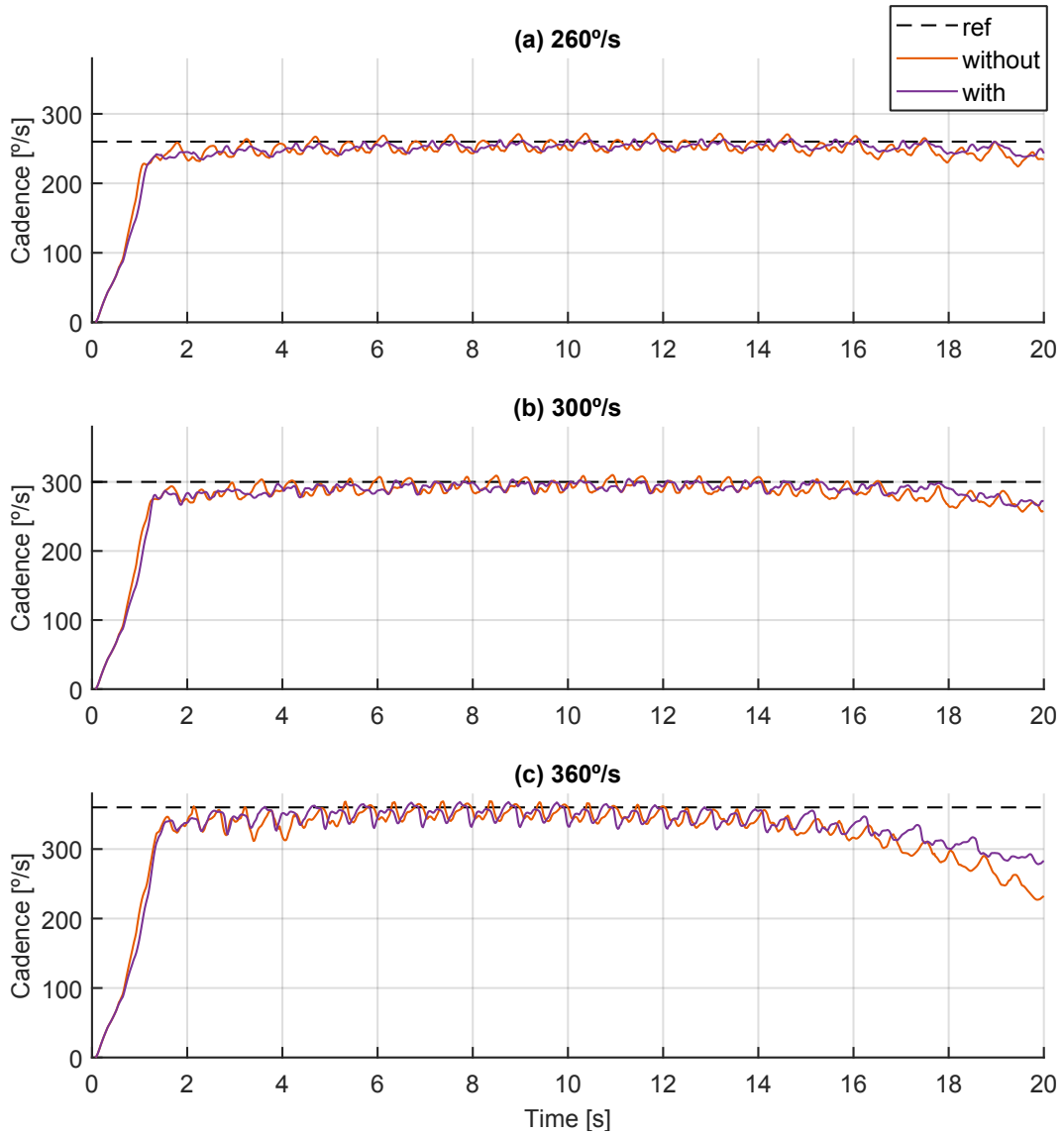
Figure 6.35: Cycling cadence simulations through 20 seconds of PID controller with orthoses. In this simulation $L = 0.01$ and $F = 10$.

Source: prepared by the author.

6.3.5 Discussion

The higher cadences result with passive orthoses not necessarily lead to tolerable elastic constant values for the spring, as we showed in the example for the PID control in Section 6.3.4.1. As this project requirement was to keep this constant lower than 0.5 Nm/°, we only observed the torque and range parameters that attend these specifications.

The PID controller adjusts the muscle excitation to maintain a reference cadence. Therefore, the average cadences at the last cycle remain alike with and without passive orthoses. Figures 6.32 to 6.35 and Tables 6.9 to 6.11 confirm that most er-

Table 6.9: Spring performance parameters with the PID controller for 260°/s reference.

$F{=}0$ $L{=}0$ Orthoses	$\bar{\theta}_c$	$\sigma_{\dot\theta}$	e_{max}	e_{RMSE}	t_r	$\{\Phi_Q, \Phi_H, \Phi_G\}$
without	260.0	9.5	20.4	9.5	0.7	$\{0.091, 0.057, 0.046\}$
with	259.9	4.9	9.9	4.9	0.8	$\{0.081, 0.076, 0.070\}$
	0.0%	-92.8%	-105.7%	-92.8%	10.0%	$\{-12.1\%, 24.5\%, 33.6\%\}$

$F{=}0$ $L{=}0.01$ Orthoses	$\bar{\theta}_c$	$\sigma_{\dot\theta}$	e_{max}	e_{RMSE}	t_r	$\{\Phi_Q, \Phi_H, \Phi_G\}$
without	260.0	8.1	17.3	8.0	1.0	$\{0.136, 0.099, 0.073\}$
with	260.0	4.6	8.2	4.6	0.9	$\{0.122, 0.112, 0.092\}$
	0.0%	-75.2%	-110.0%	-75.2%	-11.4%	$\{-11.4\%, 12.0\%, 20.8\%\}$

$F{=}10$ $L{=}0$ Orthoses	$\bar{\theta}_c$	$\sigma_{\dot\theta}$	e_{max}	e_{RMSE}	t_r	$\{\Phi_Q, \Phi_H, \Phi_G\}$
without	254.2	9.5	20.9	9.5	0.7	$\{0.031, 0.013, 0.011\}$
with	257.0	4.3	8.4	4.2	0.8	$\{0.028, 0.018, 0.024\}$
	1.1%	-124.0%	-150.3%	-124.0%	12.5%	$\{-11.1\%, 31.2\%, 53.0\%\}$

$F{=}10$ $L{=}0.01$ Orthoses	$\bar{\theta}_c$	$\sigma_{\dot\theta}$	e_{max}	e_{RMSE}	t_r	$\{\Phi_Q, \Phi_H, \Phi_G\}$
without	239.6	8.5	20.1	8.4	0.8	$\{0.043, 0.040, 0.029\}$
with	247.5	6.6	12.5	6.5	0.9	$\{0.041, 0.040, 0.029\}$
	3.2%	-29.3%	-60.7%	-29.3%	12.9%	$\{-6.5\%, -0.3\%, -1.7\%\}$

rors ($\sigma_{\dot\theta}$, e_{RMSE} and e_{max}) decreased with passive orthoses when compared to the cycling without orthoses assistance. In some results, the passive orthoses decreased more than half (e.g., e_{max} decreased 150.3% with $F = 10$ and $L = 0$, for 260°/s reference). These results also confirm the polar plot explanation for the effect of the passive orthoses in Section 6.3.3.1.

The most compelling difference happened in Figure 6.35c (Table 6.11), the final average cadence with orthoses was 288°/s (11% higher than the result without passive orthoses of 255°/s). This increase in cadence is evidence that the use of passive orthoses may reduce the demand for muscular activation, delaying fatigue. Besides, this specific configuration is the closest to a real system with a subject with SCI: there is fatigue, load, and the cadence is around 360°/s.

One adverse effect of passive orthoses is the slightly higher rising time (t_r), i.e., the spring makes it harder to start the cycling. Although the spring provides energy to the system half the time, the other half it acts as an extra load. At lower cadences, this extra load interferes further at the system due to the lack of cycling inertia. This rising time increase did not entirely block the cycling movement at the beginning of

Table 6.10: Spring performance parameters with the PID controller for 300°/s reference.

$F{=}0$	$L{=}0$					
Orthoses	$\bar{\theta}_c$	$\sigma_{\dot\theta}$	e_{max}	e_{RMSE}	t_r	$\{\Phi_Q,\Phi_H,\Phi_G\}$
without	297.2	8.0	19.0	7.9	0.8	{0.119,0.087,0.051}
with	297.6	5.5	10.5	5.5	0.9	{0.108,0.098,0.063}
	0.1%	-44.6%	-81.3%	-44.6%	4.7%	{-10.1%,10.7%,18.1%}

$F{=}0$	$L{=}0.01$					
Orthoses	$\bar{\theta}_c$	$\sigma_{\dot\theta}$	e_{max}	e_{RMSE}	t_r	$\{\Phi_Q,\Phi_H,\Phi_G\}$
without	302.0	8.1	13.5	8.0	0.9	{0.130,0.092,0.043}
with	300.1	5.6	5.8	5.6	0.9	{0.118,0.108,0.057}
	-0.7%	-43.4%	-131.3%	-43.4%	2.2%	{-9.5%,14.8%,24.4%}

$F{=}10$	$L{=}0$					
Orthoses	$\bar{\theta}_c$	$\sigma_{\dot\theta}$	e_{max}	e_{RMSE}	t_r	$\{\Phi_Q,\Phi_H,\Phi_G\}$
without	291.7	8.1	17.2	8.1	0.8	{0.033,0.022,0.013}
with	295.7	6.1	8.3	6.0	0.9	{0.041,0.019,0.003}
	1.4%	-33.5%	-108.0%	-33.5%	6.8%	{19.2%,-15.2%,-360.2%}

$F{=}10$	$L{=}0.01$					
Orthoses	$\bar{\theta}_c$	$\sigma_{\dot\theta}$	e_{max}	e_{RMSE}	t_r	$\{\Phi_Q,\Phi_H,\Phi_G\}$
without	269.3	8.1	17.7	8.0	0.9	{0.043,0.042,0.029}
with	272.6	5.6	11.3	5.6	1.0	{0.041,0.039,0.029}
	1.2%	-43.5%	-56.8%	-43.5%	8.1%	{-4.2%,-6.5%,1.4%}

the simulation, probably due to a small K_e. Therefore, these parameters still attend to the initial project requirements.

Tables 6.9 to 6.11 show that the simulations with orthoses usually presented a lower muscles excitation (e.g., Φ_{QUAD}, Φ_{HAMS} and Φ_{GLUT} decreased more than 5% for 7 of the 12 simulations). At the point where the quadriceps must be excited, the spring already provided energy and increased the cadence (cf. Section 6.3.3.1), a similar effect happens to the hamstrings and gluteus. With a higher cadence, the controller tends to decrease the control signal u.

Table 6.11: Spring performance parameters with the PID controller for 360°/s reference.

$F{=}0$	$L{=}0$					
Orthoses	$\bar{\theta}_c$	$\sigma_{\dot{\theta}}$	e_{max}	e_{RMSE}	t_r	$\{\Phi_Q,\Phi_H,\Phi_G\}$
without	359.7	9.7	15.0	9.6	0.9	{0.111,0.093,0.076}
with	360.0	9.3	14.1	9.2	0.9	{0.109,0.099,0.044}
	0.1%	-4.3%	-6.1%	-4.3%	2.3%	{-2.2%,6.4%,-72.3%}

$F{=}0$	$L{=}0.01$					
Orthoses	$\bar{\theta}_c$	$\sigma_{\dot{\theta}}$	e_{max}	e_{RMSE}	t_r	$\{\Phi_Q,\Phi_H,\Phi_G\}$
without	360.1	8.8	15.1	8.7	1.0	{0.150,0.133,0.091}
with	360.1	9.6	15.2	9.5	1.0	{0.141,0.130,0.067}
	0.0%	8.8%	0.7%	8.8%	3.7%	{-6.2%,-2.0%,-35.2%}

$F{=}10$	$L{=}0$					
Orthoses	$\bar{\theta}_c$	$\sigma_{\dot{\theta}}$	e_{max}	e_{RMSE}	t_r	$\{\Phi_Q,\Phi_H,\Phi_G\}$
without	337.5	8.9	15.4	8.8	0.9	{0.039,0.040,0.027}
with	341.6	8.2	14.0	8.1	1.0	{0.044,0.039,0.029}
	1.2%	-8.2%	-10.2%	-8.3%	4.2%	{11.2%,-0.3%,5.0%}

$F{=}10$	$L{=}0.01$					
Orthoses	$\bar{\theta}_c$	$\sigma_{\dot{\theta}}$	e_{max}	e_{RMSE}	t_r	$\{\Phi_Q,\Phi_H,\Phi_G\}$
without	255.1	18.9	35.2	18.7	0.8	{0.040,0.042,0.030}
with	288.0	4.5	6.5	4.5	1.0	{0.040,0.042,0.030}
	11.4%	-316.3%	-443.2%	-316.7%	17.8%	{0.8%,-1.2%,-0.7%}

7 EXPERIMENTAL STUDIES ON CONTROL STRATEGIES FOR FES CYCLING

The simulation results in Chapter 6 led to the conclusion that it was worth to develop and test this type of passive orthoses in FES cycling. Therefore, we established the experimental environment described in Section 7.1, then we determined the protocol (Section 7.2) for comparing the results (Section 7.3) of experiments with and without the passive knee orthoses.

7.1 EXPERIMENTAL ENVIRONMENT FOR FES CYCLING

In our experiments, we used the bang-bang (BB) controller based on the profile described in Figure 7.1. We stimulated only the quadriceps muscles based on a similar range of the Figure 6.15. Using only one channel minimizes the effects of nonlinearities and time-dependent actuation of stimulation. Further, one of the possible applications of the knee orthoses is to replace additional electrodes (IBRAHIM et al., 2008). As we performed experiments with a subject with complete SCI, the system required a robust experimental environment, described in Section 7.1.1, 7.1.2, and 7.1.3.
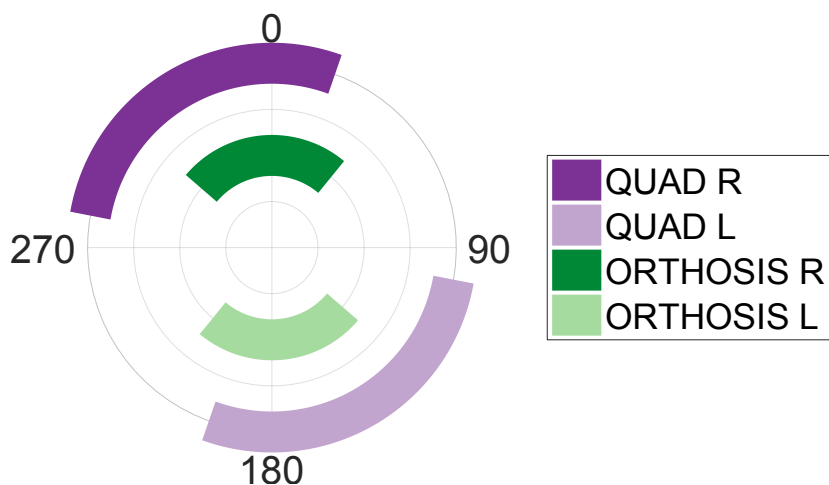
Figure 7.1: Muscles and spring range angles for excitation during a pedal stroke. Right and left quadriceps (QUAD R and L) in purple and right and left orthoses in green (ORTHOSIS R and L). We represent the left side in light colors and the right side in dark colors.

Source: prepared by the author.

7.1.1 Equipment

The experimental setup contains the stimulator, the wireless sensor, the EMA tricycle setup, the passive orthoses, and the computer running the control system.

We used the RehaStim (Hasomed, Germany), an 8-channel stimulator that provides biphasic current pulses and enables online update of stimulation amplitude and PW. We kept the stimulation frequency at $50\,Hz$, and the pulse width at $500\,us$, and we adapted the stimulation current during training; if the cycling was interrupted (probably due to fatigue), we increased the stimulation current by 2mA. For later data analysis, we look for period times with similar stimulation currents.

To calculate the crankset cadence, we first measured the angle with an inertial sensor composed of 3-axis accelerometer, gyroscope, and magnetometer. The sensor (3-space, YEI Technology, USA) features onboard quaternion-based Kalman filtering algorithms to estimate angles. From this data, we discretely differentiated angles for cadence. The sensor was attached to the tricycle crankset, providing real-time information at approximately $160\,Hz$.

For cycling, we adapted a tadpole tricycle (HP3 Trikes, Brazil). The tadpole tricycle contains two wheels at the front and one at the back, which improves stability compared to delta tricycles (one wheel at the front and two at the back). We also adapted orthopedic boots with a structure to be attached to the pedals. The boot supports the entire foot and shins to prevent motion outside the sagittal plane, which may be insecure for a volunteer with SCI. Further, the boots keep the ankle joint 90º at all times. Over the seat, we set cushions to avoid any direct contact with harder parts of the tricycle. For stationary training, we used a passive cycling roller, in which we may increase the load during cycling. Figure 7.2 illustrates the complete system, with detail of the wireless sensor, and the orthopedic boots attached to the pedals (cf. Appendix A for more details about the equipment).

To validate the concept of energy storage devices in FES cycling, we developed a pair of passive knee orthoses with torsion spring support (Figure 7.3). Table 7.1 summarizes the design specifications of the prototype. To guarantee knee support without any harmful effect, we adapted a commercial knee orthosis (Knee Brace R.A, Salvapé, Brazil), replacing the original mechanical structure to insert the elastic element. The knee orthosis accommodates the full range of cycling leg motion, only limiting knee hyperextension. We fabricated a spring holder prototype with 3D printed PETG material (PETG XT Snow White, 3D Fila, Brazil) plastic to position the spring over the knee, and to create torsion in a specific range of cycling. We added two pieces of equal-stiffness torsion AISI 1080 carbon steel springs to our design. It is possible to change these springs to different stiffness for future evaluation. In these experiments,
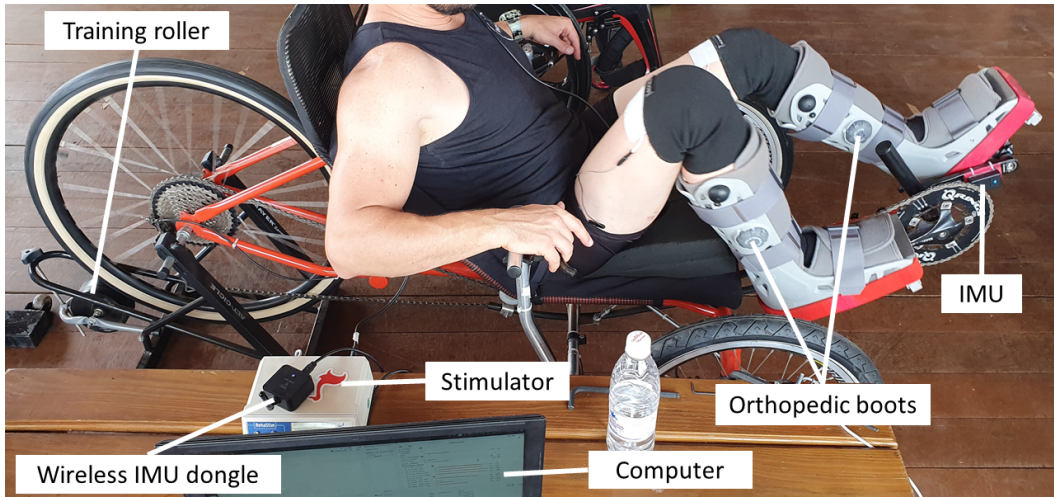
Figure 7.2: The EMA trike complete system. The computer provides the signal to the stimulator based on the crankset angle measured by the IMU. Through surface electrodes on the subject, the stimulator applies the corresponded signal to the muscles to cycle the tricycle. The orthopedic boots attached to the pedals avoid the ankle movement of the volunteer and aligns the legs so it does not fall out of the sagittal plane.

Source: prepared by the author.

we used a 0.125N.m/º stiffness around each knee joint, in which a spring stores energy from knee flexion to release it as the knee extends. Figure 7.1 presents the spring range during one cycle.

Table 7.1: Design requirements of each passive knee orthosis with storage elastic devices.

Specification	Value
Range of knee flexion	complete
Starting angle of torsion spring	92º
Total stiffness around the knee joint	0.125N.m/º
Total mass (with the springs attached)	1.01 Kg (left) and 1.06Kg (right)
Additional width of lateral mechanism	48 mm (each side)
Total mass of each spring	26g

7.1.2 Control system

For control design, we integrated the crankset angle information with the stimulator signal using the Robot Operating System (ROS[1]) and Python scripts. With the ROS platform, we developed a modular system[2], which enables a faster transition

---

[1] A detailed explanation of the ROS platform is available at http://wiki.ros.org/ROS/Introduction.

[2] It is being developed and maintained in https://github.com/lara-unb/ema_fes_cycling.
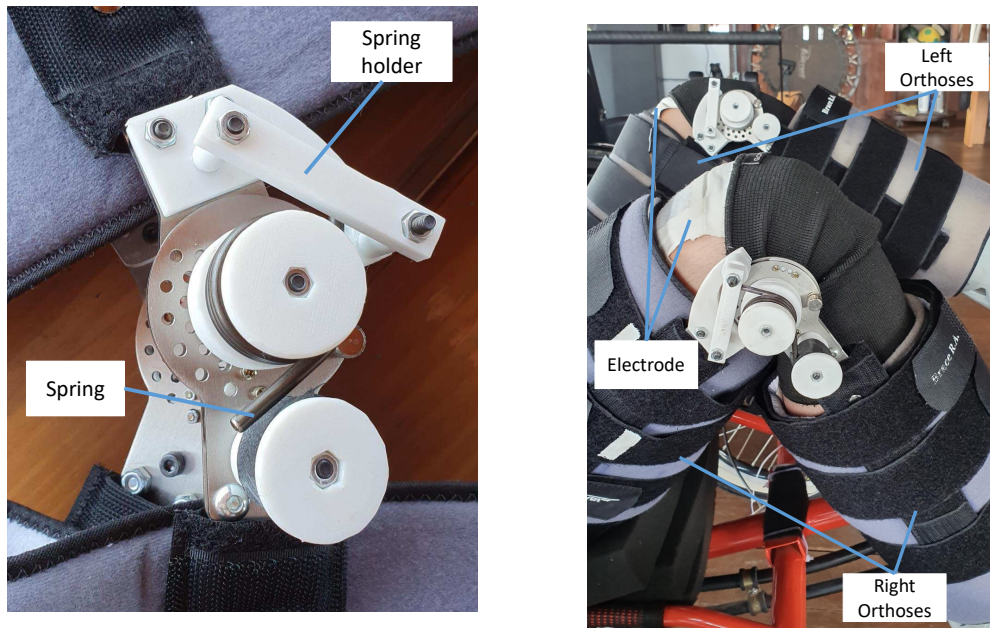
(a) Detail of a spring holder and the spring.

(b) Volunteer using the passive orthosis.

Figure 7.3: Details of the knee passive orthoses for FES cycling.

Source: prepared by the author.

to other applications. Figure 7.4 presents the basic ROS structure used in these experiments. A package is a folder with files organized regarding one or multiple parts of a system. These parts are named ROS nodes (elliptical shapes), described in an executable file (usually there is one node per package). Nodes may communicate with each other by publishing (sending data) or subscribing (receiving data) to a specific ROS topic (channel for message exchanges, arrows).
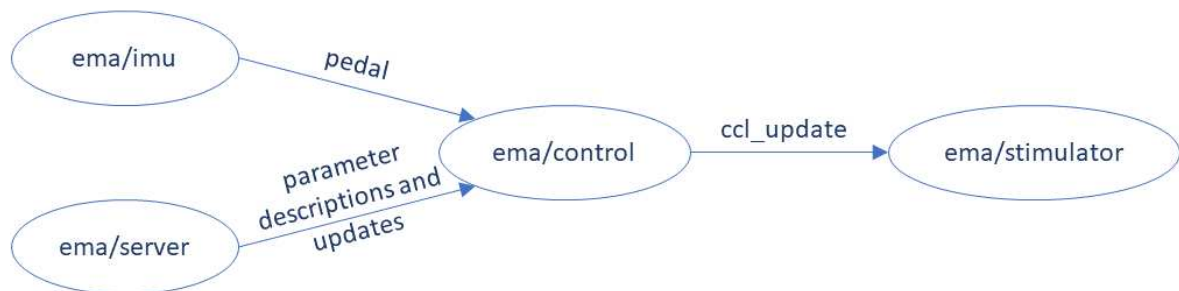
Figure 7.4: Diagram of nodes and topics of the cycling experiment. Elliptical shapes illustrate ROS nodes, and arrows illustrated ROS topics (inward and outward arrows represent subscribing and publishing, respectively).

Source: prepared by the author.

The **server node** establishes the communication between the interface, in which the user determines the maximum current, minimum pulse width, and angle range

for each muscle group. The ROS system collects this information and guarantees the communication between all topics. The **imu node** works as a driver, measuring and publishing the current crankset angle of the pedal to the **control node**. Based on these messages, the control node calculates the current cadence and determines the stimulation signal (channels, current, pulse width, and frequency) to sent them to the **stimulator node**. Figure 7.5 incorporates the BB control system developed in ROS, the equipment (stimulator and IMU), and the musculoskeletal system of the volunteer (muscles). The control executes at 50 Hz.
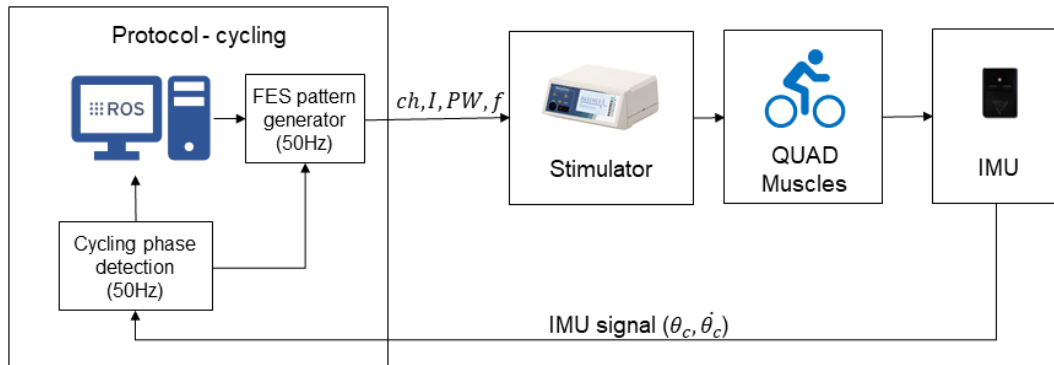
Figure 7.5: Diagram of the cycling control architecture. The controller provides a signal u_x based on the crankset angle θ_c and speed $\dot{\theta}_c$ measured by the IMU. The controller translates u_x to the stimulator, sending the channels to stimulate (ch), current (I), pulse width (PW) and frequency (f). Through surface electrodes on the subject, the stimulator applies the corresponded signal to the quadriceps (QUAD) muscles.

Source: prepared by the author.

7.1.3 Volunteer

Our volunteer with SCI was a 41-year-old male, with American Spinal Injury Association Impairment Scale designation A (AIS A), level T9, injured seven years earlier. This volunteer already uses FES daily and presents a normal cardiovascular response to stress and physical exercise, along with healthy skin. As a subject with AIS A SCI, our cyclist has no sensibility at the lower limbs. While cycling, there are two points of contact with his lower limbs and the tricycle: (1) the pelvis on the seat, and (2) the foot on the pedals. During experiments, the team is always aware of these areas, so the system does not apply excessive pressure and compression, causing injuries. A local ethical committee[3] approved the experimental tests, and the subject provided written consent (Appendix B).

---

[3] Presentation Certificate for Ethical Appreciation (Certificado de Apresentação para Apreciação Ética, CAAE): 11717119.3.0000.0030.

7.2 EXPERIMENTAL PROTOCOL

The experimental protocol consisted of two days of FES cycling exercises. Before the experiment, the volunteer did not use any electrical stimulation at the quadriceps for at least 24h. During exercises, the user used the passive knee orthoses at all times so we could differentiate the effect of the system with and without the springs only. The cyclist performed two exercises each day, maintaining the same position over the seat, and also maintaining the same electrode positioning. Between each of these exercises, we attached or detached the springs and the volunteer rest for 5min.

We performed exercises on two days, on the first day, the user started cycling with the springs, then cycled without them; and on the second day, it was the other way around. That trade was useful so that we may look at both scenarios with the effect of fatigue over time. Each exercise (either with or without springs) consisted of two phases: the warming-up phase and the training phase. Figure 7.6 illustrates the protocol procedure.
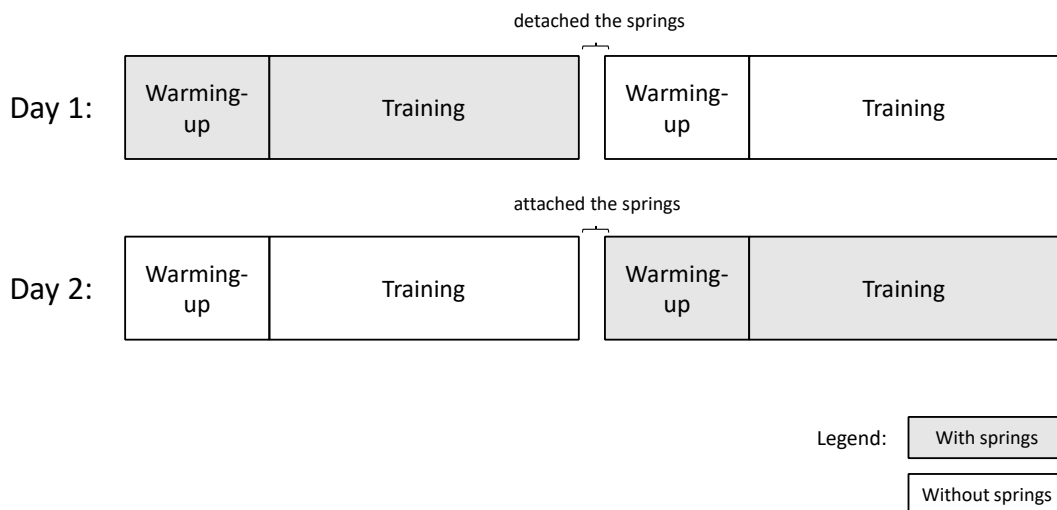
Figure 7.6: Protocol organization. During two days, the user performed two exercises. Before the experiment, the user did not use any electrical stimulation at the quadriceps for at least 24h. At each day, he cycled with and without the springs, divided by the warming-up and the training phases.

Source: prepared by the author.

After adjusting all equipment and the cyclist to the bike, we start the warming-up by manually moving the pedals. While we assist movement, we slowly increase the stimulation current applied to muscles. The warming-up aids to avoid exercise injuries to the user, guaranteeing safety. With our volunteer, if the stimulation increases too fast, it may cause several spasms, which can interfere with the control system and the safety of the user. We consider the warming-up phase finished when the cyclist could

cycle for a few cycles without any external aid; this usually happened around 50mA. Due to muscle fatigue during training, the volunteer can only keep cycling with the same stimulation current for a few minutes, usually stopping at the dead points of the pedal cycle. In the EMA trike, the dead points are around 90º or 270º; at these points, there is no stimulation on either the right or left quadriceps. Therefore, if the system stops for a few times in a row, we increased the stimulation current at steps of 2mA until a safe maximum of 90mA, and then we assisted movement by pushing the foot down. Although the stimulator may reach higher values than 90mA, it may not be safe for the volunteer. As we are continually monitoring the cadence over the graphical interface, sometimes we decides to increase stimulation before stopping movement, so the system runs more smoothly. During the entire exercise, we record the crankset angle, the cadence, and the muscle stimulation parameters.

7.3 RESULTS

On both days, the volunteer was able to cycle with and without the spring using the passive orthoses. The first day of training lasted approximately 30min of cycling, in which 14min were with springs and 16min without springs. On the second day, the volunteer cycled for around 40min, in which 20min were without springs and 20min with springs. The duration of training may differ each day due to the volunteer state (e.g., tiredness).

Figure 7.7 shows the crankset cycling speed during the entire protocol. We recorded the entire warming-up (light green) and training phases (dark green) from all exercises (except for part of the warming-up period of day 2 with the springs), then we used a moving average filter with window size 30 to present and discuss the data. During the training, we mark the point that the warming-up finishes, i.e., when the cyclist may cycle for a few cycles without any external aid. As all warming-up finishes when the stimulation current reaches around 50mA, we set this value as the end of the warming-up phase. In all pieces of training, we will look at the cycling speed between 60mA and 70mA (yellow) for the first day, and between 60mA and 70mA for the second day (yellow). With this data, we may compare within each day the cycling speed with similar muscle excitation, and similar electrodes positions. Sections 7.3.1 and 7.3.2 presents in more details the results from each day of exercise.

7.3.1 First day of training

On the first day, the training with springs lasted approximately 14min, and the training without lasted around 16 min. Figures 7.8 and 7.9 present the cycling speed between 60mA and 70mA with and without springs respectively. In each figure, we represent the cycling speed through time (Figures 7.8a and 7.9a) and over the crankset

144
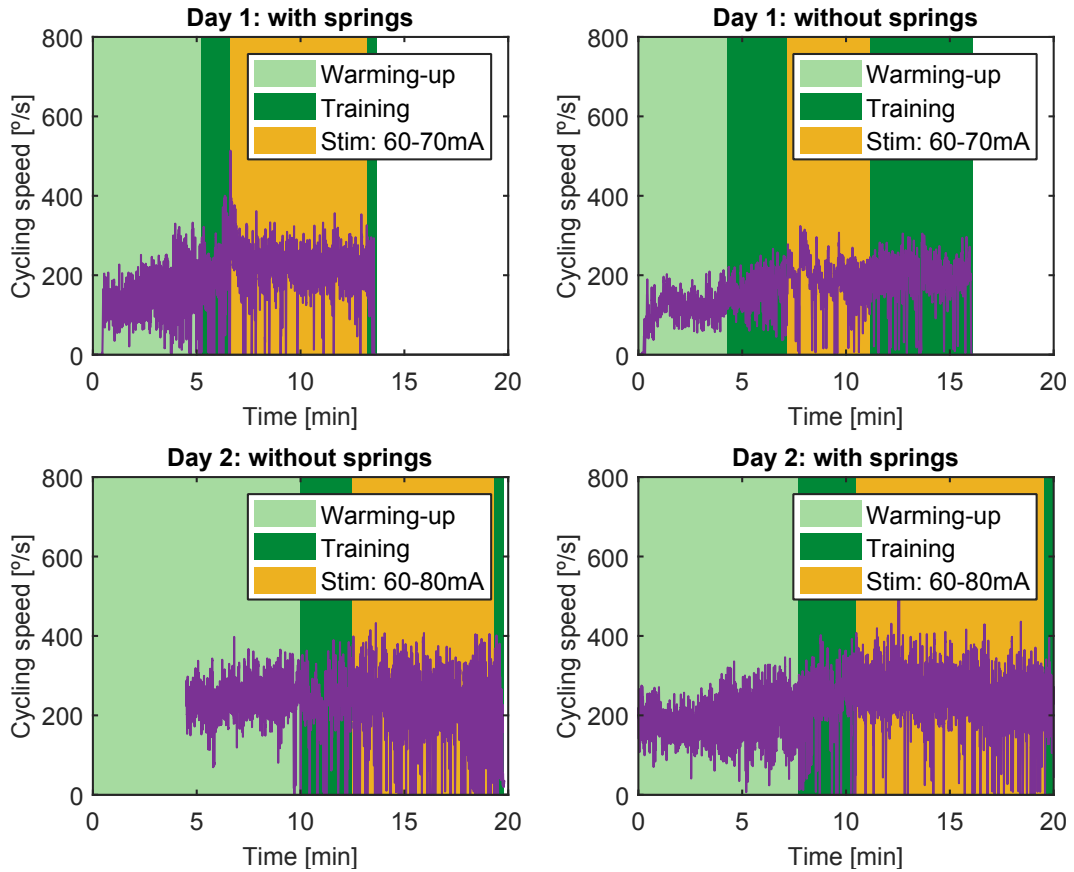
Figure 7.7: Cycling speed during both days of training. At each day, the volunteer cycled with and without the springs. The exercise divides into two phases: warming-up (light green) and training (dark green). In all pieces of training, we will look at the cycling speed between 60mA and 70mA (yellow).

Source: prepared by the author.

position (Figures 7.8b and 7.9b). In the polar plot, we represent the zero position when the left crankset forms 90º with the ground, i.e., the left foot is at the highest point over the ground (same pattern used in Chapter 6). From the polar plots, we may observe points where the cycling speed is almost reaching zero (usually over 90º and 270º). When we only excite the quadriceps, those are the dead points of the EMA trike as mentioned before. At these points, there is no stimulation on the muscles; if the volunteer did not guarantee enough force to pass those points (i.e., enough inertia), it usually stops there. We marked those points also as green crosses over the Figures 7.8a and 7.9a.

Table 7.2 shows the average cycling speed and standard deviation for both exercises. We may observe an increase of 17% of average cycling speed when we attached the springs.
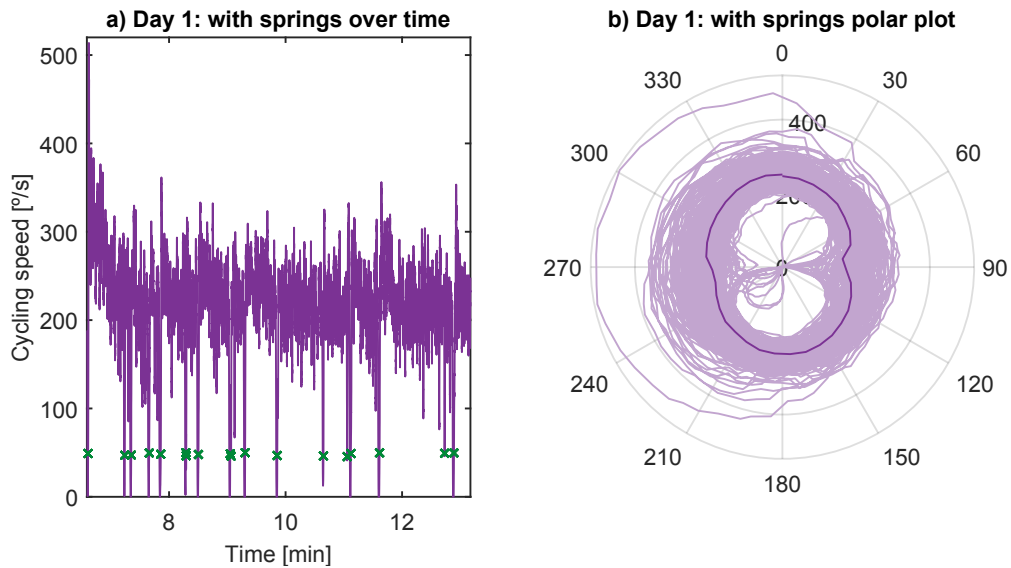
Figure 7.8: Cycling speed during first day of training with the springs for 60mA and 70mA of stimulation current (around 6min). (a) Cycling speed over time. (b) Cycling speed over the position of the crankset (left crankset forming 90º with the ground represents the zero position).
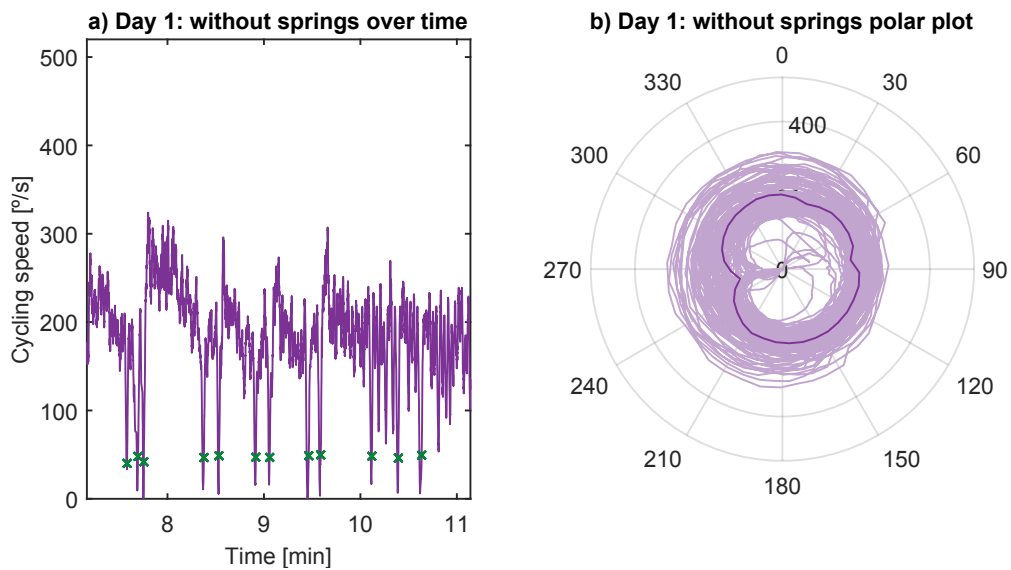
Figure 7.9: Cycling speed during first day of training without the springs for 60mA and 70mA of stimulation current (around 4min). (a) Cycling speed over time. (b) Cycling speed over the position of the crankset (left crankset forming 90º with the ground represents the zero position).

Source: prepared by the author.

7.3.2   Second day of training

On the second day, both pieces of training lasted approximately 20min. Similarly to Section 7.3.1, we represented the cycling speeds between 60mA and 80mA with and

146

Table 7.2: Average cycling speed during the first day of training for 60mA and 70mA of stimulation current.

	With springs	Without the springs
Average cycling speed	215.14°/s	183.88°/s
Standard deviation	60.30°/s	57.08°/s

without springs in Figures 7.11 and 7.10.
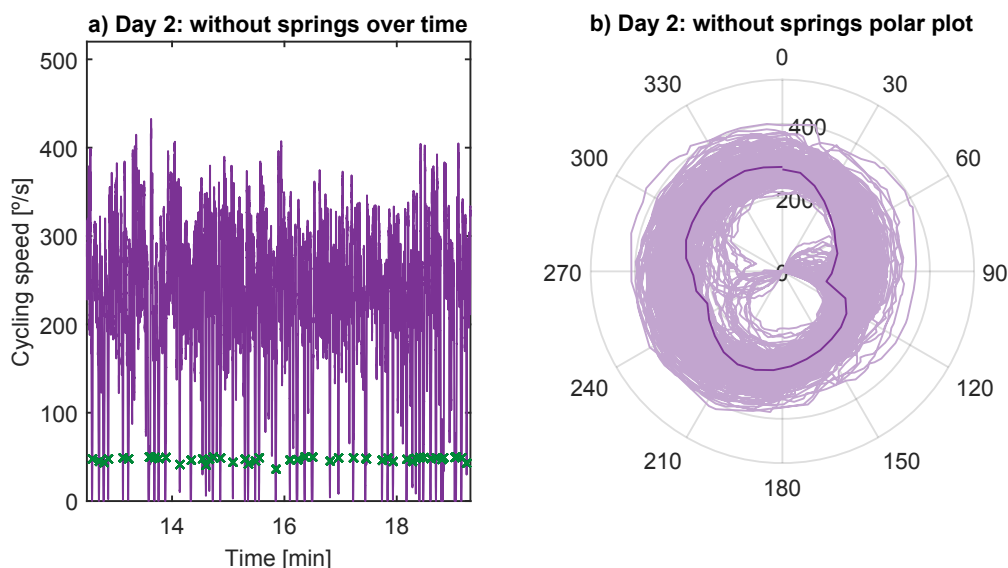
Figure 7.10: Cycling speed during second day of training without the springs for 60mA and 80mA of stimulation current (around 7min). (a) Cycling speed over time. (b) Cycling speed over the position of the crankset (left crankset forming 90º with the ground represents the zero position).

Table 7.3 shows the average cycling speed and standard deviation for both exercises. We may observe an increase of 11% of average cycling speed when we attached the springs.

Table 7.3: Average cycling speed during the second day of training for 60mA and 80mA of stimulation current.

	With springs	Without the springs
Average cycling speed	245.35°/s	220.42°/s
Standard deviation	74.81°/s	92.39°/s

7.3.3 Discussion

Taking the results from Chapter 6, we built an orthosis to test on a volunteer with spinal cord injury during two days of FES cycling exercises. Figure 7.7 shows how
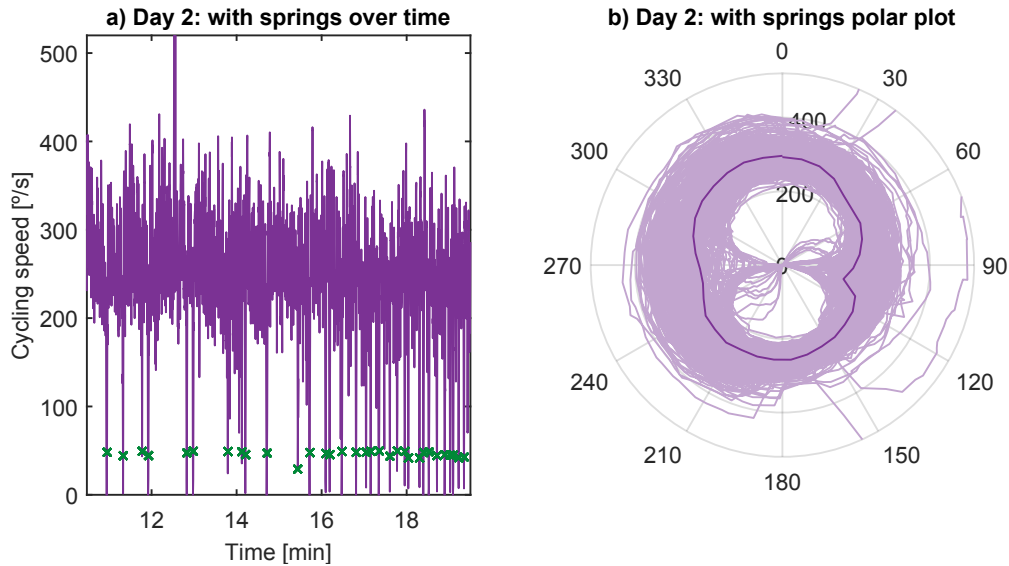
Figure 7.11: Cycling speed during second day of training with the springs for 60mA and 80mA of stimulation current (around 9min). (a) Cycling speed over time. (b) Cycling speed over the position of the crankset (left crankset forming 90º with the ground represents the zero position).

Source: prepared by the author.

the cyclist was always able to cycle using the designed passive knee orthoses with and without springs. However, as the passive orthoses added weight to the system, we took extra care to keep his legs in the sagittal plane, ensuring the safety of the volunteer. Therefore, the positioning of the user on the bicycle took longer than usual. This additional setup , i.e., putting the passive orthoses and repositioning on the tricycle, took about 15min.

As higher stimulation currents may create higher cadence response, we set the protocol so we can compare a part of the training with similar currents. On the first day of cycling, the volunteer cycled for 30min, starting with the springs attached to the spring holder. On the first session (with the springs attached), the average cycling speed was 17% higher when compared to the same period with similar excitation, but without the springs (Table 7.2). As the muscles may fatigue after the first session, we performed a new experiment. On the second day of training, the user cycled for 40min, starting without the springs attached to the passive orthoses. In this setup, the average cycling speed was 11% higher with the springs attached (Table 7.3). In both scenarios, the speed not only increased with the passive orthoses, but the standard deviation also decreased (Tables 7.2 and 7.3), this is similar to simulation results from Figure 6.22.

Similar to the Figure 6.24, we also present the polar coordinates of the two days of experiments in Figure 7.12. On the four sessions of cycling, the cyclist stops either around the 90º or 270º. At these points, there is no stimulation on muscles or actuation

148

of the springs (when attached), as observed in the profile in Figure 7.1. Therefore, he passes through these points by inertia provided by the extension of quadriceps. The cyclist has a history of fracture in the left knee, which causes a loss of strength in this leg. However, it is noticeable during the experiments, as both legs provide enough energy to pass the dead zones.
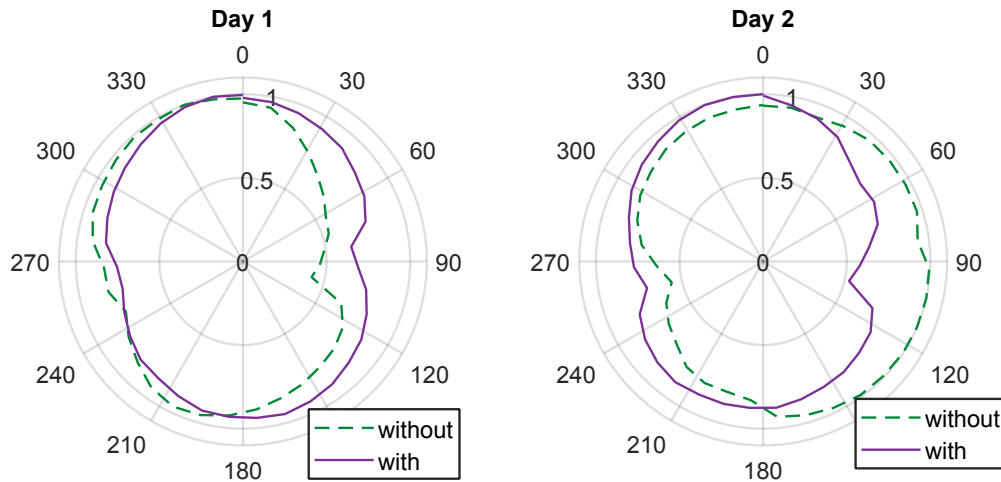
Figure 7.12: Cycling response in polar coordinates for (a) the first day and for (b) the second day (left crankset forming 90º with the ground represents the zero position).

Source: prepared by the author.

Figure 7.7 shows that the warming-up phase is usually shorter in the first session as the volunteer was performing the movement. Further, we observed that the volunteer could start to pedal without any manual push faster without the springs. This performance is similar to the simulation results presented in Figures 6.32 to 6.35 and to the results described in (CHAICHAOWARAT et al., 2017). Although the springs provide energy in part of the movement and may even increase the average cycling speed, the user also must overcome the energy that the spring is storing during knee flexion. This circumstance led to a slower start.

From the results in Sections 7.3.1 and 7.3.2, we observed that the volunteer was not only able to pedal using the orthoses, but the average cycling speed was higher with the springs attached. However, the effectiveness of the movement is still impaired when we add passive knee orthoses. This prototype pushes the skin during the pedal movements, consequently pushing the electrodes, reducing the contact area. The pedaling becomes less effective when compared to pieces of training without the orthoses. It is possible to create similar orthoses with different materials, as presented in (CHAICHAOWARAT; KINUGAWA; KOSUGE, 2018). A more rigid prototype, e.g., could be more natural to put on, decreasing the time of the setup and better guaranteeing the correct position of the springs around the knee. Depending on the

material, it is also possible to reduce its weight, consequently diminishing the effect over the cycling movement.

8 CONCLUSIONS

Usually, physiotherapists focus on repetitive strengthening exercises with specific muscles and joints, adapting the program to the patient's restrictions. Consequently, there is a constant need for more different and more efficient techniques that fit each user. This document presented three new advanced methods for lower limbs rehabilitation to improve FES control for patients with complete spinal cord injury. Each of these techniques existed in a different perspective of the control system: (1) the sensor estimation, (2) the control algorithms, and (3) the plant. Similarly to the outline of the introduction chapter, here we present the primary conclusions for each inquiry in the following sections.

8.1 SENSOR ESTIMATION USING ELECTROMYOGRAPHY

The first inquiry is related to which threshold-based method we can use to automatically detect stimulation artifacts for two channels of electromyography and stimulation on the same limb segment with a success rate higher than 95%. In Chapter 4, we have developed a method for two-channel stimulation artifact detection for EMG signals, which are not hardware-synchronized to a stimulator (SOUSA et al., 2018). Other hardware artifact detection solutions have only used one channel per limb (e.g., (PILKAR et al., 2017)) or developed synchronized hardware for this solution (e.g., (SHALABY et al., 2011)).

First, our artifact detection approach marks all potential artifacts based on one of three adaptive threshold-based detection methods (mean/standard deviation, median/MAD, and quantiles). Subsequently, for IPI extraction, we cluster the potential stimulation artifacts to cross-correlate the resulting possible stimulation artifact-vector with an expected-artifacts-vector based on the stimulation and EMG frequencies. As this detection is automatic, the method does not depend on the stimulation intensity and electrodes positioning, contrarily to the thresholds fixed manually in (ZHANG; ANG, 2007), (WIDJAJA et al., 2009), and (FANG et al., 2018). For evaluation, we performed tests on two benchmark datasets obtained from FES-assisted walking with two hardware setups. We found more than 95% success rate for both hardware setups using the adaptive threshold method independently on the selected mode for choosing the threshold. Opposed to (YOCHUM et al., 2014), (QIU et al., 2015) and (PILKAR et al., 2017), the method does not require high computation effort. Appropriately, we developed the system with the licensed Simulink®, which permits the code generation for an embedded system. The EMG amplifier would be able to preprocess EMG data

and return the EMG aligned vector with stimulation artifact. The results presented in Table 4.1 suggests that the artifact detection methods are higher than 95%, so it should be satisfactory for hardware implementation.

The accelerated muscle fatigue still is the primary challenge for FES control, substitute force sensors with eEMG in FES control for rehabilitation would cause a compelling impact for the community. Therefore, as a proof-of-concept of our artifact detection method for this application, we performed experiments comparing the torque with the eEMG. Figure 4.9 shows that after our artifact detection and estimation methods, we may find correlations between the eEMG and torque.

Even with a high success rate of artifact detection, we still found errors related either to noise or small variances on the system frequency, which may lead to unexpected responses in FES control. Therefore, even with success rates higher than 95%, we still suggest filtering the eEMG or the vEMG when using in FES control, as we have done between Figures 4.8 and 4.9. The quality of results also depends on constant EMG and FES frequencies during the entire execution, which is a similar limitation to other works, e.g., (QIU et al., 2015). To our knowledge, we have designed the first artifact detection algorithm considering two channels, yet the system is still limited to this number. However, we developed our methods using the licensed Simulink®, which may restrict extensive use in research.

For future experiments, we should also evaluate more cases, e.g., hardware, application, and subjects. With this evaluation, we could cross-correlate results, and expand conclusions for other uses. Specifically, about the parameters that we set, we should include further evaluation of the buffer size M, the parameters of the α-adaptation, and the clustering parameters concerning the computational effort in the microcontroller and the performance of artifact detection. A larger M would, e.g., improve the results of the cross-correlation but increase demands on memory and computational power.

8.2 SIMULATION ENVIRONMENTS FOR CONTROL ALGORITHMS

Using the open-source OpenSim, we created two simulation environments, in which we may evaluate errors of trajectory controllers for FES gait, and cycling cadence of speed controllers for FES cycling. As a simulation platform, OpenSim offered the possibility to conduct several experiments without fatigue impediments in real subjects.

8.2.1 FES gait

Even with previous extensive reviews of hybrid neuroprosthesis (HNPs) (DEL-AMA et al., 2012), to our knowledge, there is no comparison between several controllers

in the same environment, either simulations or experiments. After creating the simulation environment for FES gait, we simulated four trajectory controllers (BB, PID, PID-ILC, and PID-ES) to track knee movement during low-speed gait in Chapter 5.

OpenSim provided a stable environment for muscle excitation simulations combined with active torques on joints. In this platform, we could visualize that the PID-ILC and PID-ES presented lower tracking errors and higher correlation, and how the PID-ES presented slightly more precise results (Figure 5.13).

The system is available for further comparative simulation studies of other control strategies and trajectories for FES gait. However, it is still necessary to establish this environment to identify differences between the state of the art controllers. Even though we only modeled the actuator on the hip and quadriceps and hamstrings excitation for the knee, it is possible to modify features (e.g., actuators, joints, muscles) to the environment. Although we use a realistic anatomical representation of a one-leg model for muscle excitation, the model is subject-specific. Thus, we may not extend conclusions across subjects. Nonetheless, we expect future generalization once knowing the individualized anatomical details.

For future work, we may use this environment to investigate other HNPs configurations and controllers (e.g., actuators on hip, knee, and ankle, and FES to generate knee and ankle movements). This expansion is necessary to evaluate other types of HNPs presented in the literature. Furthermore, we intend to explore the use of co-activation of antagonist muscles using FES, which may improve disturbance rejection (BÓ; FONSECA; SOUSA, 2016), in addition to other control approaches, such as (MÜLLER et al., 2017) that could eliminate the oscillating behavior of the FES controller.

8.2.2 FES cycling

Similar to FES gait, to our knowledge, there was no previous simulation environment for FES cycling. So, we presented a detailed musculoskeletal model and simulated speed controllers (BB and PID) to track crankset speed during cycling using quadriceps, hamstrings, and gluteus in Chapter 6. In this platform, we could visualize the aid provided by the addition of the hamstrings and gluteus excitation (Figures 6.12), and the that the PI presented lower tracking errors (Figure 6.13). OpenSim also provided a stable environment for muscle excitation simulations combined with other models (pedals and crankset).

Further, the FES cycling environment allowed the investigation of passive knee orthoses parameters in Section 6.3. After defining the initial positions and the highest cadences, we found the knee inflection points. From these points, we modeled the

spring, considering θ_s and τ_{max}. With similar quadriceps excitation, we observed that the spring torque that extends the leg leads to higher cycling cadence (Figure 6.22).

Similarly to the FES gait environment, the model is also subject-specific. Therefore, we may not extend conclusions across subjects. Further, we should observe that the simplification of the pelvis of the cyclist locked over the seat is unrealistic. During an experiment, the pelvis moves and creates forces against the support, decreasing the overall performance. Moreover, although we were able to define some possible spring for manufacturing, the presented work still lacks considerations about torques on the knee and the pedals. As we intend to use the passive orthoses to assist FES cycling for individuals with SCI, the system must guarantee that it does not cause injuries.

8.3 PLANT CHANGES USING PASSIVE ORTHOSES

To our knowledge, no previous experiments combined passive orthoses with FES cycling in either disabled or non-disabled volunteers. Therefore, in Chapter 7, we built a pair of passive knee orthoses to determine if it was possible to change the crankset cadence in FES cyclint. We tested the prototype with a patient with complete SCI during two days of training using the passive orthoses.

The volunteer was able to cycle with and without the springs attached, while using the prototype (Figure 7.7). On the first day, the volunteer cycled for 30min, starting with the springs attached to the spring holder. In the first session (with the springs attached), the average cycling speed was 17% higher when compared to the same period with similar excitation, but without the springs (Table 7.2). On the second day, the user cycled for 40min, starting without the springs attached to the passive orthoses. In this setup, the average cycling speed was 11% higher with the springs (Table 7.3). In both scenarios, the average cadence not only increased with the passive orthoses, but the standard deviation also decreased (Tables 7.2 and 7.3), this is similar to some results from simulations (Figure 6.22).

The positioning of the user on the bicycle took longer than usual with the passive knee orthoses, as it added weight to the system, making one leg come out of the sagittal plane. Further, the use of passive orthoses makes it harder for the cyclist to start the movement, similar to the simulation results (Figures 6.32 to 6.35), and the conclusions of (CHAICHAOWARAT et al., 2017). Moreover, the prototype forces the skin during the pedal movements, consequently pushing the electrodes, reducing its effectiveness. In these conditions, the user is always able to cycle faster without the presented prototype. This study also misses a force analysis on the knee and the pedals. The forces measurements could provide a better biomechanical perception of the system, and even aid with the development of subject-specific spring parameters.

The increase of cycling speed using the springs should decrease the need for muscle excitation, consequently avoiding fatigue (one of the main challenges for FES cycling performance in the long term). However, it is necessary to guarantee that the use of passive knee orthoses does not affect the cycling movement. In the future, it is possible to create more rigid orthoses, as presented in (CHAICHAOWARAT; KINUGAWA; KOSUGE, 2018). This new prototype could decrease the time of the setup and better guaranteeing the correct position of the springs around the knee. Depending on the material, it is also possible to reduce its weight, consequently diminishing the effect over the cycling movement. The following researches also intend to evaluate other spring parameters (e.g., double and half elastic constants, as well as double and half spring ranges). These new experiments are essential to provide more robust conclusions about the use of passive orthoses for FES cycling with patients with complete SCI.

8.4 FINAL REMARKS

At each step of control design, we should take into consideration several possible pitfalls, from the sensor choice until the control parameters. This attention may lead to better methods for predicting the outcome of FES control. In this work, we presented and evaluated new techniques for FES control with simulations and experiments. Each of these techniques exists in a different perspective of the control system: (1) the use of electromyography for separating voluntary and evoked activity, (2) the use of simulation environments to evaluate control algorithms for FES gait and FES cycling, and (3) the addition of passive elements into our system environment.

Spinal cord injury poses a heavy burden on the quality of life, and the investigation of stimulation protocols for rehabilitation varies. Our approaches intended to complement other researches, always taking into account the security of the volunteer with a disability and the effectiveness of the control system. We believe that these studies may lead to better methods for improving rehabilitation for people with complete spinal cord injury.

BIBLIOGRAPHY

ABDULLA, S. C.; SAYIDMARIE, O.; TOKHI, M. O. Functional electrical stimulation-based cycling assisted by flywheel and electrical clutch mechanism: A feasibility simulation study. *Robotics and Autonomous Systems*, Elsevier B.V., v. 62, n. 2, p. 188–199, 2014. ISSN 09218890. Available in: <http://dx.doi.org/10.1016/j.robot.2013.10.005>. Cited 3 times in pages 5, 44 and 49.

AJOUDANI, A.; ERFANIAN, A. Neuro-sliding mode control with modular models for control of knee-joint angle using quadriceps electrical stimulation. *Annual International Conference of the IEEE Engineering in Medicine and Biology - Proceedings*, p. 2424–2427, 2007. ISSN 05891019. Cited 4 times in pages 37, 38, 90 and 206.

ALIBEJI, N.; KIRSCH, N.; SHARMA, N. An adaptive low-dimensional control to compensate for actuator redundancy and FES-induced muscle fatigue in a hybrid neuroprosthesis. *Control Engineering Practice*, Elsevier, v. 59, p. 204–219, 2017. ISSN 09670661. Available in: <http://dx.doi.org/10.1016/j.conengprac.2016.07.015>. Cited in page 28.

ALIBEJI, N. A.; KIRSCH, N. A.; SHARMA, N. A Muscle Synergy-Inspired Adaptive Control Scheme for a Hybrid Walking Neuroprosthesis. *Frontiers in Bioengineering and Biotechnology*, v. 3, n. December, p. 203, 2015. ISSN 2296-4185. Cited in page 42.

ALOUANE, M. A. et al. Cooperative Control for Knee Joint Flexion-Extension Movement Restoration. *IEEE International Conference on Intelligent Robots and Systems*, p. 5175–5180, 2018. ISSN 21530866. Cited 2 times in pages 50 and 201.

AMBROSINI, E. et al. A myocontrolled neuroprosthesis integrated with a passive exoskeleton to support upper limb activities. *Journal of Electromyography and Kinesiology*, Elsevier Ltd, v. 24, n. 2, p. 307–317, 2014. ISSN 18735711. Available in: <http://dx.doi.org/10.1016/j.jelekin.2014.01.006>. Cited 2 times in pages 54 and 56.

BAO, X.; KIRSCH, N.; SHARMA, N. Dynamic control allocation of a feedback linearized hybrid neuroprosthetic system. *Proceedings of the American Control Conference*, v. 2016-July, p. 3976–3981, 2016. ISSN 07431619. Cited in page 5.

BAPTISTA, P. O. *O efeito da aplicação da estimulação elétrica funcional na reabilitação em adultos com lesão medular completa*. Tese (Doutorado) — Instituto Politécnico do Porto, 2014. Available in: <https://core.ac.uk/download/pdf/47140365.pdf>. Cited in page 2.

BERRY, H. R. et al. Energetics of paraplegic cycling: Adaptations to 12 months of high volume training. *Technology and Health Care*, v. 20, n. 2, p. 73–84, 2012. ISSN 09287329. Cited 2 times in pages 6 and 199.

BESIO, W.; PRASAD, A. Analysis of skin-electrode impedance using concentric ring electrode. *Annual International Conference of the IEEE Engineering in Medicine and*

Biology - Proceedings, p. 6414–6417, 2006. ISSN 05891019. Cited 2 times in pages 31 and 32.

BESIO, W. et al. Command generation for FES enhanced grasping utilizing surface EMG in cervical injured. In: *Proceedings of the 1997 16 Southern Biomedical Engineering Conference*. IEEE, 1999. p. 414–417. ISBN 0-7803-3869-3. Available in: <http://egr.uri.edu/wp-uploads/neurorehabilitationlab/Besio_BSI99.pdf http://ieeexplore.ieee.org/document/583329/>. Cited in page 31.

BÓ, A. P. L. et al. Experiments on Lower Limb Fes Control For Cycling. *XII Simpósio Brasileiro de Automação Inteligente (SBAI)*, p. 1–6, 2015. Cited 3 times in pages 94, 95 and 206.

BÓ, A. P. L. et al. Cycling with Spinal Cord Injury: A Novel System for Cycling Using Electrical Stimulation for Individuals with Paraplegia, and Preparation for Cybathlon 2016. *IEEE Robotics and Automation Magazine*, v. 24, n. 4, p. 58–65, 2017. ISSN 10709932. Cited 6 times in pages 6, 68, 91, 92, 103 and 129.

BÓ, A. P. L.; FONSECA, L. O. da; SOUSA, A. C. C. d. FES-induced co-activation of antagonist muscles for upper limb control and disturbance rejection. *Medical Engineering and Physics*, v. 38, n. 11, p. 1176–1184, 2016. ISSN 18734030. Cited in page 153.

BOUDVILLE, R. et al. Dynamic modeling and control of FES-assisted knee ergometer for stroke patient. *Proceedings - 2012 IEEE International Conference on Control System, Computing and Engineering, ICCSCE 2012*, p. 436–439, 2013. Cited 2 times in pages 36 and 37.

BOUDVILLE, R. et al. GA-tuned fuzzy logic control of knee-FES-ergometer for knee swinging exercise. *Proceedings - 2013 IEEE International Conference on Control System, Computing and Engineering, ICCSCE 2013*, p. 608–611, 2013. Cited 2 times in pages 36 and 37.

BOUDVILLE, R. et al. Development and optimization of PID control for FES knee exercise in hemiplegic rehabilitation. *Proceedings of the International Conference on Sensing Technology, ICST*, IEEE, v. 2018-Decem, p. 143–148, 2019. ISSN 21568073. Cited 3 times in pages 37, 38 and 69.

BULEA, T. C. et al. Forward stair descent with hybrid neuroprosthesis after paralysis: Single case study demonstrating feasibility. *Journal of rehabilitation research and development*, v. 51, n. 7, p. 1077–94, 2014. ISSN 1938-1352. Available in: <http://www-.scopus.com/inward/record.url?eid=2-s2.0-84922852483&partnerID=tZOtx3y1>. Cited in page 42.

CHAICHAOWARAT, R. et al. Passive knee exoskeleton using torsion spring for cycling assistance. *IEEE International Conference on Intelligent Robots and Systems*, v. 2017-Septe, p. 3069–3074, 2017. ISSN 21530866. Cited 7 times in pages 44, 45, 49, 108, 149, 154 and 209.

CHAICHAOWARAT, R.; KINUGAWA, J.; KOSUGE, K. Cycling-enhanced Knee Exoskeleton Using Planar Spiral Spring. *Proceedings of the Annual International Conference of the IEEE Engineering in Medicine and Biology Society, EMBS*, v.

2018-July, p. 3206–3211, 2018. ISSN 1557170X. Cited 6 times in pages 44, 45, 49, 108, 149 and 155.

CHANG, S. R. et al. A stimulation-driven exoskeleton for walking after paraplegia. *Proceedings of the Annual International Conference of the IEEE Engineering in Medicine and Biology Society, EMBS*, v. 2016-Octob, p. 6369–6372, 2016. ISSN 1557170X. Cited 3 times in pages 4, 5 and 198.

CHEN, Y. et al. An FES-assisted training strategy combined with impedance control for a lower limb rehabilitation robot. In: *2013 IEEE International Conference on Robotics and Biomimetics (ROBIO)*. IEEE, 2013. p. 2037–2042. ISBN 978-1-4799-2744-9. Available in: <http://ieeexplore.ieee.org/document/6739769/>. Cited in page 42.

CHENG, L. et al. Radial basis function neural network-based PID model for functional electrical stimulation system control. *Proceedings of the 31st Annual International Conference of the IEEE Engineering in Medicine and Biology Society: Engineering the Future of Biomedicine, EMBC 2009*, p. 3481–3484, 2009. Cited 2 times in pages 37 and 38.

CORR, P. J. *Understanding biological psychology*. 1st. ed. Malden, MA, USA: Blackwell Publishing Ltd, 2006. Understanding biological psychology. xvii, 693 p. ISBN 0-631-21954-4 (Paperback), 978-0-631-21954-5 (Paperback), 0-631-21953-6 (Hardcover), 978-0-631-21953-8 (Hardcover). Available in: <http://ovidsp.ovid.com/ovidweb-.cgi?T=JS&CSC=Y&NEWS=N&PAGE=fulltext&D=psyc5&AN=2007-00725-000>. Cited 5 times in pages 9, 10, 11, 13 and 29.

COSTE, C. A.; WOLF, P. FES-Cycling at Cybathlon 2016: Overview on Teams and Results. *Artificial Organs*, v. 42, n. 3, p. 336–341, 3 2018. ISSN 0160564X. Available in: <http://doi.wiley.com/10.1111/aor.13139>. Cited 4 times in pages 3, 6, 91 and 198.

CYBULSKI, G. R.; PENN, R. D.; JAEGER, R. J. *Lower extremity functional neuromuscular stimulation in cases of spinal cord injury*. 1984. 132–146 p. Cited in page 33.

DAVOODI, R.; ANDREWS, B. J. Optimal control of FES-assisted standing up in paraplegia using genetic algorithms. *Medical Engineering and Physics*, v. 21, n. 9, p. 609–617, 1999. ISSN 13504533. Cited in page 74.

DEL-AMA, A. J. et al. Review of hybrid exoskeletons to restore gait following spinal cord injury. *The Journal of Rehabilitation Research and Development*, v. 49, n. 4, p. 497, 2012. ISSN 0748-7711. Cited 3 times in pages 42, 43 and 152.

DELP, S. L. et al. OpenSim: Open-Source Software to Create and Analyze Dynamic Simulations of Movement. *IEEE Transactions on Biomedical Engineering*, v. 54, n. 11, p. 1940–1950, 11 2007. ISSN 0018-9294. Available in: <http://ieeexplore.ieee-.org/lpdocs/epic03/wrapper.htm?arnumber=4352056>. Cited 4 times in pages 13, 68, 172 and 202.

DOLBOW, D. R.; HOLCOMB, W. R.; GORGEY, A. S. Improving the Efficiency of Electrical Stimulation Activities After Spinal Cord Injury. *Current Physical Medicine and Rehabilitation Reports*, v. 2, n. 3, p. 169–175, 2014. ISSN 2167-4833. Cited 2 times in pages 6 and 199.

DOLLAR, A. M.; HERR, H. Lower Extremity Exoskeletons and Active Orthoses: Challenges and State-of-the-Art. *IEEE Transactions on Robotics*, v. 24, n. 1, p. 144–158, 2 2008. ISSN 1552-3098. Available in: <http://ieeexplore.ieee.org/document-/4456745/>. Cited in page 39.

DOWNEY, R. J. et al. Closed-Loop Asynchronous Neuromuscular Electrical Stimulation Prolongs Functional Movements in the Lower Body. *IEEE Transactions on Neural Systems and Rehabilitation Engineering*, v. 23, n. 6, p. 1117–1127, 2015. ISSN 15344320. Cited 2 times in pages 37 and 38.

DOWNEY, R. J. et al. Switched tracking control of the lower limb during asynchronous neuromuscular electrical stimulation: Theory and experiments. *IEEE Transactions on Cybernetics*, v. 47, n. 5, p. 1251–1262, 2017. ISSN 21682267. Cited 2 times in pages 37 and 38.

DURFEE, W.; DENNERLEIN, J. EMG as a feedback signal in surfaces FES applications: issues and preliminary results. In: *Images of the Twenty-First Century. Proceedings of the Annual International Engineering in Medicine and Biology Society.* IEEE, 1989. v. 11 pt 3, p. 1009–1010. ISSN 05891019. Available in: <http://ieeexplore.ieee.org/document/96059/>. Cited 2 times in pages 26 and 30.

FANG, Y. et al. Real-time Electromyography-driven Functional Electrical Stimulation Cycling System for Chronic Stroke Rehabilitation. *Proceedings of the Annual International Conference of the IEEE Engineering in Medicine and Biology Society, EMBS*, v. 2018-July, p. 2515–2518, 2018. ISSN 1557170X. Cited 6 times in pages 33, 34, 50, 51, 151 and 201.

FARIA, E.; PARKER, D. L.; FARIA, I. E. The science of cycling: Physiology and training - Part 1. *Sports Medicine*, v. 35, n. 4, p. 285–312, 2005. ISSN 01121642. Cited in page 17.

FARIA, E. W.; PARKER, D. L.; FARIA, I. E. The science of cycling: Factors affecting performance - Part 2. *Sports Medicine*, v. 35, n. 4, p. 313–337, 2005. ISSN 01121642. Cited 2 times in pages 17 and 18.

FARRIS, R. J. et al. Design and simulation of a joint-coupled orthosis for regulating FES-aided gait. In: *2009 IEEE International Conference on Robotics and Automation.* IEEE, 2009. p. 1916–1922. ISBN 978-1-4244-2788-8. ISSN 1050-4729. Available in: <http://ieeexplore.ieee.org/lpdocs/epic03/wrapper.htm?arnumber=5152634 http://ieeexplore.ieee.org/document/5152634/>. Cited 5 times in pages 39, 43, 68, 201 and 202.

FERRANTE, S. et al. Biomimetic NMES controller for arm movements supported by a passive exoskeleton. *Proceedings of the Annual International Conference of the IEEE Engineering in Medicine and Biology Society, EMBS*, n. 248326, p. 1888–1891, 2012. ISSN 1557170X. Cited in page 50.

FERRARIN, M. et al. Standing-up exerciser based on functional electrical stimulation and body weight relief. *Medical and Biological Engineering and Computing*, v. 40, n. 3, p. 282–289, 2002. ISSN 01400118. Cited in page 35.

FREEMAN, C. et al. Iterative Learning Control in Health Care: Electrical Stimulation and Robotic-Assisted Upper-Limb Stroke Rehabilitation. *IEEE Control Systems*, v. 32, n. 1, p. 18–43, 2 2012. ISSN 1066-033X. Available in: <https://ieeexplore.ieee.org/document/6153633/>. Cited in page 73.

GHAROONI, S.; HELLER, B.; TOKHI, M. O. A new hybrid spring brake orthosis for controlling hip and knee flexion in the swing phase. *IEEE Transactions on Neural Systems and Rehabilitation Engineering*, v. 9, n. 1, p. 106–107, 2001. ISSN 15344320. Cited in page 43.

GLASER, R. M. Physiologic Aspects of Spinal Cord Injury and Functional Neuromuscular Stimulation. *Central Nervous System Trauma*, v. 3, n. 1, p. 49–62, 1986. ISSN 15579042. Cited 2 times in pages 6 and 199.

GLASER, R. M. Physiology of Functional Electrical Stimulation-Induced Exercise: Basic Science Perspective. *Neurorehabilitation and Neural Repair*, v. 5, p. 49–61, 1991. ISSN 15526844. Cited 2 times in pages 6 and 199.

Gwo-Ching Chang et al. A neuro-control system for the knee joint position control with quadriceps stimulation. *IEEE Transactions on Rehabilitation Engineering*, v. 5, n. 1, p. 2–11, 1997. ISSN 10636528. Cited 2 times in pages 35 and 42.

HA, K. H.; MURRAY, S. A.; GOLDFARB, M. An Approach for the Cooperative Control of FES with a Powered Exoskeleton during Level Walking for Persons with Paraplegia. *IEEE Transactions on Neural Systems and Rehabilitation Engineering*, v. 24, n. 4, p. 455–466, 2016. ISSN 15344320. Cited 2 times in pages 40 and 42.

HALL, J. E.; GUYTON, A. C. *Guyton and Hall Textbook of Medical Physiology*. 12th. ed. Philadelphia, USA: Saunders, 2015. ISBN 9781416045748. Cited 4 times in pages 9, 10, 11 and 13.

HIDLER, J. Robotic-assessment of walking in individuals with gait disorders. In: *The 26th Annual International Conference of the IEEE Engineering in Medicine and Biology Society*. IEEE, 2004. v. 4, p. 4829–4831. ISBN 0-7803-8439-3. Available in: <http://ieeexplore.ieee.org/document/1404336/>. Cited in page 28.

HILL, A. V.; B, P. R. S. L. The heat of shortening and the dynamic constants of muscle. *Proceedings of the Royal Society of London. Series B - Biological Sciences*, v. 126, n. 843, p. 136–195, 1938. ISSN 2053-9193. Cited 5 times in pages 5, 13, 68, 172 and 202.

HUNT, K. J. *Control Systems for Function Restoration, Exercise, Fitness and Health in Spinal Cord Injury*. Tese (Doutorado) — University of Glasgow, 2005. Cited 5 times in pages 94, 95, 96, 206 and 207.

HUNT, K. J. et al. Metabolic efficiency of volitional and electrically stimulated cycling in able-bodied subjects. *Medical Engineering and Physics*, Institute of Physics and Engineering in Medicine, v. 35, n. 7, p. 919–925, 2013. ISSN 18734030. Available in: <http://dx.doi.org/10.1016/j.medengphy.2012.08.023>. Cited 2 times in pages 6 and 199.

HUSSAIN, Z.; TOKHI, M. O.; JAILANI, R. *The use of spring-orthosis to enhance performance of FES-assisted indoor rowing exercise (FAIRE)*. IFAC, 2009. v. 14. 425–430 p. ISSN 14746670. ISBN 9783902661555. Available in: <http://dx.doi.org/10.3182/20090819-3-PL-3002.00074>. Cited in page 43.

HUXLEY, A. F.; NIEDERGERKE, R. Structural changes in muscle during contraction: Interference microscopy of living muscle fibres. *Nature*, v. 173, n. 4412, p. 971–973, 1954. ISSN 00280836. Cited in page 11.

IBRAHIM, B. S. et al. Fuzzy logic based cycle-to-cycle control of FES-induced swinging motion. *InECCE 2011 - International Conference on Electrical, Control and Computer Engineering*, p. 60–64, 2011. Cited in page 36.

IBRAHIM, B. S. K. et al. Energy-Efficient FES Cycling with Quadriceps Stimulation. *13th International FES Society Conference*, v. 53, n. 1, p. 262–264, 2008. Cited 4 times in pages 43, 44, 49 and 138.

Instituto Brasileiro de Geografia e Estatística - IBGE. Características Gerais da População, Religião e Pessoas Com Deficiência. *Censo Demográfico 2010*, p. 71–89, 2010. Cited 2 times in pages 1 and 196.

JAILANI, R. et al. PID Control of Knee Extension for FES-Assisted Walking with Spring Brake Orthosis. In: *2010 Fourth Asia International Conference on Mathematical/Analytical Modelling and Computer Simulation*. IEEE, 2010. p. 261–266. ISBN 978-1-4244-7196-6. Available in: <http://ieeexplore.ieee.org/document/5489209-/>. Cited in page 42.

JAILANI, R. et al. Finite State Control of FES-Assisted Walking with Spring Brake Orthosis. In: *2011 UkSim 13th International Conference on Computer Modelling and Simulation*. Cambridge, United Kingdom: IEEE, 2011. p. 183–188. ISBN 978-1-61284-705-4. Available in: <http://ieeexplore.ieee.org/lpdocs/epic03/wrapper-.htm?arnumber=5754212>. Cited 2 times in pages 40 and 42.

Jia-Jin Chen et al. Muscle fatigue study in FES-induced dynamic cycling movement. In: *Proceedings of 17th International Conference of the Engineering in Medicine and Biology Society*. IEEE, 1995. v. 2, n. 2, p. 1213–1214. ISBN 0-7803-2475-7. ISSN 05891019. Available in: <http://ieeexplore.ieee.org/document/579647/>. Cited in page 30.

JORGE, M.; HULL, M. L. A Method for Biomechaniccal Analysis of Bicycle Pedalling. *Journal of Biomechanics*, v. 18, n. 9, p. 631–644, 1985. Cited in page 45.

JORGE, M.; HULL, M. L. Analysis of EMG measurements during bicycle pedalling. *Journal of Biomechanics*, v. 19, n. 9, p. 683–694, 1986. ISSN 00219290. Cited in page 18.

KAMEN, G.; GABRIEL, D. A. *Essentials of Electromyography*. Champaign, USA: Human Kinetics, 2010. ISBN 9781450408530. Cited 3 times in pages 5, 26 and 198.

KAWAI, Y.; EJIRI, K.; KAWAI, H. Co-contraction of antagonist muscles of human limb using neural network-based control. In: *2015 IEEE/SICE International*

Symposium on System Integration (SII). IEEE, 2015. p. 33–38. ISBN 978-1-4673-7242-8. Available in: <http://ieeexplore.ieee.org/document/7404893/>. Cited 4 times in pages 37, 38, 87 and 205.

KILLINGSWORTH, N. J.; KRSTIĆ, M. PID Tuning Using Extremum Seeking. *IEEE Control Systems*, v. 26, n. 1, p. 70–79, 2006. ISSN 1066033X. Cited in page 74.

KIRSCH, N. et al. Switching control of functional electrical stimulation and motor assist for muscle fatigue compensation. In: *2016 American Control Conference (ACC)*. IEEE, 2016. p. 4865–4870. ISBN 978-1-4673-8682-1. Available in: <http://ieeexplore.ieee.org/document/7526123/>. Cited 2 times in pages 3 and 197.

KIRSCH, N. et al. A semi-active hybrid neuroprosthesis for restoring lower limb function in paraplegics. In: *2014 36th Annual International Conference of the IEEE Engineering in Medicine and Biology Society*. IEEE, 2014. v. 2014, p. 2557–2560. ISBN 978-1-4244-7929-0. ISSN 1557-170X. Available in: <http://login.ezproxy.library.ualberta.ca/login?url=http://ovidsp.ovid.com-/ovidweb.cgi?T=JS&CSC=Y&NEWS=N&PAGE=fulltext&D=medl&AN=25570512 http://resolver.library.ualberta.ca-/resolver?sid=OVID:medline&id=pmid:25570512&id=doi:10.1109/EMBC-.2014.6944144&issn h>. Cited 3 times in pages 68, 201 and 202.

KIRSHBLUM, S. C. et al. Reference for the 2011 revision of the international standards for neurological classification of spinal cord injury. *The Journal of Spinal Cord Medicine*, v. 34, n. 6, p. 547–554, 11 2011. ISSN 1079-0268. Available in: <http://www.tandfonline.com/doi/full/10.1179/107902611X13186000420242>. Cited 3 times in pages 2, 3 and 21.

KLAUER, C. et al. A patient-controlled functional electrical stimulation system for arm weight relief. *Medical Engineering and Physics*, Elsevier Ltd, v. 38, n. 11, p. 1232–1243, 2016. ISSN 18734030. Available in: <http://dx.doi.org/10.1016/j-.medengphy.2016.06.006>. Cited 2 times in pages 54 and 57.

KLAUER, C.; RAISCH, J.; SCHAUER, T. Linearisation of electrically stimulated muscles by feedback control of the muscular recruitment measured by evoked EMG. *2012 17th International Conference on Methods and Models in Automation and Robotics, MMAR 2012*, p. 108–113, 2012. Cited in page 5.

KNAFLITZ, M. et al. Suppression of Simulation Artifacts from Myoelectric-Evoked Potential Recordings. *IEEE Transactions on Biomedical Engineering*, v. 35, n. 9, p. 758–763, 1988. ISSN 15582531. Cited in page 5.

KOBETIC, R.; MARSOLAIS, E. B. Synthesis of Paraplegic Gait with Multichannel Functional Neuromuscular Stimulation. *IEEE Transactions on Rehabilitation Engineering*, v. 2, n. 2, p. 66–79, 1994. ISSN 10636528. Cited in page 25.

KOBETIC, R. et al. Development of hybrid orthosis for standing, walking, and stair climbing after spinal cord injury. *Journal of Rehabilitation Research and Development*, v. 46, n. 3, p. 447–462, 2009. ISSN 07487711. Cited 4 times in pages 39, 68, 201 and 202.

KRSTIĆ, M.; WANG, H. H. Stability of extremum seeking feedback for general nonlinear dynamic systems. *Automatica*, v. 36, n. 4, p. 595–601, 2000. ISSN 00051098. Cited 2 times in pages 74 and 75.

LAUBACHER, M. et al. Stimulation of paralysed quadriceps muscles with sequentially and spatially distributed electrodes during dynamic knee extension. *Journal of NeuroEngineering and Rehabilitation*, Journal of NeuroEngineering and Rehabilitation, v. 16, n. 1, p. 1–12, 2019. ISSN 17430003. Cited in page 65.

LEYS, C. et al. Detecting outliers: Do not use standard deviation around the mean, use absolute deviation around the median. *Journal of Experimental Social Psychology*, v. 49, n. 4, p. 764–766, 2013. ISSN 00221031. Cited 3 times in pages 53, 60 and 61.

LOPES, A. D.; ALOUCHE, S. R.; HAKANSSON, N. Electromyography During Pedaling on Upright and Recumbent Ergometer. *The International Journal of Sports Physical Therapy*, v. 9, n. 1, p. 76–81, 2014. ISSN 2159-2896. Cited in page 18.

LYNCH, C. L.; POPOVIC, M. R. A comparison of closed-loop control algorithms for regulating electrically stimulated knee movements in individuals with spinal cord injury. *IEEE Transactions on Neural Systems and Rehabilitation Engineering*, v. 20, n. 4, p. 539–548, 2012. ISSN 15344320. Cited 2 times in pages 2 and 196.

MANDRILE, F. et al. Stimulation Artifact in Surface EMG Signal: Effect of the Stimulation Waveform, Detection System, and Current Amplitude Using Hybrid Stimulation Technique. *IEEE Transactions on Neural Systems and Rehabilitation Engineering*, v. 11, n. 4, p. 407–415, 2003. ISSN 15344320. Cited 2 times in pages 31 and 32.

MARTIN, R. et al. Functional electrical stimulation in spinal cord injury: From theory to practice. *Topics in Spinal Cord Injury Rehabilitation*, v. 18, n. 1, p. 28–33, 2012. ISSN 10820744. Cited 2 times in pages 2 and 196.

MASSOUD, R. Energy storage devices to support functional movements' restoration. *Energy Procedia*, v. 19, p. 63–70, 2012. ISSN 18766102. Cited 5 times in pages 7, 43, 44, 49 and 199.

MCNEAL, D. R. et al. Open-Loop Control of the Freely-Swinging Paralyzed Leg. *IEEE Transactions on Biomedical Engineering*, v. 36, n. 9, p. 895–905, 1989. ISSN 15582531. Cited in page 34.

Ministério da Saúde. *Diretrizes de atenção às pessoas com lesao medular*. Brazil, 2013. Cited 2 times in pages 1 and 196.

MIZRAHI, J. et al. EMG as an Indicator of Fatigue in Isometrically Fes-Activated Paralyzed Muscles. *IEEE Transactions on Rehabilitation Engineering*, v. 2, n. 2, p. 57–65, 1994. ISSN 10636528. Cited in page 30.

MOHAMMED, S. et al. Towards a co-contraction muscle control strategy for paraplegics. *Proceedings of the 44th IEEE Conference on Decision and Control, and the European Control Conference, CDC-ECC '05*, v. 2005, p. 7428–7433, 2005. Cited in page 36.

MOHAMMED, S.; POIGNET, P.; GUIRAUD, D. Closed loop nonlinear model predictive control applied on paralyzed muscles to restore lower limbs functions. *IEEE International Conference on Intelligent Robots and Systems*, p. 259–264, 2006. Cited in page 36.

MONTE-SILVA, K. et al. Electromyogram-Related Neuromuscular Electrical Stimulation for Restoring Wrist and Hand Movement in Poststroke Hemiplegia: A Systematic Review and Meta-Analysis. *Neurorehabilitation and Neural Repair*, v. 33, n. 2, p. 96–111, 2019. ISSN 15526844. Cited in page 5.

MÜLLER, P. et al. Iterative Learning Control and System Identification of the Antagonistic Knee Muscle Complex During Gait Using Functional Electrical Stimulation. *IFAC-PapersOnLine*, v. 50, n. 1, p. 8786–8791, 2017. ISSN 24058963. Cited in page 153.

MULLER, P.; SEEL, T.; SCHAUER, T. Experimental Evaluation of a Novel Inertial Sensor Based Realtime Gait Phase Detection Algorithm. In: *Proc. of the 5th European Conference on Technically Assisted Rehabilitation - TAR 2015*. Berlin, Germany: Gruyter, 2015. Cited in page 59.

MURAOKA, Y. et al. Specifications of an electromyogram-driven neuromuscular stimulator for upper limb functional recovery. *Proceedings of the Annual International Conference of the IEEE Engineering in Medicine and Biology Society, EMBS*, p. 277–280, 2013. ISSN 1557170X. Cited 2 times in pages 31 and 32.

NAKI, I. K. et al. Is the use of computerized electrical stimulation associated with cycloergometrics in individuals with medullary lesion beneficial for the muscular parameters? *Acta Fisiátrica*, v. 18, n. 4, p. 211–216, 2011. ISSN 0104-7795. Cited 2 times in pages 2 and 197.

NENE, A. V.; HERMENS, H. J.; ZILVOLD, G. Paraplegic locomotion: A review. *Spinal Cord*, v. 34, n. 9, p. 507–524, 1996. ISSN 13624393. Cited 2 times in pages 29 and 33.

NIGHTINGALE, E. J. et al. Benefits of FES gait in a spinal cord injured population. *Spinal Cord*, v. 45, n. 10, p. 646–657, 2007. ISSN 13624393. Cited in page 33.

Nikki. *Cycle Season is Here in Vancouver - How is your pedal stroke?* 2014. Available in: <http://www.mypersonaltrainervancouver.com/cycle-season-is-here-in-vancouver-how-is-your-pedal-stroke/>. Cited in page 19.

OBINATA, G. et al. Hybrid Control of Powered Orthosis and Functional Neuromuscular Stimulation for Restoring Gait. In: *2007 29th Annual International Conference of the IEEE Engineering in Medicine and Biology Society*. IEEE, 2007. v. 2, p. 4879–4882. ISBN 978-1-4244-0787-3. ISSN 1557-170X. Available in: <http://ieeexplore.ieee.org/document/4353433/>. Cited 4 times in pages 42, 68, 201 and 202.

ODERBERK, B. J.; INBAR, G. F. Walking cycle recording and analysis for FNS-assisted paraplegic walking. *Medical & Biological Engineering & Computing*, v. 29, n. 1, p. 79–83, 1991. ISSN 01400118. Cited in page 76.

OGATA, K. *Modern Control Engineering*. 5th. ed. New Jersey, USA: Prentice Hall, 2010. ISBN 9780135987315. Cited 2 times in pages 3 and 197.

OHASHI, T. et al. Control of hybrid FES system for restoration of paraplegic locomotion. In: *Proceedings of 1993 2nd IEEE International Workshop on Robot and Human Communication*. IEEE, 1993. p. 96–101. ISBN 0-7803-1407-7. Available in: <http://ieeexplore.ieee.org/document/367741/>. Cited in page 40.

O'KEEFFE, D. T. et al. Stimulus artifact removal using a software-based two-stage peak detection algorithm. *Journal of Neuroscience Methods*, v. 109, n. 2, p. 137–145, 2001. ISSN 01650270. Cited 3 times in pages 30, 32 and 34.

PAZ, P.; OLIVEIRA, T. R. Neuromuscular Electrical Stimulation for Stroke Patients by Deterministic Extremum Seeking. *Proceedings of the IEEE Conference on Decision and Control*, IEEE, v. 2018-Decem, n. Cdc, p. 6692–6698, 2019. ISSN 07431546. Cited 2 times in pages 74 and 75.

PEASGOOD, W. et al. EMG-controlled closed loop electrical stimulation using a digital signal processor. *Electronics Letters*, v. 36, n. 22, p. 1832, 2000. ISSN 00135194. Available in: <https://digital-library.theiet.org/content/journals/10.1049/el_20001319>. Cited 2 times in pages 31 and 32.

PEDRO, J. O.; SMITH, R. V. Real-Time Hybrid PID/ILC Control of Two-Link Flexible Manipulators. *IFAC-PapersOnLine*, Elsevier B.V., v. 50, n. 2, p. 145–150, 2017. ISSN 24058963. Available in: <https://doi.org/10.1016/j.ifacol.2017.12.027>. Cited in page 73.

PEREZ-ORIVE, J.; MAYAGOITIA, R. E. Closed-loop control system to be used with a hybrid RGO system. v. 16, n. pt 1, p. 410–411, 1994. ISSN 05891019. Cited in page 40.

PERRY, J. *Gait Analysis: Normal and Pathological Function*. New Jersey, USA: SLACK Incorporated, 1992. ISBN 978-1-55642-192-1. Cited 2 times in pages 9 and 60.

PILKAR, R. et al. Application of Empirical Mode Decomposition Combined with Notch Filtering for Interpretation of Surface Electromyograms during Functional Electrical Stimulation. *IEEE Transactions on Neural Systems and Rehabilitation Engineering*, v. 25, n. 8, p. 1268–1277, 2017. ISSN 15344320. Cited 3 times in pages 33, 34 and 151.

POPOVIĆ, D. B.; SINKJÆR, T. *Control of Movement for the Physically Disabled*. London: Springer London, 2000. v. 215. 333–333 p. ISSN 0954-4119. ISBN 978-1-4471-1141-2. Available in: <http://link.springer.com/10.1007/978-1-4471-0433-9>. Cited 18 times in pages 3, 6, 9, 10, 11, 12, 15, 16, 17, 19, 22, 23, 24, 25, 26, 40, 91 and 197.

POPOVIĆ, L. Z.; MALEŠEVIĆ, N. M. Muscle fatigue of quadriceps in paraplegics: Comparison between single vs. multi-pad electrode surface stimulation. *Proceedings of the 31st Annual International Conference of the IEEE Engineering in Medicine and Biology Society: Engineering the Future of Biomedicine, EMBC 2009*, p. 6785–6788, 2009. Cited 2 times in pages 90 and 205.

POPOVIC, M. R. Functional Electrical Stimulation. *IEEE Control Systems*, IEEE, v. 28, n. 2, p. 40–50, 4 2008. ISSN 1066-033X. Available in: <https://ieeexplore.ieee-.org/document/4472378/>. Cited in page 29.

POTVIN, J. R.; FUGLEVAND, A. J. A motor unit-based model of muscle fatigue. *PLoS Computational Biology*, v. 13, n. 6, p. 1–30, 2017. ISSN 15537358. Cited 2 times in pages 70 and 94.

PREVIDI, F. et al. Data-Driven Control Design for Neuroprotheses: A Virtual Reference Feedback Tuning (VRFT) Approach. *IEEE Transactions on Control Systems Technology*, v. 12, n. 1, p. 176–182, 2004. ISSN 10636536. Cited 2 times in pages 37 and 38.

QIU, S. et al. A stimulus artifact removal technique for SEMG signal processing during functional electrical stimulation. *IEEE Transactions on Biomedical Engineering*, v. 62, n. 8, p. 1959–1968, 2015. ISSN 15582531. Cited 4 times in pages 33, 34, 151 and 152.

QIU, S. et al. Intelligent algorithm tuning PID method of function electrical stimulation using knee joint angle. *2014 36th Annual International Conference of the IEEE Engineering in Medicine and Biology Society, EMBC 2014*, p. 2561–2564, 2014. Cited 3 times in pages 4, 36 and 37.

QUINTERN, J.; RIENER, R.; RUPPRECHT, S. Comparison of simulation and experiments of different closed-loop strategies for functional electrical stimulation: Experiments in paraplegics. *Artificial Organs*, v. 21, n. 3, p. 232–235, 1997. ISSN 0160564X. Cited in page 34.

RABISCHONG, P. et al. Present Status of the Amoll (Active Modular Orthosis for Lower Limb) Project. In: *Disability*. London: Palgrave Macmillan, London, 1979. p. 435–441. ISBN 978-1-349-04835-9. Cited in page 40.

RAINE, S.; MEADOWS, L.; LYNCH-ELLERINGTON, M. *Bobath Concept*. Oxford, UK: Wiley-Blackwell, 2009. 1–216 p. ISBN 9781444314601. Available in: <http://doi.wiley.com/10.1002/9781444314601>. Cited 2 times in pages 2 and 196.

REN, Y.; ZHANG, D. FEXO Knee: A rehabilitation device for knee joint combining functional electrical stimulation with a compliant exoskeleton. In: *5th IEEE RAS/EMBS International Conference on Biomedical Robotics and Biomechatronics*. IEEE, 2014. p. 683–688. ISBN 978-1-4799-3128-6. Available in: <http://ieeexplore-.ieee.org/lpdocs/epic03/wrapper.htm?arnumber=6913857>. Cited 2 times in pages 4 and 42.

RIEK, L. D. Healthcare robotics. *Communications of the ACM*, v. 60, n. 11, p. 68–78, 2017. ISSN 15577317. Cited 2 times in pages 2 and 196.

ROBBI, D. B. et al. Dynamical Analysis of Human Gait at Low Speeds. In: *XXVI Brazilian Congress on Biomedical Engineering*. 1st. ed. Buzios, Brazil: Springer Singapore, 2019. p. 193–199. ISBN 9789811321191. Available in: <http://dx.doi.org/10.1007/978-981-13-2119-1_63 http://link.springer.com/10.1007-/978-981-13-2119-1_30>. Cited in page 76.

SCHAUER, T. Sensing motion and muscle activity for feedback control of functional electrical stimulation: Ten years of experience in Berlin. *Annual Reviews in Control*, Elsevier Ltd, v. 44, p. 355–374, 2017. ISSN 13675788. Cited 2 times in pages 5 and 198.

SCHAUER, T. et al. Realtime EMG analysis for transcutaneous electrical stimulation assisted gait training in stroke patients. *IFAC-PapersOnLine*, Elsevier B.V., v. 49, n. 32, p. 183–187, 2016. ISSN 24058963. Available in: <http://dx.doi.org/10.1016/j.ifacol.2016.12.211>. Cited 5 times in pages 26, 29, 30, 32 and 34.

SEHNDKAR, C. V. et al. Efficacy of FES for restoring hand grasp in hemiplegia: Investigation using biosignals. *2016 International Conference on Systems in Medicine and Biology, ICSMB 2016*, n. January, p. 1–4, 2017. Cited in page 30.

SENNELS, S. et al. Functional neuromuscular stimulation controlled by surface electromyographic signals produced by volitional activation of the same muscle: Adaptive removal of the muscle response from the recorded EMG-signal. *IEEE Transactions on Rehabilitation Engineering*, v. 5, n. 2, p. 195–206, 1997. ISSN 10636528. Cited 5 times in pages xii, 26, 27, 29 and 30.

SHALABY, R. et al. Amplifier design for EMG recording from stimulation electrodes during functional electrical stimulation leg cycling ergometry. *Biomedizinische Technik*, v. 56, n. 1, p. 23–33, 2011. ISSN 00135585. Cited 2 times in pages 5 and 151.

SHARMA, N. et al. Nonlinear neuromuscular electrical stimulation tracking control of a human limb. *IEEE Transactions on Neural Systems and Rehabilitation Engineering*, v. 17, n. 6, p. 576–584, 2009. ISSN 15344320. Cited 3 times in pages 37, 38 and 88.

SOARES, S. B.; COELHO, R. R.; NADAL, J. The use of cross correlation function in onset detection of electromyographic signals. *ISSNIP Biosignals and Biorobotics Conference, BRC*, 2013. ISSN 23267771. Cited in page 5.

SOUSA, A. C. C. d.; FONSECA, L. O. da; BÓ, A. P. L. *Comparison between iterative learning and extremum seeking PID controllers for a simulated hybrid neuroprosthesis.* Toronto, Canadá: IFESS 2019, 2019. Cited in page 68.

SOUSA, A. C. C. d.; FREIRE, J. P. C. D.; BÓ, A. P. L. Integrating hip exosuit and FES for lower limb rehabilitation in a simulation environment. *IFAC-PapersOnLine*, Elsevier BV, v. 51, n. 34, p. 302–307, 2019. ISSN 24058963. Cited 4 times in pages 68, 69, 72 and 201.

SOUSA, A. C. C. d. et al. A Comparative Study on Control Strategies for FES Cycling Using a Detailed Musculoskeletal Model. *IFAC-PapersOnLine*, v. 49, n. 32, p. 204–209, 2016. ISSN 24058963. Cited 12 times in pages 91, 92, 93, 96, 99, 100, 101, 102, 103, 104, 105 and 206.

SOUSA, A. C. C. d. et al. Automatic Detection of Stimulation Artifacts to Isolate Volitional from Evoked EMG Activity. *IFAC-PapersOnLine*, v. 51, n. 27, p. 282–287, 2018. ISSN 24058963. Cited 4 times in pages 50, 55, 56 and 151.

SOUSA, A. C. C. de; SOUSA, F. S. C.; BÓ, A. P. L. Simulation of the assistance of passive knee orthoses in FES cycling. In: *2019 41st Annual International*

Conference of the IEEE Engineering in Medicine and Biology Society (EMBC). Berlin, Germany: IEEE, 2019. p. 3811–3814. ISBN 978-1-5386-1311-5. Available in: <https://ieeexplore.ieee.org/document/8857912/>. Cited 2 times in pages 109 and 110.

SZECSI, J.; STRAUBE, A.; FORNUSEK, C. A biomechanical cause of low power production during FES cycling of subjects with SCI. *Journal of NeuroEngineering and Rehabilitation*, v. 11, n. 1, p. 1–12, 2014. ISSN 17430003. Cited 2 times in pages 68 and 201.

TEPAVAC, D.; NIKOLIC, Z. A portable 8 channel surface EMG recording system. In: *Proceedings of the Annual International Conference of the IEEE Engineering in Medicine and Biology Society.* IEEE, 1992. p. 1433–1434. ISBN 0-7803-0785-2. Available in: <http://ieeexplore.ieee.org/document/96059/ http://ieeexplore.ieee.org/document/5761863/>. Cited in page 30.

The Lancet. World Report on Disability. *The Lancet*, SP, Brazil, v. 377, n. 9782, p. 1977, 6 2011. ISSN 01406736. Available in: <https://linkinghub.elsevier.com/retrieve/pii/S0140673611608441>. Cited 2 times in pages 1 and 20.

Thomas Jefferson University Hospital and Magee Rehabilitation. *Spinal Cord Injury Patient - Family Teaching Manual 21.* Philadelphia, PA, EUA, 2009. Cited 3 times in pages 1, 2 and 196.

THOMAZ, S. R. et al. Effect of electrical stimulation on muscle atrophy and spasticity in patients with spinal cord injury – a systematic review with meta-analysis. *Spinal Cord*, Springer US, v. 57, n. 4, p. 258–266, 2019. ISSN 14765624. Available in: <http://dx.doi.org/10.1038/s41393-019-0250-z>. Cited 2 times in pages 2 and 196.

THORSEN, R. An artefact suppressing fast-recovery myoelectric amplifier. *IEEE Transactions on Biomedical Engineering*, v. 46, n. 6, p. 764–766, 1999. ISSN 00189294. Cited in page 5.

THRASHER, T. A.; POPOVIC, M. R. Functional electrical stimulation of walking: Function, exercise and rehabilitation. *Annales de Readaptation et de Medecine Physique*, v. 51, n. 6, p. 452–460, 2008. ISSN 01686054. Cited 2 times in pages 3 and 197.

TIMMER, C. A. W. Cycling Biomechanics: A Literature Review. *Journal of Orthopaedic & Sports Physical Therapy*, v. 14, n. 3, p. 106–113, 9 1991. ISSN 0190-6011. Available in: <http://www.jospt.org/doi/10.2519/jospt.1991.14.3.106>. Cited in page 18.

VALLERY, H. et al. Control of a hybrid motor prosthesis for the knee joint. *IFAC Proceedings Volumes*, v. 38, n. 1, p. 76–81, 2005. ISSN 14746670. Available in: <http://linkinghub.elsevier.com/retrieve/pii/S1474667016374274>. Cited in page 42.

VELTINK, P. H. Control of FES-induced cyclical movements of the lower leg. *Medical & Biological Engineering & Computing*, v. 29, n. 6, p. NS8–NS12, 11 1991. ISSN 0140-0118. Available in: <https://onlinelibrary.wiley.com/doi/abs/10.1111/j.1525-1594.1997.tb04656.x http://link.springer.com/10.1007/BF02446096>. Cited 2 times in pages 34 and 88.

VETTE, A. H.; MASANI, K.; POPOVIC, M. R. Implementation of a physiologically identified PD feedback controller for regulating the active ankle torque during quiet stance. *IEEE Transactions on Neural Systems and Rehabilitation Engineering*, v. 15, n. 2, p. 235–243, 2007. ISSN 15344320. Cited in page 3.

WANG, X. et al. Design of Functional Electrical Stimulation Cycling System for Lower-Limb Rehabilitation of Stroke Patients. *Proceedings of the Annual International Conference of the IEEE Engineering in Medicine and Biology Society, EMBS*, v. 2018-July, p. 2337–2340, 2018. ISSN 1557170X. Cited in page 26.

WATANABE, T.; TADANO, T. Determination of Stimulation Timing Pattern based on EMG Signals for FES Cycling with Pedaling Wheelchair. In: *IFMBE Proceedings 65*. Tampere, Finland: Springer, Singapore, 2018. v. 17, n. 1, p. 394–397. ISBN 0967-3334. Cited 2 times in pages 6 and 199.

WIDJAJA, F. et al. FES artifact suppression for real-time tremor compensation. *2009 IEEE International Conference on Rehabilitation Robotics, ICORR 2009*, p. 53–58, 2009. Cited 4 times in pages 31, 32, 34 and 151.

YAHAYA, S. et al. Implementation of Cycle-to-Cycle Control with Energy Storage Element for FES-Assisted Elliptical Stepping Exercise. In: *2018 IEEE 8th International Conference on System Engineering and Technology (ICSET)*. IEEE, 2018. p. 7–11. ISBN 978-1-5386-9180-9. Available in: <https://ieeexplore.ieee.org/document/8606384/>. Cited 2 times in pages 5 and 43.

YOCHUM, M. et al. EMG artifacts removal during electrical stimulation, a CWT based technique. *IEEE TENSYMP 2014 - 2014 IEEE Region 10 Symposium*, p. 137–140, 2014. Cited 3 times in pages 33, 34 and 151.

YOUNG, A.; FERRIS, D. State-of-the-art and Future Directions for Robotic Lower Limb Exoskeletons. *IEEE Transactions on Neural Systems and Rehabilitation Engineering*, PP, n. 99, p. 1–1, 2016. ISSN 1534-4320. Available in: <http://ieeexplore.ieee.org/ielx7/7333/4359219/07393837.pdf?tp=&arnumber=7393837&isnumber=4359219 http://ieeexplore.ieee.org/document/7393837/>. Cited in page 28.

ZHANG, D.; ANG, W. T. Reciprocal EMG controlled FES for pathological tremor suppression of forearm. *Annual International Conference of the IEEE Engineering in Medicine and Biology - Proceedings*, n. 1, p. 4810–4813, 2007. ISSN 05891019. Cited 4 times in pages 32, 34, 58 and 151.

A MATERIAL: EQUIPMENT AND TOOLS

This section describes all available equipment and tools for the realization of this project: electrical stimulator and electrodes, EMG amplifier and electrodes, simulation environment, inertial measurement units (IMUs) and force sensors.

A.1 ELECTRICAL STIMULATOR AND ELECTRODES

For stimulation, we used either the current-controlled 4-channel stimulator RehaMove3 (RehaMove3, Hasomed GmbH, Germany, Figure A.1a) or the 8-channel stimulator RehaStim I (RehaStim I, Hasomed GmbH, Germany, Figure A.1b). Both stimulators provide biphasic current pulses and enable online update of stimulation amplitude and pulse-width (PW). Hence, the control signal may be the PW or the current modulation, or even the normalized pulse charge varying between zero and the maximally tolerable charge. Table A.1 resumes the technical features and specifications of the stimulation devices. To apply the stimulation to the selected muscles, we used hydro-gel electrodes with sizes depending on the muscles to be stimulated.

(a) Illustration of the RehaMove3: the 4-channel stimulator for scientists.

Source: Digital Repository of Hasomed available in the worksheet accessed in May 2018.

(b) RehaStim I: the 8-channel RehaStim stimulator with surface electrodes.

Source: Digital Repository of Derek Jones available in the article accessed in May 2018.

Figure A.1: Electrical stimulator and electrodes used.

A.2 ELECTROMYOGRAPH (EMG)

For EMG measurement, we used either the two-channel recording device RehaIngest with Galvanically isolated USB interface (RehaIngest, Hasomed GmbH, Germany, Figure A.2a) or the wireless recording device MUSCLELAB (MUSCLELAB[TM], Ergotest Innovation A/S, Norway, Figure A.2b). Table A.3 resumes the technical features and specifications of the EMG amplifiers. Both EMG devices

Table A.1: Description of the stimulator technical features and specifications.

Technical feature	RehaMove3	RehaStim I
Number of channels	4	8
Pulse width	10 to $400\mu s$, $1\mu s$ step	20 to $500\mu s$, $10\mu s$ step
Current	0 to $130mA$, $0.5mA$ step	0 to $130mA$, $2mA$ step
Stimulation frequency	1 to $500Hz$, $1Hz$ step	10 to $50Hz$, $5Hz$ step
Waveform type	Biphasic, charged balanced	Biphasic, charged balanced

feature bipolar measurement channels, which measure the selected muscles EMG with AgCl electrodes.

Figure A.2: EMG amplifiers and electrodes used.

(a) RehaIngest: The bi-channel signal amplifier for EMG with surface electrodes.

Source: Prepared by the author.

(b) MUSCLELAB: Data Sync Unit with the EMG module.

Source: Digital Repository of MUSCLE-LAB available in the product overview accessed in May 2018.

Figure A.3: Description of the EMG amplifier technical features and specifications.

Technical feature or specification	RehaIngest	MUSCLELAB
Number of channels	2	2
Sample rate	$4kHz$	$1kHz$

A.3 ROBOT OPERATING SYSTEM

Robot Operating System (ROS[1]) is an OpenSource set of libraries and tools to build applications for robots. From drivers to state-of-the-art algorithms and powerful development tools, ROS provides the framework for projects. ROS offers tools to create packages in C++ and Python. Each package may contain an arbitrary number of nodes.

---

[1] A detailed explanation of the ROS platform is available at
http://wiki.ros.org/ROS/Introduction.

With the ROS platform, we may develop a modular system, a machine (master) runs the roscore command that initializes the ROS services for the nodes to communicate. It is possible to have nodes running on different machines on the network and communicate through TCP/IP protocol. Each node may publish and subscribe to topics, i.e., a node may either write or read values of that variable.

For a friendly real-time interface, we used a software framework of ROS that implements the various graphical user interfaces (GUI) tools in the form of plugins, called rqt. We created GUI for the FES cycling control illustrated in Figures A.4.
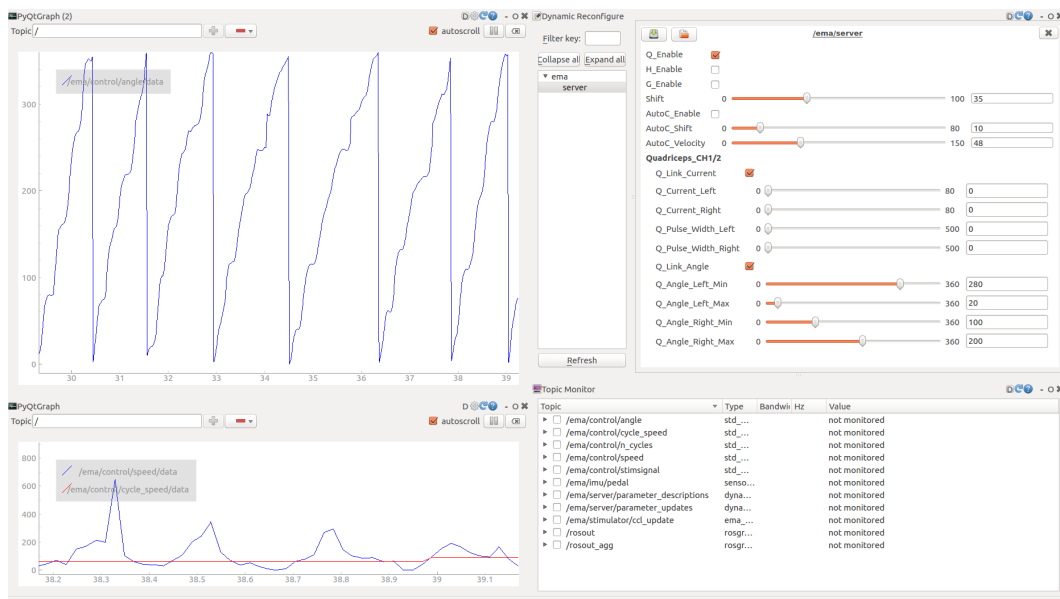
Figure A.4: ROS rqt GUI for the FES cycling control.

Source: print screen of the application on the Ubuntu 16.04 operating system.

A.4 OPENSIM AND ITS INTEGRATION WITH MATLAB

The OpenSim platform is an open-source software to simulate highly detailed musculoskeletal models (DELP et al., 2007; HILL; B, 1938)[2]. The software provides kinematics and dynamics tools to understand and analyze motions. Using a graphical interface (Figure A.5), users can generate simulations with default models or develop new models and controllers. These tools measure states variables during simulations. Users can also regulate the muscle excitation in real time for dynamic simulation (for simplicity, we define excitation as the same as stimulation level).

For functional electrical stimulation (FES) control strategies evaluations, we use the forward dynamics tool; yet, the OpenSim API only allows an open loop analysis.

---

2   Developed in maintained in https://simtk.org/projects/opensim.

There are scripting environments to use OpenSim API without any additional requirement to set up a development environment to solve the open loop analysis. It is possible to access OpenSim tools to create, simulate, and analyze models using Matlab. Basic OpenSim scripting does not enable performing dynamic simulations that integrate closed-loop artificial controllers. In our solution, we convert OpenSim models and states to Matlab components, and perform forward dynamic simulation using Matlab tools (e.g., ode45).
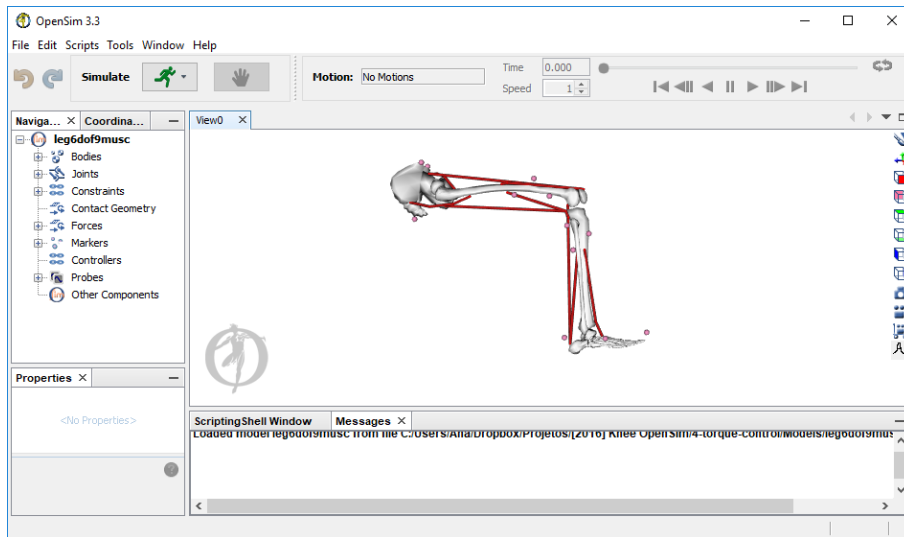
Figure A.5: OpenSim graphical interface. The navigation panel shows information and properties while the view panel shows the visualization of the model.

Source: print screen of the application on the Windows 10 operating system.

Matlab access the OpenSim source code, interacting with the API. In this way, Matlab interfaces with OpenSim libraries and use them in our scripting environment, manipulating objects and running methods. In our script, we load the model and run the forward dynamics tool for a specific time, then we read the current states, recalculate the excitations and actuation on muscles and external actuators. With the new values, the script reruns the forward dynamics tool and recalculates the control signals until the total time of simulation expires.

A.5 INERTIAL MEASUREMENT UNIT (IMU)

To measure the kinematic variables, we used inertial measurement unit (IMU) composed of 3-axis accelerometer, gyroscope, and magnetometer. The devices available for use were the 3-Space Sensor (3-Space Sensor, YEI, United States) and the RehaGait Motion Sensor (RehaGait, Hasomed GmbH, Germany). Both sensors work wired or wireless with onboard algorithms for angular estimation (e.g., Euler, quaternion-based

Kalman filtering or rotation matrix). Table A.2 resumes some features of both IMUs used.

Table A.2: Description of the IMUs technical features and specifications.

Technical feature or specification	3-Space Sensor	RehaGait
Communication	USB receiver	Bluetooth
Sample rate	$1kHz$	$1kHz$

(a) 3-Space Sensor: the USB receiver IMU.

Source: Digital Repository of Yost Labs available in the product overview accessed in May 2018.

(b) RehaGait: the bluetooth IMU.

Source: Digital Repository of Hasomed available in the motion sensors accessed in May 2018.

Figure A.6: The 3-axis accelerometer, gyroscope, and magnetometer embedded inertial sensors used.

B VOLUNTEER'S WRITTEN CONSENT

Universidade de Brasília Faculdade de Tecnologia – FT

Termo de Consentimento Livre e Esclarecido - TCLE

Convidamos o(a) Senhor(a) a participar voluntariamente do projeto de pesquisa Reabilitação de função sensório-motora em pessoas com lesão medular usando estimulação elétrica superficial, sob a responsabilidade do pesquisador Antônio Padilha Lanari Bó. O projeto busca investigar novas técnicas de terapia para lesão medular utilizadas em conjunto, e usando tecnologias inovadoras. Será utilizado estimulação elétrica superficial nos membros afetados nas atividades de ciclismo e remo, além de exercícios em posição verticalizada em que você utilizará óculos de realidade virtual e tentará controlar um boneco virtual caminhando. Nenhuma dessas atividades deve gerar dor ou desconforto, entretanto algumas podem ser cansativas. Você será sempre acompanhado por um profissional responsável pela sua segurança na atividade, e é importante seguir rigorosamente as instruções dele(a).

O objetivo desta pesquisa é justamente avaliar a recuperação de funções sensório-motoras em indivíduos com lesão medular após protocolo de reabilitação de longa duração envolvendo ferramentas tecnológicas, em especial ciclismo e remo assistidos por estimulação elétrica superficial, bem como exercícios envolvendo realidade virtual.

O(a) senhor(a) receberá todos os esclarecimentos necessários antes e no decorrer da pesquisa e lhe asseguramos que seu nome não aparecerá em lugar algum, sendo mantido o mais rigoroso sigilo pela omissão total de quaisquer informações que permitam identificá-lo(a).

A sua participação se dará por meio de sessões de fisioterapia e exames clínicos não-invasivos realizados no Departamento de Engenharia Elétrica da Faculdade de Tecnologia da Universidade de Brasília, bem como no centro de treinamento Capital do Remo. O estudo terá duração de um ano, em que serão realizadas três sessões por semana (datas específicas a combinar). O tempo estimado para a realização de cada sessão é de uma hora.

Os riscos decorrentes de sua participação na pesquisa são fraturas durante a atividade ou transferências da cadeira de rodas para os equipamentos. Esse risco é minimizado pela avaliação de composição corporal realizada previamente à participação no protocolo, além da utilização de medidas adicionais de segurança, como fixação dos pés e pernas no cicloergômetros, e botões de parada de emergência sempre ao alcance. Existe também o risco de descompensação relacionada ao esforço, como elevação de pressão arterial de forma súbita e outros problemas cardíacos. Este risco será minimizado pela avaliação de um cardiologista antes do início do protocolo e pelo regular controle da frequência cardíaca e pressão arterial durante as atividades.

Se o(a) senhor(a) aceitar participar, estará contribuindo para a geração de conhecimento científico importante para a melhoria das terapias de reabilitação de lesão medular, o que poderia impactar positivamente milhões de pessoas todos os anos. Além disso, é possível que você tenha melhorias em sua capacidade motora e funções autonômicas, o que resultaria em ganhos diretos para sua saúde e qualidade de vida.

O(a) Senhor(a) pode se recusar a responder (ou participar de qualquer procedimento) qualquer questão que lhe traga constrangimento, podendo desistir de participar da pesquisa em qualquer momento sem nenhum prejuízo para o(a) senhor(a). Sua participação é voluntária, isto é, não há pagamento por sua colaboração.

Todas as despesas que o(a) senhor(a) e seu(ua) acompanhante tiver(em) relacionadas diretamente ao projeto de pesquisa (tais como passagem para o local da pesquisa, alimentação no local da pesquisa ou exames para realização da pesquisa) serão cobertas pelo pesquisador responsável.

Caso haja algum dano direto ou indireto decorrente de sua participação na pesquisa, o(a) senhor(a) deverá buscar ser indenizado, obedecendo-se as disposições legais vigentes no Brasil.

Os resultados da pesquisa serão divulgados na Universidade de Brasília, podendo ser publicados posteriormente. Os dados e materiais serão utilizados somente para esta pesquisa e ficarão sob a guarda do pesquisador por um período de cinco anos, após isso serão destruídos.

Se o(a) Senhor(a) tiver qualquer dúvida em relação à pesquisa, por favor telefone para: Prof. Antônio Padilha Lanari Bó no Departamento de Engenharia Elétrica da Faculdade de Tecnologia da Universidade de Brasília nos telefones 061 31071040 e 061 981698477, disponível inclusive para ligação a cobrar, bem como no email antonio.plb@lara.unb.br.

Este projeto foi aprovado pelo Comitê de Ética em Pesquisa da Faculdade de Ciências da Saúde (CEP/FS) da Universidade de Brasília. O CEP é composto por profissionais de diferentes áreas cuja função é defender os interesses dos participantes da pesquisa em sua integridade e dignidade e contribuir no

Página 1 de 2

Figure B.1: The first page of the volunteer's written consent (in Portuguese).

Source: scanned document.

Universidade de Brasília Faculdade de Tecnologia – FT

desenvolvimento da pesquisa dentro de padrões éticos. As dúvidas com relação à assinatura do TCLE ou os direitos do participante da pesquisa podem ser esclarecidos pelo telefone (61) 3107-1947 ou do e-mail cepfs@unb.br ou cepfsunb@gmail.com, horário de atendimento de 10:00hs às 12:00hs e de 13:30hs às 15:30hs, de segunda a sexta-feira. O CEP/FS se localiza na Faculdade de Ciências da Saúde, Campus Universitário Darcy Ribeiro, Universidade de Brasília, Asa Norte.

Caso concorde em participar, pedimos que assine este documento que foi elaborado em duas vias, uma ficará com o pesquisador responsável e a outra com o(a) Senhor(a).

_____
Nome e assinatura do Participante de Pesquisa

_____
Nome e assinatura do Pesquisador Responsável

Brasília, ___ de _____ de _____.

Figure B.2: The second page of the volunteer's written consent (in Portuguese).

Source: scanned document.

C COMPLEMENTARY RESULTS OF CYCLING SIMU-LATIONS

In all tables, we simplify $\{\Phi_{QUAD}, \Phi_{HAMS}, \Phi_{GLUT}\}$ as $\{\Phi_Q, \Phi_H, \Phi_G\}$.

Table C.1: Performance parameters for $h = \{0.6, 0.7, 0.8, 0.9, 1.0\}$. In this simulation, we kept $F = 0$, i.e., there is no muscle fatigue effect at the model. We also kept the load crankset as zero ($L = 0$), i.e., there is no resistance at the crankset to the movement.

h	Muscles	$\bar{\dot{\theta}}_c$	$\ddot{\theta}_c$	$\sigma_{\dot{\theta}}$	e_{max}	e_{RMSE}	t_r	$\{\Phi_Q, \Phi_H, \Phi_G\}$	n_c
0.6	Q	320	9	6.51	16.09	6.45	5.19	$\{0.16\ ,\ 0.00\ ,\ 0.00\}$	14
0.6	QH	523	-1	13.03	29.28	12.83	7.83	$\{0.16\ ,\ 0.16\ ,\ 0.00\}$	22
0.6	QHG	510	25	16.48	30.10	16.24	4.66	$\{0.19\ ,\ 0.15\ ,\ 0.12\}$	23
0.7	Q	431	5	11.40	23.94	11.26	6.19	$\{0.20\ ,\ 0.00\ ,\ 0.00\}$	17
0.7	QH	505	-33	10.32	19.71	10.17	3.62	$\{0.18\ ,\ 0.20\ ,\ 0.00\}$	25
0.7	QHG	581	2	20.59	32.73	20.26	4.23	$\{0.20\ ,\ 0.20\ ,\ 0.14\}$	26
0.8	Q	518	3	13.57	29.38	13.38	9.18	$\{0.21\ ,\ 0.00\ ,\ 0.00\}$	22
0.8	QH	612	30	17.16	30.12	16.86	4.30	$\{0.22\ ,\ 0.19\ ,\ 0.00\}$	27
0.8	QHG	616	-10	20.48	31.28	20.12	2.74	$\{0.22\ ,\ 0.22\ ,\ 0.14\}$	30
0.9	Q	446	-2	18.81	29.94	18.57	3.66	$\{0.25\ ,\ 0.00\ ,\ 0.00\}$	22
0.9	QH	621	-10	19.63	39.90	19.29	3.54	$\{0.25\ ,\ 0.22\ ,\ 0.00\}$	30
0.9	QHG	677	21	20.45	33.64	20.07	2.70	$\{0.23\ ,\ 0.27\ ,\ 0.17\}$	34
1.0	Q	555	11	17.70	29.18	17.43	5.51	$\{0.27\ ,\ 0.00\ ,\ 0.00\}$	26
1.0	QH	665	-27	21.65	44.62	21.25	2.59	$\{0.30\ ,\ 0.26\ ,\ 0.00\}$	33
1.0	QHG	737	41	22.18	41.57	21.71	2.26	$\{0.29\ ,\ 0.25\ ,\ 0.21\}$	37

Table C.2: Performance parameters for $h = \{0.6, 0.7, 0.8, 0.9, 1.0\}$. In this simulation, we kept $F = 0$, i.e., there is no muscle fatigue effect at the model. We added a load resisting the movement of $L = 0.01$.

h	Muscles	$\bar{\dot{\theta}}_c$	$\ddot{\theta}_c$	$\sigma_{\dot{\theta}}$	e_{max}	e_{RMSE}	t_r	$\{\Phi_Q, \Phi_H, \Phi_G\}$	n_c
0.6	Q	241	1	6.51	14.64	6.47	9.29	$\{0.17 , 0.00 , 0.00\}$	9
0.6	QH	381	6	7.50	12.05	7.42	5.72	$\{0.17 , 0.17 , 0.00\}$	15
0.6	QHG	487	2	13.20	28.31	13.03	8.25	$\{0.16 , 0.16 , 0.11\}$	19
0.7	Q	251	5	5.94	13.11	5.89	4.71	$\{0.20 , 0.00 , 0.00\}$	12
0.7	QH	518	0	12.17	26.58	11.99	7.88	$\{0.19 , 0.19 , 0.00\}$	22
0.7	QHG	475	-65	27.09	63.09	26.73	4.33	$\{0.20 , 0.20 , 0.13\}$	23
0.8	Q	342	3	8.82	17.89	8.74	4.98	$\{0.23 , 0.00 , 0.00\}$	15
0.8	QH	531	-36	12.54	26.91	12.35	4.85	$\{0.24 , 0.21 , 0.00\}$	24
0.8	QHG	591	-20	17.89	37.39	17.59	3.69	$\{0.24 , 0.21 , 0.13\}$	28
0.9	Q	456	-1	12.37	25.18	12.21	10.03	$\{0.23 , 0.00 , 0.00\}$	19
0.9	QH	581	-49	11.44	26.84	11.26	3.13	$\{0.23 , 0.23 , 0.00\}$	29
0.9	QHG	634	-1	20.02	32.64	19.66	2.62	$\{0.26 , 0.23 , 0.19\}$	31
1.0	Q	529	1	14.54	32.84	14.33	8.91	$\{0.29 , 0.00 , 0.00\}$	23
1.0	QH	644	17	17.07	31.53	16.76	2.85	$\{0.32 , 0.25 , 0.00\}$	31
1.0	QHG	691	-10	23.65	49.17	23.20	2.71	$\{0.27 , 0.27 , 0.23\}$	35

Table C.3: Performance parameters for $h = \{0.6, 0.7, 0.8, 0.9, 1.0\}$. In this simulation, we added the muscle fatigue effect with a constant time of $F = 10$ for each muscle group. We kept the load crankset as zero $(L = 0)$, i.e., there is no resistance at the crankset to the movement.

h	Muscles	$\bar{\dot{\theta}}_c$	$\ddot{\theta}_c$	$\sigma_{\dot{\theta}}$	e_{max}	e_{RMSE}	t_r	$\{\Phi_Q, \Phi_H, \Phi_G\}$	n_c
0.6	Q	55	-11	30.15	55.90	30.11	0.85	$\{0.00 , 0.00 , 0.00\}$	5
0.6	QH	79	-10	22.77	37.86	22.72	1.11	$\{0.00 , 0.00 , 0.00\}$	7
0.6	QHG	85	-12	26.61	44.28	26.54	1.03	$\{0.00 , 0.00 , 0.00\}$	9
0.7	Q	94	-12	19.15	33.81	19.10	0.87	$\{0.00 , 0.00 , 0.00\}$	8
0.7	QH	41	-25	70.50	130.61	70.42	0.39	$\{0.00 , 0.00 , 0.00\}$	7
0.7	QHG	55	-30	63.98	102.61	63.88	0.53	$\{0.00 , 0.00 , 0.00\}$	10
0.8	Q	73	-17	26.33	72.24	26.27	0.49	$\{0.00 , 0.00 , 0.00\}$	9
0.8	QH	96	-34	42.70	71.51	42.59	0.63	$\{0.00 , 0.00 , 0.00\}$	14
0.8	QHG	118	-31	24.95	65.76	24.87	0.69	$\{0.00 , 0.00 , 0.00\}$	16
0.9	Q	202	-15	12.21	24.64	12.14	1.41	$\{0.02 , 0.00 , 0.00\}$	15
0.9	QH	230	-32	16.26	25.42	16.15	1.11	$\{0.01 , 0.01 , 0.00\}$	21
0.9	QHG	262	-32	13.74	25.64	13.64	0.85	$\{0.01 , 0.01 , 0.01\}$	23
1.0	Q	275	-12	10.88	18.97	10.80	1.55	$\{0.04 , 0.00 , 0.00\}$	18
1.0	QH	359	-18	11.49	17.58	11.38	1.25	$\{0.04 , 0.04 , 0.00\}$	24
1.0	QHG	404	-16	12.64	28.14	12.50	1.05	$\{0.04 , 0.04 , 0.03\}$	26

Table C.4: Performance parameters for $h = \{0.6, 0.7, 0.8, 0.9, 1.0\}$. In this simulation, we added the muscle fatigue effect with a constant time of $F = 10$ for each muscle group. We added a load resisting the movement of $L = 0.01$.

h	Muscles	$\bar{\dot{\theta}}_c$	$\ddot{\theta}_c$	$\sigma_{\dot{\theta}}$	e_{max}	e_{RMSE}	t_r	$\{\Phi_Q, \Phi_H, \Phi_G\}$	n_c
0.6	Q	0	0		- -	-	-	$\{$ - , - , - $\}$	0
0.6	QH	0	0	-	-	-	-	$\{$ - , - , - $\}$	0
0.6	QHG	0	0	-	-	-	-	$\{$ - , - , - $\}$	0
0.7	Q	0	0	0.00	0.00	0.00	0.00	$\{0.00 , 0.00 , 0.00\}$	1
0.7	QH	34	-25	53.95	142.29	53.90	0.63	$\{0.00 , 0.00 , 0.00\}$	5
0.7	QHG	35	-33	81.57	181.15	81.49	0.65	$\{0.00 , 0.00 , 0.00\}$	6
0.8	Q	33	-22	66.97	134.41	66.91	0.35	$\{0.03 , 0.00 , 0.00\}$	4
0.8	QH	37	-27	53.68	129.86	53.62	0.39	$\{0.01 , 0.01 , 0.00\}$	7
0.8	QHG	47	-39	65.17	153.75	65.08	0.47	$\{0.01 , 0.01 , 0.00\}$	10
0.9	Q	55	-31	79.20	122.42	79.08	0.39	$\{0.05 , 0.00 , 0.00\}$	8
0.9	QH	80	-41	60.39	95.86	60.26	0.53	$\{0.03 , 0.02 , 0.00\}$	13
0.9	QHG	116	-40	31.66	77.28	31.55	0.69	$\{0.02 , 0.02 , 0.01\}$	17
1.0	Q	83	-18	23.68	42.02	23.62	0.44	$\{0.06 , 0.00 , 0.00\}$	10
1.0	QH	225	-32	15.66	28.43	15.57	1.11	$\{0.04 , 0.04 , 0.00\}$	21
1.0	QHG	287	-30	15.07	25.35	14.94	0.91	$\{0.04 , 0.04 , 0.03\}$	24

Table C.5: Performance parameters for the PID controller. In this simulation, we kept $F = 0$, i.e., there is no muscle fatigue effect at the model. We also kept the load crankset as zero ($L = 0$), i.e., there is no resistance at the crankset to the movement.

Muscles	$\bar{\dot{\theta}}_c$	$\ddot{\theta}_c$	$\sigma_{\dot{\theta}}$	e_{max}	e_{RMSE}	t_r	$\{\Phi_Q, \Phi_H, \Phi_G\}$	n_c
Q	360	0	9.74	15.12	9.64	2.14	$\{0.14 , 0.00 , 0.00\}$	18
QH	360	0	10.69	18.32	10.59	1.17	$\{0.13 , 0.11 , 0.00\}$	18
QHG	360	-1	9.71	15.63	9.61	0.93	$\{0.12 , 0.09 , 0.08\}$	19

Table C.6: Performance parameters for the PID controller. In this simulation, we kept $F = 0$, i.e., there is no muscle fatigue effect at the model. We added a load resisting the movement of $L = 0.01$. Each muscle group set is represented by red, blue and green lines, respectively, Q, QH, and QHG.

Muscles	$\bar{\dot{\theta}}_c$	$\ddot{\theta}_c$	$\sigma_{\dot{\theta}}$	e_{max}	e_{RMSE}	t_r	$\{\Phi_Q, \Phi_H, \Phi_G\}$	n_c
Q	360	0	9.70	13.32	9.60	2.99	$\{0.20 , 0.00 , 0.00\}$	17
QH	360	0	10.68	17.05	10.57	1.34	$\{0.17 , 0.14 , 0.00\}$	18
QHG	360	1	8.80	15.10	8.71	0.99	$\{0.15 , 0.13 , 0.09\}$	18

Table C.7: Performance parameters for the PID controller. In this simulation, we added the muscle fatigue effect with a constant time of $F = 10$ for each muscle group. We kept the load crankset as zero, i.e., there is no resistance at the crankset to the movement.

Muscles	$\bar{\dot{\theta}}_c$	$\ddot{\theta}_c$	$\sigma_{\dot{\theta}}$	e_{max}	e_{RMSE}	t_r	$\{\Phi_Q, \Phi_H, \Phi_G\}$	n_c
Q	242	-16	11.74	21.60	11.66	1.43	$\{0.04 , 0.00 , 0.00\}$	16
QH	323	-9	7.53	15.27	7.46	1.13	$\{0.04 , 0.04 , 0.00\}$	18
QHG	338	-2	8.86	15.44	8.78	0.93	$\{0.04 , 0.04 , 0.03\}$	18

Table C.8: Performance parameters for the PID controller. In this simulation, we added the muscle fatigue effect with a constant time of $F = 10$ for each muscle group. We added a load resisting the movement of $L = 0.01$.

Muscles	$\bar{\dot{\theta}}_c$	$\ddot{\theta}_c$	$\sigma_{\dot{\theta}}$	e_{max}	e_{RMSE}	t_r	$\{\Phi_Q, \Phi_H, \Phi_G\}$	n_c
Q	77	-17	30.55	42.90	30.48	0.38	$\{0.07 , 0.00 , 0.00\}$	10
QH	200	-29	19.06	31.46	18.95	1.07	$\{0.04 , 0.04 , 0.00\}$	16
QHG	255	-25	18.86	35.24	18.72	0.83	$\{0.04 , 0.04 , 0.03\}$	17

Table C.9: Spring performance parameters for negative k_{max}. In these simulations, we kept $F = 0$ and $h = 1$.

Muscles	L	k_{max}	$\dot{\theta}_c$	$\ddot{\theta}_c$	$\sigma_{\dot{\theta}}$
Q	0.00	-0.40	651.08	2.50	21.98
Q	0.00	-0.35	514.65	-0.64	21.25
Q	0.00	-0.30	505.94	2.95	19.71
Q	0.00	-0.25	498.18	-0.76	19.97
Q	0.00	-0.20	529.34	7.42	11.43
Q	0.00	-0.15	489.12	2.27	19.90
Q	0.00	-0.10	516.99	-0.28	11.71
QH	0.00	-0.40	704.47	-3.70	12.92
QH	0.00	-0.35	738.17	16.34	14.88
QH	0.00	-0.30	737.60	39.07	14.20
QH	0.00	-0.25	717.53	19.08	11.41
QH	0.00	-0.20	697.37	-27.62	17.32
QH	0.00	-0.15	684.17	-38.47	20.26
QH	0.00	-0.10	689.40	-2.41	19.20
QHG	0.00	-0.40	803.76	-2.49	18.37
QHG	0.00	-0.35	794.63	23.32	15.25
QHG	0.00	-0.30	765.27	-43.15	20.81
QHG	0.00	-0.25	776.01	9.03	19.86
QHG	0.00	-0.20	770.63	30.47	18.35
QHG	0.00	-0.15	761.84	45.60	18.65
QHG	0.00	-0.10	750.65	31.44	16.69
Q	0.01	-0.40	547.10	1.36	22.76
Q	0.01	-0.35	549.23	1.52	18.47
Q	0.01	-0.30	467.96	-1.47	20.80
Q	0.01	-0.25	457.12	-1.20	19.37
Q	0.01	-0.20	448.82	0.40	18.61
Q	0.01	-0.15	445.20	4.23	18.37
Q	0.01	-0.10	436.90	-2.57	18.01
QH	0.01	-0.40	666.62	8.01	12.63
QH	0.01	-0.35	657.62	3.44	13.84
QH	0.01	-0.30	691.57	3.84	11.44
QH	0.01	-0.25	688.33	19.94	12.27
QH	0.01	-0.20	671.38	5.38	14.06
QH	0.01	-0.15	663.03	6.26	9.77
QH	0.01	-0.10	647.94	-8.80	15.06
QHG	0.01	-0.40	752.19	-27.30	21.58
QHG	0.01	-0.35	743.46	-38.49	17.89
QHG	0.01	-0.30	739.75	-34.44	21.62
QHG	0.01	-0.25	738.48	25.53	14.98
QHG	0.01	-0.20	741.02	7.47	19.89
QHG	0.01	-0.15	716.84	-25.21	20.89
QHG	0.01	-0.10	719.95	9.39	20.44

Table C.10: Spring performance parameters for negative k_{max}. In these simulations, we kept $F = 0$ and $h = 0.9$.

Muscles	L	k_{max}	$\dot{\theta}_c$	$\ddot{\theta}_c$	$\sigma_{\dot{\theta}}$
Q	0.00	-0.40	587.65	-1.37	21.27
Q	0.00	-0.35	490.33	-0.79	19.53
Q	0.00	-0.30	481.38	1.52	19.37
Q	0.00	-0.25	475.06	0.57	18.47
Q	0.00	-0.20	463.94	-0.92	18.62
Q	0.00	-0.15	459.31	2.03	17.92
Q	0.00	-0.10	456.18	0.58	17.74
QH	0.00	-0.40	683.38	26.64	9.59
QH	0.00	-0.35	645.37	2.33	14.86
QH	0.00	-0.30	681.26	18.74	11.77
QH	0.00	-0.25	673.81	27.88	11.50
QH	0.00	-0.20	662.43	9.67	12.24
QH	0.00	-0.15	653.11	12.82	11.82
QH	0.00	-0.10	637.95	-17.82	17.43
QHG	0.00	-0.40	741.60	-23.25	18.63
QHG	0.00	-0.35	744.99	4.45	16.58
QHG	0.00	-0.30	740.13	14.28	18.19
QHG	0.00	-0.25	729.85	2.12	17.87
QHG	0.00	-0.20	711.37	15.16	14.38
QHG	0.00	-0.15	690.56	-29.74	16.47
QHG	0.00	-0.10	696.81	23.53	17.88
Q	0.01	-0.40	406.12	-2.29	22.53
Q	0.01	-0.35	522.76	0.26	17.44
Q	0.01	-0.30	456.84	5.33	16.94
Q	0.01	-0.25	439.71	-3.43	19.23
Q	0.01	-0.20	428.08	0.09	16.75
Q	0.01	-0.15	421.63	1.84	16.93
Q	0.01	-0.10	414.70	-1.19	16.62
QH	0.01	-0.40	625.87	-10.11	13.42
QH	0.01	-0.35	600.13	1.81	16.20
QH	0.01	-0.30	615.88	17.27	8.28
QH	0.01	-0.25	597.07	-38.43	17.07
QH	0.01	-0.20	610.39	18.94	10.35
QH	0.01	-0.15	607.77	21.11	10.45
QH	0.01	-0.10	619.47	8.25	13.11
QHG	0.01	-0.40	676.19	-4.20	14.70
QHG	0.01	-0.35	684.39	-39.00	19.92
QHG	0.01	-0.30	679.09	-39.35	20.51
QHG	0.01	-0.25	687.32	4.88	14.92
QHG	0.01	-0.20	674.29	1.41	16.32
QHG	0.01	-0.15	661.57	7.78	15.13
QHG	0.01	-0.10	649.72	3.21	16.59

Table C.11: Spring performance parameters for negative k_{max}. In these simulations, we kept $F = 0$ and $h = 0.8$.

Muscles	L	k_{max}	$\dot{\theta}_c$	$\ddot{\theta}_c$	$\sigma_{\dot{\theta}}$
Q	0.00	-0.40	545.61	0.81	16.88
Q	0.00	-0.35	463.47	0.33	18.29
Q	0.00	-0.30	451.54	-1.42	17.47
Q	0.00	-0.25	445.97	0.46	16.94
Q	0.00	-0.20	438.54	-2.11	16.47
Q	0.00	-0.15	433.92	-3.25	16.75
Q	0.00	-0.10	433.01	-4.18	16.58
QH	0.00	-0.40	600.71	-1.59	15.70
QH	0.00	-0.35	588.02	0.65	16.05
QH	0.00	-0.30	585.18	-1.12	16.72
QH	0.00	-0.25	606.51	16.96	10.80
QH	0.00	-0.20	597.70	10.99	9.91
QH	0.00	-0.15	597.46	-3.40	11.82
QH	0.00	-0.10	606.03	-12.87	12.60
QHG	0.00	-0.40	657.89	-0.00	14.04
QHG	0.00	-0.35	644.99	-0.08	16.10
QHG	0.00	-0.30	669.97	2.05	15.93
QHG	0.00	-0.25	669.12	30.27	11.56
QHG	0.00	-0.20	655.70	8.23	13.78
QHG	0.00	-0.15	635.55	-29.51	12.92
QHG	0.00	-0.10	633.46	-13.78	18.56
Q	0.01	-0.40	493.66	-0.91	17.57
Q	0.01	-0.35	494.96	-0.22	17.15
Q	0.01	-0.30	485.08	-1.75	16.21
Q	0.01	-0.25	476.60	0.7	15.94
Q	0.01	-0.20	469.38	0.40	15.72
Q	0.01	-0.15	393.58	-5.44	15.48
Q	0.01	-0.10	369.76	-1.16	14.08
QH	0.01	-0.40	520.25	0.85	18.09
QH	0.01	-0.35	511.05	1.36	17.45
QH	0.01	-0.30	506.10	-0.97	16.10
QH	0.01	-0.25	502.45	1.13	15.64
QH	0.01	-0.20	495.95	-2.93	15.26
QH	0.01	-0.15	491.39	-0.37	15.19
QH	0.01	-0.10	527.24	-19.69	9.53
QHG	0.01	-0.40	612.01	-23.65	15.06
QHG	0.01	-0.35	601.52	-2.27	16.71
QHG	0.01	-0.30	588.61	8.08	17.10
QHG	0.01	-0.25	601.77	-36.07	18.92
QHG	0.01	-0.20	611.72	18.66	12.32
QHG	0.01	-0.15	600.62	13.48	12.77
QHG	0.01	-0.10	615.84	-6.29	13.71

Table C.12: Spring performance parameters for negative k_{max}. In these simulations, we kept $F = 0$ and $h = 0.7$.

Muscles	L	k_{max}	$\dot{\bar{\theta}}_c$	$\ddot{\theta}_c$	$\sigma_{\dot{\theta}}$
Q	0.00	-0.40	520.71	1.94	16.35
Q	0.00	-0.35	453.69	11.56	17.72
Q	0.00	-0.30	432.02	0.28	15.81
Q	0.00	-0.25	424.16	-0.93	15.44
Q	0.00	-0.20	416.74	0.67	14.96
Q	0.00	-0.15	409.92	-1.03	14.64
Q	0.00	-0.10	403.46	0.04	14.49
QH	0.00	-0.40	513.54	1.96	17.26
QH	0.00	-0.35	503.03	-0.50	16.83
QH	0.00	-0.30	501.94	1.28	15.65
QH	0.00	-0.25	496.52	1.37	15.71
QH	0.00	-0.20	489.60	0.7	14.98
QH	0.00	-0.15	485.17	-1.28	14.68
QH	0.00	-0.10	562.15	31.02	9.33
QHG	0.00	-0.40	585.25	-0.7	16.56
QHG	0.00	-0.35	583.46	3.88	17.13
QHG	0.00	-0.30	573.62	0.62	18.13
QHG	0.00	-0.25	576.25	-31.88	18.81
QHG	0.00	-0.20	591.47	5.74	11.68
QHG	0.00	-0.15	586.40	6.42	9.96
QHG	0.00	-0.10	584.40	9.11	15.41
Q	0.01	-0.40	459.27	2.73	17.53
Q	0.01	-0.35	449.95	1.92	16.56
Q	0.01	-0.30	439.38	-0.56	15.46
Q	0.01	-0.25	427.96	-0.56	14.18
Q	0.01	-0.20	414.83	0.01	13.91
Q	0.01	-0.15	403.48	1.98	12.96
Q	0.01	-0.10	388.46	-0.80	13.27
QH	0.01	-0.40	471.69	0.26	18.41
QH	0.01	-0.35	464.78	-0.80	16.91
QH	0.01	-0.30	460.47	0.79	15.81
QH	0.01	-0.25	458.03	0.36	15.06
QH	0.01	-0.20	458.44	3.86	14.27
QH	0.01	-0.15	458.83	0.04	13.58
QH	0.01	-0.10	450.82	1.23	12.63
QHG	0.01	-0.40	512.00	-1.33	16.58
QHG	0.01	-0.35	506.23	1.26	15.60
QHG	0.01	-0.30	499.59	-0.71	15.45
QHG	0.01	-0.25	494.11	0.10	14.64
QHG	0.01	-0.20	489.16	-1.71	15.01
QHG	0.01	-0.15	485.89	-1.80	15.00
QHG	0.01	-0.10	538.57	8.52	11.98

Table C.13: Spring performance parameters for negative k_{max}. In these simulations, we kept $F = 0$ and $h = 0.6$.

Muscles	L	k_{max}	$\dot{\theta}_c$	$\ddot{\theta}_c$	$\sigma_{\dot{\theta}}$
Q	0.00	-0.40	486.84	-0.46	15.51
Q	0.00	-0.35	487.67	0.76	15.10
Q	0.00	-0.30	476.33	-0.40	14.71
Q	0.00	-0.25	468.19	-1.10	14.24
Q	0.00	-0.20	384.00	-4.71	12.89
Q	0.00	-0.15	371.78	-4.11	12.22
Q	0.00	-0.10	359.69	-1.31	12.15
QH	0.00	-0.40	469.73	0.15	17.41
QH	0.00	-0.35	464.68	-0.28	16.02
QH	0.00	-0.30	459.29	0.18	15.22
QH	0.00	-0.25	458.15	-1.41	13.86
QH	0.00	-0.20	460.43	1.15	12.69
QH	0.00	-0.15	455.68	-0.61	13.15
QH	0.00	-0.10	554.48	-0.07	10.46
QHG	0.00	-0.40	500.12	0.32	15.81
QHG	0.00	-0.35	494.79	1.35	15.36
QHG	0.00	-0.30	489.05	-0.18	14.64
QHG	0.00	-0.25	483.50	-0.25	14.68
QHG	0.00	-0.20	479.83	1.54	14.14
QHG	0.00	-0.15	476.19	1.37	14.12
QHG	0.00	-0.10	493.56	28.93	15.08
Q	0.01	-0.40	402.01	-0.18	18.13
Q	0.01	-0.35	388.14	1.09	16.76
Q	0.01	-0.30	373.43	0.39	15.16
Q	0.01	-0.25	357.06	2.04	13.58
Q	0.01	-0.20	339.84	0.35	11.98
Q	0.01	-0.15	322.43	1.55	10.30
Q	0.01	-0.10	306.79	1.51	8.96
QH	0.01	-0.40	439.91	-11.22	17.20
QH	0.01	-0.35	433.23	4.85	14.48
QH	0.01	-0.30	413.96	0.07	14.53
QH	0.01	-0.25	405.25	-0.21	13.37
QH	0.01	-0.20	400.56	-0.50	12.47
QH	0.01	-0.15	391.98	-0.51	11.07
QH	0.01	-0.10	425.99	1.30	6.00
QHG	0.01	-0.40	460.95	0.87	15.68
QHG	0.01	-0.35	453.55	1.32	14.52
QHG	0.01	-0.30	448.32	-0.92	13.52
QHG	0.01	-0.25	448.02	-3.79	13.14
QHG	0.01	-0.20	448.24	0.58	12.12
QHG	0.01	-0.15	439.76	-0.40	12.45
QHG	0.01	-0.10	434.27	-1.14	12.38

Table C.14: Spring performance parameters for all θ_s. In these simulations, we kept $F = 0$ and $h = 1$.

Muscles	L	θ_s	$\bar{\ddot{\theta}}_c$	$\ddot{\theta}_c$	$\sigma_{\dot{\theta}}$
Q	0.00	52.00	505.94	11.77	19.71
Q	0.00	62.00	503.39	11.77	20.47
Q	0.00	72.00	500.65	11.77	20.66
Q	0.00	82.00	496.83	11.77	19.79
Q	0.00	92.00	670.80	11.77	15.93
Q	0.00	102.00	668.30	11.77	14.17
QH	0.00	52.00	737.60	11.77	14.20
QH	0.00	62.00	735.10	11.77	13.39
QH	0.00	72.00	731.81	11.77	13.82
QH	0.00	82.00	731.73	11.77	14.30
QH	0.00	92.00	728.16	11.77	14.43
QH	0.00	102.00	722.87	11.77	16.12
QHG	0.00	52.00	765.27	11.77	20.81
QHG	0.00	62.00	782.38	11.77	13.66
QHG	0.00	72.00	779.52	11.77	15.71
QHG	0.00	82.00	776.33	11.77	12.22
QHG	0.00	92.00	770.87	11.77	18.86
QHG	0.00	102.00	756.34	11.77	22.43
Q	0.01	52.00	467.96	11.77	20.80
Q	0.01	62.00	466.51	11.77	20.50
Q	0.01	72.00	464.80	11.77	20.86
Q	0.01	82.00	455.66	11.77	20.01
Q	0.01	92.00	450.17	11.77	18.17
Q	0.01	102.00	444.05	11.77	18.04
QH	0.01	52.00	691.57	11.77	11.44
QH	0.01	62.00	676.18	11.77	11.93
QH	0.01	72.00	658.37	11.77	17.69
QH	0.01	82.00	689.71	11.77	9.72
QH	0.01	92.00	688.07	11.77	10.51
QH	0.01	102.00	671.80	11.77	19.44
QHG	0.01	52.00	739.75	11.77	21.62
QHG	0.01	62.00	739.36	11.77	21.45
QHG	0.01	72.00	749.73	11.77	14.06
QHG	0.01	82.00	745.52	11.77	16.87
QHG	0.01	92.00	736.95	11.77	19.26
QHG	0.01	102.00	722.73	11.77	21.14

Table C.15: Spring performance parameters for all θ_s. In these simulations, we kept $F = 0$ and $h = 0.9$.

Muscles	L	θ_s	$\bar{\dot{\theta}}_c$	$\ddot{\theta}_c$	$\sigma_{\dot{\theta}}$
Q	0.00	52.00	481.38	11.77	19.37
Q	0.00	62.00	476.75	11.77	19.80
Q	0.00	72.00	476.96	11.77	19.21
Q	0.00	82.00	471.69	11.77	18.81
Q	0.00	92.00	465.46	11.77	17.73
Q	0.00	102.00	462.32	11.77	17.84
QH	0.00	52.00	681.26	11.77	11.77
QH	0.00	62.00	675.97	11.77	11.54
QH	0.00	72.00	662.23	11.77	16.80
QH	0.00	82.00	683.62	11.77	9.73
QH	0.00	92.00	655.18	11.77	15.14
QH	0.00	102.00	666.11	11.77	12.14
QHG	0.00	52.00	740.13	11.77	18.19
QHG	0.00	62.00	742.94	11.77	18.12
QHG	0.00	72.00	723.73	11.77	20.40
QHG	0.00	82.00	730.53	11.77	14.90
QHG	0.00	92.00	726.14	11.77	20.62
QHG	0.00	102.00	718.84	11.77	20.90
Q	0.01	52.00	456.84	11.77	16.94
Q	0.01	62.00	452.40	11.77	19.94
Q	0.01	72.00	445.30	11.77	18.89
Q	0.01	82.00	432.64	11.77	18.09
Q	0.01	92.00	431.47	11.77	16.76
Q	0.01	102.00	429.23	11.77	15.96
QH	0.01	52.00	615.88	11.77	8.28
QH	0.01	62.00	595.59	11.77	16.99
QH	0.01	72.00	607.99	11.77	11.18
QH	0.01	82.00	590.07	11.77	13.94
QH	0.01	92.00	615.13	11.77	10.14
QH	0.01	102.00	612.37	11.77	10.93
QHG	0.01	52.00	679.09	11.77	20.51
QHG	0.01	62.00	680.29	11.77	21.15
QHG	0.01	72.00	682.56	11.77	18.35
QHG	0.01	82.00	693.38	11.77	16.81
QHG	0.01	92.00	684.84	11.77	15.92
QHG	0.01	102.00	679.40	11.77	14.62

Table C.16: Spring performance parameters for all θ_s. In these simulations, we kept $F = 0$ and $h = 0.8$.

Muscles	L	θ_s	$\bar{\theta}_c$	$\ddot{\theta}_c$	$\sigma_{\dot{\theta}}$
Q	0.00	52.00	451.54	11.77	17.47
Q	0.00	62.00	452.22	11.77	18.32
Q	0.00	72.00	448.99	11.77	18.36
Q	0.00	82.00	446.67	11.77	17.23
Q	0.00	92.00	444.18	11.77	15.63
Q	0.00	102.00	443.53	11.77	15.77
QH	0.00	52.00	585.18	11.77	16.72
QH	0.00	62.00	603.66	11.77	7.34
QH	0.00	72.00	612.60	11.77	9.43
QH	0.00	82.00	601.28	11.77	9.49
QH	0.00	92.00	594.45	11.77	22.47
QH	0.00	102.00	596.92	11.77	20.97
QHG	0.00	52.00	669.97	11.77	15.93
QHG	0.00	62.00	681.86	11.77	15.10
QHG	0.00	72.00	677.23	11.77	12.19
QHG	0.00	82.00	677.17	11.77	12.81
QHG	0.00	92.00	671.02	11.77	13.63
QHG	0.00	102.00	659.44	11.77	15.98
Q	0.01	52.00	485.08	11.77	16.21
Q	0.01	62.00	425.61	11.77	21.75
Q	0.01	72.00	416.23	11.77	19.30
Q	0.01	82.00	398.82	11.77	16.48
Q	0.01	92.00	388.92	11.77	14.60
Q	0.01	102.00	384.10	11.77	13.68
QH	0.01	52.00	506.10	11.77	16.10
QH	0.01	62.00	506.31	11.77	17.07
QH	0.01	72.00	503.65	11.77	16.73
QH	0.01	82.00	500.91	11.77	16.44
QH	0.01	92.00	660.45	11.77	10.51
QH	0.01	102.00	569.41	11.77	9.32
QHG	0.01	52.00	588.61	11.77	17.10
QHG	0.01	62.00	605.81	11.77	15.91
QHG	0.01	72.00	626.50	11.77	11.03
QHG	0.01	82.00	604.08	11.77	20.97
QHG	0.01	92.00	611.91	11.77	12.09
QHG	0.01	102.00	613.78	11.77	14.53

Table C.17: Spring performance parameters for all θ_s. In these simulations, we kept $F = 0$ and $h = 0.7$.

Muscles	L	θ_s	$\bar{\theta}_c$	$\ddot{\theta}_c$	$\sigma_{\dot{\theta}}$
Q	0.00	52.00	432.02	11.77	15.81
Q	0.00	62.00	431.66	11.77	16.95
Q	0.00	72.00	428.56	11.77	16.98
Q	0.00	82.00	426.63	11.77	16.25
Q	0.00	92.00	421.39	11.77	14.52
Q	0.00	102.00	415.76	11.77	13.72
QH	0.00	52.00	501.94	11.77	15.65
QH	0.00	62.00	501.39	11.77	16.09
QH	0.00	72.00	500.63	11.77	16.66
QH	0.00	82.00	498.33	11.77	16.01
QH	0.00	92.00	658.72	11.77	10.87
QH	0.00	102.00	595.15	11.77	14.99
QHG	0.00	52.00	573.62	11.77	18.13
QHG	0.00	62.00	606.22	11.77	10.77
QHG	0.00	72.00	580.11	11.77	17.34
QHG	0.00	82.00	588.09	11.77	11.27
QHG	0.00	92.00	582.70	11.77	10.43
QHG	0.00	102.00	593.53	11.77	14.05
Q	0.01	52.00	439.38	11.77	15.46
Q	0.01	62.00	439.95	11.77	16.14
Q	0.01	72.00	435.11	11.77	16.17
Q	0.01	82.00	430.88	11.77	14.80
Q	0.01	92.00	420.67	11.77	13.12
Q	0.01	102.00	407.89	11.77	13.09
QH	0.01	52.00	460.47	11.77	15.81
QH	0.01	62.00	462.10	11.77	16.89
QH	0.01	72.00	498.97	11.77	11.97
QH	0.01	82.00	470.26	11.77	15.49
QH	0.01	92.00	505.35	11.77	5.93
QH	0.01	102.00	571.04	11.77	10.06
QHG	0.01	52.00	499.59	11.77	15.45
QHG	0.01	62.00	502.53	11.77	15.75
QHG	0.01	72.00	498.74	11.77	15.38
QHG	0.01	82.00	497.33	11.77	14.71
QHG	0.01	92.00	656.02	11.77	10.86
QHG	0.01	102.00	627.67	11.77	13.23

Table C.18: Spring performance parameters for all θ_s. In these simulations, we kept $F = 0$ and $h = 0.6$.

Muscles	L	θ_s	$\bar{\dot{\theta}}_c$	$\ddot{\theta}_c$	$\sigma_{\dot{\theta}}$
Q	0.00	52.00	476.33	11.77	14.71
Q	0.00	62.00	406.83	11.77	16.44
Q	0.00	72.00	402.34	11.77	17.05
Q	0.00	82.00	383.71	11.77	14.07
Q	0.00	92.00	379.44	11.77	12.32
Q	0.00	102.00	375.46	11.77	11.16
QH	0.00	52.00	459.29	11.77	15.22
QH	0.00	62.00	459.77	11.77	16.17
QH	0.00	72.00	462.13	11.77	15.97
QH	0.00	82.00	465.54	11.77	14.34
QH	0.00	92.00	555.61	11.77	5.97
QH	0.00	102.00	492.45	11.77	8.15
QHG	0.00	52.00	489.05	11.77	14.64
QHG	0.00	62.00	489.61	11.77	15.16
QHG	0.00	72.00	488.50	11.77	15.07
QHG	0.00	82.00	487.27	11.77	14.20
QHG	0.00	92.00	548.23	11.77	10.18
QHG	0.00	102.00	611.95	11.77	14.38
Q	0.01	52.00	373.43	11.77	15.16
Q	0.01	62.00	371.15	11.77	16.56
Q	0.01	72.00	365.55	11.77	16.46
Q	0.01	82.00	356.23	11.77	14.56
Q	0.01	92.00	343.78	11.77	11.56
Q	0.01	102.00	327.73	11.77	8.82
QH	0.01	52.00	413.96	11.77	14.53
QH	0.01	62.00	412.13	11.77	15.97
QH	0.01	72.00	410.15	11.77	16.08
QH	0.01	82.00	407.10	11.77	14.32
QH	0.01	92.00	404.82	11.77	11.88
QH	0.01	102.00	402.11	11.77	9.83
QHG	0.01	52.00	448.32	11.77	13.52
QHG	0.01	62.00	457.48	11.77	13.44
QHG	0.01	72.00	461.54	11.77	13.62
QHG	0.01	82.00	458.85	11.77	13.08
QHG	0.01	92.00	453.58	11.77	11.43
QHG	0.01	102.00	447.63	11.77	11.77

D COMPLEMENTARY RESULTS OF GAIT SIMULATI-ONS

Figure D.1: Knee trajectory through 10-steps of simulation of the four controllers for $g_s = 0.1$. In this simulation, $F = 312$.

Source: prepared by the author.

Figure D.2: Knee trajectory through 10-steps of simulation of the four controllers for $g_s = 0.3$. In this simulation, $F = 312$.

Source: prepared by the author.
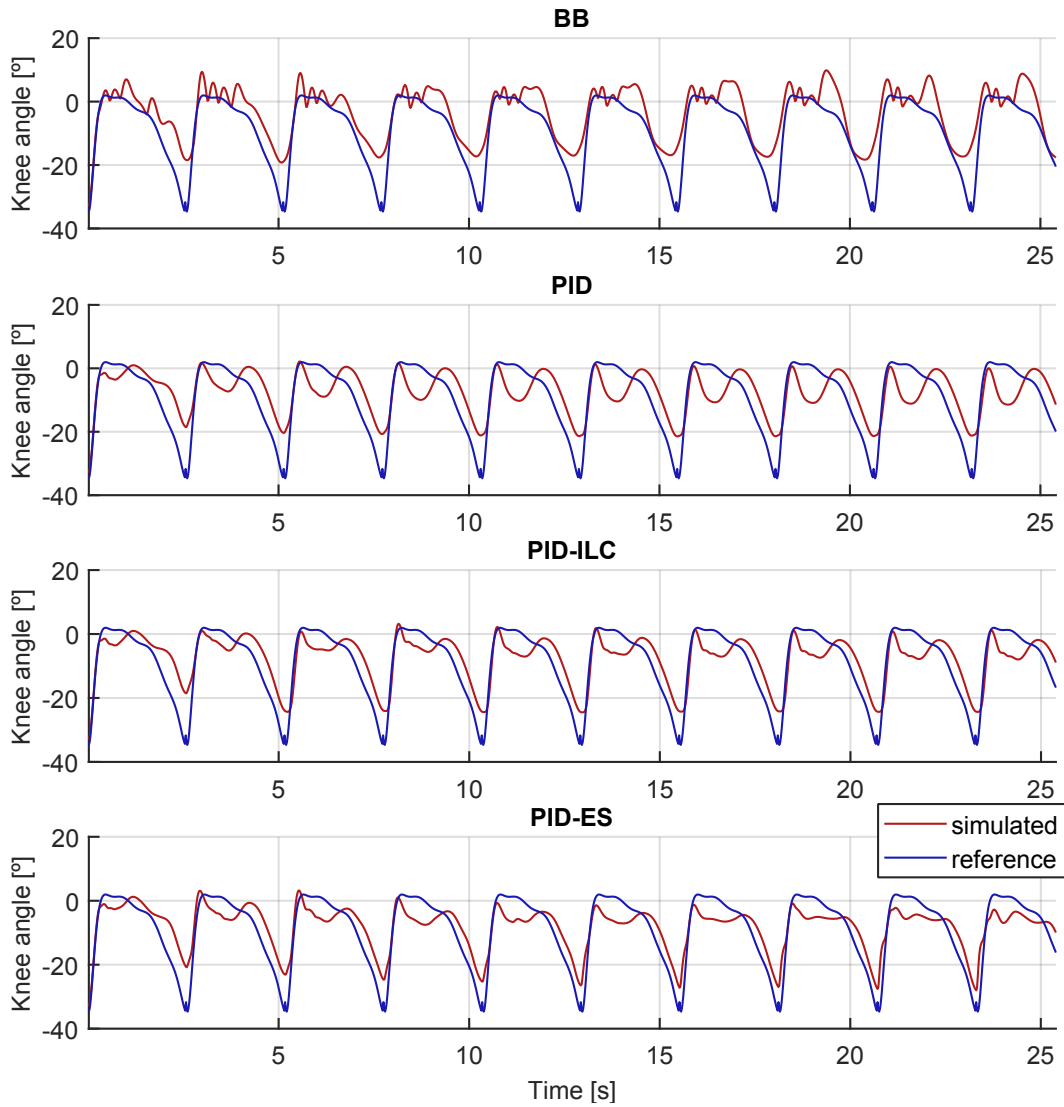
Figure D.3: Knee trajectory through 10-steps of simulation of the four controllers for $g_s = 0.1$. In this simulation, $F = 1250$.

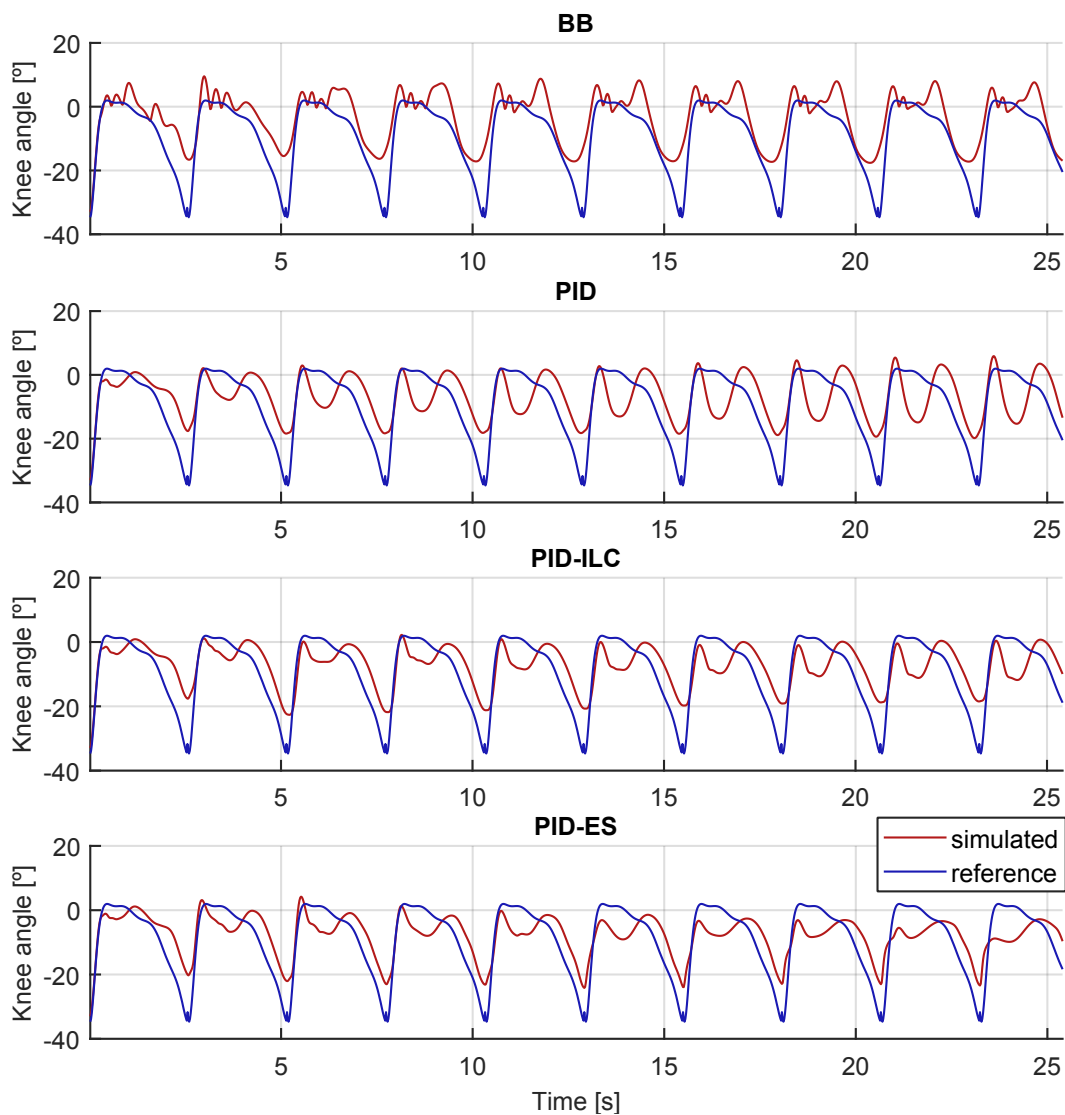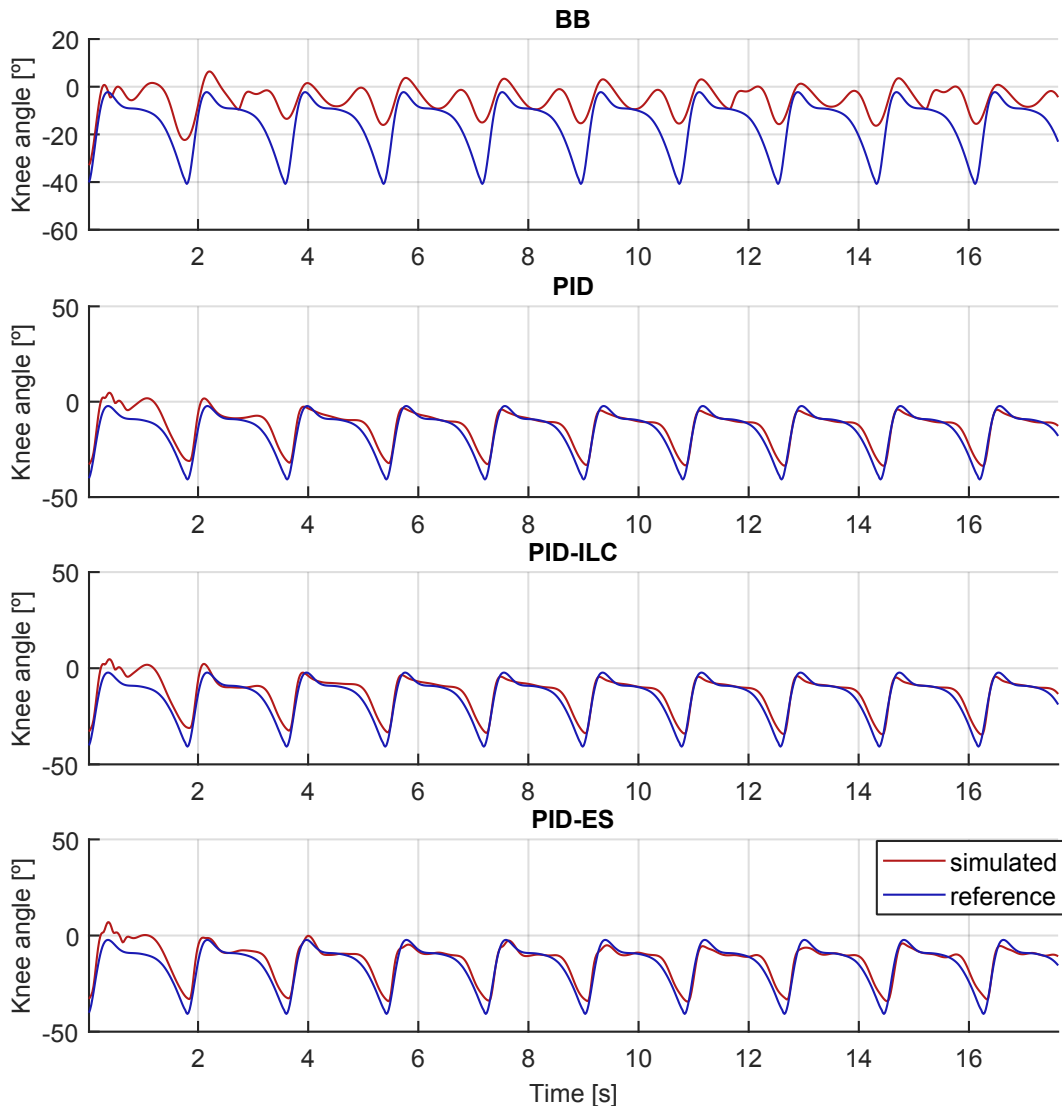Source: prepared by the author.
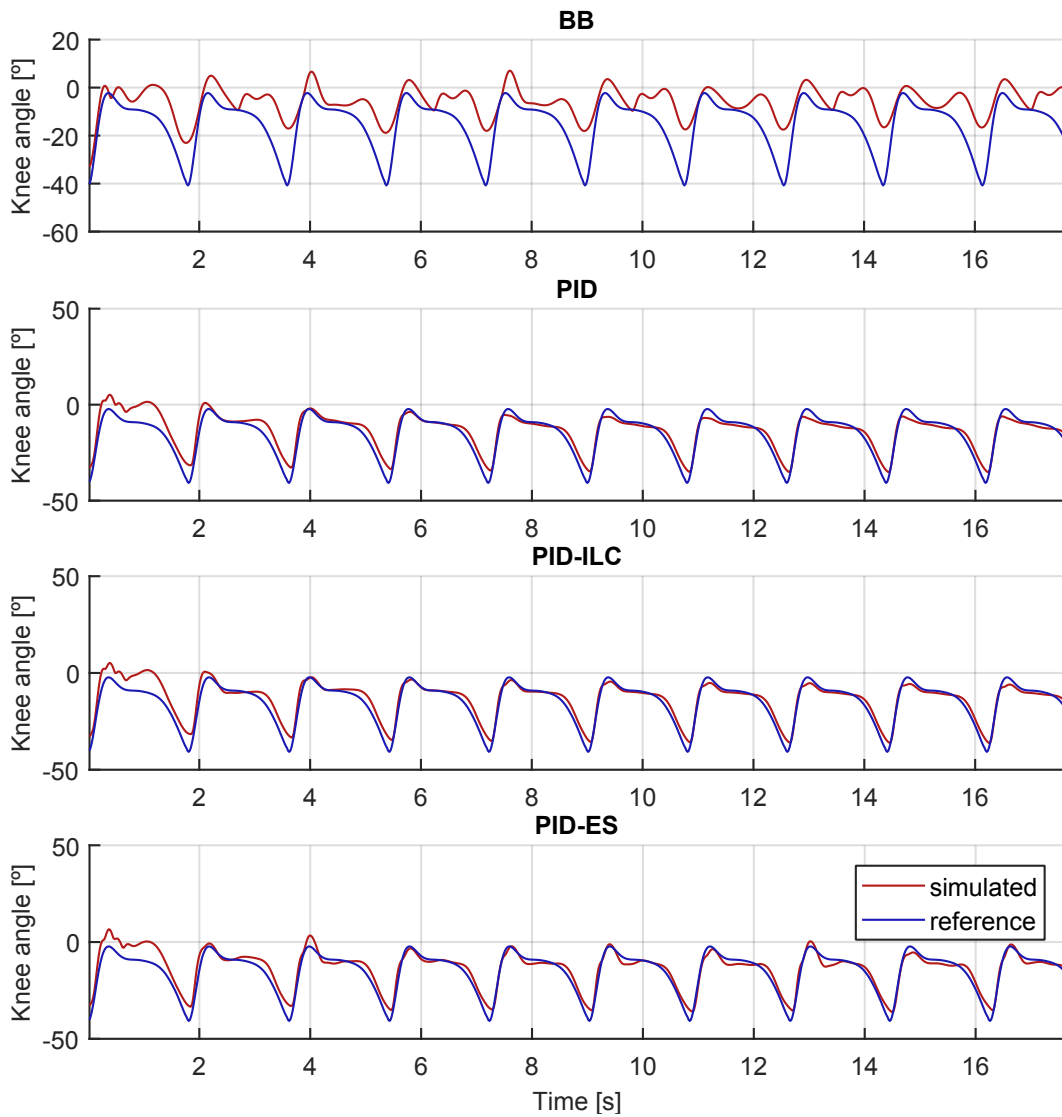
Figure D.4: Knee trajectory through 10-steps of simulation of the four controllers for $g_s = 0.3$. In this simulation, $F = 1250$.

Source: prepared by the author.

Table D.1: Performance results at the last step for $g_s = 0.1m/s$.

Controller	F	$corr_\beta$	e_{max_β}	σ_β
BB	0	0.68	16.63	8.29
PID	0	0.82	11.97	7.02
PID-ILC	0	0.93	8.79	4.95
PID-ES	0	0.96	14.69	4.84
BB	1250	0.85	21.70	5.96
PID	1250	0.71	13.59	8.07
PID-ILC	1250	0.87	10.41	6.16
PID-ES	1250	0.94	15.50	5.59
BB	312	0.86	21.93	5.96
PID	312	0.54	16.54	9.64
PID-ILC	312	0.64	16.32	8.68
PID-ES	312	0.72	16.54	8.34
BB	78	0.53	17.23	10.03
PID	78	0.53	17.24	9.99
PID-ILC	78	0.53	17.10	9.99
PID-ES	78	0.54	17.30	9.50

Table D.2: Performance results at the last step for $g_s = 0.3m/s$.

Controller	F	$corr_\beta$	e_{max_β}	σ_β
BB	0	0.68	16.63	8.29
PID	0	0.91	11.04	5.09
PID-ILC	0	0.92	9.66	4.47
PID-ES	0	0.97	7.57	3.46
BB	1250	0.82	24.18	6.97
PID	1250	0.99	6.68	3.00
PID-ILC	1250	0.99	4.36	2.58
PID-ES	1250	0.99	6.78	2.43
BB	312	0.72	25.30	8.25
PID	312	0.97	8.17	3.21
PID-ILC	312	0.98	7.50	2.99
PID-ES	312	0.97	9.40	3.50
BB	78	0.73	25.09	8.10
PID	78	0.87	14.62	5.54
PID-ILC	78	0.87	13.42	5.50
PID-ES	78	0.88	16.34	5.46

A RESUMO EXPANDIDO EM PORTUGUÊS

A.1 INTRODUÇÃO

A lesão medular (LM) é uma das lesões mais graves com severas repercussões física, psíquica e social. No entanto, os dados atuais sobre deficiência no Brasil remontam ao censo do IBGE de 2010 e não permitem a diferenciação entre deficiências motoras ou suas causas (Instituto Brasileiro de Geografia e Estatística - IBGE, 2010). Portanto, o coeficiente de incidência de LM no Brasil é desconhecido, e não existem dados precisos sobre sua incidência e prevalência, pois essa condição não está subordinada a uma notificação ao governo (Ministério da Saúde, 2013). Hoje, temos apenas algumas estimativas, como 10 mil novos casos por ano, nos quais 80% das vítimas são homens e 60% têm entre 10 e 30 anos (Ministério da Saúde, 2013). Neste trabalho, focamos em uma população com movimentos remanescentes acima do tronco, mas nenhum movimento dos membros inferiores (i.e., lesão abaixo da T8). Há um conjunto de exercícios de reabilitação para fortalecimento muscular, melhora da circulação, liberação de pressão e melhora da densidade óssea. Os fisioterapeutas se concentram em músculos e articulações específicas, adaptando o programa às restrições, limitações e avanços do paciente (Thomas Jefferson University Hospital and Magee Rehabilitation, 2009).

Para membros inferiores, os pesquisadores já apresentaram dispositivos auxiliares vestíveis com sensores para aumentar a eficiência da reabilitação (RIEK, 2017). Amplamente utilizada na reabilitação e assistência nas AVDs, a estimulação elétrica funcional (ou eletroestimulação ou estimulação) produz uma estimulação nervosa através de sinais elétricos, permitindo contração dos músculos paralisados, podendo produzir torque (LYNCH; POPOVIC, 2012; MARTIN et al., 2012). Hoje, os fisioterapeutas já utilizam a estimulação na reabilitação de LM devido suas vantagens, como aumento da força muscular, diminuição da perda óssea, melhora cardiovascular e respiratória (THOMAZ et al., 2019).

A completa ausência de função motora e sensorial abaixo da área da lesão não significa necessariamente ausência de nervos intactos, apenas que eles não estão funcionando adequadamente. Portanto, a eletroestimulação ainda é possível de ser usada em lesões completas e incompletas. Essa técnica é simples, barata e não invasiva, já indicada para diversos fins terapêuticos (RAINE; MEADOWS; LYNCH-ELLERINGTON, 2009).

Contexto

Indivíduos com LM completa não obtêm muitas vantagens da reabilitação sem movimento funcional (NAKI et al., 2011). Geralmente, esse movimento funcional é realizado por um sistema de controle, ou seja, um conjunto de equipamentos e dispositivos que gerenciam o comportamento dos sistemas físicos. Para isso, é necessário realizar a modelagem matemática da planta, seguida pelo projeto do controlador com base nos sensores disponíveis. Poderíamos aumentar o número de estudos de reabilitação com pacientes com LM completa se facilitarmos o desenvolvimento desse tipo de sistema. O controle por eletroestimulação contém não linearidades (POPOVIĆ; SINKJÆR, 2000), o que requer técnicas sofisticadas de controle de feedback.

O controle de feedback (ou malha fechada) é uma operação que, na presença de algum distúrbio, tende a reduzir a diferença entre a saída de um sistema e alguma entrada de referência (OGATA, 2010). A Figura A.1 ilustra um controle por eletroestimulação de malha fechada com um controlador que altera os parâmetros da estimulação com base na resposta dos sensores para obter a resposta desejada da planta. Uma planta é qualquer objeto físico a ser controlado; no nosso caso, os músculos dos membros inferiores através da estimulação da superfície.
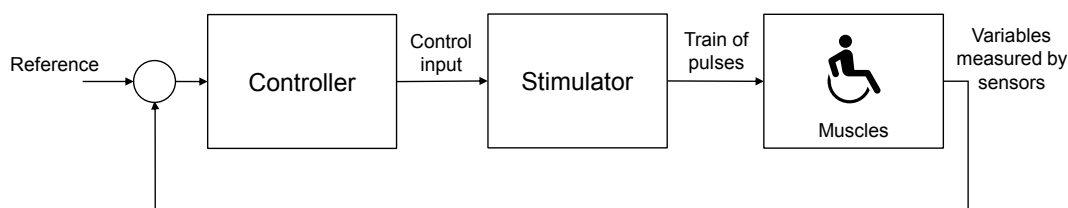
Figure A.1: Exemplo de um diagrama de blocos de um controle por eletroestimulação de malha fechada. Com base na referência e nas variáveis medidas pelos sensores, o controlador calcula uma entrada de controle e a envia ao estimulador, que por sua vez usa essa mensagem para criar um trem de pulsos que será aplicado aos músculos de um voluntário com LM completa através de eletrodos superficiais.

Fonte: preparado pela autora.

A fadiga muscular rápida continua sendo a principal limitação do uso da estimulação por longos períodos (THRASHER; POPOVIC, 2008). Os resultados dos controladores que tentam compensar a fadiga aplicando modelos dinâmicos ainda são insuficientes (KIRSCH et al., 2016). Outras complexidades da estimulação também incluem: coordenação de múltiplos músculos, não-linearidade, atrasos eletromecânicos e dependência do tempo. Esta tese visa contribuir para o desempenho geral e a interação natural entre o usuário e o sistema.

Neste documento, pretendemos então avaliar três técnicas avançadas de reabilitação de membros inferiores para melhorar o controle em pacientes com LM completa.

Cada um desses avanços existe em uma perspectiva diferente do sistema de controle: (1) **estimativa de sensores**, (2) **controle de algoritmos** e (3) **planta**.

Definição do problema

Um tipo de estimativa da atividade muscular que alguns trabalhos já utilizaram é a **eletromiografia** (EMG) (e.g., (SCHAUER, 2017)), uma técnica eletrodiagnóstica para avaliar e registrar a atividade elétrica produzida pelos músculos (KAMEN; GABRIEL, 2010). O EMG é a detecção do potencial elétrico gerado pelas fibras musculares quando ativadas eletricamente ou neurologicamente. Para extrair as informações dos sinais EMG durante a eletroestimulação, precisamos primeiro encontrar os intervalos entre os pulsos de estimulação. E, em seguida, precisamos extrair a informação do sinal EMG evocado pela estimulação. Projetos anteriores sincronizaram o amplificador EMG e o estimulador durante a estimulação para reduzir ou até mesmo remover completamente os artefatos, diretamente por hardware. No entanto, esse tipo de equipamento não está comercialmente disponível. Então, etapas adicionais de processamento de sinal (software) são necessárias para detectar com precisão os artefatos de estimulação. O sinal também se altera durante a execução dos experimentos, necessitando uma detecção automática. Nesse contexto, esta tese visa responder à primeira pergunta:

> **Como os métodos baseados em limiar detectam automaticamente artefatos de estimulação para dois canais de eletromiografia e com que seria a taxa de sucesso?**

Circunstâncias adversas exigem ambientes de simulação específicos para o controle por eletroestimulação. A maioria dos ambientes cria modelos musculoesquelético não-lineares com base em princípios como recrutamento de fibras e fadiga muscular. Ainda assim, os resultados de simulação não são totalmente comparáveis, pois a maioria dos pesquisadores não fornece o ambiente, o modelo completo ou os parâmetros utilizados. Na reabilitação, a eletroestimulação tem sido usada para produzir movimento de membros inferiores para indivíduos com LM em exercícios como marcha (e.g., (CHANG et al., 2016)) e ciclismo (e.g., (COSTE; WOLF, 2018)). Hoje, a literatura é incapaz de fornecer um cenário no qual possamos comparar adequadamente controladores em condições semelhantes. Os sistemas experimentais exigem um custo anormalmente alto, e até o momento não há modelo musculoesquelético detalhado para esse tipo de exercício. Nesse contexto, esta tese visa responder à segunda investigação:

> **Que ambiente de simulação podemos usar para comparar e avaliar erros de controladores de trajetória na marcha por eletroestimulação? Que ambiente de simulação podemos usar para comparar**

e avaliar a cadência dos controladores para o controle de ciclismo por estimulação?

Ainda existem desafios com o ciclismo por eletroestimulação relacionados à baixa eficiência e baixa potência (BERRY et al., 2012; HUNT et al., 2013). Trabalhos anteriores (GLASER, 1986; GLASER, 1991) sugerem que a biomecânica desfavorável pode ser um fator contribuinte para essa baixa eficiência. Essas biomecânicas incluem recrutamento imperfeito de grupos musculares, momento não ideal da ativação muscular e falta de controle articular sinérgico e antagônico. A maioria dos pesquisadores concentra-se em otimizar o recrutamento de grupos musculares (e.g., (DOLBOW; HOLCOMB; GORGEY, 2014)) e cronometrar a ativação muscular (e.g., (WATANABE; TADANO, 2018)). No entanto, quando consideramos o ambiente de concorrência, outros detalhes também devem ser considerados para um melhor desempenho. O uso de dispositivos de armazenamento de energia (e.g., molas) para o ciclismo por eletroestimulação em experimentos reais ainda não foi explorado. Órteses passivas podem armazenar energia cinética como energia potencial e liberá-la quando necessário sem nenhuma fonte de alimentação externa (MASSOUD, 2012). Nesse contexto, esta tese também visa responder à última pergunta:

É possível alterar a cadência no ciclismo por eletroestimulação quando um voluntário com LM completa utiliza órteses passivas no joelho?

Objetivos

Na perspectiva do sensor, propomos métodos automáticos para processamento de EMG durante a eletroestimulação, quando o hardware não está sincronizado. Esses métodos visam separar o EMG evocado por estimulação e o EMG gerado por contração voluntária (para várias frequências de amostragem EMG e taxas de estimulação). A substituição de sensores de força por EMG no controle para reabilitação deve impactar as técnicas de reabilitação, já que o EMG não requer uma estrutura externa, como plataformas de força ou faixas elásticas. Poderíamos acessar as medidas da contração muscular com apenas alguns eletrodos de superfície.

Na perspectiva do controlador, visamos desenvolver um ambiente de simulação para comparação de controladores para baixas velocidades na marcha e um ambiente de simulação para comparação de controladores de cadência para ciclismo. O software de simulação fornece ferramentas de cinemática e dinâmica para entender e analisar movimentos. Usando uma interface gráfica, podemos gerar simulações com modelos padrão ou desenvolver novos modelos e controladores. Além disso, também desenvolvemos funções adicionais para simular os efeitos de fadiga e distúrbios.
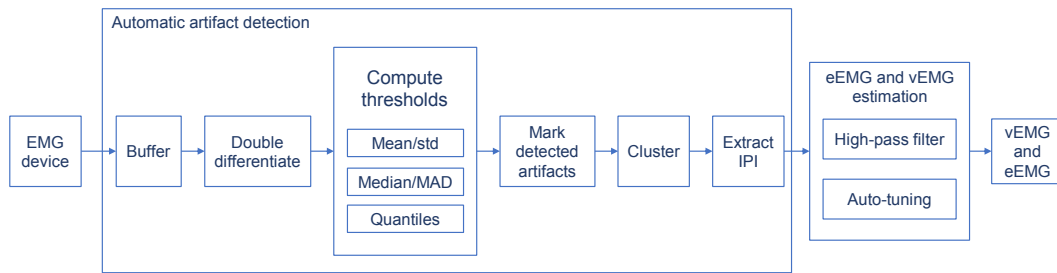
Figure A.2: A partir do sinal de EMG, a detecção automática de artefatos armazena o sinal em buffer e depois o diferencia duas vezes. A partir desse resultado, o método usa um dos três parâmetros de limiar para calcular os valores máximo e mínimo para identificar possíveis artefatos. Esses pontos são marcados e agrupados para posterior extração do IPI. Para estimar o EMG volitivo e evocado (vEMG e eEMG), o método usa um dos dois métodos de filtragem.

Fonte: preparado pela autora.

Na perspectiva da planta, o presente trabalho pretende realizar experimentos com órteses passivas de joelho para assistência no ciclismo por eletroestimulação e analisar o seu efeito na cadência. Com órteses passivas, o voluntário com LM poderia pedalar mais longe com o mesmo estímulo.

A.2 DETECÇÃO DE ARTEFATOS DE ESTIMULAÇÃO PARA ISOLAR EMG

Para extrair componentes dos sinais EMG, precisamos primeiro encontrar os intervalos entre pulsos (IPIs), ou seja, o sinal EMG entre os artefatos de estimulação. Portanto, desenvolvemos métodos para detectar os artefatos de estimulação (ínicio e fim de cada IPI) de dois canais para, em seguida, estimar o EMG voluntário e o EMG evocado pela estimulação. A Figura A.2 resume todo o método para extrair informações de EMG volitivas e evocadas. Nós testamos diferentes parâmetros do sinal para detectar os artefatos automaticamente, com dois setups de hardware diferentes.

A detecção de artefato é executada na frequência da estimulação. Deve-se considerar que a má conexão do cabo e os movimentos do usuário também geram artefatos no sinal de EMG. O método desenvolvido para a detecção de artefatos leva em consideração que a maioria dos estimuladores possui uma fonte de corrente que gera pulsos em dois canais sequencialmente em um curto período.

Para testar a estimativa de EMG volitiva e evocada, usamos duas configurações de hardware diferentes (estimuladores e amplificadores de EMG) durante a caminhada de um indivíduo hígido. Com ambos hardwares, nós encontramos uma taxa de sucesso ao encontrar os artefatos maior que 95% utilizando a detecção automática desenvolvida.

A aplicação de estratégias de controle de estimulação de malha fechada ainda enfrenta vários desafios técnicos relacionados ao projeto, como (1) a variedade de incertezas na fisiologia muscular entre diferentes pacientes e (2) as dificuldades relacionadas à predição exata da força de contração exercida pelo músculo. Essas dificuldades estão relacionadas principalmente ao mapeamento desconhecido entre os parâmetros de entrada da estimulação e a força muscular gerada (ALOUANE et al., 2018). No entanto, sabemos que a força e o sinal EMG podem estar correlacionados (FANG et al., 2018). Portanto, apresentamos, como uma prova de conceito dos métodos de detecção de artefatos automáticos, experimentos com uma pessoa com LM completa. Neste experimento, comparamos a força normalizada com a estimativa normalizada do EMG evocado pela estimulação.

Nós comparamos os sinais de força com o EMG evocado em um exercício. Durante o exercício, o EMG voluntário do participante permaneceu próximo de zero, como esperado. O algoritmo desenvolvido encontrou apenas 0.8% de artefatos incorretos, que podem ser facilmente removidos por filtros adicionais durante o controle em tempo real. O exercício isométrico causa uma fadiga muscular, que conseguimos perceber tanto no sinal de força quanto no sinal do EMG evocado, visualizado na Figura A.3.

A.3 SIMULAÇÕES DE ESTRATÉGIAS DE CONTROLE PARA MARCHA POR ELETROESTIMULAÇÃO

Durante a fisioterapia, o treinamento de marcha é um conjunto de atividades para o usuário readquirir habilidades de caminhada. Esses exercícios podem incluir: (1) treinamento de equilíbrio, para ajudar o corpo a manter seu equilíbrio em posições estáticas ou dinâmicas; (2) treinamento da postura, para intervir no alinhamento e posição do corpo com a gravidade, o centro de massa e a base de suporte; (3) e aprendizagem motora, para intervir na execução de ações qualificadas. É comum o uso da eletroestimulação com pacientes com LM completa para aumentar o tônus muscular (SZECSI; STRAUBE; FORNUSEK, 2014). Como a fadiga acelerada gerada pela estimulação limita a duração dos experimentos, desenvolvemos o ambiente de simulação para testes iniciais de controle de marcha (SOUSA; FREIRE; BÓ, 2019). Nesse ambiente, estudamos quatro estratégias de controle de estimulação combinadas com órteses ativas.

Este trabalho tem como objetivo fornecer um ambiente de simulação para comparar controladores de neuropróteses híbridas em baixas velocidades. Como a eletroestimulação com eletrodos superficiais é incapaz de recrutar adequadamente os músculos flexores de quadril (psoas major e músculo ilíaco), o sistema desenvolvido combinou o controle de joelho por estimulação com uma órtese ativa de quadril. Outros trabalhos usaram uma configuração semelhante, e.g., (OBINATA et al., 2007; KIRSCH et al.,
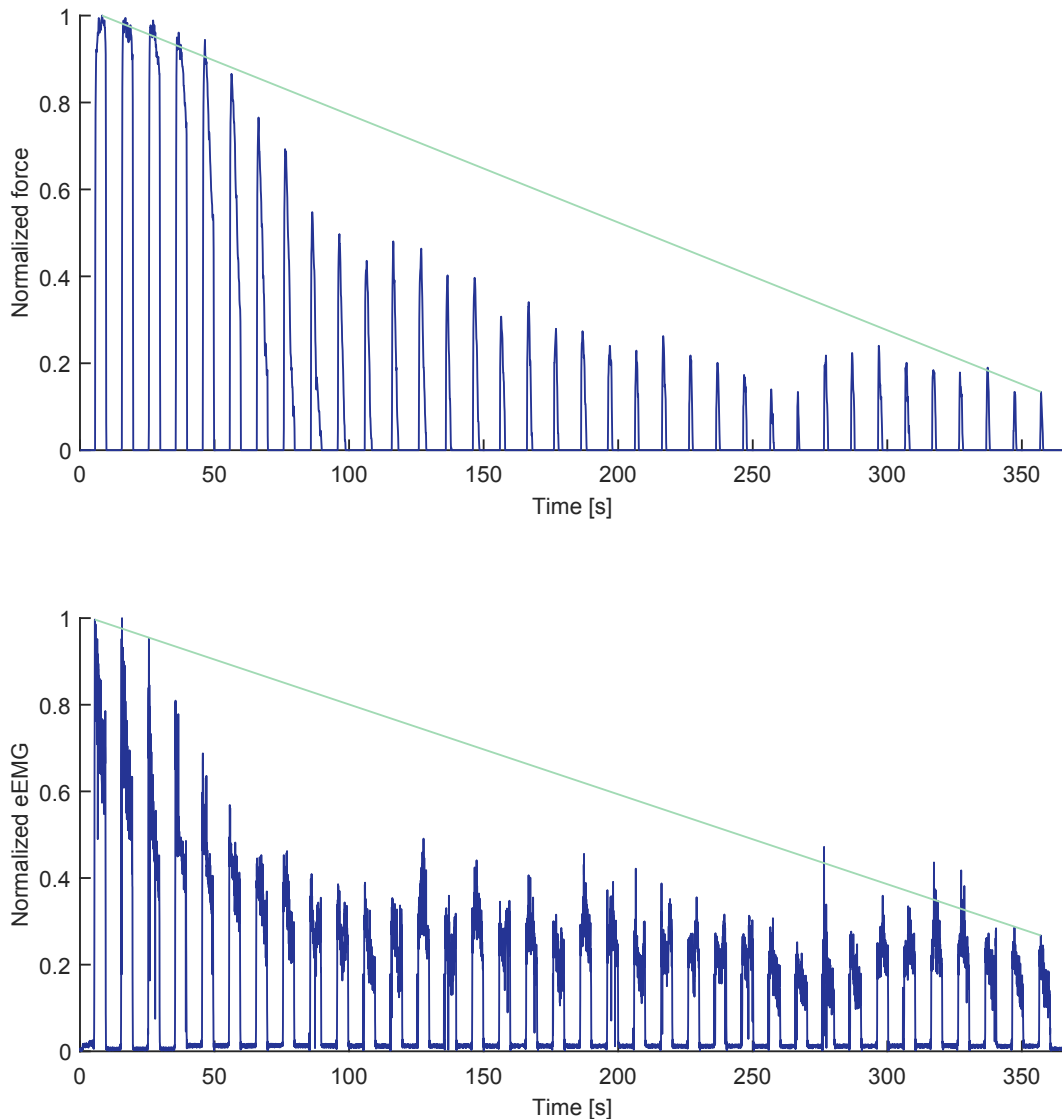
Figure A.3: Sinais normalizados de força e EMG evocado. Excluímos a detecção incorreta de artefatos e marcamos a primeira e a última medida mais alta para força e EMG evocado para mostrar a fadiga durante o exercício.

Fonte: preparado pela autora.

2014; FARRIS et al., 2009; KOBETIC et al., 2009).

Implementamos o sistema na plataforma OpenSim, um software open-source que simula modelos musculoesqueléticos (DELP et al., 2007; HILL; B, 1938). O software fornece ferramentas de cinemática e dinâmica para entender e analisar movimentos. Para implementar a marcha por eletroestimulação no OpenSim, usamos um modelo contendo os membros inferiores. A Figura A.4 ilustra o modelo resultante desenvolvido para este estudo, apresentando as órteses ativas no modelo OpenSim de uma perna.

Para simular o movimento da marcha com uma perna, integramos as articulações do quadril e do joelho com dois controladores de trajetória independentes. Por-
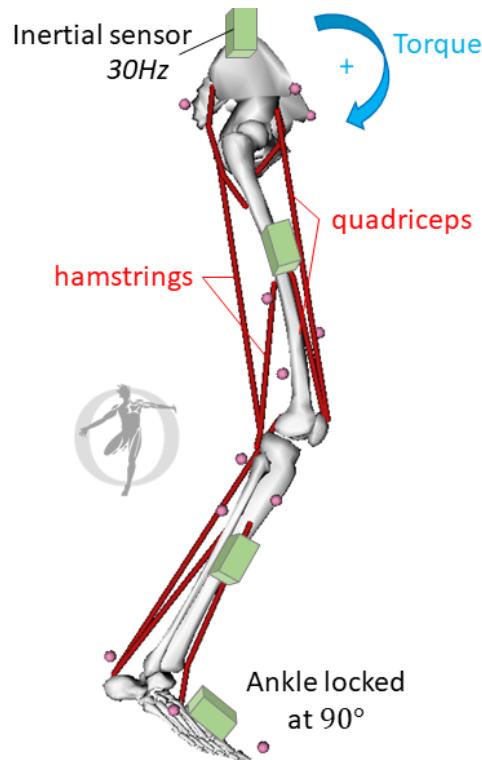
Figure A.4: O modelo completo para controle de marcha, usando estimulação para gerar movimento de joelho e órteses ativas para movimento de quadril. Linhas vermelhas representam os músculos excitáveis do quadríceps e isquiotibiais. Bloqueamos a articulação do tornozelo a 90°e deixamos o quadril se movimentar livremente pelo controle PID de torque. Cubos verdes representam os sensores inerciais (no tronco, na perna, na perna e no pé).

tanto, empregamos o controlador PID para extensão e flexão do quadril para a órtese ativa. A posição do ângulo do joelho é controlável pela excitação dos músculos, quadríceps para gerar extensão do joelho ou isquiotibiais para gerar flexão do joelho. Durante a marcha, essa integração deve considerar que diferentes velocidades de marcha geram diferentes padrões de movimento articular. Além disso, a arquitetura de controle deve combinar atuadores e estimulação, considerando as especificidades do sistema musculoesquelético e até a complexidade da marcha.

A Figura A.5 ilustra a dinâmica musculoesquelética, as trajetórias predefinidas e os controladores escolhidos. A arquitetura de controle é composta por: (1) um controlador PID (proporcional-integral-derivativo) que representa uma órtese ativa para gerar movimento do quadril e (2) um controlador de estimulação (2a) bang-bang (BB), (2b) PID, (2c) aprendizado-iterativo PID (PID-ILC) ou (2d) PID usando busca extrema (PID-ES).

Para comparar os controladores, simulamos diferentes configurações. Para todas
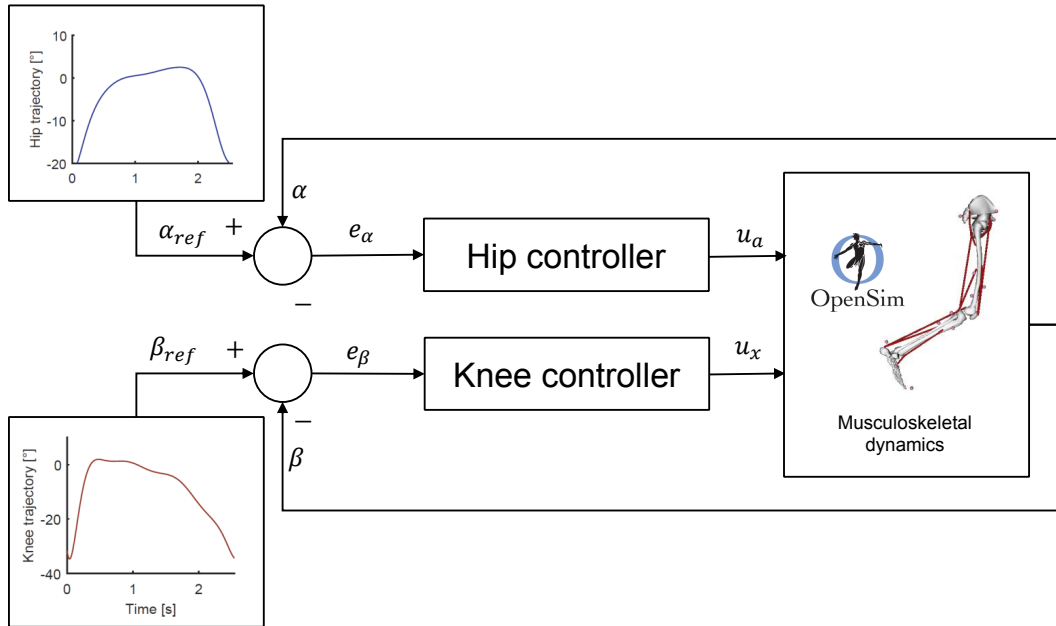
Figure A.5: Nesta arquitetura de controle da marcha, o controlador do joelho fornece um sinal de excitação para os músculos u_x com base no erro (e_β) entre o ângulo de referência da articulação do joelho β_{ref} e o ângulo medido β. O controlador de quadril fornece um sinal u_a com base no erro (e_α) entre o ângulo de referência da articulação do quadril α_{ref} e o ângulo medido α. Ambos os controladores consideram as trajetórias predefinidas do quadril e joelho. Com os sinais de controle (excitação e torque dos músculos), o OpenSim calcula a dinâmica musculoesquelética.

Fonte: preparado pela autora

essas simulações, o tempo final T_f é dez vezes o período da marcha T_{step} ($T_{step} = 1.76s$ em $0.3\,m/s$ e $T_{step} = 2.54s$ em $0.1\,m/s$), a frequência de controle f é de 50Hz e a posição inicial da articulação do quadril e joelho foram os valores no início das trajetórias (para evitar overshoots altos no início do controle). Para avaliar os controladores em condições semelhantes, simulamos cada controlador para as duas velocidades da marcha g_s ($0.1\,m/s$ e $0.3\,m/s$), além disso, simulamos esses sistemas com e sem o efeito de fadiga. Em seguida, plotamos as trajetórias de rastreamento de quadril e joelho ao longo do tempo e calculamos os parâmetros de desempenho: desvio padrão do erro no joelho (σ_β), erro máximo no joelho (e_{max_β}) e coeficiente de correlação de Pearson ($corr_\beta$).

Para ambas as velocidades, o joelho flexiona enquanto o quadril se estende (ou seja, o joelho empurra o quadril), esse efeito ocorre porque o OpenSim simula a natureza biarticular do músculo isquiotibiais, limitando a flexão do quadril. Sem nenhum observador externo do modelo musculoesquelético, os controladores testados são incapazes de manter completamente a trajetória, o que justifica o erro permanente entre a referência e a trajetória medida, semelhante às observações de (KAWAI; EJIRI;

KAWAI, 2015). Já os resultados considerando a fadiga tendem a apresentar coeficientes de correlação mais baixos e erros maiores, pois os músculos proporcionam menos torque quando fatigados, resultado esperado devido à perda de eficiência.

Para visualizar o desempenho geral dos controladores, calculamos a média de todas as correlações, desvios padrão e erros máximos do último passo da caminhada para ambas velocidades (Figura A.6). Os gráficos finais ilustram maior desempenho (maior correlação e menor desvio padrão e erros máximos) o mais longe do centro do círculo. O controlador BB apresentou baixos coeficientes de correlação e altos erros quando comparado a outros controladores, já que a falta da quantificação do erro causou altos overshoots. Em um cenário real, o controlador BB pode levar o sistema a respostas instáveis, situação perigosa para um sujeito com LM. Quando comparado ao BB, o controle PID apresentou alta correlação (> 0.9). No entanto, para velocidades mais baixas, o controle PID apresentou uma resposta inadequada mesmo em um cenário sem fadiga, esses resultados correspondem à afirmação de que o controle PID não é suficiente nas aplicações com eletroestimulação, devido às não-linearidades do comportamento muscular (POPOVIĆ; MALEŠEVIĆ, 2009).
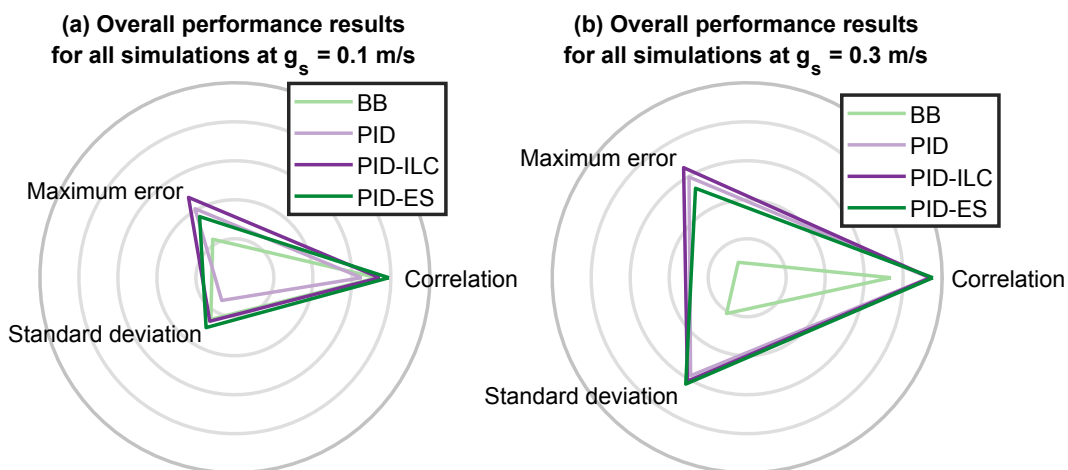

Figure A.6: Avaliação do desempenho dos controladores (BB, PID, PID-ILC, PID-ES). Esses gráficos mostram o erro máximo médio, o desvio padrão médio e os resultados da correlação média de todas as simulações em (a) $g_s = 0.1m/s$ e (b) $g_s = 0.3m/s$. Resultados maiores (fora do círculo) apresentaram melhor desempenho.

Fonte: preparado pela autora.

Em algumas configurações, especialmente para $g_s = 0.1m/s$, há uma melhoria entre os coeficientes de correlação dos controladores PID-ILC e PID-ES, quando comparados ao PID. Os controladores PID-ILC e PID-ES aumentaram a correlação e diminuíram os erros conforme os passos ocorreram. O PID-ES apresentou coeficientes de correlação ligeiramente mais altos e menores erros de desvio padrão e máximo. Mas também conseguimos observar um efeito de vibração no PID-ES, o que é indesejável

em aplicações reais (AJOUDANI; ERFANIAN, 2007).

A.4 SIMULAÇÕES DE ESTRATÉGIAS DE CONTROLE PARA CICLISMO POR ELETROESTIMULAÇÃO

Como a fadiga acelerada gerada pela estimulação limita a duração dos experimentos, também desenvolvemos o ambiente de simulação para ciclismo utilizando o OpenSim (SOUSA et al., 2016) e estudamos estratégias de controle com e sem assistência passiva de órtese. Para implementar o ciclismo, utilizamos um modelo musculoesquelético contendo os membros inferiores, bem como seu acoplamento mecânico com pedais e pé-de-vela (Figura A.7).
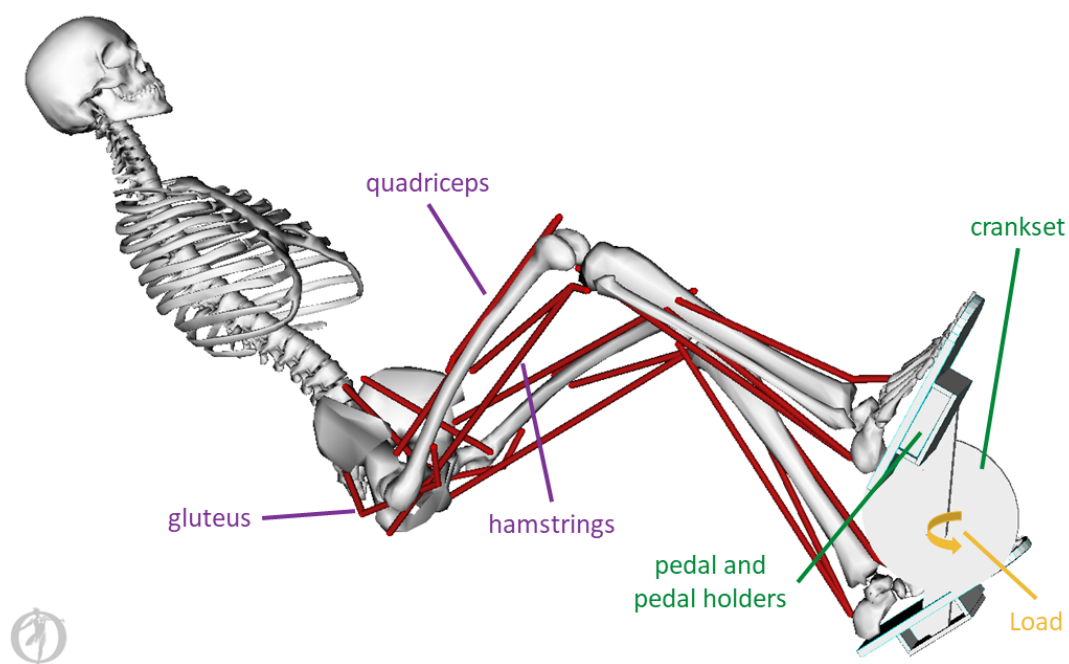

Figure A.7: Descrição do modelo para ciclismo por eletroestimulação semelhante à EMA Trike. O OpenSim representa os músculos (e.g., quadríceps, isquiotibiais e glúteo) como linhas vermelhas. Desenvolvemos o suporte para os pés com pedais e pé-de-vela, no qual também incluímos um torque para simular uma carga no pedal.

Fonte: preparado pela autora.

Aplicamos excitações coordenadas nos quadríceps, isquiotibiais e glúteo máximo, com base em controladores anteriores (HUNT, 2005; BÓ et al., 2015). Durante uma pedalada, o quadríceps é o músculo que mais fornece torque através da extensão do joelho. O glúteo máximo oferece força para a extensão do quadril após o quadríceps estender o joelho. Posteriormente, os isquiotibiais flexionam o joelho. Para um ciclismo eficiente e seguro, esses grupos musculares devem ser excitados em faixas específicas, dependendo do ângulo e da velocidade do pedal. Então, geramos pedaladas alterando

os grupos musculares da seguinte forma: (1) somente quadríceps (Q), (2) quadríceps e isquiotibiais (QH) e (3) quadríceps, isquiotibiais e glúteo máximo (QHG).

Durante o ciclismo, a cadência atual do pedal $\dot{\theta}_c$ também influencia o alcance da estimulação devido ao controlador e as atrasos neuromusculares (HUNT, 2005). Como o OpenSim também simula esses atrasos, nós desenvolvemos um ajuste de fase baseado em cadência. Posteriormente, nós também desenvolvemos controladores BB e PID.

Simulamos diferentes configurações de pedalada para cada controlador. Definimos o tempo final T_f como 20 segundos e a frequência de controle f como 50 Hz. Em seguida, calculamos os parâmetros de desempenho: cadência média, aceleração média da cadência, desvio padrão da cadência, erro máximo e erro de desvio da média quadrática da raiz (RMSE), tempo de subida, níveis de excitação muscular e número de voltas completas do pedal.

O ambiente ofereceu a possibilidade de realizar comparações entre diferentes grupos musculares, excitações, cargas, efeito de fadiga e controladores. Como esperado, com a fadiga, a cadência diminui, com mais grupos musculares, a cadencia aumenta, e com a carga, a cadência diminui.

Nós também modelamos o PID para o ciclismo, já que esse controlador considera não apenas pontos específicos nos quais o músculo deve ser excitado, mas também a intensidade de excitação para obter uma cadência de referência. Logo, foi possível controlar a cadência.

Como a fadiga muscular é rápida durante a eletroestimulação, essa é uma limitação notável para o ciclismo. Alguns ajustes podem diminuir esse efeito, nossa hipótese é que a adição de órteses passivas armazene energia (elástica com molas mecânicas) durante alguns pontos para em seguida liberá-la, auxiliando o movimento e reduzindo os efeitos da fadiga muscular e custo metabólico. Então, no ambiente de simulação de ciclismo já apresentado, nós modelamos também órteses passivas de joelho, determinando os parâmetros da mola e como eles se relacionam com a cadência média do ciclismo e a excitação muscular.

Para analisar o efeito das órteses passivas, apresentamos uma comparação entre os resultados com e sem as órteses. Nós variamos a intensidade da constante elástica e também a período de atuação da mola. As simulações indicaram que os torques negativos (mola libera energia na extensão de joelho) levaram a maiores velocidades, enquanto os positivos (libera energia na flexão) levaram a menores velocidades.

Em determinadas condições o uso das órteses passivas aumentou a cadência do ciclismo, mas não necessariamente geraram valores toleráveis para mola. Como era um requisito de projeto, simulamos também um controlador PID apenas usando os parâmetros de torque que atendem as especificações. Como esperado, as cadências

médias são semelhantes com e sem órteses. Já os erros médio e RMSE diminuíram com as órteses passivas quando comparadas ao ciclismo sem assistência. Um efeito adverso do uso das órteses é que o tempo de subida tende a ser mais alta pela dificuldade do sistema superar o torque contrário durantes as primeiras pedaladas.

A.5 EXPERIMENTOS DE ESTRATÉGIAS DE CONTROLE PARA CICLISMO POR ELETROESTIMULAÇÃO

Os resultados de simulação levaram à conclusão de que valia a pena desenvolver e testar esse tipo de órtese passiva no ciclismo por eletroestimulação. Portanto, construímos um par de órteses passivas de joelho, e estabelecemos um ambiente experimental e um protocolo para comparar os resultados de experimentos com e sem órteses passivas de joelho.

Nos experimentos, desenvolvemos um controlador BB e estimulamos apenas os quadríceps para minimizar efeitos das não-linearidades e a da dependência do tempo. Realizamos os experimentos com um voluntário com LM completa, exigindo um ambiente experimental robusto (Figura A.8). O protocolo experimental consistiu em dois dias de exercício de ciclismo com eletroestimulação. Durante o exercício, o usuário usava as órteses passivas em todo o experimento, e nós adicionamos ou retiramos as molas (para podermos diferenciar o efeito do sistema apenas com e sem molas). O ciclista realizou dois exercícios por dia, mantendo a mesma posição sobre o assento, assim como o mesmo posicionamento de eletrodos. Entre cada um desses exercícios, nós adicionamos ou nós retiramos as molas e o deixamos descansar por 5 minutos.

No primeiro dia, o usuário começou a pedalar com as molas, e em seguida sem. E no segundo dia, o contrário. Essa troca foi necessária para que possamos observar o uso das molas com e sem o efeito da fadiga. Cada exercício ainda consistia de duas fases: aquecimento e treinamento. A Figura A.9 ilustra o procedimento.

Nos dois dias, o voluntário foi capaz de pedalar com e sem as órteses. No primeiro dia, o treinamento com molas durou aproximadamente 14 minutos, e o treinamento sem molas durou cerca de 16 minutos. Podemos observar que a velocidade aumentou em 17% quando colocamos as molas (Tabela A.1). No segundo dia, os dois treinamentos duraram aproximadamente 20 minutos e podemos observar um aumento de 11% da velocidade média ao conectarmos as molas (Tabela A.2).

Como as órteses adicionavam peso ao sistema, tomamos um cuidado extra para manter as pernas no plano sagital, garantindo a segurança do voluntário. Portanto, o posicionamento do usuário na bicicleta demorou mais que o usual. Como correntes de estimulação mais alta podem gerar uma maior cadência, definimos o protocolo para que possamos comparar uma parte do treinamento com correntes semelhantes.
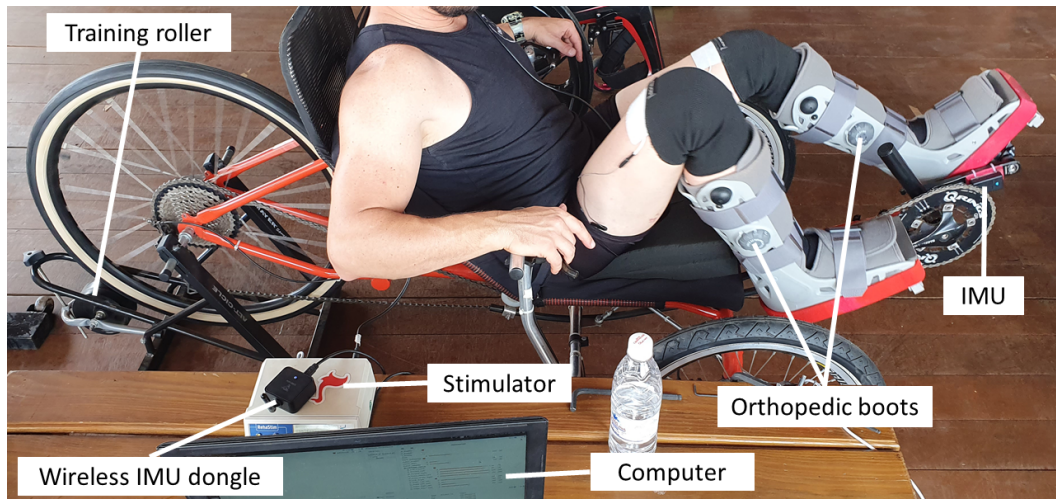
Figure A.8: O sistema completo da EMA trike. O computador fornece o sinal de estimulação com base no ângulo do pedal medido pela IMU. Através de eletrodos superficiais, o estimulador aplica o sinal correspondente aos músculos para pedalar o triciclo. As botas ortopédicas presas aos pedais evitam o movimento do tornozelo do voluntário e alinham as pernas para que não caiam do plano sagital.
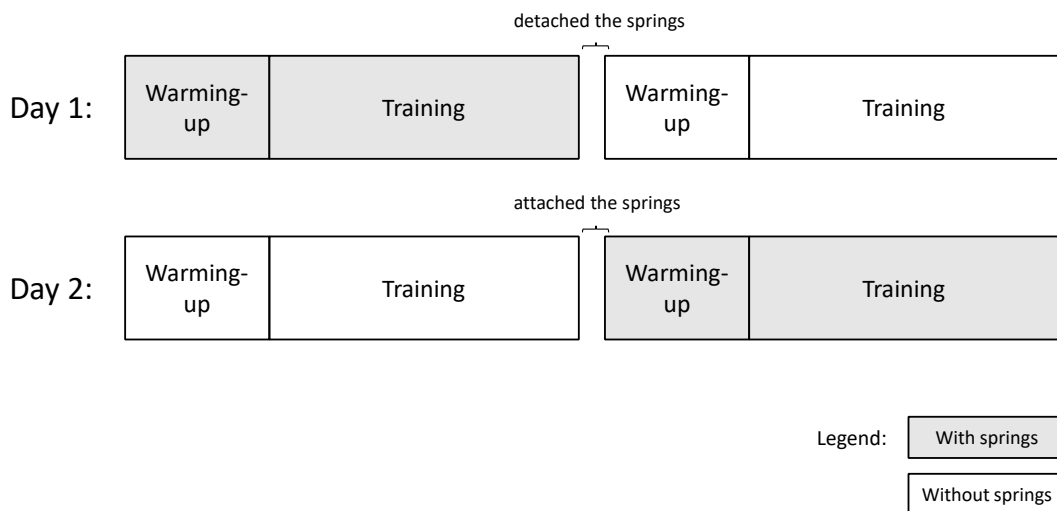
Fonte: preparado pela autora.

Figure A.9: Protocolo. Durante dois dias, o usuário realizou dois exercícios. Antes de cada dia, o usuário não usava nenhuma estimulação elétrica no quadríceps por pelo menos 24 horas. A cada dia, pedalava com e sem as molas, divididas entre as fases de aquecimento e treinamento.

Fonte: preparado pela autora.

Nós observamos que o voluntário podia começar a pedalar sem nenhum empurrão manual de forma mais rápida sem as molas. Esse desempenho é semelhante aos encontrados em simulação com o controlador PID e aos resultados descritos em (CHAI-CHAOWARAT et al., 2017). Embora as molas forneçam energia em parte do movi-

Table A.1: Cadência durante o primeiro dia de treinamento entre 60mA e 70mA (corrente de estimulação).

	Com molas	Sem molas
Cadência	215.14°/s	183.88°/s
Desvio padrão	60.30°/s	57.08°/s

Table A.2: Cadência durante o primeiro dia de treinamento entre 60mA e 80mA (corrente de estimulação).

	Com molas	Sem molas
Cadência	245.35°/s	220.42°/s
Desvio padrão	74.81°/s	92.39°/s

mento e possam até aumentar a cadência média, o usuário ainda precisa superar a energia da mola durante a flexão de joelho. De toda forma, a cadência acabou sendo sempre menor com a órtese, quando comparado sem.

A.6 CONCLUSÕES

A LM pode levar a uma grande diminuição na qualidade de vida, portanto existe uma necessidade constante de desenvolvimento de técnicas mais avançadas para se ajustarem a cada usuário. Este documento apresentou três novos métodos para melhorar a reabilitação de membros inferiores com controladores baseados em eletromiografia. Nossas abordagens visaram complementar outras pesquisas, sempre levando em consideração a segurança do usuário com deficiência e a eficácia do sistema de controle. Acreditamos que esses estudos podem levar a melhorias em métodos para reabilitação.